"Awarded for ... developing a method for ... determining essentially equal-atom crystal ... and molecular ... structures by X-ray ... analysis, having a ... profound effect ... on the practice of ... organic and biological ... chemistry."

The National Medal of Science awarded to Dr. Isabella Karle

1996 NRL REVIEW

Naval Research Laboratory, Washington, DC

19970501 083

This *1996 NRL Review* introduces you to the Naval Research Laboratory—the Navy's Corporate Laboratory—and focuses on research highlights from fiscal year 1995. In addition, it presents the special honors awarded to NRL employees and describes the programs available to NRL and non-NRL employees. This publication offers an exchange of information among scientists, engineers, scholars, and managers, and it is used as a recruiting tool.

As you read the *NRL Review*, you will become even more aware that the Naval Research Laboratory comprises a dynamic team of scientists, engineers, and support personnel working together to promote the programs that will continue to foster discoveries and scientific advances for the Navy of the future.

General information on the research described in this *NRL Review* may be obtained from the Public Affairs Office, Code 1230, (202) 767-2541. Information concerning Technology Transfer is available from Dr. Richard Rein, head of the Technology Transfer Office, Code 1004, (202) 767-7230. The sources of information on the various nonresearch programs at NRL are listed in the chapter entitled "Programs for Professional Development."

The NRL *Fact Book* lists the organization, key personnel, and major facilities for each division. Further, it contains information about Laboratory funding, programs, and field sites. A copy of the *Fact Book* may be obtained by contacting the Technical Information Division, Publications Branch, Code 5230, (202) 767-2782.

NRL's URL: http://www.cmf.nrl.navy.mil/

Quick Reference Telephone Numbers

	NRL Washington	NRL-SSC	NRL-Monterey	NRL CBD
Hotline	(202) 767-6543	(601) 688-5001	(408) 656-4737	(202) 767-6543
Personnel Locator	(202) 767-3200	(601) 688-3390	(408) 656-4706	(410) 257-4000
DSN	297- or 354-	485	878	—
Direct-in-Dialing	767- or 404-	688	656	257
Public Affairs	(202) 767-2541	(601) 688-5328	(408) 656-4708	—

DISCLAIMER NOTICE
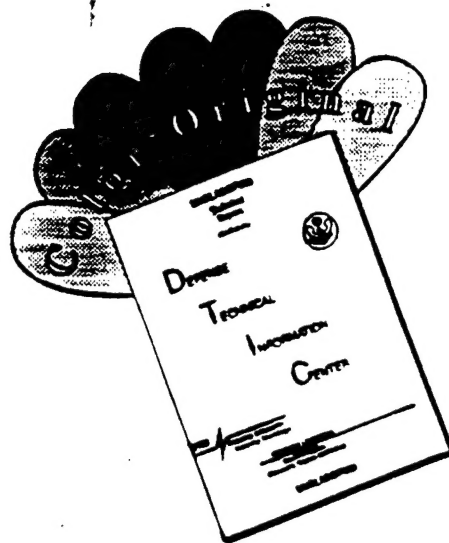
THIS DOCUMENT IS BEST QUALITY AVAILABLE. THE COPY FURNISHED TO DTIC CONTAINED A SIGNIFICANT NUMBER OF COLOR PAGES WHICH DO NOT REPRODUCE LEGIBLY ON BLACK AND WHITE MICROFICHE.

To readers of the *1996 NRL Review*:

The Naval Research Laboratory is pleased to honor one of its distinguished scientists, Dr. Isabella Karle, head of the X-ray Diffraction Section of NRL's Laboratory for the Structure of Matter. Dr. Karle is the recipient of the 1995 National Medal of Science, the highest scientific honor bestowed by the President of the United States. The medal is given in special recognition of outstanding contributions to the physical, biological, mathematical, behavioral, or engineering sciences. President Bill Clinton presented the award at the White House on October 18, 1995.

Also during 1995, Dr. Karle received the National Academy of Sciences' Award in Chemical Sciences and the Department of Defense's Distinguished Civilian Service Award.

I invite your attention to pages ii and iii, where Dr. Isabella Karle's awards and work are described in more detail.

Further, NRL's great recent success—Project *Clementine*—continues to receive awards from outside organizations. Those presented during 1995 are shown on pages iv and v.
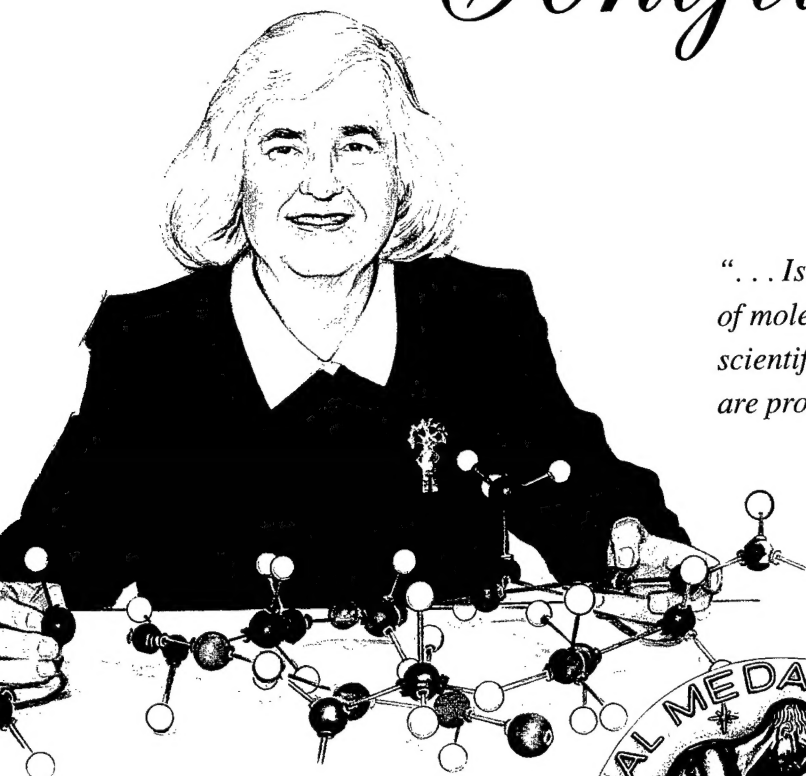
Timothy Coffey

Dr. Timothy Coffey
Director of Research

19970501 083

Congratulations . . .

". . . Isabella's contribution to the determination of molecular structures has been profound in both scientific impact and its economic impact. We at NRL are proud to have the privilege of working with her."

– Dr. Timothy Coffey
Director of Research

DR. ISABELLA KARLE

Dr. Karle has pioneered in elucidating the crystal structures of numerous complex organic substances, natural products, photorearrangement products, biologically active molecules, ionophores, peptides containing many residues, and supramolecular assemblies, which have significance in, for example, synthetic chemistry, medical drug design, materials design, reaction mechanisms, ion channel formation, molecular modeling programs, and energy calculations.

Dr. Karle and her husband, Dr. Jerome Karle, corecipient of the Nobel Prize in Chemistry in 1985, have worked at NRL for 50 years and continue to bring honor not only to themselves and the Laboratory, but to the Federal Government, as well.
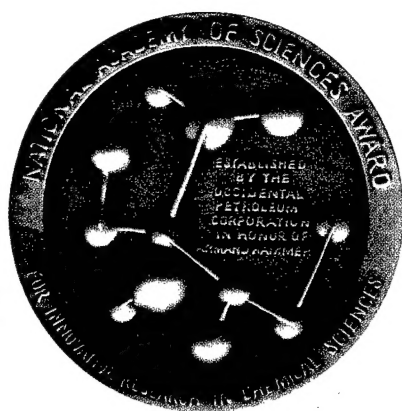
1995 NATIONAL MEDAL OF SCIENCE

President Bill Clinton presented this prestigious award to Dr. Karle for "developing a method for determining essentially equal-atom crystal and molecular structures by X-ray analysis, thereby having a profound effect on the practice of organic and biological chemistry." Her practical procedures have become adopted worldwide and have contributed to the explosive output of crystal structure analyses. The National Medal of Science is the highest scientific honor bestowed by the President of the United States in special recognition of outstanding contributions to the physical, biological, mathematical, behavioral, or engineering sciences.
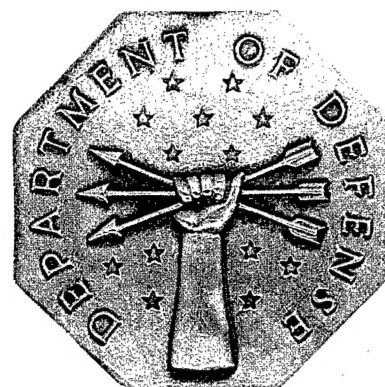
1995 DEPARTMENT OF DEFENSE DISTINGUISHED CIVILIAN SERVICE AWARD

This competitive award is the highest honor given by DoD to career employees. Dr. Karle was cited for "effecting major advances in chemistry and the chemical industry by affording an analytical tool that can determine accurately and with dispatch, the three-dimensional arrangements of atoms in a very broad range of substances . . . Dr. Isabella Karle has not only applied her methodology in her research program to many substances of importance, but also her efforts have been very greatly magnified by the worldwide adaptation and application of her methodology. Many thousands of new structures are determined each year for the valuable purpose of relating structure to function."

ii

Dr. Isabella Karle

1995 NATIONAL ACADEMY OF SCIENCES AWARD IN CHEMICAL SCIENCES

The Academy presented this award to Dr. Karle "for innovative research in the chemical sciences that, in the broadest sense, contributes to a better understanding of the natural sciences and to the benefit of humanity." Further, Dr. Karle was honored "for her development of and extensive application of a method for determining essentially equal-atom crystal molecular structures by X-ray analysis, thereby profoundly affecting the practice of chemistry."

## BOWER AWARD AND PRIZE FOR ACHIEVEMENT IN SCIENCE

This award is presented by the Franklin Institute to honor international achievement in the physical and life sciences that significantly advances human knowledge and welfare. Dr. Karle was cited for her "pioneering contributions in determining the three-dimensional structure of molecules, making use of both X-ray and electron diffraction, and in particular for her definitive introduction . . . of the symbolic addition method to reveal molecular structure directly from X-ray studies." Dr. Karle was the fourth recipient of the prize and the first woman to receive it—clearly a fitting recognition of her half-century career in science and service to the U.S. Navy and mankind.

1988 GREGORI AMINOFF PRIZE

This award was presented by the Royal Swedish Academy of Sciences, in Stockholm, Sweden. The prize honors "outstanding pioneering contributions to crystallography characterized by scientific beauty and elegance." Dr. Karle was honored for her "eminent crystallographic studies of complicated natural products."
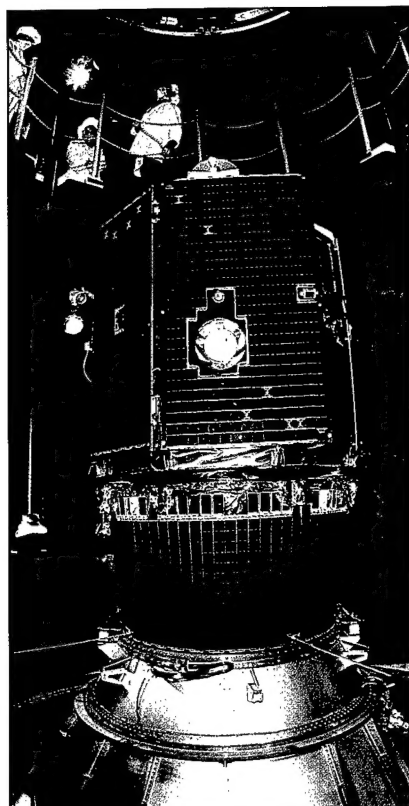
In 1990, a mission was conceived to test the latest in space-based imaging components, using the Moon and a near-Earth asteroid as celestial targets. The *Clementine* mission was the result of those early investigations. In 22 short months, the construction and integration of the sophisticated deep-space spacecraft was completed.

Clementine is the first satellite to embody the concept of "faster, cheaper, better" and represents the beginning of a new era of cooperation in space.

The Clementine *spacecraft*

Mr. Jim Campbell (left), Jet Propulsion Laboratory's Clementine *manager, Mr. Paul Regeon (center), NRL's* Clementine *project team manager, and Ms. Linda Greenway (right), NRL's Public Affairs exhibit specialist at the "Best of 1994" ceremony.*


Mr. Peter Wilhelm (right), director of NRL's Naval Center for Space Technology accepts the Stellar Award on behalf of the Clementine *team from Mr. Christopher Kraft, former director of the Johnson Space Center.*

**Popular Science Magazine's
"The Best of 1994's Top 100 Technologies"**

Clementine, the first U.S. spacecraft to visit the moon in a quarter-century, is proof that the "faster, cheaper, better" mantra is more than just rhetoric. The 500-pound spacecraft was designed and built in only 2 years, for just $80 million. Developed by DoD, DoE, and NASA, *Clementine* could be a model for future military-civilian cooperation. Like its namesake, though, *Clementine* is now "lost and gone forever," after sending back to Earth more than 1 million images of the lunar surface.
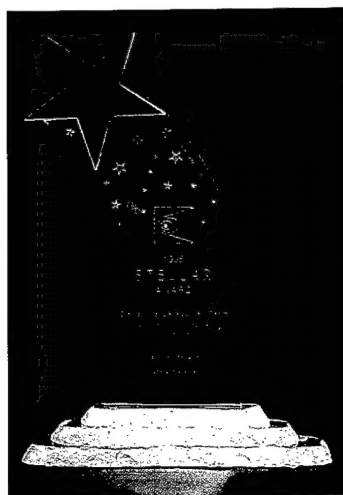
The Rotary National Award for Space Achievement Foundation's 1994 Stellar Award for Spacecraft Design

NRL's *Clementine* team was "recognized for its pioneering efforts in successfully demonstrating the first 'faster, cheaper, better' spacecraft technology, during the *Clementine I* mission that mapped the entire lunar surface; for demonstrating that it is possible to build a spacecraft like *Clementine* in only 22 months (less than one-half the usual time) for one-fifth the usual cost for similar space probes; and for opening a new pathway for reduced operational costs for future Department of Defense and NASA space missions."

Continues to Receive Recognition
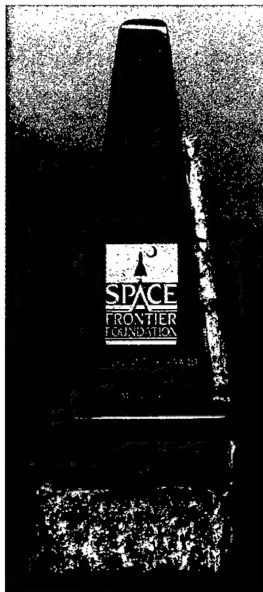
1995 Space Frontier Vision-to-Reality Award

Presented to five *Clementine* team members, including NRL's Mr. Paul Regeon. "The *Clementine* team's achievement, in acquiring an impressive quantity of high-quality multispectral, topographic and other data of the moon's surface, while testing military sensor hardware, is remarkable. Further, the demonstration of new approaches to the development, operations and program management of a planetary exploration vehicle is equally commendable. Your participation in this effort is very much appreciated by American citizens like we in the [Space Frontier] Foundation who are committed to an open frontier in space."
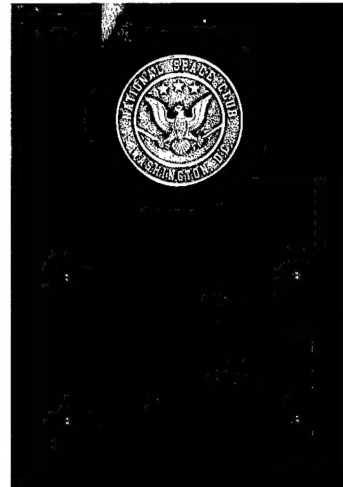
The National Space Club's Nelson P. Jackson Aerospace Award

The *Clementine* team was cited "for innovative spacecraft design, development and operations, and the production of meaningful scientific data that was used to build the most comprehensive, multispectral geologic lunar map to date."
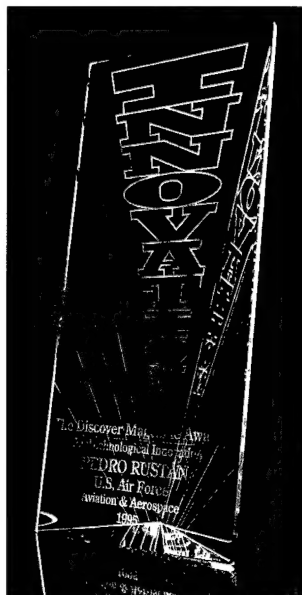
1995 Award for Technological Innovation

Discover Magazine selected *Clementine* as the winner in the Aerospace and Aviation category, one of seven for which awards were presented. A total of 4,000 technologies were considered.
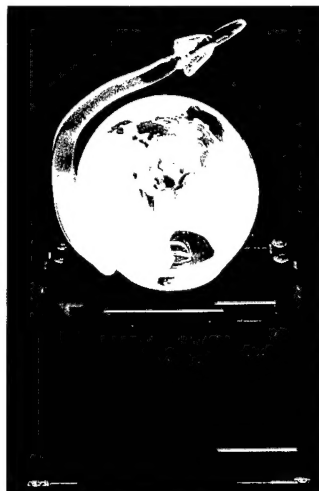
Aviation Week and Space Technology's 1994 Laureate Award

Presented to Col. Pedro Rustan, Mission Director, and NRL's Mr. Paul Regeon. "This year's space laureates had a 'supporting cast' composed of an exceptionally talented and dedicated cadre of engineers and scientists . . . *Clementine* fully realized its defense technology goals, and it produced splendid new lunar science as a bonus. In an era in which 'faster, cheaper, better' has become a mantra in space circles, *Clementine* is the premier example of a return to the practices that once characterized all space science missions."

1996 NRL Review

CHEMICAL/BIOCHEMICAL RESEARCH

ELECTRONICS AND ELECTROMAGNETICS

ENERGETIC PARTICLES, PLASMAS, AND BEAMS

INFORMATION TECHNOLOGY AND COMMUNICATION

MATERIALS SCIENCE AND TECHNOLOGY

OCEAN AND ATMOSPHERIC SCIENCE AND TECHNOLOGY

OPTICAL SCIENCE

REMOTE SENSING

SIMULATION, COMPUTING, AND MODELING

SPACE RESEARCH AND SATELLITE TECHNOLOGY

SPECIAL AWARDS AND RECOGNITION

PROGRAMS FOR PROFESSIONAL DEVELOPMENT

GENERAL INFORMATION

Mission

To conduct a broadly based multidisciplinary program of scientific research and advanced technological development directed toward maritime applications of new and improved materials, techniques, equipment, systems, and ocean, atmospheric, and space sciences and related technologies.

The Naval Research Laboratory provides

- primary in-house research for the physical, engineering, space, and environmental sciences;

- broadly based exploratory and advanced development programs in response to identified and anticipated Navy needs;

- broad multidisciplinary support to the Naval Warfare Centers;

- space and space systems technology development and support.

Reflections

The dawning of the post-Cold War era offers the Department of the Navy the unique opportunity to plan a new force structure. While the worldwide responsibilities of our naval forces have not changed, our mission, threats, and potential adversaries have.

Our challenge today is greater than it ever has been—we must plan for, in the words of Secretary Dalton "the Navy after next"—one whose enemies are not yet known, but one that must have the technological edge to win.

The naval research and development community is charged with ensuring that our smaller Fleet of sailors and marines have the crucial force-multiplying weaponry and the supporting state-of-the-art systems needed to win in combat and capably defend American interests and policies. The science and technology (S&T) investments we make today will determine the technological superiority of the future Navy and Marine Corps, so it is imperative that we lay that foundation with informed vision.

Fleet operational requirements drive the need for S&T integration. We work closely with the developers to put improved products in the Fleet. Affordability, jointness, and transition—to the Fleet and to industry— are fundamental to our plan's success. The S&T investment program maintains our strong commitment to work with other services, with other government agencies to leverage our resources, with academia and industry, and, as appropriate, with our foreign allies to support U.S. naval S&T needs. The Office of Naval Research continues to look beyond traditional partnerships with defense contractors to include new partnerships with commercial industries, and we are ever more dependent on the high quality products of the Navy's corporate lab—the Naval Research Laboratory (NRL). Through its research divisions, which conduct programs embracing virtually all the physical science disciplines, the Laboratory has responded effectively to solve many of the short- and long-term problems of the Navy and the nation. It has gained a reputation as an institution that searches for and insists on excellence. When it comes to developing affordable, innovative, and superior military technologies from concept through demonstration, NRL has always been a leader.

This year, an exciting year for the Lab, brought such noteworthy achievements as: the Polar Ozone and Aerosol Measurement Experiment (POAM II), which has provided scientists with unique data on ozone chemistry and processes that affect ozone depletion; the development of a new concept for antiship missile defense—the new, AN/SPQ-9B radar, which provides a new, low-cost, quality sea-skimmer detection capability to the Fleet. NRL researchers developed a technique to

RADM Marc Y.E. Pelaez

extend the useful range of rare-Earth solid-state lasers into the mid-infrared (IR) range with potential applications that include illuminators for IR imaging and countermeasure systems, as well as chemical and biological sensing.

NRL's standing among the world's leading scientific institutions stems from the caliber and achievements of the people who work here and carry out magnificently the Laboratory's mission to conduct a broadly based multidiscipline program of scientific research and advanced technological development directed toward new and improved materials, equipment, techniques, system, and related operational procedures for the Navy. NRL researchers continue to be recognized for their stellar efforts. To name just a few—the *Clementine* trajectory team won an award in the area of Technology Transfer for their work in the trajectory analysis for the *Clementine* mission; Dr. Isabella Karle received the 1995 National Medal of Science, the DoD Distinguished Civilian Service Award, and the National Academy of Sciences Award in Chemical Sciences; Dr. Brenda Little received the 1995 WISE Scientific Achievement Award; and Dr. Thomas Reinecke received the 1994 Humboldt Research Award for Senior U.S. Scientists.

Science and technology are looking for order-of-magnitude changes and paradigm breakers in naval capability. NRL is the key organization in moving the Navy to entirely new paradigms of systems platforms and ways of operating.

1

CAPT Richard M. Cassidy

The past year has been an extraordinary one in shaping the future of the Navy and, by extension, the Naval Research Laboratory. A commitment to a balanced budget and a recognition that all segments of the economy will be subject to significant readjustments over the next 7 to 10 years are factors we must deal with. It will require us to continuously reexamine what we are about. As we undertake this reexamination, we must bear in mind that preparing the Navy for the future is why we exist.

It is often said that one should look to the past in order to prepare for the future. If we look to our past experience (which for most of us spans the period from World War II to today) and examine those conditions compared to a much longer stretch of world history, we find that the last 50 years turn out to an anomaly. In fact the multipolar, confusing, and nationalistic environment of today is a more normal condition than the bipolar, U.S. vs Soviet Union situation that has prevailed during the lifetimes of most of us.

The struggle to produce a coherent strategy for this new (to us) situation has led to much volatility. In the last decade, we've seen such schemes as modernization through acquisition. We've seen truncation of development before production such that technology can be on the shelf when we need it. We've seen a push to develop technologies that can be inserted in legacy systems. We've seen the COTS [commercial off-the-shelf] call to arms. We've seen the development of systems strictly to preserve the industrial base. And we've seen the push to get the Government out of hands-on activity and to let the private sector do it. Clearly some of these are mutually exclusive strategies, but that does not preclude them from coexisting in today's confused environment.

Given that recent history is a poor predictor and that we have no clear path to follow, how should the Naval Research Laboratory proceed? If we consider the situation at the time of the founding of the Lab, the issues are amazingly similar to those of today. The Balkans are in an uproar, the proper role for the U.S. in world affairs is being debated in Congress, national defense is not a priority, and the role of government labs is under intense scrutiny.

If we examine why in 1915 Edison felt the need for " a great government laboratory" and contrast it with today's environment, we'd find that the original reasons he and the Naval Consulting Board had for establishing the Naval Research Laboratory are still valid. If there wasn't an NRL, we'd soon discover that we needed one, as would industry. Recall it was industry that sensed the need for a great laboratory—not the government. These historical antecedents are important because, in most cases, the key to the future of any institution is its ability to examine its roots and to continuously focus on the basics that make it great.

How will these basics enable us to meet our

responsibilities in a certain future? Let's start by asserting a few things which are certain over the next 10 years:

- Today's Fleet will be 10 years older, and a substantial number of ships and airplanes will be approaching the end of their service lives.
- Today's threat will be at least two generations better (or worse from our perspective), if you assume that the rest of the world operates on 5-year plans. So we can't declare victory and stop working in areas where we excel today.
- Somewhere in the world where the U.S. has an interest, there will be armed conflict.
- The defense budget will not return to the levels we've seen in the recent past nor will the S&T budgets.

These certainties imply several things to the Naval Research Laboratory. On the one hand, there will be continued pressure to downsize the shore establishment, which frees up limited funds to recapitalize the operating forces. These freed-up funds are always in danger of being eaten up by contingency operations, as in Bosnia, further putting pressure on the shore establishment. On the other hand, since the work we do is threat-driven, there will be a clear need to improve our weapons systems and avoid technological surprise. The fundamental question will be "who should do that and to what extent?".

This is where the basics of NRL's mission and excellence come into play. A broadly based, multidisciplinary program of science and applied technology, which is characteristic of NRL, doesn't exist in industry or in any one university. This broad base frees the Lab from the restriction

Dr. Timothy Coffey

of having only a narrow pathway into the market-place, as would a company with a limited product line. It allows a focus on the long-term needs of the Navy, rather than on compliance with a contract. It provides a stable source of technical expertise in areas the Navy needs. Finally, it provides a source of advice not encumbered by a programmatic agenda.

The key in each of the above areas is a sustained excellence and an ability to persevere in those areas not currently in vogue. It will be the responsibility of NRL management and the Laboratory's workforce to ensure that the scientific and technical excellence that has characterized the Laboratory throughout its history will be maintained as we adjust to the new realities. We must also work with the Navy policymakers, sponsors, and program managers to ensure that we maintain investment and competence in those areas that are of long-term importance to the Navy while at the same time shedding those areas whose time is forever past.

NEW COMMANDING OFFICER
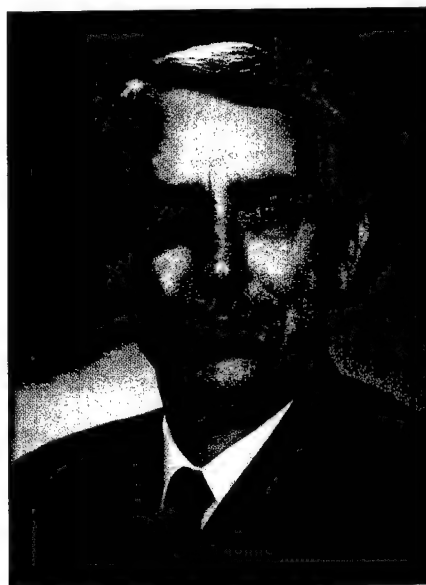
On January 26, 1996, CAPT Bruce W. Buckley replaced CAPT Richard M. Cassidy as the Naval Research Laboratory's Commanding Officer.

Captain Bruce W. Buckley, a native of Lancaster, Ohio, graduated from the United States Naval Academy in 1973. CAPT Buckley entered flight training and was designated a Naval Aviator in December 1974 at Naval Air Station Chase Field, Texas. After completing replacement pilot training in the F-14A at Fighter Squadron 124, he served a fleet assignment as an F-14A pilot in Fighter Squadron Twenty Four.

Following his fleet assignment in Fighter Squadron Twenty Four, CAPT Buckley began accumulating extensive experience in research, development, engineering, and project management with a tour on the Joint Test Force of the Air Combat/Air-to-Air Missile Evaluation at Nellis Air Force Base, Nevada. He then attended the Naval Postgraduate School at Monterey, California, where he earned a Master of Science in Electrical Engineering, with Distinction. While at postgraduate school, CAPT Buckley was selected to be designated an Aerospace Engineering Duty Officer (AEDO).

As an AEDO, CAPT Buckley has had positions of increasing responsibility in engineering and program management, including F/A-18 F404 Project Officer

at the Naval Plant Representatives Office, Lynn, Massachusetts; Avionics and Electro-Optics Projects Manager in the F/A-18 Program Management Office, Assistant to the Program Director of Tactical Aircraft Programs, F404 Engine Program Manager, and Program and Policy Branch Head in the Propulsion Division, all at the Naval Air Systems Command Arlington, Virginia. CAPT Buckley then served in two positions—as the F-14 Aircrew Systems Program Manager and as the Deputy Director of the Research and Engineering Department of the Naval Training Systems Center in Orlando, Florida. Returning to Washington and the Naval Air Systems Command in July 1993, he served as the Associate Director of the Evaluations Division and as the Director of the Propulsion and Power Division before assuming his last position as the Executive Assistant to the Commander, Naval Air Systems Command.

CAPT Buckley's decorations include the Legion of Merit, the Meritorious Service Medal, a Joint Service Commendation, and three Navy Commendations. CAPT Buckley is married to Janice E. (Faller) Buckley, formerly of Miami, Florida, and they reside with their two daughters, Michele and Sandra, in Lake Ridge, Virginia.

The
Naval
Research
Laboratory

NRL — Our Heritage

Today, when government and science seem inextricably linked, when virtually no one questions the dependence of national defense on the excellence of national technical capabilities, it is noteworthy that in-house defense research is relatively new in our Nation's history. The Naval Research Laboratory (NRL), the first modern research institution created within the United States Navy, began operations in 1923.

Thomas Edison's Vision — The first step came in May 1915, a time when Americans were deeply worried about the great European war. Thomas Edison, when asked by a *New York Times* correspondent to comment on the conflict, argued that the Nation should look to science. "The Government," he proposed in a published interview, "should maintain a great research laboratory.... In this could be developed...all the technique of military and naval progression without any vast expense." Secretary of the Navy Josephus Daniels seized the opportunity created by Edison's public comments to enlist Edison's support. He agreed to serve as the head of a new body of civilian experts — the Naval Consulting Board — to advise the Navy on science and technology. The Board's most ambitious plan was the creation of a modern research facility for the Navy. Congress allocated $1.5 million for the institution in 1916, but wartime delays and disagreements within the Naval Consulting Board postponed construction until 1920.

The Laboratory's two original divisions — Radio and Sound — pioneered in the fields of high-frequency radio and underwater sound propagation. They produced communications equipment, direction-finding devices, sonar sets, and perhaps most significant of all, the first practical radar equipment built in this country. They also performed basic research, participating, for example, in the discovery and early exploration of the ionosphere. Moreover, the Laboratory was able to work gradually toward its goal of becoming a broadly based research facility. By the beginning of World War II, five new divisions had been added: Physical Optics, Chemistry, Metallurgy, Mechanics and Electricity, and Internal Communications.

The War Years and Growth — Total employment at the Laboratory jumped from 396 in 1941 to 4400 in 1946, expenditures from $1.7 million to $13.7 million, the number of buildings from 23 to 67, and the number of projects from 200 to about 900. During WWII, scientific activities necessarily were concentrated almost entirely on applied research. New electronics equipment — radio, radar, sonar — was developed. Countermeasures were devised. New lubricants were produced, as were antifouling paints, luminous identification tapes, and a sea marker to help save survivors of disasters at sea. A thermal diffusion process was conceived and used to supply some of the ^{235}U isotope needed for one of the first atomic bombs. Also many new devices that developed from booming wartime industry were type tested and then certified as reliable for the Fleet.

NRL Reorganizes for Peace — Because of the major scientific accomplishments of the war years, the United States emerged into the postwar era determined to consolidate its wartime gains in science and technology and to preserve the working relationship between its armed forces and the scientific community. While the Navy was establishing its Office of Naval Research (ONR) as a liaison with and supporter of basic and applied scientific research, it was also encouraging NRL to broaden its scope and become, in effect, its corporate research laboratory. There was a transfer of NRL to the administrative oversight of ONR and a parallel shift of the Laboratory's research emphasis to one of long-range basic and applied investigation in a broad range of the physical sciences.

However, rapid expansion during the war had left NRL improperly structured to address long-term Navy requirements. One major task — neither easily nor rapidly accomplished — was that

of reshaping and coordinating research. This was achieved by transforming a group of largely autonomous scientific divisions into a unified institution with a clear mission and a fully coordinated research program. The first attempt at reorganization vested power in an executive committee composed of all the division superintendents. This committee was impracticably large, so in 1949, a civilian director of research was named and given full authority over the program. Positions for associate directors were added in 1954.

The Breadth of NRL—During the years since the war, the areas of study at the Laboratory have included basic research concerning the Navy's environments of Earth, sea, sky, and space. Investigations have ranged widely from monitoring the Sun's behavior to analyzing marine atmospheric conditions to measuring parameters of the deep oceans. Detection and communication capabilities have benefitted by research that has exploited new portions of the electromagnetic spectrum, extended ranges to outer space, and provided means of transferring information reliably and securely, even through massive jamming. Submarine habitability, lubricants, shipbuilding materials, fire fighting, and the study of sound in the sea have remained steadfast concerns, to which have been added recent explorations within the fields of virtual reality, superconductivity, and biomolecular science and engineering.
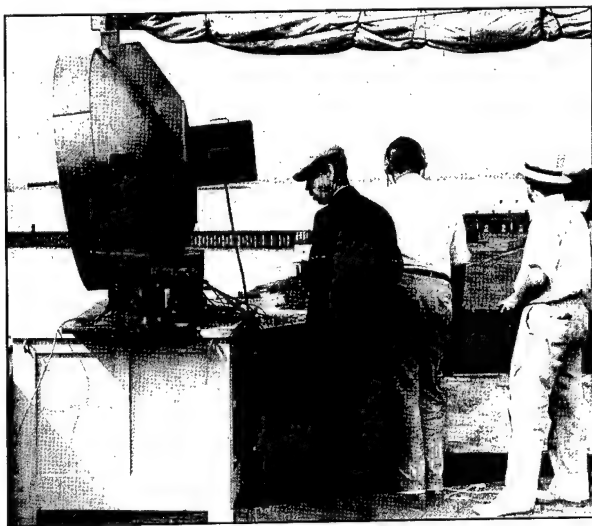
Dr. A.H. Taylor, Dr. C.E. Cleeton, and Mr. J.P. Hagen operate the Navy's first high-power communication transmitter from the roof of Building 1 (early 1937).

The Laboratory has pioneered naval research into space from atmospheric probes with captured V-2 rockets through direction of the *Vanguard* project—America's first satellite program—to involvement in such projects as the Navy's Global Positioning System. Today NRL is the Navy's lead laboratory in space systems research, fire research, tactical electronic warfare, microelectronic devices, and artificial intelligence.

The consolidation in 1992 of NRL and the Naval Oceanic and Atmospheric Laboratory, with centers at Bay St. Louis, Mississippi, and Monterey, California, added critical new strengths to the Laboratory. NRL now is additionally the lead Navy center for research in ocean and atmospheric sciences, with special strengths in physical oceanography, marine geosciences, ocean acoustics, marine meteorology, and remote oceanic and atmospheric sensing. The expanded Laboratory is focusing its research efforts on new Navy strategic interests and needs in the post-Cold War world. Although not abandoning its interests in blue-water operations and research, the Navy is also focusing on defending American interests in the world's littoral regions. NRL scientists and engineers are working to give the Navy the special knowledge and capabilities it needs to operate in these waters.

Scientists within NRL's Radar Division during the last year have developed a new concept for an antiship missile defense. The new AN/SPQ-9B radar maintains present gun-fire control-systems MK 86 support while providing low-cost, quality sea-skimmer detection capability for the Fleet. The system will provide significantly increased sensitivity, along with an improved ability to detect targets in clutter. Researchers in the Laboratory's Tactical Electronic Warfare Division have developed a portable electronic warfare (EW) environment simulator capable of generating high-fidelity signals. The simulator can be used for EW training and for checkout of modern shipboard or airborne platforms, while remaining small and inexpensive enough to be placed on every Navy ship.

During FY 95, NRL-Monterey signed a memorandum of agreement with Lawrence Livermore Laboratory for collaborative research on and transfer of two NRL numerical weather prediction models. The models will be used in predicting atmospheric variables important to forecasting

Secretary of the Navy James Forrestal addresses those assembled on the mall to observe NRL's 20th Anniversary (1943).

the movement and dispersion of hazardous airborne particles and gasses.

Scientists and engineers at NRL have also helped establish a new world record in superconducting motor performance using high-temperature superconductors. The motor reached an output of 167 horsepower using high Tc field windings. This is more than 30 times greater than the previous record. The goal of the NRL effort is the development of high-temperature superconducting wire suitable for military and commercial applications. A different NRL research team has used scanning tunneling microscopy in conjunction with supercomputer-based calculations to arrive at a complete structural model for a recently discovered stable surface of silicon — Si(5 5 12). The determination of this structure will greatly improve our understanding of silicon surfaces, which are widely used for semiconductors.

Fiscal year '95 saw Laboratory research personnel make innovative discoveries across a wide-range of scientific specialties. In astronomy, NRL's Oriented Scintillation Spectrometer (OSSE) on NASA's Gamma Ray Observatory revealed neutron star AO535+26 to possess one of the strongest magnetic fields ever measured in the Milky Way galaxy. Its total field strength corresponded to a magnetic field 10-trillion times stronger than Earth's. In a different experiment, NRL scientists were part of a research team that detected three neutron stars in our local astronomical neighborhood. The detection was made using the Extreme Ultraviolet Explorer (EUVE) satellite. Two of the

neutron stars are only a few million years old, while the third is an ancient millisecond pulsar estimated to be about 5 billion years in age. Another NRL astronomical detector, the Far-Ultraviolet Imaging Spectrograph (FUVIS) experiment was launched on the space shuttle *Discovery* on February 3, 1995. The objective of the FUVIS detector is to study astronomical and artificially induced sources of diffuse far-ultraviolet radiation in order to help improve our understanding of the composition, properties, and distribution of the interstellar medium.

A little closer to home, NRL researchers have been studying the solar atmosphere in an attempt to understand and predict its dynamic effect upon the Earth. One Laboratory scientist has investigated the Sun's corona in an attempt to explain why it is so much hotter than the solar surface. Coronal heating is directly responsible for solar X-ray and ultraviolet radiation, which in turn controls the dynamics and chemistry of Earth's middle and upper atmosphere. Other NRL scientists, in related work, have developed a comprehensive model of Earth-influencing solar-wind structures. The model will aid in increasing the accuracy of scientific predictions of geomagnetic storms that can cause severe disturbances in our communication and navigational systems.

In a different space-related effort, the team of NRL engineers responsible for system integration and performance of 1994's *Clementine* satellite continued to receive rave national and international reviews for their efforts. Some of the

team's awards include *Popular Science Magazine*'s "Best of 1994's Top 100 Technologies;" "The 1994 Stellar Award for Spacecraft Design," from Rotary National; "The Nelson P. Jackson Aerospace Award," from the National Space Club; *Aviation Week & Space Technology*'s "1994 Laureate Award;" and the 1995 *Discover Magazine's* "Award for Technological Innovation." (See pp. iv and v.)

Two NRL satellite detectors are playing a big part in providing expanded information on the Earth's atmosphere. The Laboratory's Middle Atmosphere High Resolution Spectrograph Investigation (MAHRSI) has given researchers new information on two trace constituents—nitric oxide and the hydroxyl radical—that are believed to determine the natural balance of ozone in the area above 30 kilometers. The detector has also provided high-quality measurements of ozone in the middle atmosphere. NRL's Polar Ozone and Aerosol Measurement Experiment (POAMII) has provided scientists with data on ozone chemistry and the processes affecting ozone depletion in the polar region. The detector has produced important information on the formation of polar stratospheric clouds, which are indirectly involved in the chemical destruction of ozone by chlorine in the Antarctic ozone hole.

Another NRL environmental detector, the Water Vapor Millimeter-wave Spectrometer (WVMS), is producing ground-based measurements for monitoring the middle atmosphere. The WVMS provides the best current instrumental platform for detecting long-term trends in mesospheric water vapor. The latter is expected to increase due to man-made effects on methane emission. Yet one more recent NRL detector developed with environmental sensing in mind is the Portable Hyperspectral Imager for Low-Light Spectroscopy (PHILLS). It facilitates the collection and analysis of high-quality broadband hyperspectral data in near-real time. PHILLS will greatly expand our capability to detect and identify airborne, land, or water pollution and potentially may also be used for damage assessment from natural disasters.

In further environmentally directed research, NRL personnel have developed an environmentally friendly antifouling coating for use on the water intakes of electric power plants; created a chemically resistant nontoxic epoxy lining for water pipes to help keep impurities out of drinking water; and demonstrated the viability of a manufacturable, hand-held biosensor for detecting the presence of TNT in field sites slated for environmental clean-up.

Also this year, the Laboratory's Nike Krypton Fluoride Laser Facility was dedicated. NRL began development of the Nike KrF laser in the late

CAPT Bruce W. Buckley and CAPT Richard M. Cassidy cut the ceremonial cake at the Change of Command and Retirement Cermony held on January 26, 1996. CAPT Buckley becomes NRL's 32nd commanding officer.

1980s because of its potential ability for producing a more uniform laser beam. The high uniformity holds the potential for high-gain fusion targets. This high gain would be attractive for both military and fusion reactor applications.

Technology Transfer — NRL was active last year in transferring technology developed at the Laboratory to private industries for production and marketing. While the majority of Cooperative Research and Development Agreements (CRADAs) are with industrial firms, several are also with universities and nonprofit organizations. To date, NRL has signed over 100 CRADAs and patent license agreements. K&L Microwave of Salisbury, Maryland, signed a pair of 1-year CRADAs with NRL to develop high-temperature superconductor-based dielectric resonator filters for applications in cellular communication ground-based receivers. NRL and K&L will also develop and demonstrate the manufacturability of microwave devices based on high-temperature superconductors as a potential commercial application.

NRL also signed a CRADA with the Westinghouse Electric Corporation to investigate the advantages of using a SiGe-grown base in a high-power microwave transistor. This CRADA will combine the expertise of the two organizations to build a structure that has a high probability of operation. A local start-up firm, REPTECH, Inc., of Pasadena, Maryland, signed a patent-licensing agreement with NRL to produce rare Earth-based materials for the magnet industry. REPTECH, Inc., intends to work with the University of Maryland's Engineering Center for assistance in developing the technology required to manufacture the magnetic alloys.

A further illustration of technology transfer activity during FY 95 is the patent-licensing agreement between NRL and Allied-Signal ELAC Nautik GmbH of Kiel, Germany, to manufacture an NRL-developed high-resolution acoustic sedimentation classifications system (HR ASCS). The licensing of the HR ASCS is another example of state-of-the-art Navy-developed technology being transferred into the private sector for use in civilian and commercial applications.

NRL and K&L Microwave researchers show the superconducting filter, cryogenic cooler, and microwave test equipment.
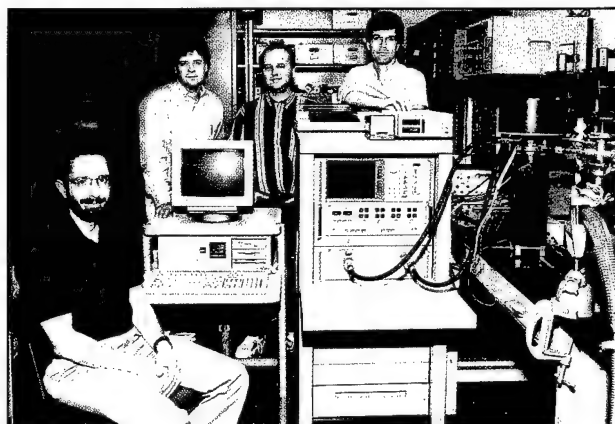
NRL Today

ORGANIZATION AND ADMINISTRATION

The position of NRL within the Navy is that of a field command under the Chief of Naval Research.

Heading the Laboratory with joint responsibilities are the naval Commanding Officer, CAPT Bruce W. Buckley, USN, and the Civilian Director of Research, Dr. Timothy Coffey. Line authority passes from the commanding officer and the director of research to three associate directors of research, planning, a director of the Naval Center for Space Technology, and an associate director for business operations. Research is performed in the following areas:

- Systems Directorate
- Materials Science and Component Technology
- Ocean and Atmospheric Science and Technology
- Naval Center for Space Technology.

Through FY 95, NRL operated as a Defense Business Operating Fund (DBOF) activity. As a DBOF activity, all costs, including overhead, were charged to various research projects. Funding in FY 95 came from the Chief of Naval Research, the Naval Systems Commands, other Navy sources; government agencies, such as the U.S. Air Force, Advanced Research Projects Agency, the Department of Energy, and the National Aeronautics and Space Administration; and several nongovernment activities.

PERSONNEL DEVELOPMENT

At the end of FY 95, NRL employed 3803 personnel—46 officers, 133 enlisted, and 3624 civilians. In the research staff, there are 876 employees with doctorate degrees, 450 with masters degrees, and 597 with bachelors degrees. The support staff assists the research staff by providing administrative, computer-aided design, machining, fabrication, electronic construction, publication, personnel development, information

NRL headquarters, located off Interstate 295 in S.W. Washington, as viewed from the east.

retrieval, large mainframe computer support, and contracting and supply management services.

Opportunities for higher education and other professional training for NRL employees are available through several programs offered by the Employee Development Branch. These programs provide for graduate work leading to advanced degrees, advanced training, college course work, short courses, continuing education, and career counseling. Graduate students, in certain cases, may use their NRL research for thesis material.

For non-NRL employees, several postdoctoral research programs exist. There are also cooperative education agreements with several universities, summer and part-time employment programs, and various summer and interchange programs for college faculty members, professional consultants, and employees of other government agencies.

NRL has active chapters of Women in Science and Engineering, Sigma Xi, Toastmasters International, Federally Employed Women, and the Federal Executive and Professional Association. Three computer clubs meet regularly—NRL Microcomputer User's Group, NeXT, and Sun NRL Users Group. An amateur radio club, a drama group (the Showboaters), and several sports clubs are also active. NRL has a Recreation Club that provides basketball and softball leagues and swim, sauna, whirlpool bath, gymnasium, and weight-room facilities. The Recreation Club also offers classes in martial arts, aerobics, swimming, and water walking.

The Community Outreach Program traditionally has used its extensive resources to foster programs that provide benefits to students and other community citizens. Volunteer employees assist with and judge science fairs, give lectures, tutor, mentor, coach, and serve as classroom resource teachers. The program also sponsors Black History Month art and essay contests for local schools, student tours of NRL, a student Toastmasters Youth Leadership Program, an annual holiday party for neighborhood children in December, an equipment loan program that provides surplus equipment to partnership schools, a book donation program for both students and teachers, and an annual collection for Children's Hospital. Through the Community Outreach Program, NRL has active partnerships with four District of Columbia public schools.

NRL has an active, growing Credit Union, with assets over $163 million and a membership numbering over 20,000. The NRL Federal Credit Union offers competitive and innovative financial services.

Public transportation to NRL is provided by Metrobus. Metrorail service is 3 miles away.

For more information, see the *NRL Review* chapter entitled, "Programs for Professional Development."

SCIENTIFIC FACILITIES

In addition to its Washington, D.C. campus of about 130 acres and 102 main buildings, NRL maintains 14 other research sites, including a vessel for fire research and a Flight Support Detachment. The many diverse scientific and technological research and support facilities are described in the following paragraphs.

Research Facilities

Radar

NRL has gained worldwide renown as the "birthplace of radar" and, for a half-century, has maintained its reputation as a leading center for radar-related research and development. An impressive array of facilities managed by NRL's Radar Division continues to contribute to this reputation.
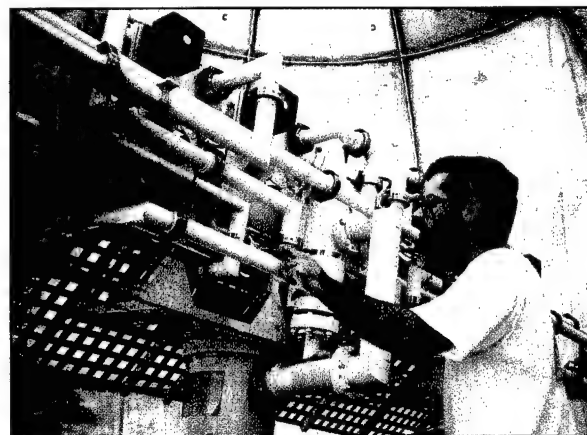
A researcher examines the space-time adaptive processing (STAP) array.

In connection with airborne radar, the division uses a Radar Imaging Facility, consisting of an inverse synthetic aperture radar (ISAR) that can be deployed to collect radar-imaging data from the air in a P-3 aircraft or a trailer for ground or ship installation. New technology associated with aircraft early warning (AEW) radar uses a rooftop space-time adaptive processing (STAP) array and associated processors. In connection with ship-based radar, the division operates a Radar Test Bed Facility at the Chesapeake Bay Detachment (CBD), Randle Cliffs, Maryland. Represented are test bed radars and related data-processing facilities for long-range air search, point defense, and surface search. Concepts and engineering developments in connection with target identification are explored by using an experimental Cooperative Aircraft Identification (CAI) System. Other installations operated by the division include an Electromagnetic Interference (EMI) Facility, a Radar Signature Calculation Facility for complex electromagnetic radar target modeling, a Compact Antenna Range (operated jointly with the Space Systems Development Department) for antenna design and development, and a Computer-aided Engineering (CAE) Facility.

Information Technology

The Information Technology Division (ITD) is at the forefront of DoD research and development in artificial intelligence, telecommunications, computer networking, human-computer interaction, information security, parallel computation, and computer science.

The division maintains local area computer networks to support its research and hosts test-beds for advanced high-performance fiber-optic network research. These networks make available hundreds of high-performance computers to local and remote users. The ITD research networks are part of NRL's internal network and also connect via T1 lines to the regional SURAnet, to DISnet, and via ATM/SONET links to ATDnet, an experimental wide-area network connecting a number of research organizations in the metropolitan area.

Major shared resources include the systems and networks available in the division's Center for Computational Science, including two Connection Machines, a 32-processor CM-5E and a
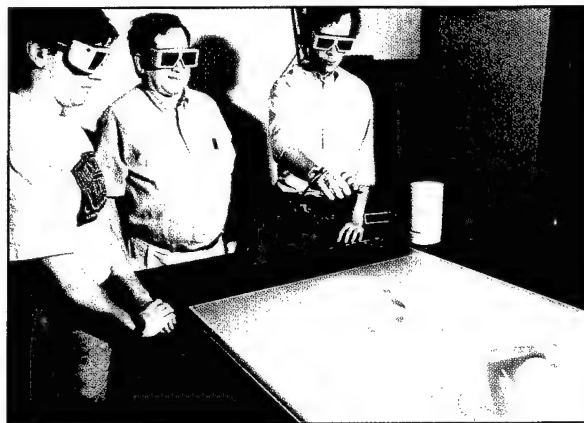
Researchers examine a 3-D virtual human body using the ITD VR Lab's "virtual workbench." With a team leader, users interact with the 3-D image rising above the workbench by using a combination of gestures and voice recognition. The workbench is being used for medical, design, and C2 applications.

256-processor CM-5E with 32 gigabytes of memory, and a 25 terabyte robotic D2 tape-storage system; dual processor Cray Y-MP EL, 1.5-terabyte file server/archiver, and Scientific Visualization Lab. The center manages and operates the NRL local area network (NICEnet), which includes a new FDDI network. NICEnet provides external connections to networks worldwide.

The division facilities also include an Information Security Engineering Laboratory and an experimental facility with special displays, eye and gesture trackers, and speech I/O devices for research in human computer interaction.

A Virtual Reality (VR) Laboratory was launched in FY 95. In addition to an extensive set of typical VR equipment (a high-speed graphics workstation, head-mounted displays, a boom, high-end projection systems, magnetic trackers, voice recognition, data gloves, and a video/sound suite), the VR lab designed and fabricated the first U.S. version of the "virtual workbench." The workbench is a major advance in VR that allows users to see and interact with a 3-D virtual image above a table while maintaining the ability to see and communicate with each other.

Optical Sciences

The Optical Sciences Division has a broad program of basic and applied research in optics and electro-optics. Areas of concentration in electro-optics include fiber optics, integrated
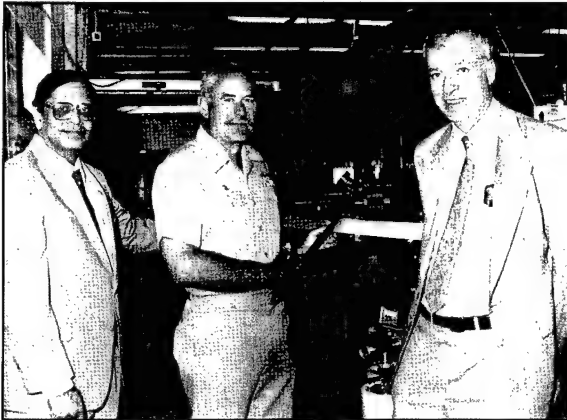
CAPT Cassidy cuts the ribbon at the EPICENTER dedication on July 11, 1995, while Dr. Rath (left) and Dr. Coffey (right) look on. The EPICENTER is a shared facility involving the Electronic Science and Technology, Materials Science and Technology, and Chemistry Divisions. The Center provides growth and assessment capabilities for technologically promising semiconductor and magnetic materials.

optical devices, fiber-optic sensors, high-power diode lasers, and diode-pumped solid-state lasers. Modern electro-optic sensors such as infrared focal plane arrays are developed by NRL as well as signal processors, digital processors, computer algorithms, and digitized background scene imagery to allow computer-augmented sensor design for naval applications. The division also maintains a capability to perform optical field measurements from ground-based, water-based, or air-based platforms at appropriate sites away from NRL. The Optical Sciences Division has recently occupied the newly constructed Electro-Optics Research Facility (Buildings 215-216). These two buildings together provide 87,000 ft² of modern office and laboratory spaces. Together with recently renovated spaces in Buildings A-12 and A-50, the division now occupies some of the most modern optical facilities in the country. These facilities allow work to be performed in the areas of fiber optics, integrated optics, optical information processing, infrared sensors and modeling and testing of sensors, optical components, and signal processing. Facilities include the following:

Ultralow-Loss, Fiber-Optic Waveguides — NRL has developed record-setting ultrahigh transparency infrared waveguides. These fluoride glass materials offer the promise of long-distance communications without the need of signal amplification or repeaters. The high temperature IR glass technology is also useful for bulk optical materials and

as a host for laser ions or other species in devices such as chemical detectors.

Focal Plane Evaluation Facility — This facility has extensive capabilities to measure the optical and electrical characteristics of infrared focal plane arrays being developed for advanced Navy sensors.

IR Missile-Seeker Evaluation Facility — This facility performs open-loop measurements of the susceptibilities of infrared tracking sensors to optical countermeasures.

Large Optic, High-Precision Tracker — NRL has developed a tracker system with an 80-cm primary mirror for atmospheric transmission and target signature measurements. By using a quadrant detector, the servo system has demonstrated a 12-mrad tracking accuracy. An optical correlation tracker system tracks objects without a beacon.

High-Energy Pulsed Hydrogen Fluoride, Deuterium Fluoride Laser — NRL has constructed a pair of pulsed chemical lasers, each capable of producing up to 30 J of laser energy at 2.7 to 3.2 mm and 3.8 to 4.5 mm in a 2-ms pulse. This facility is used to investigate a variety of research areas, including stimulated Brillouin scattering, optical phase conjugation, pulsed laser amplification, propagation, and beam combining.

Fiber-Optics Sensors — The development and fabrication of fiber-optic sensor concepts, including acoustic, magnetic, and rate-of-rotation sensors, are conducted in several facilities within the Laboratory's Optical Sciences and Acoustics Divisions. Equipment includes facilities for evaluating optical fiber coatings, fiber splicers, an acoustic test cell, a three-axis magnetic sensor test cell, a rate table, and various computers for concept analysis.

Digital Processing Facility — This facility is used to collect, process, analyze, and manipulate infrared data and imagery from several sources.

Emittance Measurements Facility — NRL routinely performs measurements of directional hemispherical reflectance from 2 to 16 mm in the infrared by using a diffuse gold-integrating sphere and a Fourier transform spectrophotometer (FTS). Sample temperatures can be varied from room temperature to 250° C and incidence angles from 0° to 60°.

Diode-Pumped Solid-State Lasers — Two micrometer lasers operate in an eye-safe region of the

optical spectrum, an important issue for laser use in industry or in cases where eye damage to the public could be a safety and liability issue. Research at NRL in the 1980s had a major role in demonstrating room temperature flash-lamp and diode-pumped lasers. The lamp-pumped lasers have found wide usage in laser surgery while diode-pumped lasers appear to be leading candidates for eye-safe laser radars for aircraft and for laser sources to counter IR missile seek-ers. Newer lasers have been found that operate from 0.400 μm in the near UV to beyond 5 μm in the IR.

Electronic Warfare

The scope of research and development at NRL in the field of electronic warfare covers the entire electromagnetic spectrum—from basic technology research, component, and subsystem development—to system design and effectiveness evaluation. Major emphasis is placed on providing the methods and means to counter enemy hostile actions in all battle phases, from the beginning—when enemy forces are mobilized for an attack—through the final engagement stages. For this purpose, NRL has constructed special research and development laboratories, anechoic cham-bers, and facilities for modeling and simulation. NRL has also added extensive new facilities where scientists can focus on the coordinated use of all organic defensive and offensive resources now present in the Fleet.

Structure of Matter

The laboratory investigates the atomic arrangements in materials to improve them or facilitate the development of new substances. Various diffraction methodologies are used to make these investigations. Subjects of interest include the structural and functional aspects of energy conversion, ion transport, device materi-als, and physiologically active substances such as drugs, antibiotics, and antiviral agents. Theo-retical chemistry calculations are used to comple-ment the structural research. A real-time graphics system aids in modeling and molecular dynamics studies.

Chemistry

NRL has been a major center for chemical research in support of naval operational require-ments since the late 1920s. The Chemistry Divi-sion continues its tradition with a broad spectrum of basic and applied research programs concerned with controlled energy release (fuels, fire, com-bustion, countermeasure decoys, explosives), sur-face chemistry (corrosion, adhesion, tribology, adsorbents, film growth/etch), advanced polymeric materials (high-strength/low-weight structures, drag reduction, damping, special function), and advanced detection techniques (environment, chemical/biological, surveillance). Facilities for research include a wide range of the modern photon/electron, magnetic and ion-based spec-troscopic/microscopic techniques for bulk and surface analysis; nanometer-scale fabrication and characterization; multiple facilities for materials synthesis and physical/chemical characterization; a 11,400 ft^3 fire research chamber (Fire I); and a 475-ft ex-USS Shadwell (LSD-15) advanced fire research ship.

The Chemistry Division is upgrading its nuclear magnetic resonance (NMR) capability with a state-of-the-art 11.7 T multinuclear NMR spectrometer. NMR spectroscopy is used
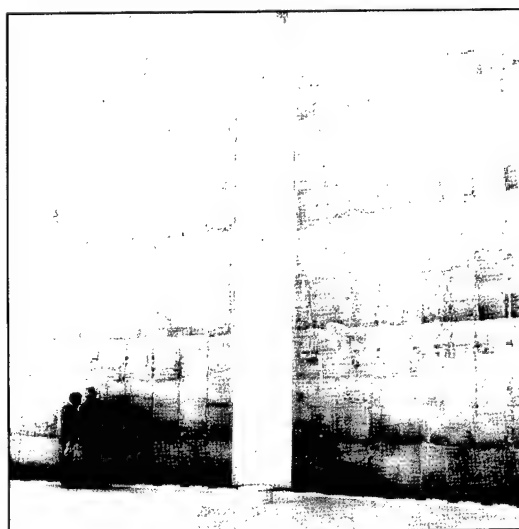
Interior view of a typical fuel storage tank of the floating roof type, for which scientists in the Chem-istry Division have developed a fluoropolymer lining; the lining prevents corrosion in the steel tanks, helps keep the fuel clean, and seals minor leaks.

to investigate the structure and dynamics of materials in the solid and liquid states. Through its significantly higher magnetic field, the new spectrometer affords greater sensitivity and spectral resolution than existing spectrometers, particularly when observing quadrupolar nuclei such as those found in many ceramics and glasses. The higher magnetic field allows exploration of the use of the induced magnetization to transfer NMR coherence over the distance of 1 μm for the practical purpose of imaging. New capabilities include triple resonance in liquids and solids, gradient spectroscopy, variable-angle sample spinning, and self-diffusion measurements in liquids and gases. These capabilities will significantly enhance studies of organic polymers, biomaterials, inorganic materials, and molecules in solution.

Materials

NRL has capabilities for X-ray and electron diffraction analyses and for electron and Auger spectroscopy. Scanning, transmission, and combined scanning-transmission electron microscopes are used to study surface and/or internal microstructures. The division has a secondary ion mass spectrometer for surface analysis that significantly extends the diagnostic capability of the technique. A high-resolution, reverse-geometry mass spectrometer is used to probe reactions between ions and molecules. The Laboratory has a fully equipped fatigue and fracture laboratory, a modern vacuum arc melting furnace for reactive metals, an ultrasonic gas atomization system for making metal powders, and hot isostatic press facilities. The Laboratory's cryogenic facilities include dilution refrigerators and superconducting magnetic sensors for measuring ultrasmall magnetic fields. Also available are two molecular beam epitaxy devices for growing thin films.

Laboratory for Computational Physics and Fluid Dynamics

The Laboratory for Computational Physics and Fluid Dynamics is in round-the-clock production for computational studies in the fields of compressible and incompressible fluid dynamics, reactive flows, fluid-structure interaction (including submarine, ship, and aerospace applications), atmospheric and solar magnetoplasma dynamics, and for application of parallel processing to large-scale problems, such as unstructured grid generation for complex flows, target tracking and correlations for battle management, and other disciplines of continuum and quantum computational physics. The system is used to develop and maintain state-of-the-art analytical and computational capabilities in fluid dynamics and related fields of physics, to establish in-house expertise in parallel processing and on-line graphical rendering for large-scale scientific computing, to perform analyses and computational experiments on specific relevant problems, and to transfer this technology to new and ongoing projects through cooperative programs.

The Parallel High Performance Computer/ Graphics Facility is a heterogeneous high-performance computer system composed of a number of autonomous computers with a composite peak speed equivalent to about 15 Cray 90 processors. The system is coupled directly to the advanced video recording center described below. The main computational engine is comprised of three Intel iPSC/860 Touchstone Gamma parallel supercomputers supported by the hardware and software environment necessary to develop, debug, and benchmark parallel simulations. With multi-MFLOP processors as building blocks, the Intel iPSC/860 is a MIMD-distributed memory machine configured as a hypercube. These three machines comprise a block of 224 parallel nodes with a peak computational speed of 18 GFLOPS with a cross-connected disk farm file system and network connections.

The facility's disk farm also supports three IBM RS/6000 and three DEC AXP high capacity compute-server computers, providing the facility with medium-to-large-scale memory and computational power enabling heterogeneous simulations with a significant scalar component, algorithm development, and diagnostic and postprocessing for large simulations. Special software allows simultaneous use of these computers on a single problem. Access to various other HPCC capabilities around the U.S. is accomplished through this system by using the new DoD high-bandwidth communication networks. A six-processor, five-gigabyte SGI Onyx provides the division with state-of-the-art high performance visualization.

A high-quality video studio has been created around a Sony D2 digital recording system, with a coupled Lyon-Lamb animation controller and a large memory Silicon Graphics ONYX workstation.

Scientists in the Condensed Matter and Radiation Sciences Division have developed a method to deposit biocompatible ceramic coatings using the pulsed-laser deposition technique. The method may have applications in dental and orthopedic implants, as well as percutaneous catheters.
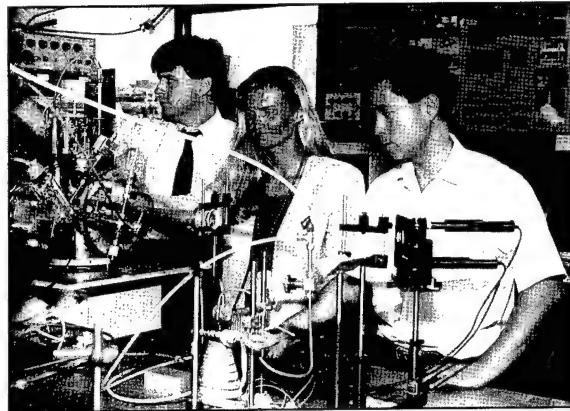
Through the network, other graphics stations, including the extensive resources of NRL's Visualization Laboratory, can create and record high-quality graphical images of simulation data for analysis and presentation by using digital recording techniques.

Condensed Matter and Radiation Sciences

The Condensed Matter and Radiation Sciences Division is the primary Navy center studying the effects of radiation on materials, electronic equipment, satellites, etc., and the production of thin films on diverse objects. The facilities for production and employment of photons, ions, and hypervelocity projectiles available to the division include:

High-Power Microwave (HPM) Facility — The large anechoic chamber (4.9 m × 4.9 m × 9.8 m) can be used at frequencies ranging from 0.5 to 94 GHz. Effects, susceptibility, and survivability of systems are the major research areas of interest.

Laser Facilities — Pulses of up to several joules are available from one system, while time resolutions down to 100 femtoseconds are produced by another. Synchronized Q-switched oscillators are configured for pump-probe experiments.

Thin-Film Preparation Facilities — The division has several major capabilities for preparation of thin films of advanced materials, such as high-temperature superconductors and active dielectrics. These include ion-assisted evaporation (which produces dense, adherent films), various dc plasma sources (which can etch as well as deposit films), and pulsed laser deposition (for production of chemically complex films).

X-ray Facility — Laboratory X-ray sources, monochromators, detectors, and related equipment are available for X-ray energies from 0.7 to 25 keV and dose rates up to 10^5 rads/s.

Synchrotron Radiation Facility — Intense, monochromatic X-ray photon beams tunable from 10 eV to 12 keV are available from the three beam lines developed by NRL at the National Synchrotron Light Source at the Brookhaven National Laboratory. Environmental target chambers can span a pressure range from 10^{-12} to 10^5 atmospheres and temperatures from 10 to 1500 K.

Ion Implantation Facility — The facility consists of a 200-keV ion implanter with specialized ultrahigh vacuum chambers and associated in situ specimen analysis instrumentation.

3-MeV Tandem Van de Graaff — This facility is used to study charged-particle radiation damage effects such as occur in space, to provide high-sensitivity analysis of materials, and to perform MeV energy implants in materials.

Hypervelocity Impact Facilities — Three facilities are used for ballistics research at speeds exceeding 6 km/s with inert or explosive targets while measuring projectile velocity, orientation, and dynamic projectile-target interaction.

Plasma Physics

The Plasma Physics Division is the major center for in-house Navy and DoD plasma physics research. The division conducts a broad experimental and theoretical program in basic and applied research in plasma physics, which includes laboratory and space plasmas, pulsed-power sources, plasma discharges, intense

The Plasma Physics Division's Nike KrF Facility.

electron and ion beams, atomic physics, laser physics, plasma processing, nonlinear dynamics and chaos, and numerical simulations. The facilities include an extremely high-power laser—Pharos III—for the laboratory simulation of space plasmas and nuclear weapons effects studies, a short pulse, high-intensity Table-Top Terawatt (T^3) laser to study intense laser-plasma, laser-electron beam, and laser-matter interactions. The division also has an 11-m^3 space chamber capable of reproducing the near-Earth space plasma environment and a radar antenna laboratory where the interaction of high-frequency microwaves and a sheet plasma distribution (agile mirror) is studied. The division has developed a variety of pulsed-power sources to generate intense electron and ion beams, powerful discharges, and various types of radiation. The largest of these pulsers—GAMBLE II—is used to study the production of megampere electron and ion beams and for producing very hot, high-density plasmas. Other generators are used to produce particle beams that are injected into magnetic fields and/or cavities to generate intense microwave pulses (e.g., the Relativistic Klystron Amplifier (RKA), in the 1 to 10 GHz regime). A large array of high-frequency microwave sources (35 to 120 GHz) are available to conduct research on microwave processing of advanced ceramic materials.

A major 3-kJ KrF laser facility opened on 13 June 1995. This facility is being initiated to provide intense radiation for studying inertial confinement fusion target heating at short wavelengths (0.25 microns).

Electronics Science and Technology

In addition to specific equipment and facilities to support individual science and technology programs, NRL operates the Nanoelectronics Processing Facility (NPF), the Penthouse Processing Facility (PPF), the Laboratory for Advanced Material Synthesis (LAMS), and the EPICENTER. The NPF's mission is to provide service to both NRL and external organizations requiring micro- and nanofabrication processing support. Lithography is a particular strength of the NPF, with definition of feature sizes down to 150 Å possible with an e-beam nanowriter. The NPF can supply items ranging from individual discrete structures and devices to circuits with very-large-scale integration complexity. The recently completed PPF is dedicated to processing III-V semiconductor devices and circuits in addition to serving the hands-on fabrication needs of individual NRL scientists. The PPF employs a single-pass air-ventilation system to minimize human risk to potentially hazardous III-V semiconductor processes and associated chemicals, thereby further

meeting existing safety standards. The LAMS' mission is to support NRL programs that require thin film III-V or refractory semiconductor technology. The LAMS employs organometallic vapor phase epitaxy to synthesize a wide range of thin films such as InSb, InGaP, InP, and GaN. The EPI-CENTER (a joint activity of the Electronic Science and Technology, Materials Science and Technology, and Chemistry Divisions) is dedicated to the production of multilayer microstructures using in-situ surface analytical techniques in either of two ultrahigh vacuum, molecular-beam-epitaxy growth chambers—one for III-V semiconductors and the other for magnetic materials and II-VI semiconductors.

Bio/Molecular Science and Engineering

The Center for Bio/Molecular Science and Engineering conducts research and development using biotechnological approaches to solve problems for the Navy, DoD, and the nation at large. Problems currently being addressed include advanced material development (for electronic, biomedical, and structural applications), combat casualty care, environmental quality (including pollution cleanup and control), and biological warfare defense. The approach to these problems involves long-term research focused on the study of complex materials systems, coupled with integrated exploratory and advanced development programs. The staff of the center is an interdisciplinary team who performs basic and applied research and development in areas that require expertise in bio- and surface chemistry, biophysics, genetic engineering, cell biology, advanced organic synthesis, solid-state and theoretical physics, and electronics and materials engineering. In addition, the center has many collaborations throughout the Laboratory, at universities, and in industry to ensure that a broad base of the required expertise and critical evaluations are part of the research and development programs. Highlights of the program include the development of liposome-based blood substitutes, the manipulation of biologically derived structures on the nanometer scale, the development of ferro-electric liquid crystal systems with microsecond response times, discovery of an advanced resist system for high-speed, high-density integrated circuits, the patterning of neuronal cells to form neural networks, and the development of biosensors for environmental monitoring.
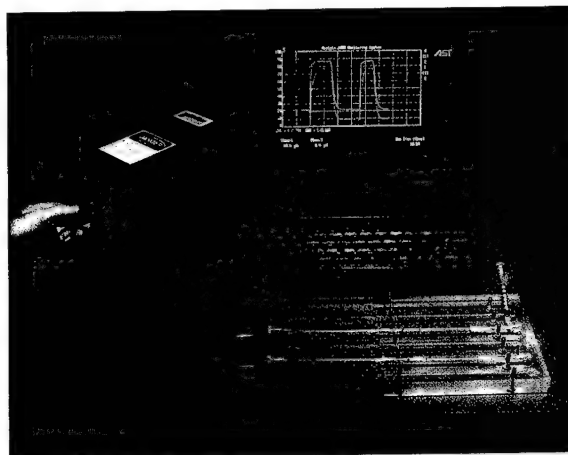
The fiber-optic biosensor is a portable detection system capable of analyzing ppb (ng/ml) concentrations of hazardous chemicals and pathogenic agents. It is fast (< 10 minutes), easy to use, and capable of simultaneous analysis for multiple analytes. It has been field tested for the detection of pollutants and biological warfare agents.

In October 1994, the center occupied newly renovated laboratories and offices in Building 30. These modern facilities, designed to be used into the next century, include general laboratories for research in chemistry, biochemistry, molecular biology, and physics. Specialized areas include a 600-ft^2 Class 1000 clean room; an advanced Electron Microscope facility; and a Scanning Probe Microscope laboratory. In addition, instrument rooms in the new building provide access to a variety of spectrophotometers (IR, GC-MS, NMR, and UV-Vis) and other equipment used in biochemical or physical analyses of biomaterials. In the near future, laboratories will be set up to accommodate an X-ray diffraction instrument, a liquid crystal fabrication facility, and equipment for advanced electronics and biosensor programs.

Acoustics

The Acoustics Division has three integrated acoustic pool facilities supporting research in submarine target characteristics for ASW, submarine acoustic design and quieting, sensors for hull-mounted sonars, and structural acoustics for mine countermeasures. Scaled submarine targets, real mine structures, sensors mounted on hull simulators, and underwater buried objects can all be examined with advanced nearfield holographic and scanning 3-D laser vibrometer systems to measure and visualize the sound fields near a
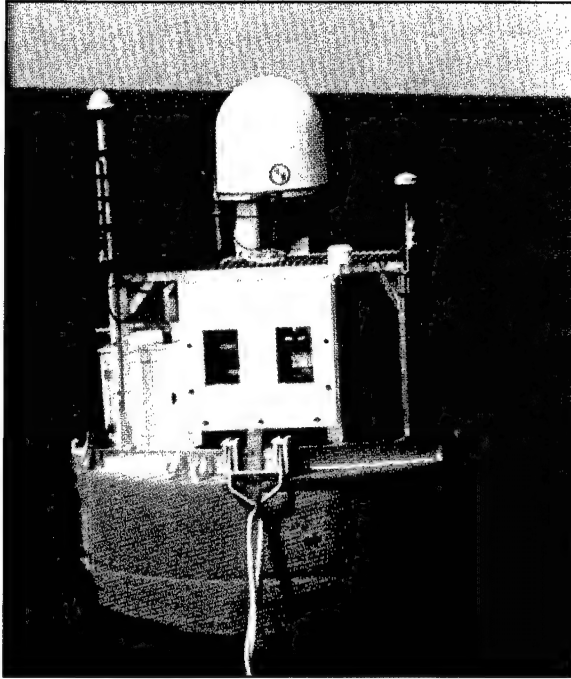
The Satellite Vertical Line Array (SLVA) system collects acoustic and oceanographic data and transmits it to a remote shore station in real time.

structure, the vibrations of the structure itself, the resulting farfield sound fields, and the physics of the sound-structure-fluid interactions.

The division operates several acoustic projectors and receive arrays for the generation and collection of experimental data. Source projectors include five towed XF4 flextensional transducers, two moored WEBB organ-pipe projectors, and a WEBB battery-operated arbitrary-waveform projector system. Receive systems include a moored, 32-element (up to 800 Hz) vertical-array with a RF telemetry system, a 64-element (75 to 600 Hz) towed oil-filled seismic-type array, and a 64-element (100 to 400 Hz) oil-filled array that can either be deployed along the ocean bottom or moored vertically. The 64-element arrays use direct-link cabling to a 64-channel (expendable to 1024 channel), 20 kHz bandwidth data acquisition and processing system. The division also has unique, self-recording digital acquisition buoy systems (DABS) that are used to obtain multi-channel (up to 128) acoustic data in the 10 Hz to 5 kHz regime. These systems provide up to 250 gigabytes of data on a single 15-inch reel of one-inch tape. The division has recently developed the Satellite Vertical Line Array (SLVA) system to collect acoustic and oceanographic data and transmit selected data to a remote shore station in real time. The buoy has a local-area network and computers on board to control the collection, preprocessing, and transmission of data. The multichannel data are sent via high-speed satellite channel at speeds in excess of 1 Mbit/s, using commercial Ku-band satellites.

The division operates high-frequency (up to 600 kHz) acoustic measurement systems to obtain scattering, target strength, and propagation data using bottom-moored instrumentation towers and a high-speed, remotely operated vehicle. These data are used to simulate the performance of weapons and mine countermeasure sonars (including advanced synthetic aperture sonars) in shallow and very shallow water environments.

The Tactical Oceanography Simulation Laboratory (TOSL) is a modeling and simulation architecture consisting of a set of tools for ingesting and processing climatological and real-time environmental data and applying energy propagation models to that data to determine acoustic and nonacoustic propagation loss. TOSL is coupled with a storage repository of environmental data and a wide-area network (WAN), which allows full participation in a distributed simulation environment. TOSL features a high-performance computational capability able to provide real or near-real-time calculations in support of training, war games, operations rehearsal, and other distributed simulation functions.

Remote Sensing

The Remote Sensing Division conducts a program of basic research, science, and applications to develop new concepts for sensors and imaging systems for objects and targets on the Earth and in the near-Earth environment and in deep space. The research, both theoretical and experimental, leads to discovering and understanding the basic physical principles and mechanisms that give rise to the background environmental emissions and targets of interest and to absorption and emission mechanisms of the intervening medium. Accomplishing this research requires the development of sensor systems' technology. The developmental effort includes active and passive sensor systems used for the study and analysis of the physical characteristics of phenomena that evolve from naturally occurring background radiation, such
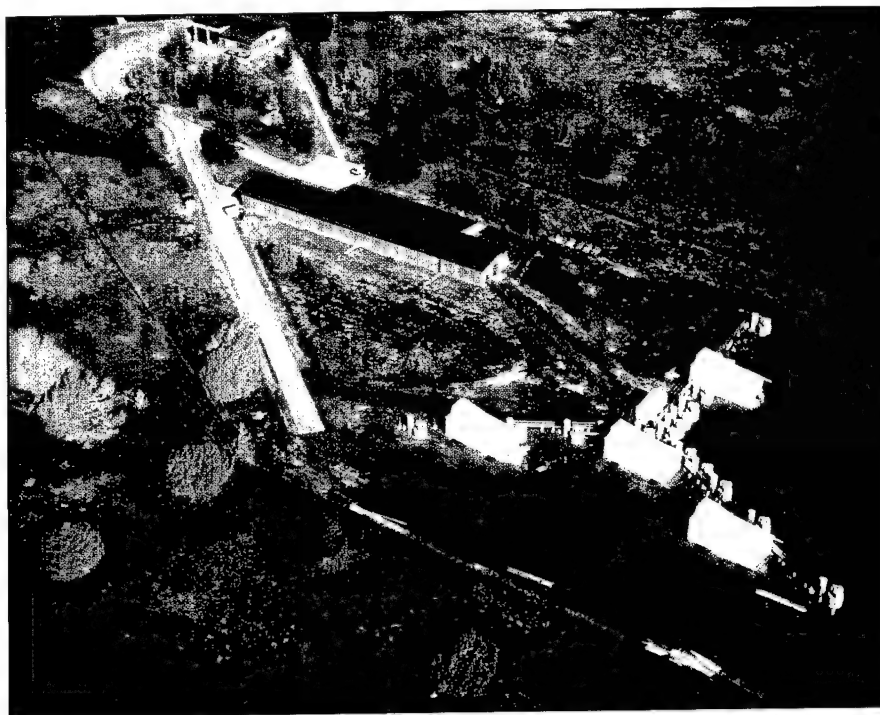
The Navy Protoype Optical Interferometer makes high-angular-resolution optical measurements of stars. This view shows the four buildings housing the astrometric siderostats, the "Y" array of exterior piers for the imaging siderostats, and the optical lab where the light is combined. The facility is located near Flagstaff, Arizona.

as that caused by the Earth's atmosphere and oceans and man-made or induced phenomena, such as ship/submarine hydrodynamic effects. The research includes theory, laboratory, and field experiments leading to ground-based, airborne, or space systems for use in remote sensing, astrometry, astrophysics, surveillance, nonacoustic ASW, improved meteorological/oceanographic support systems for the operational Navy, and the environmental/global climate change initiatives. Special emphasis is given to developing space-based platforms and exploiting existing space systems.

The Navy Prototype Optical Interferometer (NPOI), a major new facility of the Remote Sensing Division, is actually two colocated instruments for making high-angular-resolution optical measurements of stars. Light from widely separated individual siderostats will be combined simultaneously to synthesize the angular resolution of a telescope tens to hundreds of meters in diameter. Four siderostats are placed in an array with extremely accurate metrology, to enable very-high-precision measurements of stellar positions (wide-angle astrometry). These measurements are used by the U.S. Naval Observatory to refine the celestial reference frame, determine Earth rotation parameters, and thus satisfy Navy requirements for precise time and navigation data. They also provide determinations of basic astrophysical parameters, such as stellar masses and diameters. Additional relocatable siderostats can be placed out to distances of 250 m from the array center and used to construct very-high-resolution images of stars. These images will provide fundamental astrophysical information on stellar structure and activity. When complete, the NPOI will be the most advanced high-resolution imaging optical interferometer in the world.

Oceanography

The Oceanography Division is the major center for in-house Navy research and development in oceanography. It is known nationally and internationally for its unique combination of theoretical, numerical, and experimental approaches to oceanographic problems. Researchers make extensive use of the Maury Oceanographic Library (jointly operated by NRL-Stennis Space Center
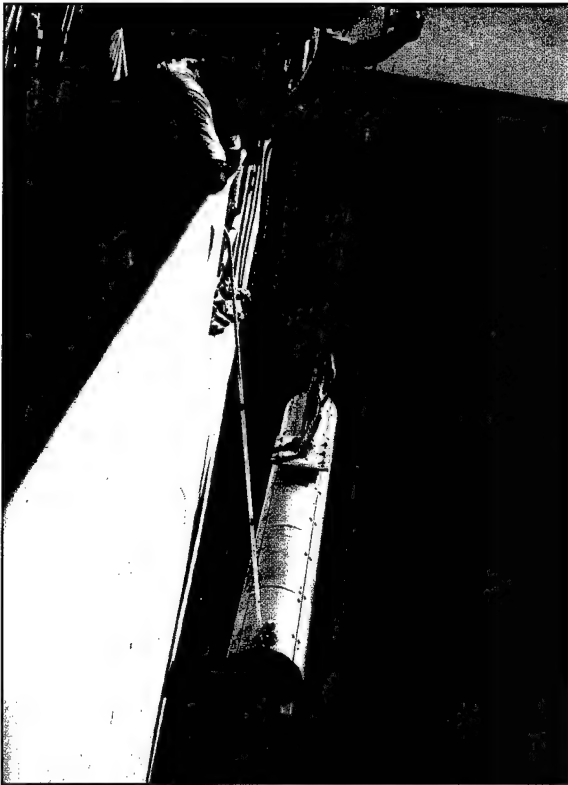
Deployment of an under-way sensor system aboard R/V *Thompson* in the Arabian Sea.

Marine Geosciences

The Marine Geosciences Division is the major center for in-house naval research and development in marine geology, geophysics, geoacoustics, and geotechnology. It is also the Navy's lead activity for mapping, charting, and geodesy research and development. The division has acquired unique instrumentation suites for its studies of the seafloor and its subbottom. These include sidescan sonar systems; deep-towed, low-frequency acoustic-reflection systems; parametric acoustic-swath subbottom-mapping systems; remotely operated vehicles; and electromagnetic mapping sensors. These systems allow studies ranging from sediment classification to mapping of inclusions and changes in the seafloor subbottom structure. The division deploys ocean bottom and subbottom seismometer systems for use in studies ranging from tectonic noise to studies of whale migration. Specialized seafloor probes

(NRL-SSC) and the Naval Oceanographic Office), which is recognized as one of the best and most comprehensive oceanographic libraries in the world. The division numerically models the ocean and coastal areas of the world. This modeling is conducted on the Navy's and DoD's most powerful vector and parallel-processing machines. To study the results of this intense modeling effort, the division operates a number of highly sophisticated graphic systems to visualize ocean and coastal dynamic processes. The seagoing experimental programs of the division range worldwide. Unique measurement systems include: towed sensor and advanced microstructure profiler systems for studying micro- and fine-scale ocean structure, an integrated absorption cavity and optical profiler system for studying ocean optical characteristics, and self-contained bottom-mounted upward-looking acoustic profilers for measuring ocean variability. In the laboratory, the division operates an environmental scanning electron microscope and a laser confocal scanning microscope for detailed studies of biocorrosion in naval materials.

The Remotely Operated Vehicle ORCA being deployed for tests of a hydrographic survey sensor suite at Gulfport, Mississippi, in January 1995.

allow measurement of the water pressure in sediment pores and acoustic compression and shear wave velocity and attenuation. Laboratory equipment includes a transmission electron microscope with an environmental cell to carry out sediment-fabric and sediment-pollutant adsorption studies.

The Map Data Formatting Facility, a collection of computers and work stations with associated graphics manipulation software, is used to compress map information onto a CD-ROM for Navy and Marine Corps aircraft digital moving maps. The division also operates the NRL Magnetic Observatory at SSC. This facility includes two specially built wooden buildings with minimal ferrous content and arrays of magnetometers that extend radially from the building. The Magnetic Observatory measures the ambient magnetic field, its changes, and other magnetic phenomena. The observatory is part of a worldwide observing system.

In addition to in-house laboratory work, the division incorporates the Chief of Naval Operations (CNO)-sponsored Center for Tactical Oceanographic Warfare Support, which develops high-resolution atmospheric, oceanographic, and bathymetric instrumentation systems and measurement techniques in support of CNO-endorsed requirements.

Marine Meteorology

The Marine Meteorology Division is located in Monterey, California. NRL-Monterey (NRL-MRY) performs both basic and applied research in meteorology in applications relevant to both central-site and shipboard meteorological analyses and forecasts. Located adjacent to the Fleet Numerical Meteorology and Oceanography Center (FNMOC), the Navy's operational forecast center, NRL-MRY has developed both the global and regional forecast systems that are run at FNMOC and that provide worldwide Navy forecasts. NRL-MRY is also the technical direction agent for TESS(3), a minicomputer-based environmental diagnosis/forecast system designed for shipboard use. Advanced technologies in use include satellite meteorology, advanced numerical techniques, and artificial intelligence.

Space Science

NRL is the Navy's main laboratory for conducting basic research and development in the space sciences. The Space Science Division conducts and supports a number of space experiments in the areas of upper atmospheric, solar, and astronomical research aboard NASA, DoD, and other Government-agency space platforms. Division scientists are involved in major research thrusts that include ultraviolet remote sensing of the upper atmosphere, spectrographic studies of the solar atmosphere, and astronomical radiation ranging from the ultraviolet through cosmic rays. In support of this work, the division maintains facilities to design, construct, assemble, and calibrate space experiments. A network of computers, workstations, image-processing hardware, and special processors are used to analyze and interpret space data. Among the division's space science data acquisition and analysis efforts are the following:

• mission operations and data analyses of the NRL's Oriented Scintillation Spectrometer Experiment (OSSE) for NASA's Compton Observatory;

• observation of the Sun's interaction with the upper-Earth atmosphere through the Solar Ultraviolet Spectral Irradiance Monitor (SUSIM) experiment in support of NASA's Upper Atmosphere Research Satellite (UARS) and Atmospheric Laboratory for Application and Science (ATLAS) missions; and

• observation of selected celestial targets in the ultraviolet and X-ray bands by three Advanced Research and Geophysical Observation Satellite (ARGOS) experiments—Global Imaging of the Ionosphere (GIMI), High-Resolution Atmospheric and Auroral Spectroscopy (HIRAAS), and Unconventional Stellar Aspect (USA).

The Space Science Division also operates the BMDO's Background Data Center (BDC)—a center of expertise for backgrounds phenomenology data that provides archival, management and analysis services, and value-added products for preserving and applying data collected by satellite experimental programs. The BDC's architecture consists of fully functional classified and unclassified processing environments that include operational data processing systems and science analysis stations. Automatic data processing equipment includes Digital Equipment Corporation (DEC) VMS, and Unix platforms, Sun workstations, Silicon Graphics workstations, Macintoshes, and IBM-compatible personal computers. These platforms

support a wide variety of standard scientific analyses software packages, including Ingres RDBMS, IRAF, IDL, KHOROS, and the MOSAIC/World Wide Web. Unclassified processing environments are linked to scientists throughout the world via the Internet. Data files can be received by or sent from the BDC by using FTP or other protocol. Information about the BDC, the programs it supports, and the services it provides can be obtained via the BDC World Wide Web Home Page—http://bradbury.nrl.navy.mil/.

Space Technology

In its role as a center of excellence for space systems research, the Naval Center for Space Technology (NCST) designs, builds, analyzes, tests, and operates spacecraft, as well as identifies and conducts promising research to improve spacecraft and their support systems. NCST facilities that support this work include large and small anechoic radio frequency chambers, clean rooms, shock and vibration facilities, an acoustic reverberation chamber, large and small thermal/vacuum test chambers, control system interaction laboratory, satellite command and control ground stations, fuels test facility, and modal analysis test facilities. NCST has a facility for long-term testing of satellite clock time/frequency standards under thermal/vacuum conditions linked to the Naval Observatory; a 5-m optical bench laser laboratory; and a hologram research laboratory to conduct research in support of the development of space systems.
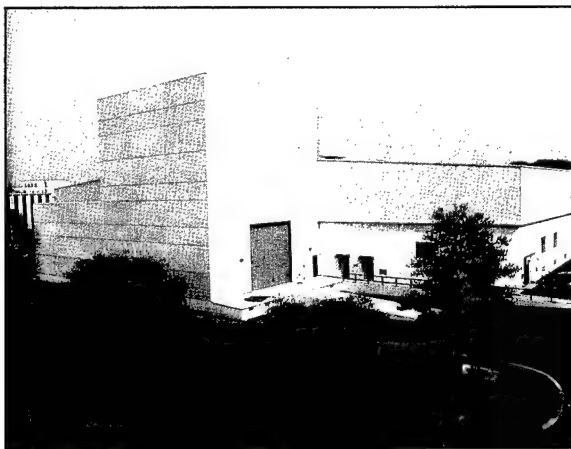
Building A59 was recently renovated for NCST occupancy.

Research Support Facilities

Technical Information Services

The Ruth H. Hooker Research Library and Technical Information Center contains more than 1 million items, including journals, books, conference proceedings, technical reports, and more than a thousand microcomputer software packages. Its collections can be searched by computer-based catalogs. The Library provides interlibrary loans, on-line literature searches, access to CD-ROM and commercial databases, loans of microcomputer software, and a full range of reference services. The Library offers desktop access to its catalogs and databases through its menu-driven InfoNet information system, which can be accessed from offices and laboratories as well as from home. A number of these services are also available via the World Wide Web through the Library's InfoWeb interface. The InfoWeb links to the Library's networked document dissemination system called TORPEDO (The Optical Retrieval Project: Electronic Documents On-line), offering full-text search capabilities and on-line display and printing of selected journals, research reports, and NRL Press Releases.

Publication services include writing, editing, composition, phototypesetting, publications consultation, and printing management. The primary focus is on using computer-assisted publishing technology to produce scientific and technical information containing complex artwork, equations, and tabular material.

The research conducted at NRL requires a diversity of graphic support such as technical and scientific illustrations, computer graphics, design services, photographic composites, calligraphy, display panels, sign making, and framing. A high-end workstation provides and delivers a new level of electronic airbrushing and photographic retouching.

Photographic services include high-speed motion picture, video, and still-camera coverage for data documentation both at NRL and in the field. A photographic laboratory offers custom processing and printing of black and white and color films. Photographic images can also be captured with state-of-the-art digital cameras and still video. Video services include producing video reports of scientific and technical programs. A video studio and editing facility with high-quality

The Technical Information Division has recently installed this Noritsu photographic minilab to process up to 120-size film and make prints up to 8 in. by 10 in.

Beta Cam and VHS editing equipment are available to support video production.

The Visual Design/Imaging Center offers high-quality output from computer-generated files in EPS, PostScript, PICT, TIFF, Photoshop, and PowerPoint. The Captivator film recorder produces high-resolution 35-mm slides, viewgraphs, and negatives. Photographic quality color prints and viewgraphs are available from Kodak dye-sublimation printers. High-resolution scanning to a Macintosh or PC disk is available. The Linotron Imagesetter produces gray-scale prints and transparencies at 1693 dpi.

Center for Computational Science

The Center for Computational Science (CCS) conducts research and development to further the advancement of computing and communications systems to solve Navy problems. Promising technologies are transitioned to production systems. The CCS operates and maintains computer systems and networks that provide support for NRL, Navy, and DoD research. The CCS features two Connection Machines (massively parallel computer systems), a 32-processor CM-5E, and a 256-processor CM-5E with 32 gigabytes of memory and a 25 terabyte robotic D2 tape storage system. The CCS operates high-performance network testbeds, including an ATM/SONET experimental wide-area network. These leading-edge systems and networks are being investigated and developed by the CCS.

The CCS also manages and operates production computer systems and networks. A Cray Y-MP EL provides support for vector computing. The CCS supplies lab-wide data storage support with NRL's File Server/Archiver (FS/A) system. The FS/A provides 70 gigabytes of on-line storage and 25 terabytes of near-line storage, featuring advanced robotics from Storage Technology in an automated tape cartridge system.

The CCS Scientific Visualization Lab functions as an information center, video production unit, and training center for the latest tools in scientific visualization. By using powerful workstations, graphics workstations, and a networked digital video editor, researchers can conveniently turn the results of their computations into color prints, 35-mm slides, or animations on video tape. The Scientific Visualization Lab also provides assistance and training in workstation system administration and clustered workstation programming.

The CCS facilities are accessed through NRL's local area network, NICEnet, which includes a new local FDDI network. NICEnet provides external connections to network and computer systems worldwide. Dial-in modem access is also available.

FIELD STATIONS

NRL has acquired or made arrangements over the years to use a number of major sites and facilities for research. The largest facility is located at the Stennis Space Center (NRL-SSC) in Bay St. Louis, Mississippi. Others include a facility at the Naval Postgraduate School in Monterey, California (NRL-MRY), and the Chesapeake Bay Detachment (CBD) in Maryland. Additional sites are located in Maryland, Virginia, Alabama, and Florida.

Flight Support Detachment (NRL FSD)

Located aboard the Patuxent River Naval Air Station in Lexington Park, Maryland, NRL FSD operates and maintains five uniquely configured P-3 Orion turboprop aircraft as airborne research platforms. The FSD conducts single aircraft, worldwide detachments in support of a wide range of scientific research.

In FY 95, NRL FSD provided flight support for diverse research programs, including Project

Flight Support Detachment aircraft, BUNO 154589, parked in front of Hangar 109 at the Patuxent River Naval Air Station.

Birdseye, involving hydroacoustic research; Fly's Eye, an infrared threat warning system; Airborne Multisensor Pod System (AMPS), a multisensor data collection system; Airborne Geophysical Sensor Suite (AGSS), involving data and gravimeter testing to detect variations in the ocean floor; and MAKO, an ECM study of received signals.

The NRL FSD aircraft are the sole airborne platforms for numerous projects, such as bathymetry, electronic countermeasures, gravity mapping, and radar development research. The detachment has an impressive safety record of over 50,880 accident-free flight hours amassed over a 32-year period.

Chesapeake Bay Detachment (CBD)

CBD occupies a 168-acre site near Chesapeake Beach, Maryland, and provides facilities and support services for research in radar, electronic warfare, optical devices, materials, communica-

tions, and fire research. Because of its location high above the Chesapeake Bay on the western shore, unique experiments can be performed in conjunction with the Tilghman Island site 16 km across the bay from CBD. Some of these experiments include low clutter and generally low-background radar measurements. By using CBD's support vessels, experiments are performed that involve dispensing chaff over water and radar target characterizations of aircraft and ships. Basic research is also conducted in radar antenna properties, testing of radar remote-sensing concepts, use of radar to sensor ocean waves, and laser propagation. CBD also hosts facilities of the Navy Technology Center for Safety and Survivability, which conducts fire research on simulated carrier, surface, and submarine platforms.

Marine Corrosion Test Facility

Located on Fleming Key at Key West, Florida, this facility offers an ocean-air environment and clear, unpolluted, flowing seawater for studies of environmental effects on materials. Equipment is available for experiments involving weathering, general corrosion, fouling, and electrochemical phenomena, as well as coatings, cathodic protection devices, and other means to combat environmental degradation.

Naval Research Laboratory-Stennis Space Center (NRL-SSC)

NRL-SSC, a tenant activity at NASA's Stennis Space Center, is located in the southwest corner
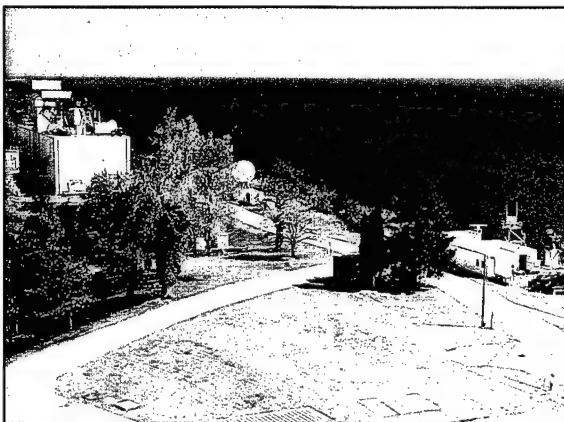
The radar facility located at the Chesapeake Bay Detachment.
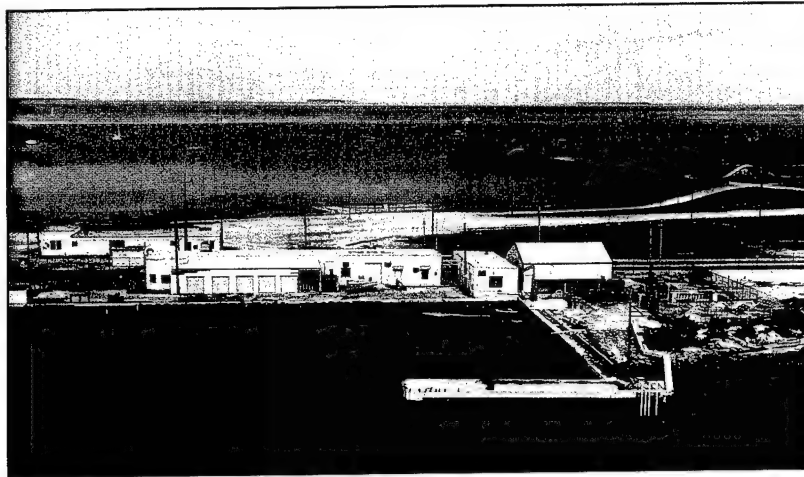
The Marine Corrosion Facility, located at Key West, Florida.

of Mississippi, about 50 miles northeast of New Orleans, Louisiana, and 20 miles from the Mississippi Gulf Coast. NRL-SSC encompasses over 200 square miles of land area, including a perimeter buffer zone to insulate surrounding civilian communities from the noise of rocket-engine testing by NASA. Other Navy tenants at NRL-SSC include the Commander, Naval Meteorology and Oceanography Command and the Naval Oceanographic Office, who are major operational users of the oceanographic and atmospheric research and development performed by NRL. The Naval Oceanographic Office provides access for NRL researchers to one of the Navy's largest supercomputers. This unique concentration of operational and research oceanographers makes NRL-SSC the center of naval oceanography and the largest such grouping in the Western world.

NRL-SSC provides administrative and business operations support for NRL's Center for Environmental Acoustics, Remote Sensing Applications Branch, Oceanography Division, and Marine Geosciences Division. NRL-SSC occupies over 200,000 square feet of research, computation, laboratory, administrative, and warehouse space. Facilities include a number of large antennas to receive available oceanographic and meteorological satellite data, a Magnetic Observatory building constructed of nonferrous materials in an electromagnetically quiet area of NRL-SSC, a Pattern Analysis Laboratory, a Map Data Formatting Facility, a water-wave channel, and numerous laboratories for acoustic and oceanographic computation,

instrumentation, analysis, and testing. Special areas are available for constructing, staging, refurbishing, and storing sea-going equipment.

Marine Meteorology Division
Monterey, California (NRL-MRY)

Located in Monterey, California, as a tenant activity of the Naval Postgraduate School (NPS), this facility is collocated with the Fleet Numerical Meteorology and Oceanography Center (FNMOC) to support development and upgrades of numerical atmospheric forecast systems and related user products. NRL-MRY's mission has broadened considerably to include basic research and support to other customers. Collocation with FNMOC allows NRL-MRY access to the Navy's largest vector supercomputer mainframe and workstation resources. This access provides real time as well as archived global atmospheric and oceanographic databases for research on-site and at other NRL locations. Interfaces to the Defense Research and Engineering Network through FNMOC and Defense Simulation Internet at NPS have been established. Locally, NRL-MRY has a DEC Alpha Workstation and data archives system for in-house researchers to conduct numerical weather prediction experiments.

NRL-MRY's experience extends to prototype regional and shipboard atmospheric prediction systems. A third-generation Navy system, the Tactical Environmental Support System (TESS(3)), developed for SPAWAR, is installed and has

undergone various upgrades on-site to provide networking capabilities in line with the Copernicus architecture and remote workstation access. TESS(3) is functioning as an R&D testbed for new tactical/environmental decision aids (TDAs/EDAs), object-oriented databases, and Motif/X Windows-user interfaces. State-of-the-art graphics workstations (SGIs), network file-servers (Suns), and TAC 3 (HP) systems have been acquired for use by researchers. Environmental components of future shipboard systems are being developed within a system rooted in commercially available distributed database management software.

Other Sites

Some field sites have been chosen primarily because they provide favorable conditions to operate specific antennas and electronic subsystems and are close to NRL's main site. Pomonkey, Maryland, a field site south of NRL, has a free-space antenna range to develop and test a variety of antennas. The antenna model measurement range in Brandywine, Maryland, has a 4.6-m diameter turntable in the center of a 305-m-diameter ground plane for conducting measurements on scale-model shipboard and other antenna designs.

A site on the cliffs overlooking the Chesapeake Bay provides an over-the-water range of approximately 10 miles to Tilghman Island.

Midway Research Center

The Midway Research Center (MRC) is located on a 158-acre site in Stafford County, Virginia. Located adjacent to the Quantico Marine Corps' Combat Development Command, the MRC has 10,000 square feet of operations and administration area and three precision 18.5-m-diameter parabolic antennas housed in 100-ft radomes. The MRC, under the auspices of the Naval Center for Space Technology, provides NRL with state-of-the-art facilities dedicated solely to space-related applications in naval communications, navigation, and basic research.

Research Platforms

Mobile research platforms contribute greatly to NRL's research. These include five P-3 Orion turboprop aircraft and one ship, the ex-USS *Shadwell* (LSD-15), birthed in Mobile Bay, Alabama. The ex-*Shadwell* is used for research on fire suppression techniques on-board ship.
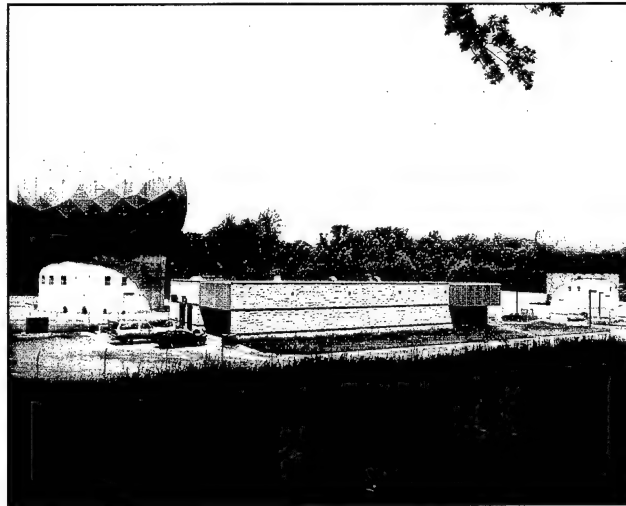
View of the Midway Research Facility space-tracking facility.

NRL in the Future

In order to provide preeminent research for tomorrow's Navy, NRL must maintain and upgrade its scientific and technological equipment to keep it at the forefront of modern research facilities. The physical plant to house this equipment must also be state of the art. NRL has embarked on a Corporate Facilities Plan to accomplish these goals. This plan and future facility plans are described below.

THE CORPORATE FACILITIES INVESTMENT PLAN (CFIP)

The CFIP is a financial spending plan to provide modern research facilities at NRL by the year 2000. The plan calls for both Congressional and Laboratory investment and is updated and altered as changes occur in scientific emphasis and Congressional attitude. Over the past several years, Congressionally approved military construction (MILCON) funds were used to construct the new Electro-Optics Laboratory and a high-bay facility for the Naval Center for Space Technology. Funds have been requested for the construction of a new building for nanoscience research.

To complement these efforts, overhead funds have been used to renovate and upgrade laboratory and support areas in several existing buildings. To date we have provided modern laboratory facilities for the Center for Bio/Molecular Science and Engineering, the Material Sciences and Technology Division, and the Remote Sensing Division. Work that is currently in progress will provide new facilities for the Acoustics Division, the Information Technology Division, and the Radar Division.

Center for Computational Sciences

The Center for Computational Science has a procurement in process for a scalable, massively parallel processing (MPP) computer system. The system will be used to continue innovative exploration and evaluation of MPP technology for the solution of significant military-relevant problems relating to computational and information sci-

ence. The planned system will allow for continuing research into heterogeneous parallel processing in connection with the NRL Thinking Machines Corporation CM-5E systems and other computational assets.

Optical Sciences

The NRL infrared (IR) test chamber, or IR range, was installed in Building 216 in December 1995 and became fully operational in the second quarter of FY 96. This ultradry chamber is used to measure the IR signature of new surface treatments, scale models, and components used for observables control on ships, aircraft, and missiles. The IR range can simulate the infrared radiance from the Earth and sky at target altitudes ranging from 0 to 30,000 feet. Included in the facility are a midwave solar simulator, a versatile target mount with control over yaw, pitch, and temperature, and seven ports to view the target with IR sensors. This facility complements the NRL Compact Radar Range in Building A59 and is only the second IR Range ever built. It can supply calibrated signature data sufficient to meet the needs of both the Navy and Air Force.

Plasma Physics

The division has established a new facility for research on high-frequency microwave processing of advanced ceramic materials. It features a unique, tunable (60 to 120 GHz) quasi-optical gyrotron, 35 and 94 GHz fixed-frequency gyrotrons, and a 6 kW, 2.45 GHz industrial microwave source. The facility is being used to investigate the scientific basis for understanding and controlling microwave processes, such as sintering/densification, coating, and joining, for low-loss, refractory ultrafine-grain polycrystalline ceramic materials.

Electronics Science and Technology

Important division emphasis is focused on the continual upgrading of the Nanoelectronics

Processing Facility (NPF) and the Penthouse Processing Facility (PPF) and expanding activities in the nanoelectronics, heterostructures, and vacuum electronics science and technology programs. The Laboratory for Advanced Material Synthesis Facility will continue to upgrade its organometallic vapor-phase epitaxy equipment to meet program needs for thin-film semiconductors. Upgrades include safer and more environmentally benign processing and waste disposal techniques. The EPICENTER (a joint activity of the Electronic Science and Technology, Materials Science and Technology, and Chemistry Divisions) will continue to provide new insight into epitaxial semiconductor growth processes. Knowledge of these growth processes will be used for improved control of film properties for use in the electronic devices of tomorrow.

Ocean Acoustics Research Laboratory

NRL's Ocean Acoustics Research Laboratory (MILCON Project P-006), a 52,000-square-foot building, will place 90% of NRL-SSC in one closely located area. This project will provide secure laboratory and computing facilities for research and development in ocean science and technology. Completion and occupancy should occur by the end of 1999.

Vacuum Ultraviolet Space Instrument Test Facility

The Space Science Division facilities include an ultraclean solar instrument test facility in Building A-13 on the main NRL campus. The new facility is designed to satisfy the rigorous contamination requirements of state-of-the-art solar spaceflight instruments. The facility has a 400-square-foot Class 10 clean room and a large Solar Coronagraph Optical Test Chamber (SCOTCH). This completely dry-pumped, 550-cubic-foot vacuum chamber is maintained at synchrotron levels of cleanliness. Solar instrumentation up to 1 m in diameter and 5 m in length may be physically accommodated in the chamber. The instrument's optical performance is probed and calibrated with a variety of visible and XUV sources mounted on the chamber's 11-m beamline. The optical testing and characterization of the Large-Angle Spectrometric Coronagraph (LASCO) instrument for the European Space Agency's Solar Heliospheric

Observatory satellite was conducted in this chamber. Coronagraph stray-light characterization was carried out by mounting a set of baffles in the main beamline, illuminating the instrument with a simulated solar beam, and measuring the residual radiation. A stray light background measurement of 10^{-12} was successfully measured in the LASCO C3 channel. Coronagraph calibration was carried out by installing back-illuminated, calibrated opals in front of the instrument entrance aperture. Instrument polarization properties were analyzed by using a variety of polarizers installed in a wheel located between the opal and the instrument. The wheel was remotely controlled from outside the chamber. Instrument Mueller matrices were verified with a 12-in. diameter, two-plate partial polarizer. Calibration and focus of XUV solar instrumentation are accomplished by exposing the instrument to an XUV windowless collimator at the end of the tank. The facility also has a small thermal bake/vacuum test chamber used for vacuum conditioning and thermal testing of spaceflight components and subassemblies. Both the SCOTCH and the small test chamber are instrumented with temperature-controlled quartz-crystal monitors and residual gas analyzers for real-time, quantitative measurements of volatile contamination.

Remote Sensing

To validate numerical and theoretical efforts ongoing within the Remote Sensing Division, extensive hierarchical-coupled experiments are planned within a new, Free-Surface Hydrodynamics Laboratory. This laboratory will be used to study free-surface turbulence interactions, wave-generation phenomena, jet-flow phenomena, vorticity dynamics, and free-surface/surfactant interactions. Of particular importance is the detailed study of surfactant materials, both in shear and surface wave flows. State-of-the-art diagnostic tools are available, such as Langmuir film balance to measure the properties of surface films, hot-wire and laser-Doppler anemometry, together with the new quantitative flow techniques of laser speckle, particle tracking, and particle image velocimetry. These experimental diagnostic techniques use high-powered lasers, high-tolerance optical lenses, and extensive ultra-high-resolution video-imaging hardware and PC-based computerized systems. Further

computational assets consist of powerful graphical computer work stations, the NRL Connection Machine, and other off-site CRAY supercomputer systems.

Marine Geosciences

The Marine Geosciences Division will greatly enhance the capabilities and quality of seafloor sediment fabric analyses through purchase, installation, and staff training for a 300 kV transmission electron microscope (TEM) and accompanying environmental cell (EC) in FY 96. The TEM-EC will be housed in a specially built facility imparting a null effect on the functioning of the TEM-EC electronics. The new facility will improve transition of developed capabilities and sediment fabric understanding to applied issues of acoustic and shock-wave propagation, mine burial, and mine countermeasures.

REHABILITATION OF SCIENTIFIC FACILITIES

Specialized facilities are being installed or upgraded in several of the research and support divisions.

Flight Support Detachment

NRL's Flight Support Detachment (FSD) has continued to improve both capabilities and diversity among its aircraft platforms. Aircraft 153442 was transferred to the Naval Air Depot, Jacksonville, Florida, in preparation for extensive aircraft modifications required to install a "roto-dome" antenna and full AEW radar system on the aircraft. These modifications will support the Navy's Theater Air Defense programs, while providing a testbed for advanced EW radar research. Additionally, Aircraft 154589 and 154587 completed modifications to enhance interoperability and support pod-based research programs, such as the Advanced Multipod System (AMPS) and the Integrated Electronic Warfare System (IEWS). These upgrades and modifications will ensure that NRL will have the finest airborne research capabilities well into the next century.

Information Technology

The Information Technology Division continues to upgrade its local area network and

research into high-performance network testbeds, including ATM/SONET technology. The 256-processor CM-5E massively parallel computer will be upgraded in FY 96. The upgrade will include the addition of 100 gigabytes of scalable disk array, 32 additional processor nodes, device/processor expansion cabinets, and an upgraded interprocessor router. An additional scalable massively parallel computer system will be acquired. The new system will allow for continuing research into heterogeneous parallel processing in connection with the existing NRL CM-5E and will provide an alternative globally shared memory programming paradigm. The need for additional facilities to supplement research in virtual environments and Global Grid demonstrations will lead to gradual development of a demonstration/VR and conference center in Building 34. An upgrade for the Human-Computer Interaction Laboratory will integrate and enhance its video and audio presentation and recording capabilities.

Materials Science and Technology

Renovation is in progress for Building 3, which is composed of two of the original five buildings at NRL, to contain modern laboratories for studies of thin-film deposition and characterization, superconducting materials, magnetic materials, and other materials science projects. The new space will feature the most modern molecular beam epitaxy and other materials synthesis and processing equipment, an up-to-date fatigue and fracture laboratory, and state-of-the-art diagnostic equipment, including electron microscopes, spectrometers, and electron and X-ray diffraction equipment. The renovated building will also contain office and laboratory space for approximately 70 technical personnel.

Plasma Physics

A state-of-the-art short-pulse (<1 ps), high-intensity (>1 TW) Table-Top Terawatt (T^3) laser has been procured for a variety of physics studies. The T^3 laser will be integrated into the Pharos III Nd-laser facility to boost its power into the 10 to 100 TW range. This will provide a facility to do fundamental physics experiments in intense laser-plasma interactions and intense laser electron beam interactions.

A low-frequency (300 MHz to 10 GHz), high-power microwave facility that uses a relativistic

klystron concept is being upgraded to produce multigigawatt coherent radiation pulses.

A compact spectral imager, which records 2-D images of scenes with up to 500 spectral bands and 500 pixel spatial resolution, has been developed. This hyperspectral imager can be deployed on aircraft or on the ground for remote-sensing applications.

Remote Sensing

From 1920 through 1990, Building 2 (one of five original buildings at the Laboratory) housed the Engineering Service Division (ESD). ESD is no longer an active division, and renovation of Building 2 to house the Remote Sensing and Acoustics Divisions is currently in progress and scheduled for completion in 1996. After completion, Build-ing 2 will house office and laboratory space for over 125 personnel of the Remote Sensing Division.

Marine Geosciences

In September 1995, the division's Mapping, Charting, and Geodesy Branch, located at NRL-SCC, moved into newly refurbished facilities located in the same building with the division's Sea-floor Sciences Branch and Administrative Offices. This colocation will enhance interaction, efficiency, and research product quality of the division elements. Accompanying the change of quarters is an upgrade in hardware to improve electronic data transfer rate and efficiency internal and external to the division and NRL.

Highlights of NRL Research in 1995

The Transition of Low Observable Technology
into the SPS-49 MPU Program
Radar Division

The SPS-49 MPU (Medium Pulse-Repetition Frequency (PRF) Upgrade) radar is the Navy's principal long-range, shipboard, 2-D, air surveillance radar that is used on major combatant vessels. This radar system was recently upgraded to enhance the Fleet's ability to detect fast, low-cross-section targets. The SPS-49 MPU signal-processing technique initially developed at NRL determines the radial velocity of a contact on a single scan. This velocity estimation and an estimate of target cross-section are then used to reject unwanted, slow-moving contacts resulting from birds and clutter while retaining full sensitivity against desired low-cross-section targets. Analysis of the test data by NRL has led to a number of performance-enhancing modifications to the radar and tracker that will be implemented into production versions. The MPU upgrade will initially be applied to LSD 41 class amphibious ships as part of the Ship's Self-Defense System Program and to Cort FFGs. Follow-on production contracts will upgrade Aegis cruisers, DDG-993, LHD-1, DD-997, and CV/CVN-class ships.

AN/SPQ-9B Radar Program
Radar Division

The current AN/SPQ-9 radar's sensitivity is too low to detect difficult threats, and it cannot deal effectively with clutter. Thus the AN/SPQ-9B program objective was to add a low-cost, quality sea-skimmer detection capability to an existing shipboard radar as an ordinance alteration kit, with subsequent rapid introduction into the Fleet. The resulting upgrade provides significantly increased sensitivity and improved ability to detect large targets in clutter while maintaining current operating modes. An improved surface mode maintains the current MK 86 gun-fire control-system support, and a new air mode provides the capability of detecting sea-skimmer targets in a high clutter environment. The air mode of an advanced development model radar (AN/SPQ-9B advanced development model) has been successfully tested at Wallop's Island and in an at-sea shipboard environment. This program will provide a large number of Navy ships with a low-cost, low-RCS, sea-skimmer detection capability in clutter using the pedestal and below-deck spaces of the present AN/SPQ-9A radar.

Data and Voice Integration Advanced Technology Demonstration
Information Technology Division

Historically, military communication systems have implemented separate links and networks for each different application, such as voice tactical data, surveillance, intelligence, and command and control. This mode of operation is excessively expensive and wasteful and must be replaced by networks that are shared by multiple missions, multiple users, and multiple applications, including simultaneous voice and data. This capability is almost nonexistent over military tactical wireless networks. The Data/Voice Integration Advanced Technology Demonstration provides technology to integrated digital voice and data services over bandwidth-constrained tactical networks, using low-data-rate vocoder technology, unique

multiplexing schemes that support both datagram and virtual-circuit services, and advanced wireless network control schemes. A capability has been demonstrated for high- frequency surface-wave wireless systems operating at link rates as low as 2400 bps. The technology developed under this ATD provides essential capabilities that are needed to share a common wireless network among multiple missions, multiple users, and multiple applications.

Infrared (IR) Ocean Surface Modeling
Optical Sciences Division

The Navy requires ocean surface IR models to assess the performance of ship-defense IR surveillance systems and to develop ship signature-reduction techniques. These models must provide rapid and accurate IR imagery in a wide range of environmental conditions. A statistical model for infrared radiance emitted by the ocean surface near the horizon has been developed. This analytical model provides the mean and clutter radiances emitted by the ocean surface and is in good agreement with field-test imagery. Near-field IR models are currently being developed that use an ocean surface topographic realization based on the Pierson-Moskowitz wave-height power-spectral density. This model provides fast and accurate computation of the ocean surface IR imagery for marine IR background simulation models. The upgraded sea-surface model will provide a full spectral description of the mean and clutter radiances.

Ultrahigh Sensitivity Fiber Bragg Grating Laser Sensor
Optical Sciences Division

Substantial progress has been made in the use of optical fibers for sensing acoustic fields and other physical measurands. With the introduction of fabricating optical Bragg gratings directly in the optical fiber, new types of optical fiber sensors are emerging. These fiber Bragg grating devices are attractive for their small size, their ease of fabrication, the potential affordable mass production, and relative high sensitivity. An ultrahigh sensitivity fiber sensor configuration has been developed based on the modulation of the optical frequency of a small all-fiber Bragg grating-based fiber laser. Sensitivity to laser cavity strain on the order of 10^{-14} have been demonstrated, and the sensor can be serially multiplexed along a single fiber. This sensor provides a very high sensitivity to weak measurand fields in a compact, passively activated, and interrogated implementation. Also, this type of sensor could have a significant impact on the development of small, high-sensitivity devices for a range of Navy applications, particularly in underwater surveillance.

Self-Navigating Drone Expendable/Recoverable (SENDER)
Tactical Electronic Warfare Division

A need existed to develop a quickly deployed platform capable of carrying miniature radiosondes for atmospheric measurements. SENDER, a man-portable, low-cost, autonomous unmanned airplane capable of performing several military and dual-use missions, such as countermeasures deployment, reconnaissance/surveillance, covert payload delivery, and chemical/biological agent sampling, fills this need. SENDER has been designed to carry a three-pound payload for up to 100 nmi (no wind conditions) at an airspeed of 40 to 50 knots. SENDER's portability, rapid deployability, and low cost will allow radiosonde measurements to be taken within the immediate test area of a live missile firing exercise, before, during, and following the exercise.

Enzyme-based Detection of Environmentally Important Trace Metals
Laboratory for the Structure of Matter

Current methods for determining trace metals possess sufficient sensitivity but suffer from problems involving sample pretreatment and analysis time. It would be desirable to measure trace metals in situ, thus eliminating problems caused by sampling and storage—a currently impractical approach. A system for detecting zinc and cobalt using the metallo-enzyme carbonic anhydrase has been extensively studied; the apocarbonic anhydrase can be reactivated by either metal ion. Enzymes sensitive to copper, cadmium, and lead have also been identified. A prototype flow-through system to determine zinc in the low μM concentration range has been constructed. Such a system will allow near real-time monitoring of metal-ion concentrations. Analysis of trace concentrations of metal ions is important in the environmental and health sciences. The flow-through system currently under development will allow continuous monitoring and should be of great benefit in both environmental monitoring and in studies of the natural environment.

Force-Amplified Biological Sensor (FABS)
Chemistry Division

The DoD needed reliable point-detection systems capable of detecting biological agents below incapacitating levels in order to provide the user in a battlefield scenario with early-warning and contamination-avoidance information. NRL's task was to develop a sensor technology capable of detecting and identifying biological agents at extremely low concentrations (potentially a single molecule in a 100 microliter sample volume) using minimal instrumentation, without resorting to elaborate chemical amplification schemes. Based on previous experience with the direct measurement of the binding interaction between individual ligand-receptor molecules and complementary strands of DNA and of the development of a micromachined force transducer that is rugged, compact, and fast, this biosensor concept has been reduced to a prototype sensor called the Force Amplified Biological Sensor (FABS). The projected biosensor sensitivity of FABS will dramatically affect our ability to collect and identify biological agents, usually in the form of toxins, viruses, and bacteria. The ultrasensitivity of FABS reduces the sample collection time from hours or days to minutes, and the small size and portability of FABS are amendable to new collection and use scenarios.

Development of a Superconducting Motor Using High T_c Materials
Materials Science and Technology Division

Scientists and engineers at NRL and the Naval Surface Warfare Center and partners from private industry have successfully fabricated a motor using coils made from a high T_c-oxide superconductor that establishes a new record for generation of power using this technology. The demonstration represents a major step in the development of HTS wire suitable for military and commercial applications. The motor demonstration may have direct impact on ongoing Navy programs in minesweeping, electric drive, and superconductive magnet energy storage and may benefit other applications such as transportation, electric power transmission and distribution, magnetic-resonance imaging, and other medical devices.

Synthesis and Characterization of New Mercury/Thallium-based High-Temperature Superconductors
Materials Science and Technology Division

The discovery of high-temperature superconductors has spawned a search for new materials with ever higher superconducting transition temperature, T_c, in order to motivate and test theoretical treatments

of the mechanisms responsible for high-temperature superconduction, which still is not understood. A long-desired application of high-temperature superconductors is in the fabrication of high-current wires. Since these superconductors are complicated, multicomponent materials with short coherence lengths, fabrication of such wires has been difficult. NRL's results disclose a novel, one-step process that produces large, dense Hg-based HTS with a critical current density, J_c, which while still limited by sample granularity, is approximately 1.5 orders of magnitude better than samples synthesized using a conventional process. The discovery of the new materials will motivate the continued search for new materials with higher T_c's.

Piezoelectric Ceramics with Functional Gradients: A New Application in Material Design Metamorphic Materials
Materials Science and Technology Division

Piezoelectric ceramics have been designated for use in many applications as displacement transducers, micropositioners, and rotary actuators. A new type of monomorph uses a built-in functional gradient that is attained by doping PZT bars with varying amounts of additives across their thickness. The voltage-induced piezoelectric strain of these monomorph bars is more than double that of homogeneous bars. This new monomorph has no discernible internal seams or boundaries. The advantage of making a monomorph in such a way is that failure from internal debonding or from stress peaks developed in conventional bimorphs is avoided. This functional graded monomorph is to be used as an actuator in smart structures and for active flow control. In addition, it is being evaluated as large area multiple integrated sensor arrays, accelerometer structures, and motor elements.

Hydrogen Storage Materials
Materials Science and Technology Division

The current state of development of Mg-based metal-hydride storage alloys has led to the concept of producing power compacts with varying amounts of Ni, which aids the kinetics of hydrogen absorption and desorption by catalyzing the dissociation of the H_2 molecule. Mixing and attriting Mg and Ni powers by high-energy ball milling, then compacting the mixture under high pressure, produces an alloy which absorbs and desorbs hydrogen much more rapidly than conventional alloys or power compacts and does so at reasonable temperatures and pressures. The improved behavior is obtained even with very low Ni content, thereby maintaining the low density of the alloy. The development of a low-density, efficient hydride-based hydrogen storage alloy will permit hydrogen to be used as a fuel in seagoing vessels, aircraft, and land vehicles. The current results with ball-milled Mg-Ni alloys are a major step toward that goal.

Modeling of Diamond Growth in Chemical Vapor Deposition Reactors
Laboratory for Computational Physics and Fluid Dynamics

Much effort has been directed toward producing reliable, reproducible, and economic growth of thin diamond films using chemical vapor deposition techniques. Thin diamond films exploit the high thermal conductivity and hardness—yet low electrical conductivity—of diamond in coatings for cutting tools, high-transmittance optical windows, thermal spreaders for electrical devices, and high-performance semiconductors. Theoretical analysis and modeling have been applied to understand and optimize the growth of thin diamond films in chemical vapor deposition reactors, using mixtures of alcohol and water vapor as feedstocks in the process. Three-dimensional simulations of flow in geometrically complex reactors were used to develop inflow and outflow configurations that promote mixing and optimal uniformity of the reactants over the growth surfaces. Improvements in the uniformity and robustness of

the growth process promise significant economies of scale in the production of diamond wafers for a variety of technological applications, including several relevant to the military in general and the Navy, in particular. The reactive flow modeling described is contributing to these goals.

Exciton-phonon Coupling in Semiconductor Nanocrystals
Condensed Matter and Radiation Division

Resonant and nonresonant exciton-polar complexes have been observed in nanoscale semiconductor quantum dots for the first time. A theory of exciton coupling with spherical phonons has been developed, which quantitatively describes the nanocrystal size dependence of the nonresonant and resonant hybrid exciton-phonon complexes. The sources of the discrepancy between calculated and experimental coupling strengths can now be investigated. This shows for the first time that we fundamentally understand exciton-phonon interactions in nanosize semiconductor crystals. Now we can proceed to investigate the sources of the discrepancy between calculated and experimental coupling strengths.

Transparent Conducting Oxide-stabilized Zirconia Films
Condensed Matter and Radiation Division

Transparent conducting films of metallic oxides (TCO) such as In_2O_3, SnO_2, and Sn-doped In_2O_3 have gained renewed attention recently because of their possible applications in solar cells, electrical heaters, antistatic coatings, transparent electrodes, display devices, and optical waveguides. In_2O_3 and SnO_2 are degenerate n-type semiconductors with high electrical conductivities and a wide bandgap that produces a high transparency in the visible but have an undesirable low melting temperature; they are unstable at $\geq$ 400° C. An electrically conducting film has been produced that one can see through. These could have practical applications in devices such as solar cells, electrical heaters for aircraft windows, antistatic coatings on instrument panes, transparent electrodes for ferroelectric photoconducting storage devices, display devices, and optical waveguides.

Prediction of Negative Electron Affinity for a Diamond Surface
Condensed Matter and Radiation Division

Electron emission from semiconductor surfaces can be enhanced by orders of magnitude if the conduction band minimum can be made—by suitable surface treatment—to lie higher in energy than the vacuum level. Electrons excited into the conduction band will be spontaneously emitted into the vacuum. Local density functional techniques and large-scale DoD computing facilities have been applied to address the problem of achieving electron emission from surfaces that are stable in hostile environments. Diamond is a very stable semiconductor, and several methods for growing diamond films have been developed during the past decade. It is found that a diamond (100) surface that is clean, oxygenated, and then cesiated, will have a surface electronic structure that is conducive to strong emission. Possible applications include photomultipliers for night-vision goggles, long-lived unheated photocathodes, flat panel displays, and high definition TV.

Laboratory Investigation of Velocity-Shear-Driven Plasma Instabilities
Plasma Physics Division

A major experimental effort in the Space Physics Simulation Chamber (SPSC) has produced the first verification of a mechanism thought to be responsible for observations of ions with more energy than typically found in the auroral ionospheres. The basis of the study is the production of a localized electric

field contained within the plasma column of the SPSC. Azimuthally rotating waves are produced by this field and are believed to be responsible for the observed ion energization. Both the waves and the enhanced energy levels are being investigated. Understanding the physical processes associated with basic plasma physics acceleration mechanisms has wide-ranging implications for the space environment and the direction of new research in this area. Understanding microscale physics, which result in macroscale phenomena, is necessary in ionospheric applications such as ground-to-satellite and satellite-to-satellite communications. Possible macroscale disturbances of the plasma environment must be understood as fully as possible when designing these communication links. Results of this nature have also been previously demonstrated in vastly different plasma physics parameter regimes, and the extrapolation to even more widely separated regimes is plausible.

GaN Materials and Devices for High-Temperature and Microwave-Frequency Applications
Electronic Science and Technology Division

The interest in the GaN material system has grown recently because of the development of high-efficiency blue-light-emitting diodes. These devices are being applied to flat panel displays and to automotive indicator lights. Although GaN technology is much less developed for electronics application, characteristics of this material offer significant advantages for high-temperature electronics, microwave power generation, and power-switching applications. Because of their excellent electrical characteristics and outstanding thermal and chemical stability, GaN and related III-IV materials are showing great promise for high-temperature active electronic devices. High quality GaN epitaxial layers on sapphire substrates have been achieved at NRL. Several types of applications for this technology are envisioned. Microwave FETs will find use in a wide range of radar and communications systems; GaN devices have potential as electric power control devices for all electric platforms such a motor vehicles, ships, and aircraft; and materials inherent high tolerance to radiation-induced displacement damage along with chemical inertness and high-temperature operation make GaN devices applicable to operation in hostile environments such as spacecraft. The progress in GaN materials and devices described here has brought these applications close to feasibility and has made the NRL research team one of the leaders in the field.

Visible Light Emission from Porous Silicon
Electronic Science and Technology Division

NRL has engaged in a broad-ranging program aimed at understanding the optical properties of porous silicon. We have shown that the luminescence properties of etched porous silicon nanostructures are not the result of quantum confinement but the result of emission from oxide-related defect center present at the surface of the silicon crystallites. This work has shown the importance of surfaces and interfaces in describing the optical properties of fabricated semiconductor nanostructures and also prevents futile efforts from being made in the manufacture of laser and other devices whose operation depended critically on quantum confinement. We may now be in a better position to provide optimized light-emitting diodes, chemical gas sensors, and optical down-converters making use of porous silicon luminescence properties.

In situ Detection of Environmental Contaminants Using the Flow Immunosensor
Center for Bio/Molecular Science and Engineering

An NRL flow immunosensor developed to provide instrumentation for detection of explosives in cargo and baggage areas—and later adapted to detection of drugs of abuse—has been adapted for the

detection of explosive contaminants at Navy and DoD bases. The sensor is based on antigen displacement of fluorescently-labeled antigen from antibodies immobilized on beads. Antigen is injected into a flow stream that passes over a column of antibody-coated beads saturated with fluorescently-labeled antigen. The displacement of the labeled antigen causes a proportional increase in fluorescence observed downstream. In field tests at DoD cleanup sites, the flow immunosensor was successful in detecting in parts-per-billion RDX and TNT present in ground-water and leachate samples. The NRL method has a clear advantage over other assays based on cost, analysis time, and simplicity. As a result of this success, the EPA has selected the NRL approach for a year-long field demonstration at the Naval Submarine Base at Bangor, Washington. Using this sensor for on-site testing, sample numbers could be increased at little or no additional cost to the user, providing more complete characterization as well as real time monitoring of cleanup efforts.

Forward-Scatter Detection of Quiet Submarines
Acoustics Division

The detection of diesel submarines in shallow-water environments is problematic, especially when the slow-moving diesel is operating on its electric power supply. In this case, active acoustic systems must be exploited. However, conventional active system concepts suffer from two major complications: the active target strength is low and markedly dependent on target aspect and multipath and boundary reverberation mask the desired target returns. Advances in our understanding of forward-scattering target physics and development of modally based source/receiver filtering approaches have led to the development of an exciting new concept to actively detect quiet targets (submarines) in shallow water. This approach has been demonstrated by simulation studies—first for beam aspect and then for multiaspect in a typical shallow-water acoustic environment. Further simulation studies demonstrated large area coverage possibilities and the ability to extract the "free field" target signatures from the complex acoustic returns. This demonstrated concept may provide the only practical approach to long-range detection of quiet diesel submarines operating in shallow-water regions.

First Light with the Navy Prototype
Optical Interferometer (NPOI)
Remote Sensing Division

Interferometric techniques have enabled astronomers to attain the highest angular resolution views of the universe. A successful interferometer requires the concurrent operation of a number of complex subsystems: telescope control, narrow-angle tracking, metrology, real-time fringe tracking, beam combination, vacuum, and data monitoring. NRL, world leader in the use of optical interferometry to attain high-precision stellar positions, has developed and operated the Mark III Optical Interferometer on Mt. Wilson. Operation of the Mark III showed it was possible to build a larger interferometer to meet the stringent requirements of Navy systems. NRL (with the Naval Observatory and ONR) has worked to construct a much larger NPOI facility on Anderson Mesa. The culmination of the first phase of construction of the larger facility was achieved with the detection of interference rings from several stars. The NPOI has now demonstrated that there are no potential problems in achieving full operational status and in providing absolute stellar positions with an accuracy of a few milliarcseconds. It will enable precise measurement of spectroscopic binary star orbits to provide direct measurements of stellar distances and masses, and it will provide a thousand-fold improvement in the angular resolution available to stellar astronomers.

Water Vapor Millimeter-Wave Spectrometer (WVMS)
Remote Sensing Division

Water vapor plays a central role in aeronomic processes in the mesosphere. It is the reservoir of odd hydrogen that catalytically destroys ozone. In addition, chemical time scales for water vapor in the mesosphere are sufficiently long and are excellent tracers of atmospheric motions. These measurements are made using a 22 GHz radiometer, which takes advantage of the change in the shape of the water vapor profile with pressure to obtain information on water vapor as a function of altitude from 40 to 80 km; that is, from a very dry "middle" atmosphere to a very "wet" troposphere. Two NRL-built WVMS instruments have provided continual measurements of water vapor in the middle-atmosphere from California and New Zealand. These instruments have provided the first continuous set of ground-based observations of middle atmospheric water vapor. The retrieved water-vapor profiles show an encouraging interannual consistency, and the seasonal variations show both the annual and semiannual cycles predicted by models of atmospheric transport. The WVMS data are being used to assist in the calibration of the UARS instruments.

Development of a Feature Model for Low-Grazing-Angle Sea Scatter
Remote Sensing Division

Low-grazing-angle radar backscatter from the sea surface exhibits polarization anomalies not observed at more moderate incident angles. An example are "sea spikes"—large echoes for which the horizontally polarized radar cross sections are often larger than those for the vertically polarized cross sections. Similar behavior has also been observed for the small-scale breaking associated with current rips and other mesoscale features resulting from strong wave-current interactions. A feature model has been developed that predicts many aspects of low-grazing-angle sea scatter not explained by other models. This model is the first to successfully explain many of the polarization anomalies that characterize low-grazing-angle sea scatter. Conventional models fail to account for scattering events for which the horizontally polarized echo strength exceeds that for vertical, yet these events often dominate backscatter in this regime. The model has also been used to explain distinctive features observed in the ultrawideband frequency and polarization responses of breaking waves in a wave tank.

The Importance of Coastal Filaments to the Northern Arabian Sea Phytoplankton Bloom During Southwest Monsoon
Oceanography Division

The Arabian Sea is an area with steady wind forcing during the regularly alternating northeast and southwest monsoons, with wind lulls in Spring and Fall. It is associated with plankton blooms and extremely high productivity during the southwest monsoon and with reduced productivity during the other monsoon. Impoverishment occurs during the Spring transition. These cycles of high productivity alternating with impoverishment are so extreme that they represent end numbers in the range of open-ocean productivity values. The coastal filaments, which are formed by the interaction of the northeast-ward flowing Omani coastal current with the prominent capes along the coast, extend offshore as jets with width scales of up to 100 km and surface velocities as large as 100 cm/s. The Navy needs all available environmental data for operational analyses and forecast models in variable littoral environments. Assessments of model predictions for specific environments are needed to extrapolate findings to areas lacking sufficient databases for operational requirements.

MCM Tactical Environmental Data System (MTEDS)
Marine Geosciences Division

Mine countermeasure (MCM) operations are significantly impacted by environmental influences on the performance of its combat systems. This is especially significant because this warfare area is almost exclusively conducted within the highly dynamic littoral regions of the world. The MCM force has limited capability in measuring needed environmental information in situ. The alleviation of this deficiency is the major purpose of the MTEDS program, which now has achieved most of its planned objectives. These include a major at-sea demonstration off Key West, Florida, designed to show that selected environmental data (bathymetry, current velocity profile, seafloor sediment classification, sound-speed profile, mine-hunting sonar-reverberation statistics, and differential GPS) can be measured in situ while a ship is underway, stored in a database within an on-board computer, and used for assisting in tactical decision making. With this capability clearly demonstrated at sea, the MCM community can transfer this technology to its surface ships using off-the-shelf technology. Also, on-board TAC 3 or 4 computers can be used to store the data, display it, and compute tactically significant information (for example, mine-burial probability).

Improved Tropical Cyclone Forecasts Using the Navy
Operational Global Atmospheric Prediction System (NOGAPS)
Marine Meteorology Division

Since the assimilation of the synthetic tropical cyclone (TC) observations into NOGAPS, NOGAPS has displayed significant TC forecast skill at 48 h and 72 h but little skill at 24 h. It was hypothesized that this lack of skill was largely due to deficiencies in the depiction of the TC steering flow by the NOGAPS initial state. To improve the depiction of the steering flow, the synthetic TC observations were modified to incorporate information of storm motion. An extensive impact experiment was conducted, and it was determined that this enhancement resulted in TC forecast track improvements of 20%, 10%, and 5% at 24 h, 48 h, and 72 h, respectively. After an operational implementation of this enhancement, the TC forecast performance of NOGAPS in the Atlantic was evaluated for Summer 1995. In comparison with the primary TC track-forecasting aid used by NOAA's Tropical Prediction Center, NOGAPS demonstrated forecast improvement of 5%, 13%, and 21% at 24 h, 48 h, and 72 h, respectively. The marked improvement in the NOGAPS 24-h forecasts, resulting from the incorporation of storm motion information along with more modest improvements to its demonstrated skill at 48 h and 72 h, has made NOGAPS one of the primary tools of Atlantic hurricane forecasters.

High-Efficiency Multilayer-Coated Gratings
Space Science Division

All materials have low reflectance at normal incidence in the extreme ultraviolet (XUV) and X-ray regions. Instruments operating in these wavelength regions typically use grazing-incidence optics that are costly to fabricate and align. These difficulties are overcome by using multilayer interference coatings that selectively reflect the waveband of interest at normal incidence. Diffraction gratings that have dramatically enhanced efficiency at normal incidence in the XUV ultraviolet wavelength region have been developed. These gratings have multilayer interference coatings that preferentially reflect wavebands of importance for the study of laboratory, solar, and astrophysical plasmas. The use of multilayer-coated gratings in the design of spectrometers extends the operating range of normal-incidence gratings to shorter wavelengths and allows the use of traditional normal-incidence instruments that are less costly and have lower weight and smaller size. These are important considerations for flight instruments that are designed for solar and astrophysical studies.

Germanium Strip Detectors
Space Science Division

Future progress in several areas of research and radiological applications requires the development of imaging-gamma-ray detectors with excellent energy resolution. Germanium strip detectors provide the best spectroscopy possible of any radiation detector now in use. They combine the excellent energy resolution typical of (coaxial) germanium detectors and the fine spatial resolution possible in a strip detector. These features are required to increase sensitivity to the gamma-ray line emission associated with nuclear decay in research and applications. They are applicable to and/or enable sensitive, high-spectral resolution, imaging gamma-ray detectors using coded-aperture, Compton telescope, or hard X-ray focusing techniques. The excellent performance of germanium compared to other detector types is essential to make the order-of-magnitude improvements in sensitivity required for the next major space mission.

Next-Generation Global Positioning System (GPS) Space Clocks
Space Systems Development Department

The design and construction of atomic clocks for satellites has required unique and highly specialized groups to produce one-of-a-kind designs, thereby limiting the availability and quality of these devices used primarily by the GPS program. The availability of production sources of these units has been a problem. A key design advance in clock technology for use in future GPS satellites has been demonstrated at NRL. An experimental cesium clock that is capable of using beam tubes from four different manufacturers was assembled and tested. This laboratory model exhibited performance at least as good as the tubes provided in their original vendor-built clock electronics. Previous cesium clocks used an analog signal of a few nanoamps to provide frequency error information from the beam tube to the servo-control electronics, and the beam tube received low-level signals back from the electronics. The primary feature of the new clock is a digital approach to interfacing the cesium beam tube to the control electronics. With the new NRL approach to a nearly all-digital electronic design to separate the cesium beam tube from the electronics, not only are the error sources and control instability significantly reduced or eliminated, but the design provides the basis for improved clock diagnostic and test information to be gathered and processed.

Smart Structure Technology Studies
Spacecraft Engineering Department

Analytical tools have been developed that enable implementation of smart structure technology into future Navy spacecraft missions. Smart structures refer to the active sensing and augmentation of system dynamics using integrated sensors and actuators for feedback and control. Three-dimensional and planar flexible body dynamics models of a spacecraft with two 50-m booms have been developed to study how on-orbit disturbances affect spacecraft pointing and the accuracy of space-based interferometric measurements, as well, and to analytically implement and simulate the performance of control strategies. A laboratory facility has been constructed as a test bed for experimental implementation of smart structure hardware and control algorithms. The 3.7-m, 12-bay truss is equipped with integrated proof-mass actuators and piezoelectric active struts for control and fiber-optic strain-gage sensors, force and displacement sensors, and accelerometers for feedback. In recent experiments, truss tip motion caused by a disturbing vibration was attenuated by a factor of 40, with an increase of damping by a factor of 20. Precision control of vibration in spacecraft structures will enable lighter and more capable space-based sensors that include multispectral instruments and radio and optical interferometers.

Meet the Researchers

NRL is proud of its numerous researchers. Every year, we feature some of these people so that you may get to know them and, as a result, understand how their diverse backgrounds come together to keep the Laboratory on the horizon of discovery.

Mr. H. Edward Senasack, Jr. is the acting superintendent of the Spacecraft Engineering Department (SED), one of two departments within the Naval Center for Space Technology (NCST). The SED team provides inhouse capability to develop new spacecraft and space systems through all program phases (from conception through operations). The facilities include state-of-the-art design, analysis, test, and fabrication functions, supporting an integration and test area housed in Building A59.

"NRL has built and launched more than 80 satellites and has continued the success of advanced technology demonstrations such as GPS development and, most recently, the *Clementine* mission. From its unique position within the Government, the SED draws on the best in new technology—the resources of NRL and other research institutes—to demonstrate and transition to industry new, more capable, lower cost components, subsystems, and systems that will better serve the military, scientific, and commercial space communities."

Mr. Senasack has worked with the engineers and scientists within the SED, NCST, and NRL for 25 years, to play a leadership role in how the vantage point of space is used for military and scientific missions.

Ms. Linda M. Schaus is an electronics engineer in the Radar Division and is principle investigator for the NAVSEA AN/SPQ-9B radar project. This project is a low-cost upgrade of the SPQ-9B radar that will provide it with an automatic sea-skimmer detection and tracking capability. Ms. Schaus is a key member of the design team that continues to implement an advanced development model (ADM) of the SPQ-9B. She is responsible for the radar signal processor, and she is a member of the team that tested the ADM at Wallops Island, Virginia, and on board the NAVSEA Self-Defense Test Ship.

"My career at NRL has been exciting and ever-changing. I have had the rare privilege of working on a new radar—from concept, through development and testing—and now implementation into the Fleet. NRL has provided me the opportunity to work with and learn from some of the most intelligent, respected, and enthusiastic engineers in the radar field. The SPQ-9B project has been successful not only because the concept was sound but because the engineering team was motivated and had the unique ability to work as a team. I look forward to continuing my work as a radar engineer at NRL."
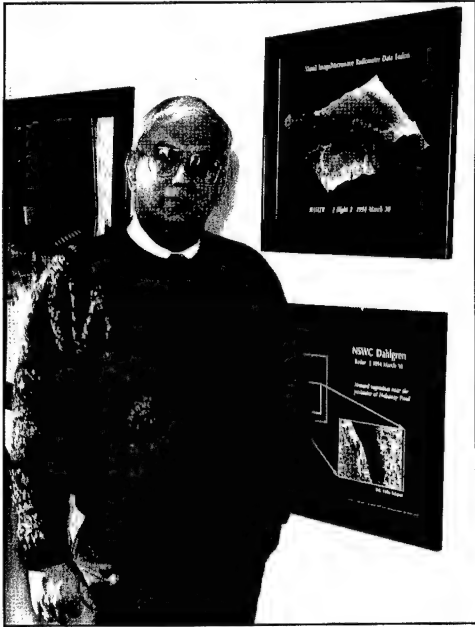
Dr. Philip R. Schwartz is superintendent of the Remote Sensing Division. The division is committed to the dual goals of bringing modern environmental remote sensing products to the operating Navy and Marines and to injecting advanced DoD sensing technology into the remote sensing community. Dr. Schwartz's own current research activities are focused on sensing and understanding the stratosphere, but he maintains a lively interest in astrophysics research. He has also been a prime mover in the use of classified data and systems for environmental research and for military operational support.

"Remote sensing overlaps many other areas at NRL but indirect measurement is its organizing principle. Because we are trying to measure some physical property or phenomenon from a distance, we usually measure a proxy—a radiance, a reflectivity, or some other influence. The trick is then to retrieve the quantity of interest and also to understand the errors or biases resulting from such an indirect measurement. Thus, although the result may be a practical technology, the path to its realization leads through very basic physics. This also explains how the areas of our scientific interest can be so diverse, ranging from astrophysics to the oceans, while the techniques end up being similar."

Mr. Steven Payne is a meteorologist and is associate superintendent of the Marine Meteorology Division in Monterey. The division is focused on developing and improving our capability to understand and predict both the weather and its influence on military operations around the world. This research effort is closely linked to DoD requirements for accurate environmental information and coordinates extensively with operational prediction centers within DoD and in the wider civilian community. The computer prediction models used operationally within DoD were developed by the staff at NRL Monterey.

"When I joined the laboratory in Monterey, it was not part of NRL. We were closely aligned with an operational center and could view first hand the impact of our projects and transitions. Many of us viewed our merger into NRL with some concern, worried that we might lose both our autonomy and our focus on operational transitions. But the merger has proven to be a success. NRL has supported our small research team approach while encouraging us to broaden horizons through training, professional travel, joint research projects, and temporary assignments. I continue to work in a challenging research field with the knowledge that my efforts contribute directly to the safety and success of Naval operations and now, also, to larger DoD and international environmental programs. Most importantly, NRL supports good people, friends and colleagues, role models, and mentors who have believed in my potential and encouraged my efforts. I am fortunate to be a part of NRL."

45

Featured Research

Naturally Occurring Biological Molecules as Environmentally Acceptable Corrosion Inhibitors

E. McCafferty and D.C. Hansen
Materials Science and Technology Division

Biological polymers that exhibit a strong affinity for metal surfaces are increasingly becoming important in the development of environmentally friendly, nonpolluting corrosion inhibitors and surface treatments. Recent research on iron and aluminum surfaces has involved the use of various metal complexing agents (siderophores) isolated from bacteria, the adhesive protein isolated from the common blue mussel (*Mytilus edulis* L), and simple catechols found in plant roots. A combined electrochemical and surface chemical approach has been used to determine the adsorption and effectiveness of the various organic molecules as corrosion inhibitors. Parabactin, a catecholate siderophore, was effective in inhibiting both the corrosion of iron in acid solutions and the pitting of aluminum in sodium chloride. The adhesive protein from the blue mussel was also effective in inhibiting the pitting corrosion of aluminum. These results are interpreted in terms of the molecular structure of the various organic molecules. Future research directions are also addressed.

INTRODUCTION

In recent years, there has been much interest in the development of environmentally acceptable, nonpolluting corrosion inhibitors. Chromates, for example, are excellent corrosion inhibitors and are used routinely in a variety of applications, including the surface treatment of aluminum alloys for commercial and military aircraft. However, there are major problems with the use of chromates as corrosion inhibitors or for the surface treatment of metals due to the toxicity of chromates to aquatic plants and animals, as well as their prolonged residence time in the environment.

Natural products constitute a new class of potentially useful corrosion inhibitors and/or additives for incorporation into anodized films or organic coatings. Such compounds are of interest because (1) they generally contain surface-active adsorbable functional groups, and (2) naturally occurring molecules are environmentally unobjectionable.

One of the current research thrusts in the area of corrosion has been the study and development of environmentally acceptable corrosion inhibitors. This article discusses recent research in the Materials Science and Technology Division [1,2] on metal-binding biological molecules — called siderophores, which are isolated from bacteria and on an adhesive protein isolated from the common blue mussel *M. edulis*.

Pure iron and pure aluminum were used as substrates. In the case of iron, deaerated 1 N HCl was used as the aqueous medium to provide a relatively high uninhibited rate and to allow dissolution of the air-formed oxide film on iron so as to focus on metal-inhibitor interactions. In addition, the behavior of iron in acid solutions is relevant to corrosion within confined geometries such as crevices or stress corrosion cracks, within which localized acidities develop. The pitting corrosion of pure aluminum was studied in deaerated 0.1 M sodium chloride solution, and the effect of selected inhibitors on the initiation of corrosion pits was determined.

BIOMOLECULES

Siderophores

Micro-organisms such as bacteria require ferric ions, which are normally very insoluble at physiological pH's. In response to this problem, bacteria excrete relatively low molecular weight chelators, called siderophores, which solubilize ferric ion for transport into their cells [3]. Three siderophores isolated from bacteria and one from a yeast have been studied as possible corrosion inhibitors for iron. These compounds are aerobactin, rhodotorulic acid, enterobactin, and parabactin; Fig. 1 shows their molecular structures. These compounds are also of interest because of the repetitive number of surface-active functional groups present in each molecule.

Based on their structural features, siderophores can be classified into two major types: hydroxamates or catechols. Aerobactin and rhodotorulic acid are hydroxamate siderophores while enterobactin and parabactin are catechol types. It is well known that in aqueous solutions, these siderophores form complexes with dissolved ferric ions through coordination of the hydroxamate or catechol groups. In the present work, where the aqueous medium is deaerated hydrochloric acid, the incipient air-formed oxide film on iron is dissolved away so that the various siderophores interact directly with the bare iron surface.

One of these compounds—parabactin—was also used as a corrosion inhibitor for the pitting of oxide-covered aluminum.

Mussel Adhesive Protein

The blue mussel, *M. edulis*, has evolved an opportunistic and permanent adhesive strategy in seawater that relies on the use of adhesive proteins contained in a holdfast [4]. This structure is composed of byssal threads ending in adhesive plaques at the points of attachment to the substrate (Fig. 2). Many of these proteins have a
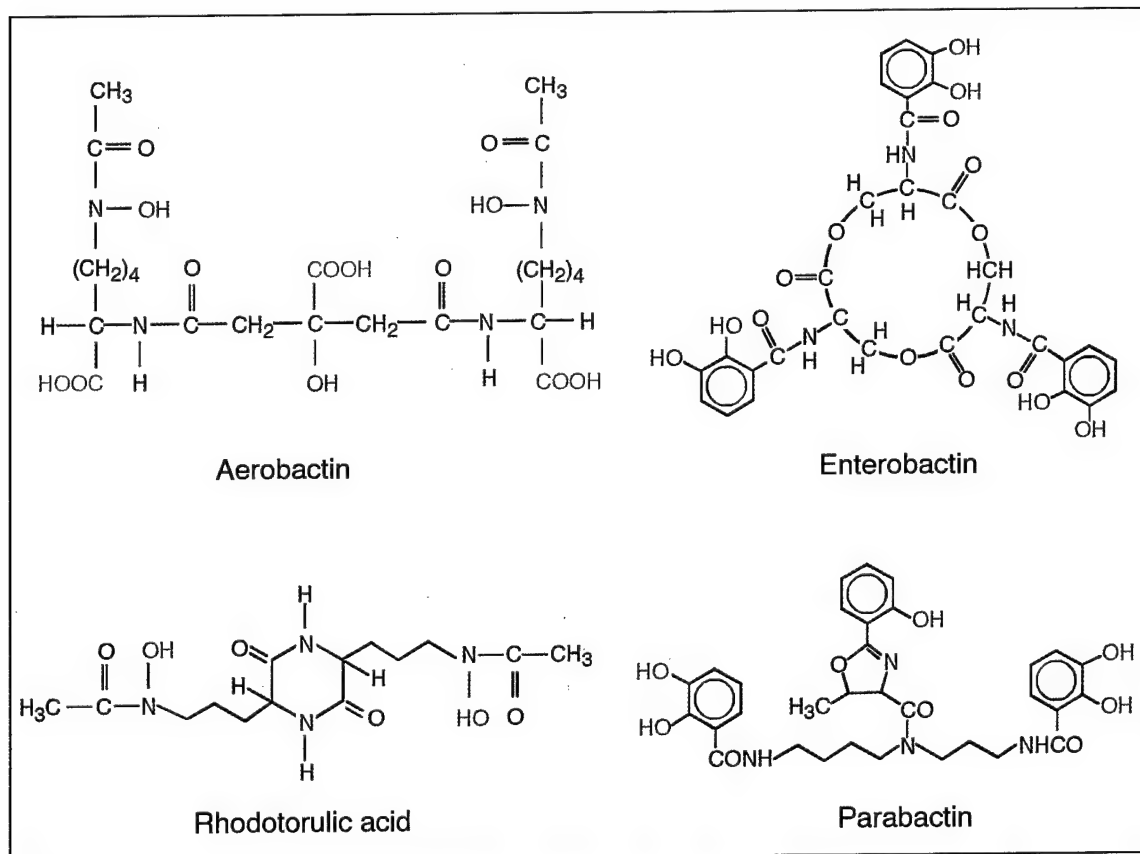
Fig. 1 — Structural formulas for the four siderophores.
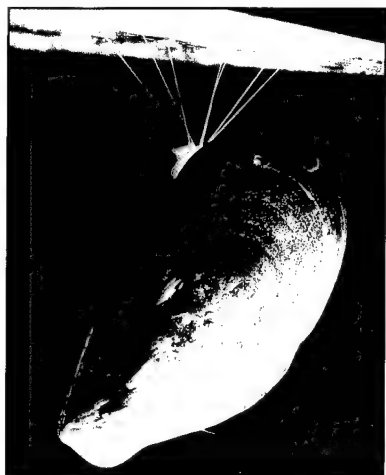
Fig. 2 — A mussel suspended by byssal threads from a glass plate to which it has attached itself.

common feature in containing varying amounts of the unique catecholic amino acid 3,4-dihydroxy-phenyl-L-alanine (dopa). The most abundant of these proteins is known as the mussel adhesive protein (MAP) and has a high molecular weight (> 100,000), is basic, and in addition to dopa, contains primary amines, hydroxyls, and phenols. The protein consists largely of a linear tandem array of decapeptide repeats, the consensus sequence of which is presented in Fig. 3. This sequence is repeated approximately 70 times in a linear fashion, and it is clear that the protein presents an overwhelming number of potential binding sites to a metal surface, including hydrogen bonding, dipole-dipole, and coulombic interactions. More importantly, dopa, like other catecholic groups, has the capability to chelate or couple to the metallic ions or metal oxides that are present at the metal-solution interface. The tenacity with which a mussel is attached to a piling or jetty is testimony to the irreversibility of the binding of MAP to a surface, even in the presence of water.

Recent evidence suggests that MAP, which is primarily contained within the adhesive plaques, is also distributed over the entire byssus as a natural coating or varnish. It has been proposed that this protein has a helical structure that places lysine and dopa residues on adjacent polymer chains within close proximity of one another so that intramolecular cross-linking can occur. The byssus of the blue mussel has been described as a quinone-tanned structure, the result of an oxidative process that leads to the polymerization of dopa-containing proteins. The first step in this process is the oxidation of dopa groups to o-quinones. In the second step, o-quinones are unstable and undergo nucleophilic attack from a nearby lysine residue, resulting in a covalent bond between two adjacent MAP molecules (Fig. 4).
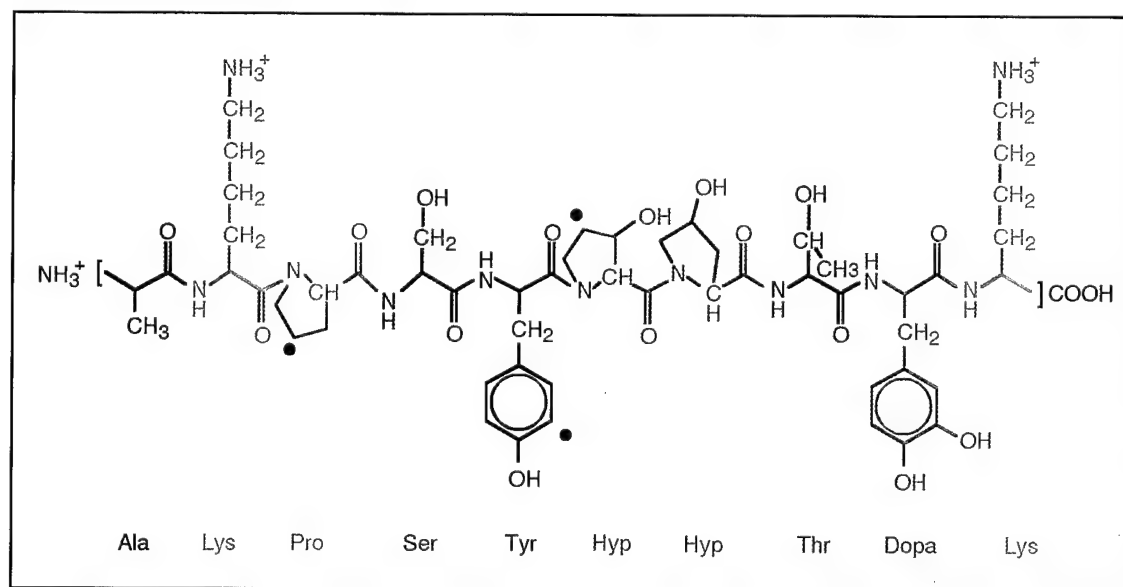
Fig. 3 — The repeating decapeptide sequence of the mussel adhesive protein (MAP) isolated from the blue mussel *M. edulis*. Dots on proline, tyrosine, and hydroxyproline denote positions of optional hydroxylation.
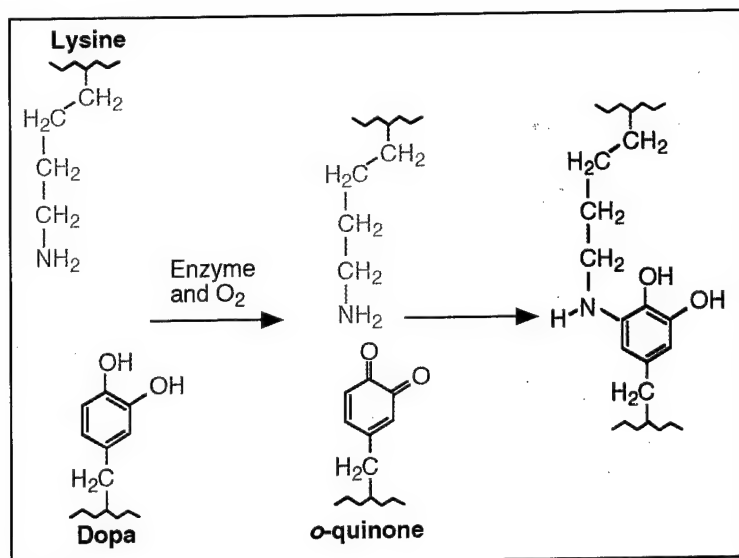
Fig. 4 — Possible cross-link reaction between dopa and lysine residues on adjacent MAP polymer chains.

A varnish is a transparent surface coating applied as a liquid, which then cures or polymerizes into a tough, solid thin film. Quinone-tanned structures, once fully cured and hardened, are insoluble in water, detergents, denaturants, organic solvents, cold dilute or concentrated hydrochloric, nitric, and sulfuric acids, have low antigenicity, and are highly resistant to proteases. These characteristics make the mussel protein a prime candidate as a potential corrosion-inhibitive coating when applied and cross-linked on a metal surface.

EXPERIMENTAL TECHNIQUES

Parabactin, enterobactin, and aerobactin were isolated from bacteria, and rhodotorulic acid was isolated from a yeast. All compounds were kindly provided by Dr. James V. McArdle, of SmithKline Beecham Pharmaceuticals and formerly of the University of Maryland. Isolation procedures were slightly different for each of the four siderophores, but each consisted of using a culture of the appropriate bacterium or yeast in an iron medium to form a ferric complex, from which the siderophore itself was subsequently isolated. In the case of rhodotorulic acid, for example, *Rhodotorula rubra* was cultured in a low-iron medium, the cells removed by centrifugation, the supernatant liquid concentrated and cooled, and the cystalline product purified by filtration through charcoal and recrystallization from hot methanol-water.

The mussel protein used in our experiments was purified from the feet of approximately 1000 mussels, using a method previously described [5]. In brief, the mussel feet were extracted with 0.7% perchloric acid, and the protein precipitate was solubilized in 5% acetic acid. Partial purification of the soluble protein was achieved via gel filtration liquid chromatography. Final purification was attained using reverse-phase, high-performance liquid chromatography (HPLC). This procedure yields approximately 30 mg of pure MAP.

The effectiveness of these various natural products in inhibiting the general corrosion of iron or the pitting of aluminum was investigated using standard dc and ac electrochemical methods in conjunction with surface analytical techniques.

SIDEROPHORES AS CORROSION INHIBITORS FOR IRON

Figure 5 shows corrosion rates (that is, current densities) for iron in 1 N HCl with and without an added dissolved siderophore. These corrosion rates were determined from electrochemical polarization curves (not shown) in which linear portions of the log current vs electrode potential are extrapolated back to the open-circuit corrosion potential to give the freely corroding rate. Aerobactin, enterobactin, parabactin, and rhodotorulic acid are each corrosion inhibitors in 1 N HCl.
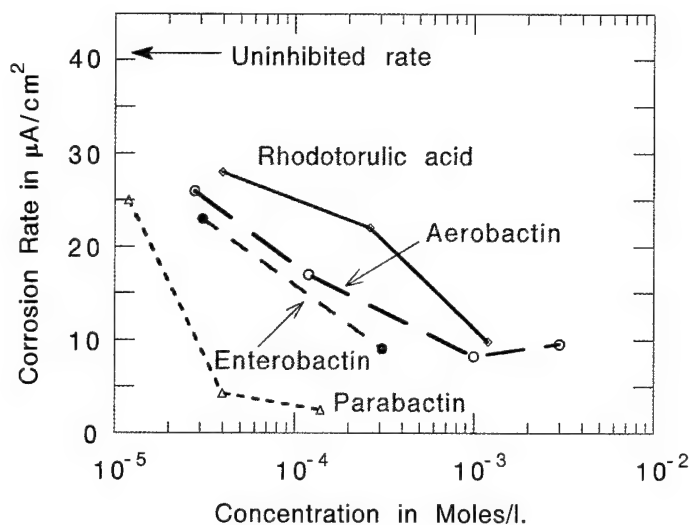
Fig. 5 — Effect of various siderophores on the
corrosion current density of iron in deaerated 1 N HCl.

For a given siderophore, the corrosion rate decreases with increasing concentration of added inhibitor. For a fixed concentration of siderophore, the corrosion rates in 1 N HCl follow the order:

rhodotorulic acid > aerobactin > enterobactin > parabactin,

with parabactin providing 93% inhibition at its solubility limit, where % inhibition = [i(uninhibited) - i(inhibited)]/i(uninhibited).

Figure 6 shows ac impedance data for uninhibited iron in 1 N HCl and for iron in 1 N HCl containing 3×10^{-3} M aerobactin. The data are displayed as Cole-Cole plots, in which the imaginary part of the complex impedance is plotted vs the real part. The best semicircle fitted through the data points intersects the X-axis at the values R_s and $(R_s + R_p)$, where R_s is the solution resistance and R_p, the more meaningful parameter, is the resistance to charge transfer processes. The higher R_p, the lower the corrosion rate. The addition of 3×10^{-3} M aerobactin increases the value
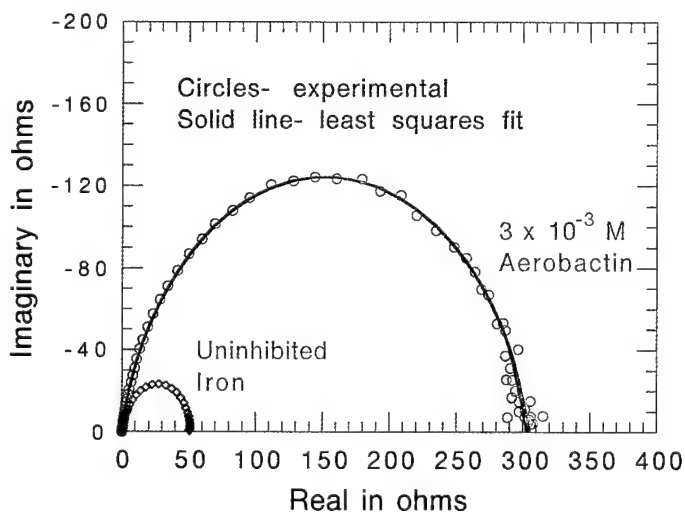
Fig. 6 — Cole-Cole plots for iron in deaerated 1 N HCl.

of R_p by a factor of nearly 10. For the four sidero-phores, the order of the R_p values in 1 N HCl in either a saturated solution or 10^{-3} M of the sidero-phore is:

rhodotorulic acid $\approx$ aerobactin $<$ enterobactin $<$ parabactin.

Thus, the order of effectiveness of the sidero-phores in increasing R_p is the same as the trend in decreasing corrosion rates.

The siderophores reduce the corrosion rate of iron by adsorption at the metal/solution interface. That adsorption occurs was confirmed by both electrochemical measurements and surface analy-sis. Double layer capacitances C_{dl} calculated from the Cole-Cole plots, as described previously [1], decrease from 89 $\mu F/cm^2$ for uninhibited iron to 35-55 $\mu F/cm^2$ in the presence of the various sid-erophores. This decrease in C_{dl}, which can result from a decrease in local dielectric constant and/ or an increase in the thickness of the electrical double layer, suggests that the siderophores func-tion by adsorption at the iron/solution interface.

Adsorption of the siderophores (rhodotorulic acid) at the iron/solution interface was verified by X-ray photoelectron spectroscopy (XPS). Figure 7 shows nitrogen 1s spectra for iron in solutions of rhodotorulic acid in deaerated hydrochloric acid or in methanol, as well as the result for the con-trol sample. The presence of the nitrogen 1s peak (and its absence in the control) clearly shows that rhodotorulic acid chemisorbs from solution onto the iron surface.

To understand the behavior of a series of inhibitors, account must be taken of the molecular area and the electron donating ability of the adsorbing inhibitor. Construction of molecular models shows that a multiple number of function-al groups can interact with the metal surface if the siderophore chemisorbs in a horizontal (flat) con-figuration. Table 1 lists the cross-sectional areas (in Å^2) for the siderophores in the horizontal con-figuration as determined from molecular models, which shows that the smaller the molecular cross-sectional area, the less effective the siderophore in reducing the corrosion rate—other factors be-ing equal.

The electron donating ability of a series of organic molecules can be estimated from their
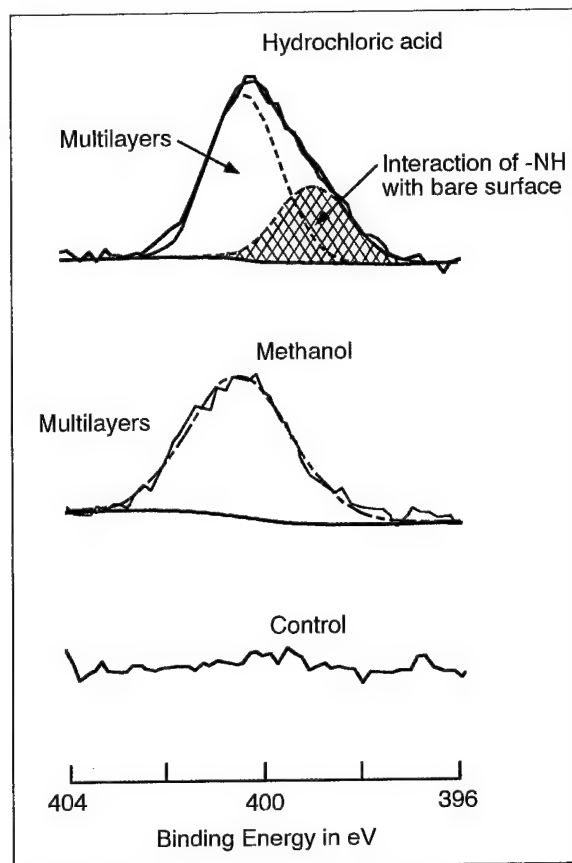
Fig. 7 — Nitrogen 1s XPS spectra for iron emersed from hydrochloric acid or methanol solutions of rhodotorulic acid.

acid dissociation constants pK_a. Table 1 also lists the first acid dissociation constants for the four siderophores used in this study. Larger values of pK_{a1} imply stronger conjugate bases and hence better electron donors. The two most efficient inhibitors—enterobactin and parabactin—have the optimum combination of relatively high values of pK_{a1} and the largest molecular cross-sectional areas. The increased efficiency of parabactin com-pared to enterobactin may be attributed to the presence of hydrocarbon linkages in the para-bactin molecule that do not occur in enterobactin. That is, the $-(CH_2)_4-$ and $-(CH_2)_3-$ chains in parabac-tin provide the molecule with a degree of flexibili-ty in accommodating itself onto the iron surface during the adsorption process so that a close-packed adsorbed layer is more likely to be formed than with enterobactin.

Table 1 — Molecular Cross Sectional Areas and Acid Dissociation Constants for the Four Siderophores.

Compound	Rhodotoruic Acid	Aerobactin	Enterobactin	Parabactin
Corrosion rates	Corrosion rates decrease in this order ⟶			
Cross sectional areas in ($\mathring{A}^2$)	39	55	91	88
First acid dissociation constant $pK_{a,1}$	8.49	3.11	7.6	7.89

NATURAL PRODUCTS AS INHIBITORS FOR ALUMINUM

Mussel Protein and Parabactin

The mussel protein used in our experiments was purified from the feet of approximately 1000 mussels, as described earlier, yielding a white powder that we used to make numerous solutions at various pH ranges and concentrations. The protein readily adsorbs from solution onto metal, therefore making application of the protein to a test sample very easy. Aluminum samples (99.995% pure) were incubated in one of the several protein solutions prior to the corrosion experiments. The corrosion experiments consisted of measuring the critical pitting potential of the metal samples in a 0.1 M sodium chloride solution. A positive shift in the critical pitting potential relative to the un-treated sample indicates an increase in the corrosion resistance of the metal.

For the samples treated with the protein solutions at the various pH ranges and concentrations, we found the best result to be for adsorbing the protein at a pH of 2.5, which resulted in a shift of the critical pitting potential by approximately +85 mV.

Figure 8 also shows that the pitting potential of parabactin saturated in 0.1 M NaCl raised the pitting potential of aluminum by a similar amount of approximately +85 mV.

Adsorption and Cross-linking of the Mussel Protein

Since the mussel protein was effective in inhibiting the corrosion of aluminum when it was adsorbed onto the metal from solution, the next step was to determine if we could cross-link the protein after it was adsorbed. In the mussel, this cross-linking is facilitated by an enzyme catechol oxidase and has been only partially character-ized. Instead, we used a commercially available enzyme — mushroom tyrosinase — that exhibits simi-lar activity on MAP. To do this, we adsorbed the protein from solution onto the aluminum samples as we had done before, only this time the protein solution was buffered to neutral pH with 0.05 M sodium phosphate and then the mushroom tyrosi-nase was added. The samples were allowed to air-dry and then immersed in sodium chloride solu-tion, and their pitting potentials were measured.

Figure 8 shows that the aluminum sample treated with MAP and tyrosinase exhibits a critical pitting potential of approximately −580 mV, which is a +100 mV shift compared to that of the untreated sample. The sample treated with buffer alone resulted in no significant shift of the pitting potential.

AC Impedance

To further determine what effect the MAP was having on the electrochemical behavior of aluminum, ac impedance measurements were made over a 12-day period. Figure 9 shows that the polarization resistance R_p values are higher for the aluminum sample treated with the MAP-tyrosinase than for either the MAP adsorbed at acidic pH, parabactin adsorbed from solution, or the untreated sample. This indicates that the oxide film on the MAP-tyrosinase sample has the highest resistance to charge transfer processes and is more resistant to breakdown by chloride ions.
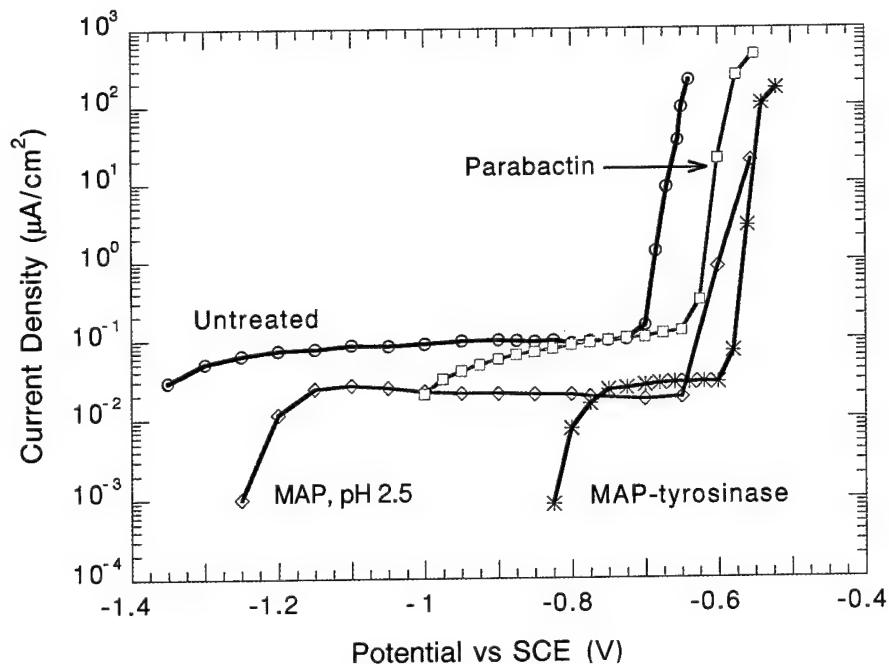
Fig. 8 — Anodic polarization curves of aluminum samples treated with MAP, MAP-tyrosinase, the bacterial siderophore parabactin, and an untreated sample.
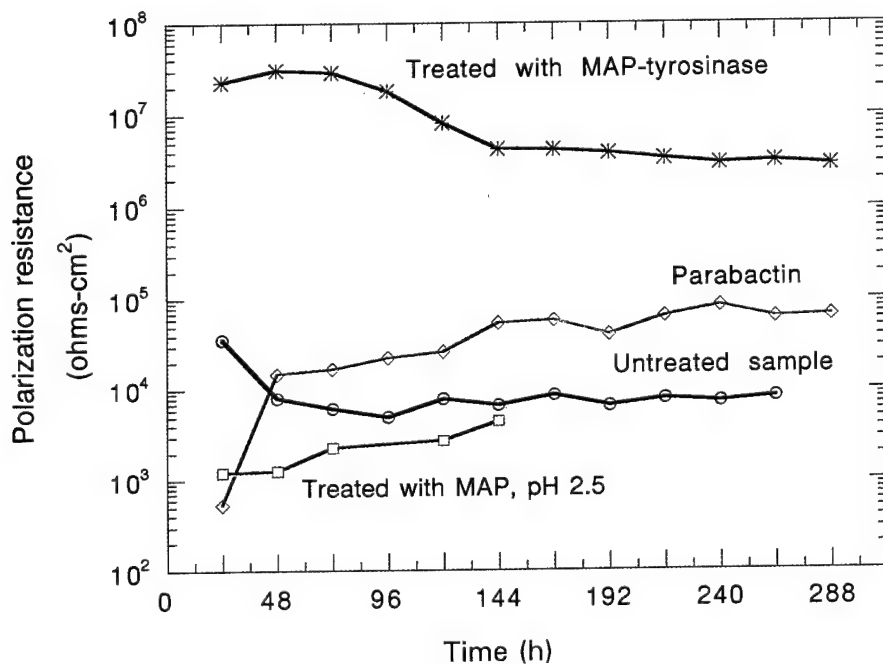
Fig. 9 — Polarization resistance values for aluminum samples treated with MAP, MAP-tyrosinase, the bacterial siderophore parabactin, and an untreated sample in deaerated 0.1M NaCl as a function of time.

Binding Sites at the Oxide Surface

A previous detailed study by the present authors using Fourier transform IR analysis of parabactin adsorbed onto aluminum from solution [2] has indicated that the catecholic functionalities are responsible for the adsorption of the siderophore to the aluminum sample. This adsorption is accomplished via the formation of a complex with the aluminum oxide layer by displacement of the −OH groups from the oxide, with the result being that parabactin acts as a surface chelator. In order to facilitate the binding of the catechols to the metal oxide surface, the siderophore is oriented in a horizontal plane.

Whereas parabactin relies primarily on its catecholic functionalities for adsorption to the metal oxide surface, the mussel protein presents a host of potential binding sites at the metal oxide/solution interface. Figure 10 is a summary of the various amino acid side chains and their roles as potential binding sites at the surface/solution/protein interface. Hydrogen bonding, dipole-dipole, and coulombic interactions can occur in conjunction with the coordination and chelation of metallic ions or oxides by the catecholic functional groups (that is, dopa). This heterogeneity in binding capabilities gives this biological polymer, and thus the mussel, the ability to adhere to a multitude of surfaces in the marine environment.

SUMMARY AND PROSPECTUS

The siderophores rhodotorulic acid, aerobactin, enterobactin, and parabactin are corrosion inhibitors for the general dissolution of iron in deaerated 1 N HCl. Parabactin and an adhesive protein isolated from the blue mussel *M. edulis* inhibit the pitting of aluminum in 0.1 M sodium chloride solution. These organic molecules function by adsorption at the iron/solution or oxide-covered aluminum/solution interfaces. These studies show that natural products have great promise as corrosion inhibitors.

Present research is focused on optimizing the effect of the mussel adhesive protein. Additional natural products and their analogs will also be considered. Future applications should address their potential incorporation into anodized films or organic coatings.

[Sponsored by ONR]

References

1. E. McCafferty and J.V. McArdle, "Corrosion Inhibition of Iron in Acid Solutions by Biological Siderophores," *J. Electrochem. Soc.* **142**, 1447 (1995).

2. E. McCafferty and D.C. Hansen, "The Corrosion Inhibition of Iron and Aluminum by Various Naturally Occurring Biological Molecules,"
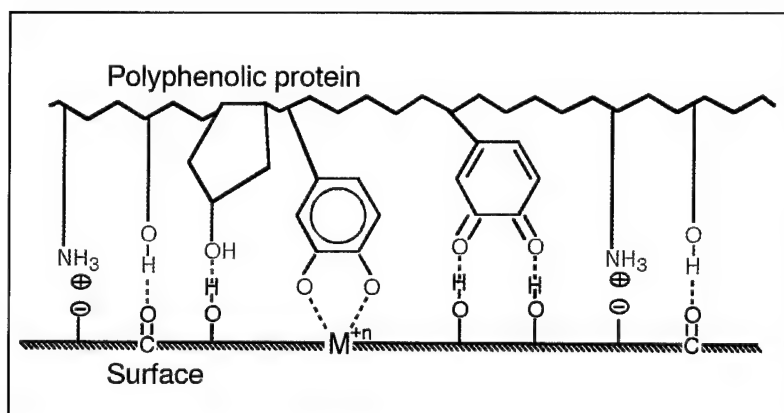
Fig. 10 — Possible molecular interactions between the adhesive protein isolated from the blue mussel and a surface.

in *Advances in Corrosion and Wear Resistant Coatings*, A.R. Srivatska, C.R. Clayton, and J.K. Hirvonen, eds., TMS, (1995), p. 183 and references therein.

3. S.R. Cooper, J.V. McArdle, and K.N. Raymond, "Siderophore Electrochemistry: Relation to Intracellular Iron Release Mechanism," *Proc. Nat. Acad. Sci.* **75**, 3551 (1978).

4. J.H. Waite, "Adhesion in Byssally Attached Bivalves," *Biol. Rev.* **58**, 209 (1983).

5. L.M. Rzepecki, S.S. Chin and J.H. Waite, "Molecular Diversity of Marine Glues: Polyphenolic Proteins from Five Mussel Species," *Mol. Mar. Biol. and Biotech.* **1**, 78 (1991). ∎

THE AUTHORS

EDWARD MCCAFFERTY is head of the Surface Protection Section in the Environmental Effects Branch at NRL. His areas of interest include corrosion science, electrochemistry, physical chemistry of surfaces, and surface modification. Dr. McCafferty holds a B.S. in chemistry from Wilkes College and an M.S. and Ph.D. in chemistry from Lehigh University. He will also receive an M.S. in applied mathematics from Johns Hopkins University in May 1996. He is the author or coauthor of nearly 80 publications, coeditor of two books, and has made over 70 technical presentations. He has received several awards, including the 1992 NRL Sigma Xi Award in Pure Science, the Victor K. LaMer Award of the American Chemical Society, and the William Blum Award of the National Capital Section of the Electrochemical Society. He has received NRL Publication Awards in 1974, 1984, and 1990. His professional experience also includes service as scientific officer in the Office of Naval Research and as a part-time faculty member at George Washington University.

DOUGLAS C. HANSEN received a B.S. degree in marine biology from Stockton State College in 1982, an M.S. degree in 1989, and a Ph.D. degree in 1993, both from the Marine Biology/Biochemistry Department at the University of Delaware. For his dissertation, he measured and characterized the adsorption and anticorrosive effect of the mussel adhesive protein on 304L stainless steel in seawater. He joined NRL as a National Research Council postdoctoral fellow in 1993, investigating organic corrosion inhibitors on aluminum. He joined the staff of the Environmental Effects Branch, Surface Protection Section in 1995 as a research chemist. His research interests continue in the field of natural products as corrosion inhibitors, specifically the interaction of biological polymers with metal surfaces, and biomaterials. Dr. Hansen is author or coauthor of more than 10 scientific papers.

A Deep Western Boundary Current in the North Pacific

Z.R. Hallock, W.J. Teague, and E.R. Fillenbaum
Oceanography Division

A Pacific deep western boundary current (DWBC) was discovered flowing southward along the continental slope of Japan. This discovery is based on 2 years of current velocity observations from four moorings arrayed across the Japan Trench near 35° N. Hydrographic measurements conducted at the beginning of the observational period provide further evidence that the DWBC is, to some degree, part of the global thermohaline circulation. Concurrent inverted echo sounder records and TOPEX altimetric data provide a time history of fluctuating Kuroshio positions. Similar fluctuations in DWBC volume transports suggest a link between Kuroshio and deep variability. These observations were made as part of the Naval Research Laboratory's Kuroshio Extension Regional Experiment.

INTRODUCTION

A Pacific deep western boundary current (DWBC) was discovered flowing southward along the continental slope of Japan. The significance of this discovery is comparable to the discovery of the North Atlantic DWBC, almost 4 decades ago [1]. The Pacific DWBC discovery is based on 2 years of current velocity observations from four moorings arrayed across the Japan Trench near 35° N [2]. Seawater property measurements conducted at the beginning of the observational period provide further evidence that the Pacific DWBC is, to some degree, part of the global thermohaline circulation.

In the Atlantic Ocean, where the Gulf Stream separates from the eastern seaboard, a DWBC passes beneath as a southward flow. The Atlantic DWBC is largely the result of the thermohaline circulation, which is predicted by the abyssal circulation theory of H. M. Stommel and A. B. Arons [3]. In this theory, the abyssal circulation is forced by uniform upwelling throughout the world's oceans. The upwelling is compensated by localized downwelling sources, primarily in the polar regions of the Atlantic. The resulting abyssal circulation consists of broad, slow flows in ocean basin interiors and concentrated return currents along northern and western boundaries. The downwelling sources affect the strength and sense of the boundary flows but not their locations. Hence, northern and western deep boundary currents are predicted for the other oceans as well. The presence of the primary downwelling source in the Greenland/Norwegian Sea area accounts for the prominence of the Atlantic DWBC. In the North Pacific, the theory predicts a boundary flow westward along the Aleutians and southward along the Kamchatka Peninsula and the coast of Japan to about 30° N. North Pacific deep boundary currents are predicted to be considerably weaker than those in the Atlantic due to the lack of downwelling sources of deep water.

While it is not reasonable to expect a Pacific DWBC comparable in magnitude to that found in the Atlantic, we present evidence that a diminished, but significant, deep boundary flow does exist. We further show an apparent link between fluctuations in Kuroshio position and volume transport of the deep flow. The observations described here include 2 years of current meter velocities, inverted echo sounder, and satellite altimeter sea surface heights shoreward of, in, and seaward of the Japan Trench. The location of

these observations, which include four current meter moorings (each with two to four instruments), is shown in Fig. 1 (which also shows locations of other investigations). This effort was part of the Kuroshio Extension Regional Experiment (KERE) conducted by the Naval Research Laboratory (NRL) and the Office of Naval Research.

BACKGROUND

As a test of the proposition of a deep northern boundary flow in the Pacific, B.A. Warren and W.B. Owens, of the Woods Hole Oceanographic Institution [4], conducted temperature and salinity (hydrographic) profile measurements of sections across the Aleutian Trench along 175° E, 175° W, and 165° W (Fig. 1). They also placed current meter moorings along the central section. From hydrographic properties and directly measured currents, they concluded that a narrow current flows westward north of the trench, but a broader, eastward current exists above the trench and Aleutian Rise. In sections across the Kuril-Kamchatka Trench near 47° N, tracer distributions indicate northward flow above the trench, but an extremely narrow southward boundary flow inshore of the trench [5]. The relatively instantaneous nature of accompanying acoustic Doppler current profiler and geostrophic velocities calculated from density gradients may explain disparities with inferences from the tracers, which are

more representative of mean conditions. Long-term direct current measurements were not part of these studies.

Much earlier, a southward flowing current was found near 3000 m off the coast of Japan, using neutrally buoyant floats [6]. However, these observations were relatively short-term, Lagrangian measurements carried out at different locations at different times. The result most pertinent to those presented here is a southwestward current at 3000 m, above the seaward flank of the trench at 38° N, having a 3-day average magnitude of 1 to 4 cms^{-1}. There have been other measurements of this type that also suggest southward flow inshore of the Japan Trench, but as with the earlier observations, data were rather time-limited and not necessarily representative of long-term mean conditions.

More recently, Japanese investigators [7] have analyzed several long current meter records from two locations on the slope off Hokkaido. The first was in water of depth 4000 m at 41°30′ N, 144°30′ E, where yearly mean currents at 3000 m were west-southwestward between mid-1990 and 1992 and between mid-1993 and 1994. Magnitudes ranged from 1 to 3 cms^{-1}. Between mid-1989 and 1990, the mean flow was about 1 cms^{-1} to the northeast. This record showed considerable variability on shorter time scales. The second, at a similar depth, was located at 42°05′ N, 145°21′ E in 3560 m of water, about
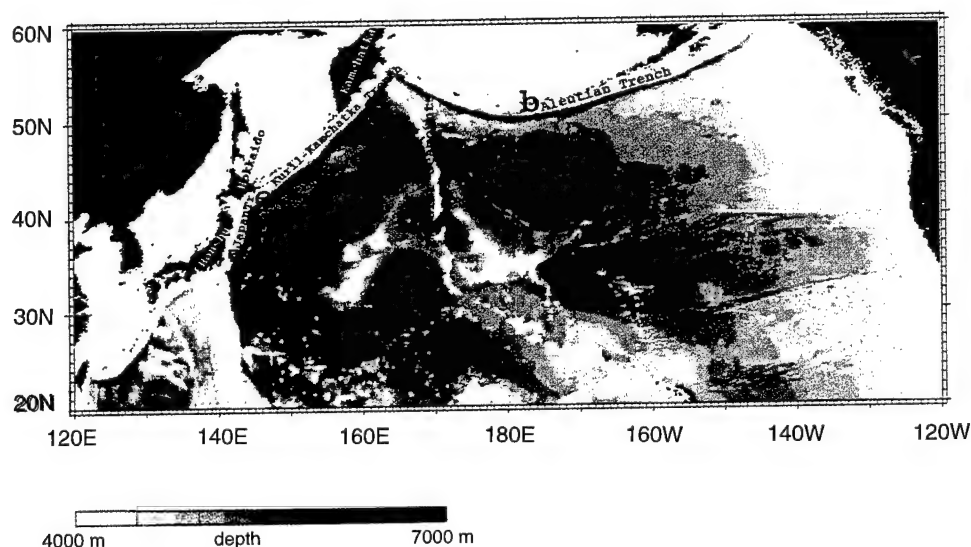
Fig. 1 — North Pacific showing locations of various observations discussed in text: KERE section (a); Warren and Owens [4] (b); Talley [5] (c); Nan'niti and Akamatsu [6] (d); Kawasaki and Kono [7] (e).

90 km to the northeast. During the first year, the current underwent a complete cycle in direction, flowing first westward for several months, northeastward for the next several months, and then southeastward, resulting in a mean speed close to zero. Speeds during the first year were less than 1 cms^{-1} most of the time. During the second year, however, the current was quite steady to the west-southwest at about 1 cms^{-1}. It is interesting to note that for the 1991-1992 period, the result from the first mooring is quite different from that of the second, even though both records are from nearly the same isobath along the slope. Different bottom slopes at the two locations may be a factor. Furthermore, bottom contours change from an essentially north-south orientation to northeast-southwest in this area, and the sill between the Japan Trench and the Kuril-Kamchatka Trench is quite close to Miyake's mooring.

Pacific Ocean simulations using an NRL eddy-resolving model [8], which do not explicitly contain thermohaline sources or sinks, reproduce both the position and major features of the Kuroshio Extension. The simulations show that there are very significant links among specific topographic features, mean currents in the abyssal layer, and mean upper-layer currents. More specifically, the instability of the Kuroshio Extension is strongly controlled by the abyssal currents and the large scale bathymetric gradient. The authors [8] hypothesize that the combined impact of baroclinic instability and specific bathymetric features are critical for determining the mean path and variability of the Kuroshio Extension; this work shows that the model produces an eddy-driven southward flow along the continental slope of Japan.

In the light of earlier results, we pose the following questions. Does a persistent deep boundary current exist along the continental slope of Japan? If so, what are its characteristics? Is it affected by local, shallower processes? Is it part of the global thermohaline circulation?

MEASUREMENTS CONDUCTED DURING THE KERE

In the region where the Kuroshio turns eastward from the coast of Japan, in-situ measurements were made between summer 1992 and summer 1994 by NRL as part of the KERE. Other NRL KERE components were numerical modeling and analysis of TOPEX/POSEIDON (T/P) satellite altimetry data.

The in-situ measurements included current meter moorings (CMMs) and inverted echo sounders (IESs) deployed for 2 years (with a reset after 1 year), temperature/salinity, and water sampler profiling (hydrography) during the 1992 deployment cruise, and expendable temperature probe (XBT) drops made at IES sites. The emphasis in this article is on the current meter observations. Some discussion of the hydrography is included, and details can be found in a companion study [9]. The locations of the CMMs and IESs are indicated in Fig. 2, which also depicts the mean path of the Kuroshio (based on satellite infrared imagery) for the 1991-1994 period. It is worth noting that the KERE section is directly beneath a T/P descending groundtrack. The two settings of the moorings are henceforth referred to as "Year 1" (Summer 1992 to Summer 1993) and "Year 2" (Summer 1993 to Summer 1994).
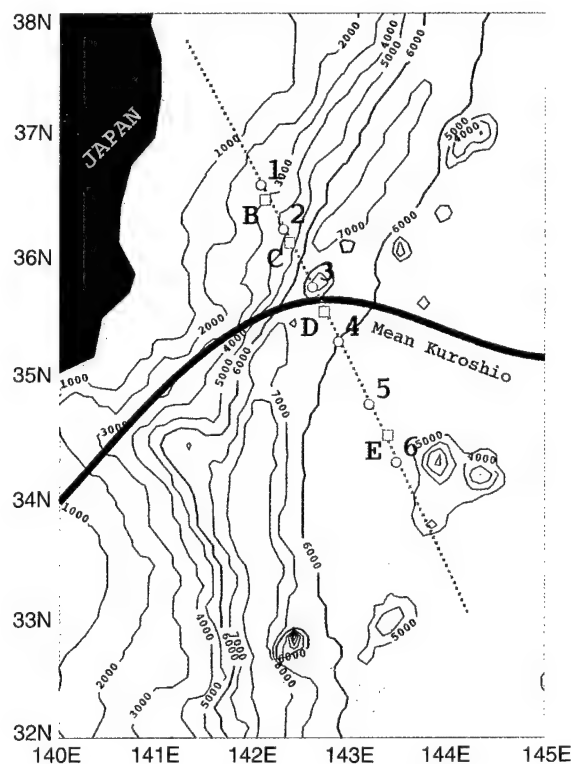
Fig. 2 — KERE area showing current meter-mooring locations (squares), inverted echo sounder locations (circles), the coincident TOPEX/POSEIDON groundtrack (dotted) and bathymetry.

61

Two of the CMMs (B and C) were located on the slope, inshore of the Japan Trench, CMM D was in the trench, and CMM E was farther southeastward. Kashima 1 Seamount, also in the trench, is near the D site and rises to a depth of about 3500 m northwest of CMM D. IESs 1 and 2 were on the slope, IES 3 was on the seamount, and IESs 4-6 were offshore on the trench. The vertical arrangement of the current meters (CMs) and IESs is shown in Fig. 3 where shading of symbols indicate data recovery. For example, a shaded right-half of a symbol indicates a full record for the second deployment (Year 2). Bottom topography in Fig. 3 is based on the Earth Topography 5 Minute (ETOP05) database, but some discrepancies were found during predeployment bathymetric surveys during the cruises. This bottom profile crosses the southern flank of Kashima 1 Seamount, which rises northeast of the mooring line. CM depths indicated in Fig. 3 are planned depths; actual minimum, deployed depths are listed in Table 1. The differences are important only for the CMs in the thermocline (near 400 m).

The CMs used were Neil Brown-EG&G acoustic current meters (ACM-II). The accuracy of the ACM-II is ± 1 cms^{-1}, or 5% (whichever is greater), for individual velocity samples. For long-term means, however, the effect of instrumental error is much reduced and insignificant relative to the statistical uncertainty of the means (discussed below). IESs measure round-trip acoustic travel time between the sea surface and the instrument (bottom). Changes in this travel time are governed by the heat content of the water column and are proportional to changes in thermocline depth. Baroclinc changes in sea surface height are then inferred from changes in thermocline depth with an rms accuracy of about 5 cm.

Good data were retrieved from 19 CMs. Data recovery was best from the second deployment. Data return was reduced because of instrument flooding (1), battery leakage (1) and electronics or recorder malfunctions (5). Some velocity records required corrections for unanticipated zero-offset errors, which reduced magnitudes and slightly changed directions of some of the means but did not change the sense of any of the meridional components. For the analyses presented here, CM velocity components and IES travel times were low-pass filtered (filter half-amplitude point at 40 h) to remove high-frequency fluctuations such as tides.

Yearly averages of horizontal velocity components (U is eastward, V is northward) are calculated for each CM record. Means (with uncertainties) and standard deviations are listed in Table 1. Tabulated uncertainties are statistical errors based on decorrelation times (T_U, T_V; also in Table 1) calculated from the data records (U, V). Each series (for example, U) is broken into ns segments of length T_U. The mean of each segment is calculated, followed by the standard deviation σ_s of these segment means about their overall mean. The error then is just $\sigma_s/\sqrt{ns}$. Mean velocity vectors are plotted over bathymetry in Fig. 4 (Year 1) and in Fig. 5 (Year 2), where CM depths are color-coded. Note that vectors for thermocline-level instruments have a different magnitude scale.
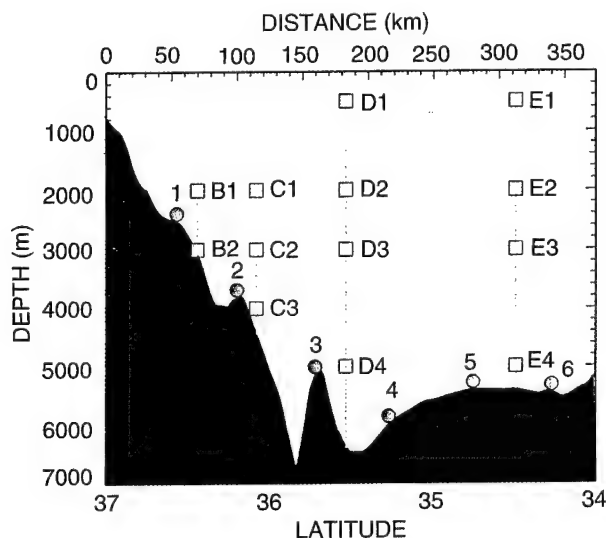
Fig. 3 — Vertical arrangement of current meters (squares) and inverted echo sounder locations (circles), with bathymetry. Shading in the symbols indicates data recovery; for example, the shaded right half of the square at C2 indicates a complete data record for Year 2 (1993-1994) but not for Year 1 (1992-1993).

Table 1 — Current Meter Statistics

Meter ID (Year 1)	Location	Depth (m)	$\bar{U}$ (cms^{-1})	T_U (days)	σ_u (cms^{-1})	$\bar{V}$ (cms^{-1})	T_v (days)	σ_v (cms^{-1})
B1	36°27′ N, 142°06′ E	2043	−1.0 ± 0.5	7	4.0	−1.6 ± 0.6	13	5.0
B2		3043	−0.3 ± 0.5	7	4.1	−0.5 ± 0.9	17	4.4
C1	36°05′ N, 142°22′ E	2160	0.6 ± 0.3	4	2.6	−1.0 ± 0.8	21	3.4
C3		4160	−0.2 ± 0.3	8	2.1	−1.9 ± 0.7	16	3.2
D1	35°31′ N, 142°43′ E	409	32.8 ± 3.8	20	15.5	10.0 ± 4.1	30	13.9
D2		1909	8.9 ± 2.0	27	5.5	3.6 ± 1.6	24	6.1
E1	34°30′ N, 143°23′ E	517	14.0 ± 3.5	47	15.9	−0.3 ± 2.8	35	13.9
E4		5017	0.0 ± 0.4	8	3.2	−4.3 ± 0.7	6	4.9

Meter ID (Year 2)	Location	Depth (m)	$\bar{U}$ (cms^{-1})	T_U (days)	σ_u (cms^{-1})	$\bar{V}$ (cms^{-1})	T_v (days)	σ_v (cms^{-1})
B1	36°27′ N, 142°07′ E	2017	−0.6 ± 0.3	7	2.5	−1.3 ± 0.6	13	3.2
C1	36°05′ N, 142°22′ E	2145	−0.3 ± 0.4	11	2.5	−0.8 ± 0.4	25	2.4
C2		3145	−1.4 ± 0.3	20	2.3	−1.4 ± 0.7	13	3.1
C3		4145	0.1 ± 0.1	4	1.2	−2.6 ± 0.6	15	2.9
D1	35°33′ N, 142°40′ E	324	26.5 ± 5.0	13	24.6	4.3 ± 1.9	6	14.6
D2		1824	5.9 ± 0.9	9	5.6	3.5 ± 0.7	5	6.5
D3		2824	3.1 ± 0.7	10	3.6	4.2 ± 0.7	12	3.6
D4		4824	−2.1 ± 0.6	5	5.3	2.4 ± 0.3	5	2.5
E2	34°30′ N, 143°23′ E	1984	3.6 ± 0.4	6	3.1	−1.0 ± 0.6	7	4.1
E3		2984	2.9 ± 0.5	7	3.4	−1.5 ± 0.6	8	4.5
E4		4984	2.8 ± 0.6	6	4.6	−4.6 ± 0.8	6	5.5
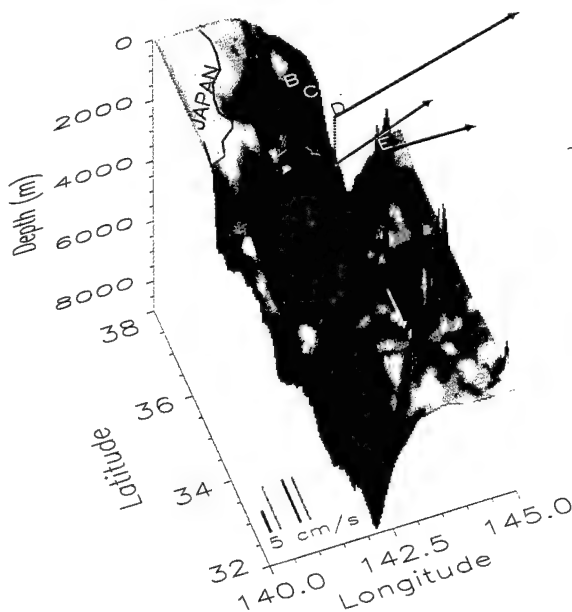
Fig. 4 — Mean velocity vectors are shown for Year 1 superimposed on the bathymetry. Depths of instruments are color-coded; actual deployed depths appear in Table 1. The vector lengths correspond to velocity magnitude (see inset scale).
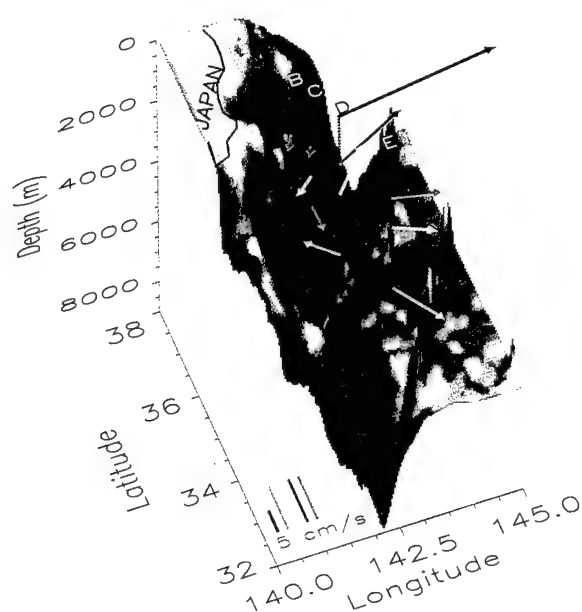
Fig. 5 — Mean velocity vectors are shown for Year 2 superimposed on the bathymetry. Depths of instruments are color-coded; actual deployed depths appear in Table 1. The vector lengths correspond to velocity magnitude (see inset scale).

The uppermost instrument on each mooring recorded pressure, which is used to estimate the vertical excursions of the CMs as a result of mooring motion. Direct mooring motion contamination of measured velocities due to lateral movement of the current meters is minimal, but thermocline instruments (D1, E1) sampled a range of depths where vertical shear was high, introducing some uncertainties in depths associated with calculated means. This effect is negligible for instruments at 2000 m and deeper. For D1 and E1, mean depths are only slightly deeper than the minimum values and standard deviations are relatively small, indicating that large excursions are anomalous. Statistics of velocity components are unchanged from those in Table 1 when recalculated after omitting segments of the D1, E1 records where depths were deeper than their respective minimum values by at least 100 m.

MEAN CURRENTS

The mean Kuroshio is apparent at D1, D2, and E1. A decrease in current speed at D1 for Year 2 is accompanied by an increase in variability (Table 1), implying increased meander or eddy activity. Counterclockwise (clockwise) changes in direction with depth at D (E) show the transition from the east-northeastward-flowing Kuroshio and the northward (southward) deep flows. At D4, which is deeper (5000 m) than the peak of the Kashima-1 Seamount, the mean flow is northwestward, consistent with predicted anticyclonic flow of a stratified Taylor column around such a feature. Inshore of the Japan Trench (B, C), the yearly mean flows are generally directed southward along the isobaths, with magnitudes ranging from about 0.5 cms^{-1} to 2.6 cms^{-1}. All but B2 (Year 1) have negative meridional components that are significantly different from zero. These magnitudes are consistent with westward annual means found inshore of the Aleutian Trench [4]. We estimate mean meridional volume transports along the slope at 2 Sv (1 Sv = 1 × 10^6 m^{3}s^{-1}), based on current records from moorings B and C.

B.A. Warren and W.B. Owens [4] use maps of potential temperature (θ) to delineate regimes of deep flow in the northwest Pacific. They associate cold tongues (minima) with the boundary between westward, along-slope flow, and eastward flow above the Aleutian Trench. We extend

their analysis of θ at 4000 m to the vicinity of the KERE observations (Fig. 6). A cold tongue (θ < 1.15° C) parallels the coast to about 35° N, where it becomes more irregular and shows signs of turning eastward. Between 150° E and 160° E, another cold feature is evident, which extends eastward. All the KERE observations fall westward of the primary cold tongue in Fig. 6, but a narrower, cold feature (θ < 1.15° C) lies along the trench. Variability at 4000 m appears to be greater south of about 40° N than father north and off the Aleutians. The horizontal variability apparent in Fig. 6 is probably more the result of aliasing of temporal changes than of real horizontal structure in the mean temperature. This view is supported by examination of the relative importance of current velocity variance in the KERE region compared with that of Warren and Owens. In particular, the ratios of the magnitude of mean currents to standard deviations calculated with the KERE CM data (as well as from the results of other investigators) are typically only one-third to one-half the ratios calculated with Warren and Owens results.
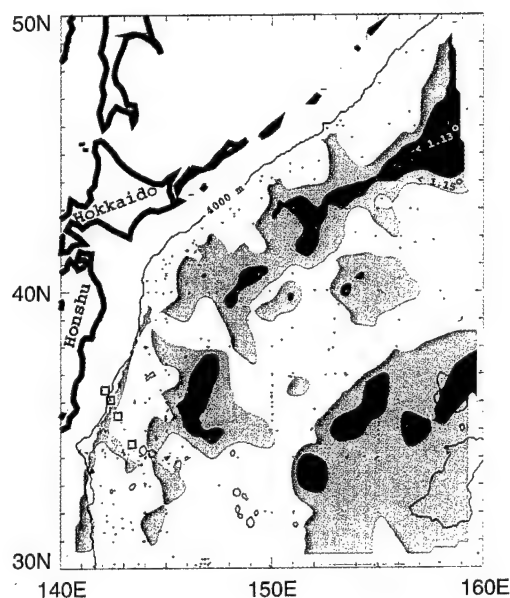
Fig. 6 — Map of potential temperature (θ) at 4000-m depth for the KERE region and northeastward. KERE current meter moorings are indicated by squares. The analysis is based on historical hydrographic observations; station locations are indicated by pluses. The 4000-m depth contour is included.

This variability tends to obscure inferences of thermohaline flow from time-limited observations such as the KERE hydrographic section and from historical data sets (Fig. 6) where temporal aliasing and smearing can occur. Anomalies of a chemical tracer (such as the concentration of silica) may indicate a distinct source of a particular flow in a more integral way, minimizing the effect of temporal aliasing [5]. Positive silica anomalies near mooring B between 2000 m and 3300 m are consistent with a southward transport of water from the Bering Sea or northeast Pacific. Likewise, a negative silica anomaly found between moorings C and D (in the same depth range) is consistent with northward flow from a southern region.

At our southeasternmost mooring, we see a 2-year mean southward component of flow. In this region, depth decreases slowly to the west with a slope of about 1×10^{-3}. According to a later study by H.M. Stommel and A.B. Arons [10] a broad, equatorward flow is consistent with a slope of this magnitude and can coexist with a narrow boundary flow such as that seen at B and C. Approaching the Japan Trench, the slope decreases and depth reaches a minimum just seaward of mooring D, where a deep northward flow is encountered. Poleward flows were not considered in their treatment. Due to the complex bottom topography in this region, deep mean flows are likely to be locally intensified and more complex than those predicted by this type of model, even when simply sloping bottoms are included. Also, narrow features may be undersampled by existing mooring data. Further potential problems with the Stommel-Arons model arise with recent observations showing that the upwelling of abyssal water is not uniform everywhere [11]. Hence, observed flows in the region are likely comprised of local recirculations driven by topography and eddy fluxes, superimposed on the large-scale thermohaline flow.

FLUCTUATIONS OF THE CURRENTS

The Kuroshio exhibits strong variability in the KERE observational area. This variability primarily takes the form of meanders (defined as changes in direction and cross-stream position). Meanders sometimes increase or decrease in amplitude as standing waves, or they can propagate alongstream (usually downstream). A useful measure of variability is the eddy kinetic energy (EKE), defined as the kinetic-energy-per-unit mass associated with the velocity field with the mean removed. This is half the sum of the variances of the velocity components (that is, from Table 1: EKE = 0.5 $(\sigma_u^2 + \sigma_v^2)$). EKE is plotted as a function of latitude for all CM records in Fig. 7. The salient results are a significant increase in EKE from Year 1 to Year 2 for the shallowest instrument in the Kuroshio (D1) and for deeper instruments on moorings D and E. There is a concurrent decrease in EKE for B1. For the D1 records, there is a corresponding decrease in the kinetic energy of the mean (see Table 1), consistent with a general increase in eddy or meander activity in the Year 2. These results further suggest a dynamic link between Kuroshio variability and that of the deep currents.

Another way to assess eddy activity is to examine the decorrelation times T for the velocity components (Table 1). Relatively longer values of T indicate the presence of longer period coherent structures or events, such as eddies. This is the case for records from instruments located in the thermocline and/or near the Kuroshio influence (D1, D2, E1). This result is anticipated near such mesoscale features. What is perhaps more interesting is that for all the deep slope instruments (on moorings B and C), with the exception of C2 (Year 2), T_v is considerably greater than T_u. The implication is that the velocity components are governed by different dynamics, with the longer time scales roughly associated with the alongslope direction, further suggesting strong topographic interaction.

While EKE and other quantities at instrument locations provide quantitative information about the flow field, more integral analyses better describe specific phenomena. We take such an approach to examine the relationship of Kuroshio changes to the strength of the DWBC. Figure 8 is a time history of surface height along the KERE section. It is based on a combined analysis of hydrography, IES records, and T/P altimetry [12]. Lateral shifting of the axis region (red band) of the Kuroshio is evident, changing on a time scale of about 100 days. Strength of the component of flow normal to the section is proportional to the height gradient along the section. Since meandering is mostly due to changes in lateral position and direction rather than flow magnitude, changes in the gradient (width of the red band) mostly
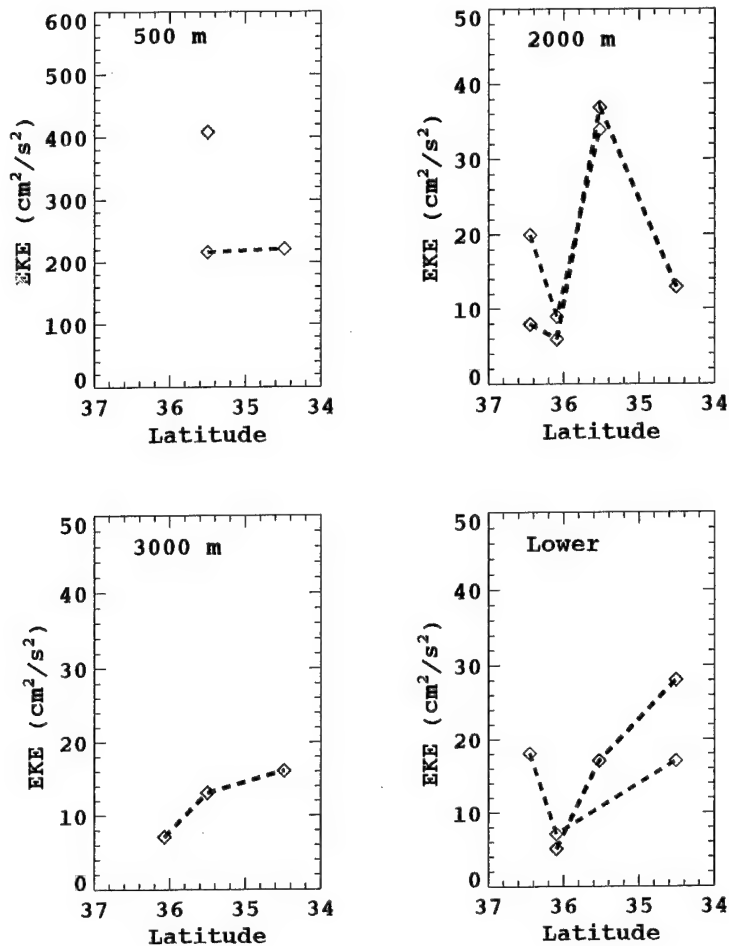
Fig. 7 — Eddy kinetic energy (EKE) for the current meter velocity records. Mooring locations A, B, C, D correspond to decreasing latitude. The label "Lower" in the lower right panel indicates the deepest instruments at those locations; they are not necessarily at the same depths. Blue curves are for Year 1, and red curves are for Year 2.

Fig. 8 — A time series of sea-surface height contours (m) along the KERE section computed from TOPEX/POSEIDON data is shown for comparison with the meridional volume transport (yellow curve) based on current measurements from moorings B and C. The transport is shifted 40 days forward in time for visual comparison purposes. The red band indicates the approximate location of the Kuroshio surface current axis.
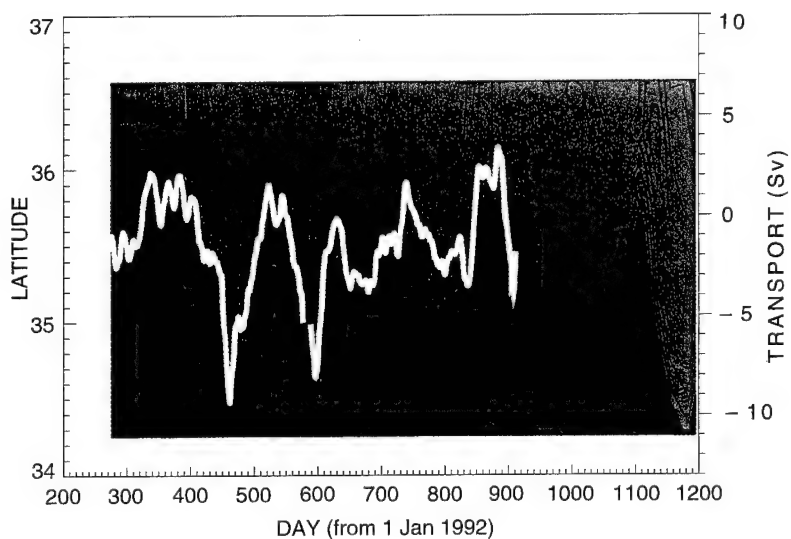
represent changes in direction relative to the orientation of the section. The deep flows exhibit similar variability scales. A time series of meridional volume transport (indicated by the yellow curve in Fig. 8), based on all CMs from moorings B and C, shows similar scales of variability. In particular, a large, negative excursion is apparent between days 400 and 450 for both the transport and Kuroshio position. That is, a large, southward shift of the Kuroshio axis corresponds to a strong, southward surge of the DWBC. However, the transport has been shifted forward in time by 40 days, and thus leads the shift of the Kuroshio axis. This is significant because it implies that the shift of the axis might be caused by the DWBC change rather than the other way around. Another possibility is that both events are the result of nonlocal forcing such as large-scale windstress changes of long Rossby-wave activity. Similar causal links have been found by others for the Gulf Stream near Cape Hatteras.

SUMMARY

A southward mean North Pacific DWBC has been found along the continental slope of Honshu Island which is, to some extent, part of the global thermohaline circulation, although eddy-driving is also likely to be a factor. This volume transport of this current is about 2 *Sv* southward but shows strong variability that may be dynamically linked to meanders of the Kuroshio. Deep mean flows near the Japan Trench are generally northward and affected by topographic features, while seaward of the trench, the deep mean currents are again southward. In-situ measurements, such as those obtained in the KERE, are essential for understanding the dynamics of western boundary currents. Such understanding is required for accurate modeling and prediction in these regimes. This work provides a touchstone for the evaluation of circulation models for the Pacific Ocean.

ACKNOWLEDGMENTS

REFERENCES

1. J.C. Swallow and L.V. Worthington, "Measurements of Deep Currents in the Western North Atlantic," *Nature* **179**, 1183-1184 (1957).

2. Z.R. Hallock and W.J. Teague, "Evidence for a North Pacific Deep Western Boundary Current," *J. Geophys. Res.*, accepted (1995).

3. H. Stommel and A.B. Arons, "On the Abyssal Circulation of the World Ocean I, Stationary Planetary Flow Patterns on a Sphere," *Deep Sea Res.* **6**, 140-154 (1960).

4. B.A. Warren and W.B. Owens, "Deep Currents in the Central Subarctic Pacific Ocean," *J. Phys. Oceanogr.* **18**, 529-551 (1988).

5. L.D. Talley, T.M. Joyce, and R.A DeSzoeke, "Transpacific Sections at 47° N and 152° W: Distribution of Properties," *Deep Sea Res.* **38**, Supp. 1, S63-S82 (1991).

6. T. Nan'niti and H. Akamatsu, "Deep Current Observations in the Pacific Ocean Near the Japan Trench," *J. Oceanogr. Soc. Japan* **22**(4), 154-166 (1966).

7. Y. Kawasaki and T. Kono, "Results of Current Measurements Southeast of Kushiro," in *Nemuro Workshop on Western Subarctic Circulation '93*, Hokkaido National Fisheries Research Institute, September 19-23, 1993.

8. H.E. Hurlburt, A.J. Wallcraft, W.J. Schmitz, P.J. Hogan, and E.J. Metzger, "Dynamics of the Kuroshio/Oyashio Current System Using Eddy-Resolving Models of the North Pacific Ocean," *J. Geophys. Res.*, accepted (1995).

9. W.J. Teague, A.M. Shiller, and Z.R. Hallock, "Hydrographic Section Across the Kuroshio

Near 35° N, 143° E," *J. Geophys. Res.* **99**(C4), 7639-7650 (1994).

10. H. Stommel and A.B. Arons, "On the Abyssal Circulation of the World Ocean V; The Influence of Bottom Slope on the Broadening of Inertial Boundary Currents," *Deep Sea Res.* **19**, 707-718 (1972).

11. J.R. Toggweiler and B. Samuels, "New Radiocarbon Constraints on the Upwelling of Abyssal Water to the Ocean's Surface," in *The Global Carbon Cycle,* M. Heimann, ed. (NATO ASI Series, Springer Verlag, Berlin, 1993), pp. 333-366.

12. W.J. Teague, Z.R. Hallock, G.A. Jacobs, and J.L. Mitchell, "Kuroshio Sea Surface Height Fluctuations Observed Simultaneously with Inverted Echo Sounders and TOPEX/POSEI-DON," *J. Geophys. Res.,* **100** (C12), 24987-24994 (1995).

THE AUTHORS

ZACHARIAH R. HALLOCK received a B.S. in physics from the Polytechnic Institute of Brooklyn in 1970, and M.S and Ph.D. degrees in physical oceanography in 1973 and 1977, respectively, from the Rosenstiel School of Marine and Atmospheric Science of the University of Miami. He then joined the U. S. Naval Oceanographic Office in 1977. In 1981, he joined the Oceanography Division at NRL (then NORDA) where he conducted research in oceanic thermohaline finestructure using observations from frontal regions. Beginning in 1985, Dr. Hallock pursued research in oceanic mesoscale variability in multidisciplinary programs. This work included field observations and analyses of moored and profile measurements in combination with satellite altimetry and model results. In addition, he conducted GEOSAT validation studies for the open ocean. In 1990, he began a study of deep boundary flows in the northwest Pacific near Japan, in collaboration with concurrent NRL remote-sensing and modeling efforts. He received the NORDA Best Publication Award in 1989, the NOARL Code 330 Best Publication Award in 1991, an *NRL Review* Publication Award in 1994, and an NRL Technology Transfer Award in 1995. He is a member of the American Geophysical Union.

WILLIAM J. TEAGUE received a B.S. degree in physics from the University of Miami in 1972 and an M.S. degree in physical oceanography from the Rosenstiel School of Marine and Atmospheric Science of the University of Miami in 1975. He is a physical oceanographer and was employed by the U.S. Naval Oceanographic Office from 1976 to 1983. He joined the Oceanography Division at NRL (then NORDA) in 1983 and was involved in collecting and analyzing hydrographic, inverted echo sounder, and altimetric data for the GEOSAT field program and in developing database management systems. More recently, he has been investigating the dynamics of the Kuroshio Extension, off the coast of Japan. Present work involves analyzing TOPEX altimetric data and studying the dynamics of the Yellow and East China Seas to winds and currents. He received an NRL Technology Award in 1995, an Alan Berman Research Publication Award in 1995, an *NRL Review* Publication Award in 1994, the best NOARL directorate publication award in 1991, best NOARL division publication awards in 1990 and 1991, and the Naval Oceanographic Office Goldsborough Publication Award in 1984. He is a member of the American Geophysical Union, TOPEX/POSEIDON Science Team, and ERS1 Science Team.

EVE R. FILLENBAUM received a B.A. degree in physics from Carleton College in 1989, and a Ph. D. in physical oceanography from the Rosenstiel School of Marine and Atmospheric Science of the University of Miami in 1994. Her dissertation research involved investigation of the variability of the meridional heat flux in the North Atlantic Ocean. In 1995, she joined NRL as a Consortium for Oceanographic Research and Education postdoctoral fellow, working on volume transports in the Kuroshio Extension area. Dr. Fillenbaum is a member of the American Geophysical Union, the Oceanography Society, and Sigma Xi.

NRL Advances in Computational Fluid Dynamics: FAST3D and FEFLO

A. Landsberg, R. Ramamurti, J.P. Boris, and W.C. Sandberg
Laboratory for Computational Physics and Fluid Dynamics

In this article we present the recent progress made in the development of new, scalable CFD technology for computing unsteady flows over complex geometries. We also discuss two approaches — FAST3D and FEFLO — and the application of that technology to both basic research studies and grand challenge problems and the role of the DoD Common High-Performance Computing Software Support Initiative (CHSSI) in developing scalable software.

INTRODUCTION

Computational fluid dynamics (CFD) is a critical, enabling technology for a broad range of scientific research and engineering design applications. CFD accounts for about half of all large-scale computing in the Department of Defense (DoD) and underpins the DoD High-Performance Computing (HPC) Modernization Program. Over the last decade, NRL's Laboratory for Computational Physics and Fluid Dynamics (LCP&FD) has been in the forefront of the thrust to develop CFD techniques and programs to accurately represent the highly complex geometries and unsteady turbulent flows found in real applications. This task is complicated by the clear technical and economic need to exploit the very highest performance parallel computers now available and those being designed for the future.

One area of research upon which CFD is critically dependent is grid generation; that is, the process of discretizing the surfaces of objects and the volume about those objects in which the numerical solution to the appropriate equations will be computed. The computations are carried out at selected points in space, and the closeness of one point to its neighbor's depends upon how finely one chooses to divide the computational domain. The three important goals of the grid generation community are: (1) to develop grid generators that are fast; (2) to develop grid generators that can represent the complex geometry found in most real applications; and (3) to develop parallel versions of the methods to take advantage of the scalability and speed of new computer architectures. Scalability means having the potential for speeding up a computation due to the structure of the code, which breaks the problem up into pieces that can be worked on in parallel by multiple processors. Significant progress has been made in meeting the first two objectives while the third has only recently begun to draw widespread attention. This increase in attention on the development of parallel grid generation methods (and flow solvers) within the DoD is primarily due to the growing availability of massively parallel computing resources, under the auspices of the High-Performance Computing Modernization Office (HPCMO). To take full advantage of this computing power, however, requires an investment in scalable code development by the DoD. An initiative of the HPCMO, namely the Common High-Performance Computing Software Support Initiative (CHSSI), focuses such an investment and is about to begin. It will enable DoD scientists and engineers to join multiservice teams with academic and industrial partners to develop general purpose, multiservice, portable, efficient, and scalable CFD software. National challenges, such as ocean and weather modeling, environmental contamination or deterioration, design and fabrication of new materials and drugs, and grand challenge

military applications, are representative of the problems being tackled under the new initiative. The military applications include submarine, aircraft and missile maneuvering, blast dynamics and structural response, fire propagation and control, electromagnetic scattering from complex surfaces, and signal processing for real-time control. Significant progress on such computational challenges will be delayed without the application of the new, parallel-computing resources. This paper describes the recent progress made at NRL in the development of scalable CFD technology and the application of that technology to both basic research questions and grand challenge problems.

GRID GENERATION TECHNOLOGY

The rapid generation of a suitable computational grid upon which to carry out a flow, structural mechanics, or electromagnetic or acoustic signature computation for a complex geometric object has been a long-time goal of the mathematical and computational communities. There are essentially three ways of representing complex geometry. The first uses structured multiblock or overset grids where the individual grid blocks are bent around various parts of the body. The second uses globally structured rectilinear grids where the body cuts smoothly through the cells of the grid. The third uses unstructured finite-element grids comprised of tetrahedra. Numerous examples of all three approaches to gridding complex shapes can be seen in Ref. [1]. At the LCP&FD, we have pursued both the structured and unstructured grid approaches. The structured grid approach is discussed first.

FAST3D AND GLOBALLY STRUCTURED GRID TECHNOLOGY

For structured grid approaches, we have developed a new, faster alternative to multiple blocks or overset grids—namely, the globally structured grid with virtual cell embedding (VCE). This approach was chosen because it allows simpler data structures aimed at efficient use of the existing and emerging highly parallel architectures with little sacrifice in speed, memory requirements, or flow-field accuracy [2]. A structured rectilinear mesh is used as the basis for VCE, but variable spacing between the grid planes and even motion of the grid planes is allowed. The method

allows surfaces of complex objects to cut smoothly through the rectilinear grid. The smooth intersection with the grid is accomplished by subdividing the mesh into very fine subcells. The method is called virtual because the subcells embedded within a cell are not stored in memory or integrated in the solution and, hence, the computation time is essentially independent of the high resolution used to replicate the geometric detail. VCE is used within the CFD program FAST3D, which is the DoD's scalable reactive flow benchmark program. FAST3D solves 3-D, time-dependent, compressible, reactive flow problems. There are three software components of the FAST3D system—the grid generator GRIDGEN, the flow solver FAST3D, and the asynchronous graphics package VOYEUR. An important aspect of VOYEUR is the ability it provides to watch the time evolution of computed data on selected visualization cross-sections while the simulation is proceeding on one of the DoD's scalable high-performance computers.

The underlying fluid dynamics algorithm in FAST3D is the high-resolution, direction-split, flux-corrected transport (FCT) algorithm called LCPFCT [3]. The FAST3D flow-solver model approximates the high Reynolds number limit solutions of the Navier-Stokes equations within the resolution limits controlled by the fundamental grid spacing chosen by the user. It is particularly advantageous to use the FCT algorithm with the VCE method since both algorithms are highly parallel. The FCT and VCE algorithms have been implemented for distributed memory parallel computers such as the Intel iPSC/860, Intel Paragon, and clustered workstation architectures. In the parallel implementation of FAST3D, domain decomposition is used to distribute the grid cells across the processors while a running transpose is used for the inter-processor communications. The VCE data structure implemented in FAST3D for complex geometry is partitioned for efficient parallel processing and communication.

An example of the power of the VCE to represent complex geometry is given in Fig. 1, which is an instantaneous snapshot of the unsteady air wake about the LHD aircraft carrier. Detailed knowledge of the unsteady air flow around a ship superstructure is necessary to assess the suitability of a platform for air operations, to predict and rank the relative merits of proposed topside design modifications, and to improve the fidelity of ship air-wake models in pilot training simulators.
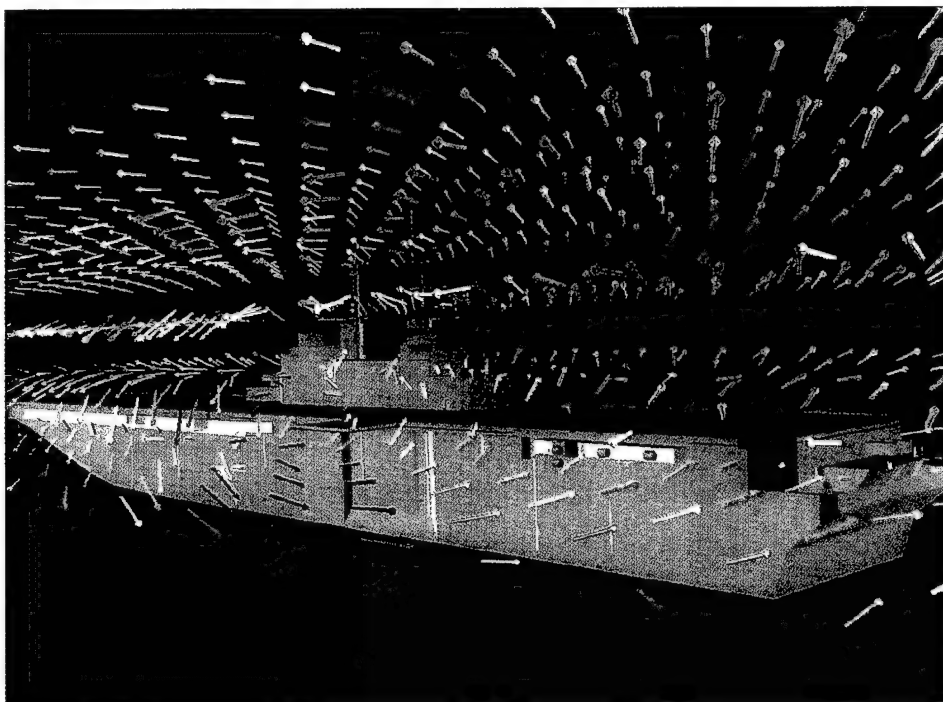
Fig. 1 — An instantaneous snapshot of the unsteady flow field about the LHD aircraft carrier. The 3-D velocity vectors show the magnitude and direction of the flow field for an incoming wind of 30 knots at 30° from starboard.

The ultimate objective of such numerical simulations is to provide the design and operational guidance needed to improve the safety of aircraft and helicopter landings. The interaction of the unsteady air wake with incoming or outgoing air vehicles is obviously critical, and FAST3D can do this computation while computing the temperature and trajectory of the hot exhaust plume from the ship's smokestacks. Large data sets of velocity vector time histories represent the unsteady air flow over the LHD and are being incorporated into the Navy's manned-flight simulator (MFS) for pilot training. This work was sponsored by the Navy MFS facility and NAVSEA.

FAST3D is also a multiphase reactive flow code and therefore can compute the flows associated with detonation of explosives, as Fig. 2 shows, or the propulsion dynamics of new weapon concepts, as Fig. 3 shows. Currently, about 400,000 tons of expired/obsolete munitions await disposal. The explosion computations are sponsored by the Army and EPA, who are jointly developing a methodology for permitting the in-place detonation of these munitions as the most environmentally sound and cheapest way to remove these hazards. FAST3D is being used to character-

ize the explosion sources in containment facilities. The results from the computations are to provide input to a NOAA atmospheric dispersion model for studying atmospheric contamination. The source characterization model requires describing the relevant parameters of the detonation processes such as the initial buoyancy of the plume, the propagation and intensity of the blast wave, the type and amount of the solids and other pollutant releases, and the plume dimensions as a function of time. Figure 2 shows a VOYEUR temperature and pressure contour plot for a detonation inside a containment facility with and without a water shield.

The computation of shock dynamics is also critical for the design of new weapon systems. The ram accelerator is a new propulsion concept to accelerate projectiles to very high velocities (up to 8-10 km/s). The basic working principle of the ram accelerator is to use shock-induced combustion to generate high pressures to propel the projectile. Figure 3 shows VOYEUR cross-sections of the fluid pressure for a projectile that has been canted in the launcher tube by uneven pressures. Such phenomena have been seen in University of Washington/Applied Research Laboratory

73

water shield   **no water shield**
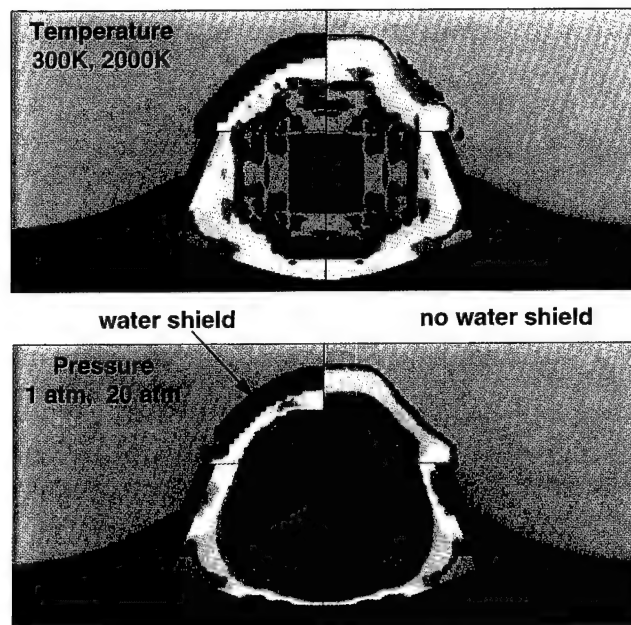
Fig. 2 — Potential design of a containment facility for open-air detonation of expired/obsolete munitions. The left half of the figures shows a solution with a water shield to reflect the explosion back into the containment facility; the right half shows the solution without the water shield.
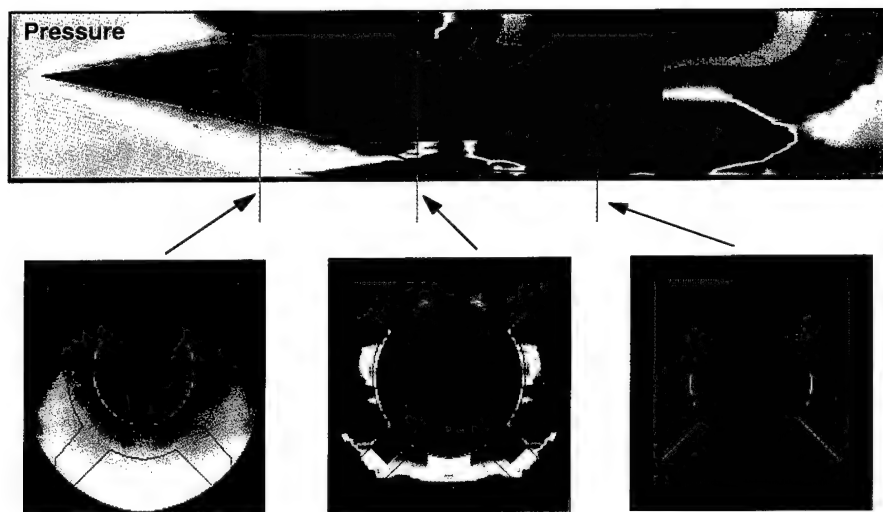
Fig. 3 — VOYEUR cross-sections of the fluid pressure for a projectile that has been canted in the launcher tube by uneven pressures. The three lower figures are axial cross-sections of pressure showing the fins rotated at a 45° angle.

experiments and represent a real concern for the efficiency and accuracy of the device. This work is sponsored by the Air Force and Navy.

In addition to computations for solving applications problems in complex geometries, we also carry out computations in simple geometries where the physical processes may be extremely complicated. One such example is in the study of the dynamics that occurs during the laser-induced ablation of initially spherical fuel pellets in inertial confinement fusion experiments. Since radiation transport hydrodynamics is important for laser-matter interaction computations, a separate version of FAST3D that incorporates radiation transport hydrodynamics has been developed at NRL under DOE and NRL sponsorship [4]. This version of FAST3D is being used to simulate the evolution of 85-μm-thick NIKE simple plastic ablator targets accelerated with prototype inertial-confinement fusion (ICF) driver conditions. In addition to assisting in the design of high-gain ICF pellets, the code is also being used to assist in the design and diagnosis of laboratory experiments on spherical pellets for the NRL NIKE KrF Laser Facility (Laser Plasma Branch, Plasma Physics Division).

Each of the above FAST3D applications was performed using several different computers. In addition to the Intel iPSC/860, Intel Paragon, Convex, IBM and DEC Workstations, and SGI Power Challenge systems used in these examples, variants of this CFD model exist for the TMC Connection Machines, Cray T3D, IBM SP2, and Cray C90. Each application, to date, has used a somewhat different version of the program. One aim of the CHSSI project is to unify these capabilities within a single portable code.

FEFLO: UNSTRUCTURED GRID TECHNOLOGY

FEFLO is an unsteady, implicit, finite element, Navier-Stokes solver that uses unstructured grids for modeling both compressible and incompressible flows. Like FAST3D, the compressible version of the flow solver uses the FCT algorithm. In addition to the compressible and incompressible flow solvers, there is a CAD/CAM interface (FECAD), a grid generator (FRGEN3D), and a flow-visualization code written especially for unstructured grids (FEPOST3D). Unstructured grids are built with triangular cells in 2-D and tetrahedral cells in 3-D. The cells surrounding any particular computational element can be, and usually are, distributed irreg-

ularly. This allows one to place tightly packed tetrahedra close to the body surface as needed to capture geometric detail or resolve viscous boundary layers while using significantly less resolution in immediately adjacent regions away from the body surface where flow gradients are moderate. Where high gradients do occur, one can adaptively remesh as needed to capture and track the evolution of the flow unsteadiness. This is very useful for unsteady separating flows where one wishes to track the shed vorticity and for flows about moving surfaces, deforming surfaces, and in time-varying computational domains. The unstructured grid-generation process in FEFLO is very fast and thus well suited for rapid regridding of geometric configuration changes, which is essential for timely design iterations.

Viscous, turbulent separating flows are an area of intense fluid dynamic research. The dynamics of these flows need to be understood in order to predict confidently the behavior of ships, submarines, torpedoes, and propulsors. FEFLO and the unstructured grid technology development were funded by ARPA and the Navy because they offer significant promise in this area and because of their ability to examine the details of unsteady separation and vorticity shedding. Figure 4 is an example of such an investigation, which gives the computed results for the distribution of vorticity at various streamwise locations for the flow over a prolate spheroid at an angle of attack. The prolate spheroid was selected because it has been the subject of several fundamental experiments to map steady and unsteady flows over bodies at an angle of attack. Comparison of the computational results with experimental results have shown quite good agreement [5] and have focused the next phase of work on turbulence models for massively separating flows.

A natural extension of prolate spheroid flow is submarine flow computation. An extremely challenging problem related to submarine flow is the prediction of forces, moments, and trajectories during the torpedo launch process. The flow fields are affected by two-body interactions, propulsor-generated flows, and unsteady water-jet interactions. Successful development of advanced launcher and unmanned underwater vehicle concepts may depend on being able to make the computations of the flow so that a range of vehicle/propulsor/control system alternatives can be assessed prior to costly prototype construction
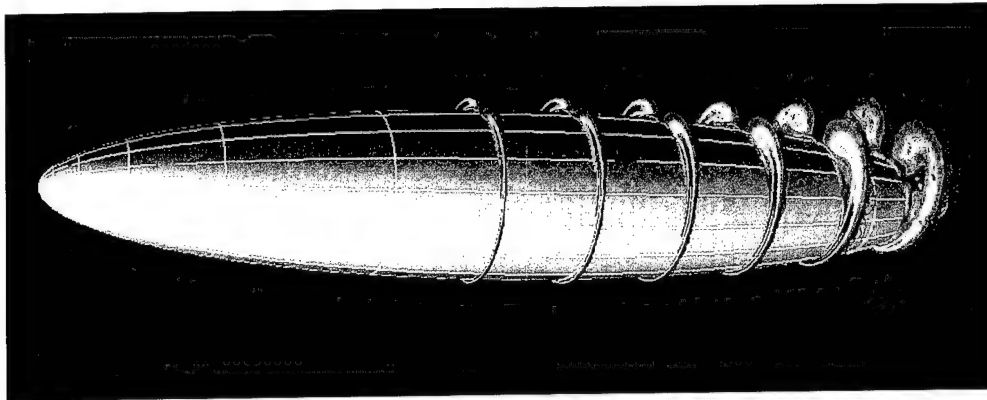
Fig. 4 — Unsteady separating flow past a 1:6 prolate spheroid, $a = 10°$, $Re = 60,000$.
Longitudinal cuts show instantaneous vorticity.

and testing. Figure 5 shows the velocity about a torpedo as it exits from the launch tube of a moving submarine. The adaptive remeshing incompressible flow solver was applied to simulate the unsteady flow throughout the entire launch process.

In addition to weapons launch, the submarine community is also challenged to predict the forces, moment, and trajectories of the submarine itself as it responds to control surface commands. An ability to compute the unsteady flow about moving control surfaces is therefore critical. Fish, such as tuna, propel themselves almost exclusively by motion of the last 10% or so of their body where their caudal fin is located. They thus provide an interesting example in nature of flows about reasonably streamlined bodies with control surface activity, such as submarines. Until now, hydrodynamic computations to model fish motion have been restricted to slender body theory. The difficulties that have heretofore prevented the development of computational capabilities for understanding the hydrodynamics of fish motion are its complex geometry, the undulatory motion of the body and the fins, as well as the interaction of the body and fin flow fields. Figure 6 shows the results of the first 3-D unsteady computations of surface pressure distribution on a swimming fish [6]. The computations included continuous fin deformation and oscillation.

Moving from the low-speed undersea world of swimming fish to the high-speed atmospheric world of recoverable rockets takes us out of the world of incompressible phenomena and into the world of compressible fluid dynamics. Computations of compressible flows were carried out using the unstructured grid code, FEFLO96. The purpose of this effort is to support the study (by NRL's Naval Center for Space Technology) of the subsonic recovery of the BLUE (Basic Launch Understanding Effort) launch vehicle. The vehicle uses a recovery system called the subsonic recovery decelerator (SRD) that deploys during descent, for a controlled landing. Figure 7 shows the simulated flow field past a re-entry vehicle with a SRD during its deployment phase. Additional FEFLO applications using a coupled CFD and computational structural dynamics (CSD) methodology, developed by Löhner and his coworkers under Air Force and DNA support, include the blast dynamics in the World Trade Center [7] and aircraft interior blast loads and structural responses.

The development of the parallel software necessary to implement these codes on massively parallel hardware began under the ARPA sponsorship. In our parallel code-development effort, we have demonstrated a robust 2-D and 3-D parallel unstructured grid generation code on the LCP&FD Intel iPSC/860 system. A domain partitioner and an implicit incompressible flow solver in both 2-D and 3-D have also been implemented on this system. The scalability and performance of the flow solver has been demonstrated for the very complicated geometry of a landing configuration tri-element airfoil using 384 processors on the Caltech Intel Delta machine. In this work, a domain decomposition algorithm that results in efficient load balancing and an optimum computation-to-communication balance was also developed. The development of scalable and portable codes for the adaptive remeshing on parallel architectures will be carried out as part of the CHSSI effort.
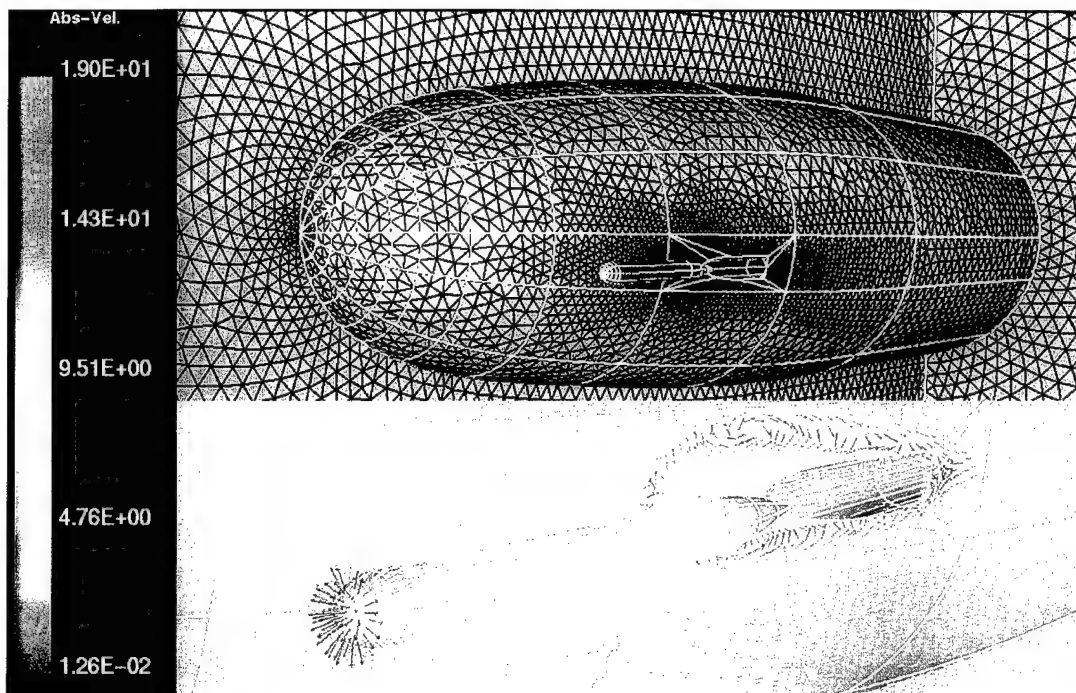
Fig. 5 — Simulation of a torpedo launch, t = 2.0 s. Surface triangulation and instantaneous velocity vectors as torpedo exits the launch tube.
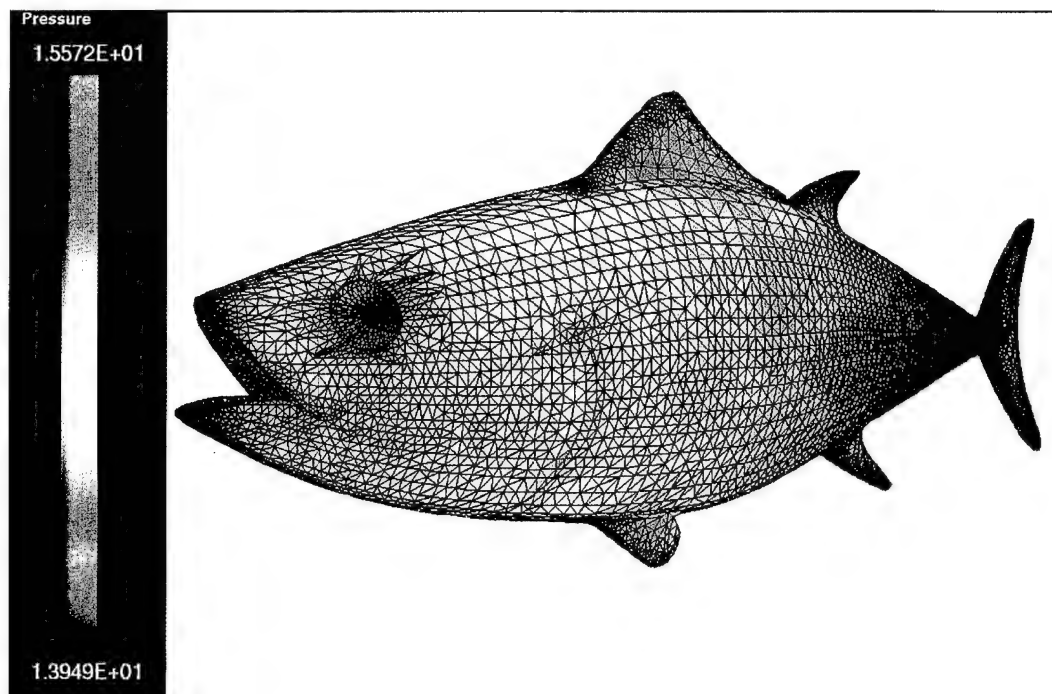
Fig. 6 — Pressure distribution about 3-D tuna with forward velocity. Caudal fin is being continuously deformed and is executing sinusoidal oscillations with amplitude and frequency of actual tuna motions.

Abs-Vel.

1.9071E+02

2.9128E-01
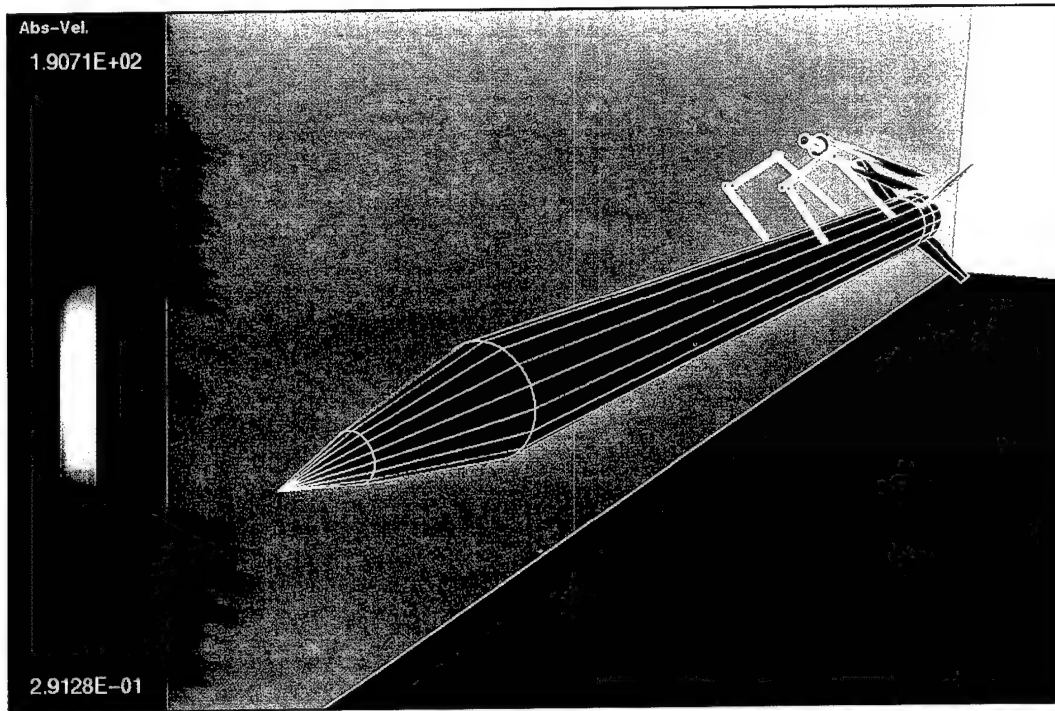
Fig. 7 — Flow past a re-entry vehicle during deployment phase.

SUMMARY

We have described several new advancements in scalable CFD technology and the progress made on a number of military and civilian computational challenges. The new, scalable, massively parallel computing architectures present a potential for increasing our rate of progress on these and other national and DoD grand challenge problems. The progress arising from timely use of DoD High-Performance Computing resources is not restricted to specific technology advances but encompasses all major technologies. Thus it should also propel the general DoD modeling and simulation community in areas of design and acquisition, training, and distributed warfare simulations.

ACKNOWLEDGMENTS

REFERENCES

1. *DoD Mission Success from High Performance Computing—March 1995*, available from the Defense Technical Information Center, AD 285359.

2. A.M. Landsberg, T.R. Young, Jr., and J.P. Boris, "An Efficient, Parallel Method for Solving Flows in Complex Three-Dimensional Geometries," AIAA Paper 94-0413, Washington, DC, (1994).

3. J.P. Boris, A.M. Landsberg, E.S. Oran, and J.H. Gardner, "LCPFCT—A Flux-Corrected Transport Algorithm for Solving Generalized Continuity Equations," NRL Memorandum Report 93-7192 (1993).

4. J.P.Dahlburg, J.H. Gardner, and D.E. Fyfe, bottom figure, p. 58, *1994 NRL Review*, Naval Research Laboratory, Washington, DC.

5. R. Ramamurti, R. Löhner, and W.C. Sandberg, "Evaluation of a Scalable 3-D Incompressible Finite Element Solver," AIAA Paper 94-0756, Washington, D.C. (1994).

6. W.C. Sandberg, R. Ramamurti, and R. Löhner, "Computing Unsteady Flow About Deforming Bodies," Review Meeting on Biolocomotion and Rotational Flow Over Compliant Surfaces, Baltimore, MD, March 1995.

7. J.D. Baum, H. Luo and R. Löhner, "Development of a Coupled CFD/CSD Methodology," *DoD Mission Success from High Performance Computing—March 1995*, available from the Defense Technical Information Center, AD 285359.

THE AUTHORS

ALEXANDRA LANDSBERG received her B.S. and M.S. degees in aeronautics and astronautics from the Massachusetts Institute of Technology in 1988 and 1991, respectively. She has been an aerospace engineer in the Laboratory for Computational Physics and Fluid Dynamics at the Naval Research Laboratory since 1991. Her research has concerned both the development and application of numerical algorithms for solving flows in complex geometries. A major contribution has been the development of the "virtual" cell embedding method for representing and solving flow in complex geometries with Cartesian grids. This method has been implemented in the parallel CFD simulation code, FAST3D. Ms. Landsberg's work on the unsteady airflow about the DDG 51 destroyer has generated interest within the U.S. Navy as well as in England, Australia, and Canada through TTCP Dynamic Interface meetings. Ms. Landsberg is currently studying molecular dynamics simulations of lattices for her Ph.D. in computational physics at George Mason University.

RAVI RAMAMURTI received his B. Tech. in mechanical engineering from the Indian Institute of Technology, Madras, India, in 1980 and his M.S. and Ph. D. degrees in aerospace engineering from University of Cincinnati, in 1983 and 1986, respectively. He is an aerospace engineer in the Laboratory for Computational Physics and Fluid Dynamics at NRL. Dr. Ramamurti has extensive experience in computational aerodynamics and hydrodynamics, including the generation of unstructured grids for complex geometries. Dr. Ramamurti's primary areas of research are in the development of codes for unsteady incompressible flows for submerged vehicles, weapon launch flows, external two-body flows, and moving and deforming surfaces. He is also active in the development of scalable software for parallel computing architectures. He is a member of AIAA and Sigma Xi.

JAY P. BORIS received his B.A. degree in physics from Princeton University in 1964, magna cum laude, and his M.A. and Ph.D. degrees in astrophysical sciences in 1966 and 1968, also from Princeton. He joined NRL in 1970. In 1978, he was appointed to the SES and established in the NRL Chair of Science in Computational Physics. As director of NRL's Laboratory for Computational Physics and Fluid Dynamics, he has conceived and led computational research efforts on many Navy and DoD fluid dynamics, many-body dynamics, reactive flow, and plasma physics problems and has developed several of the now standard simulation algorithms in use in these fields. His professional recognition includes the Navy's Captain Robert Dexter Conrad and Distinguished Achievement in Science Awards and the Arthur S. Fleming Award. Dr. Boris is a fellow of the American Physical Society and the American Institute for Aeronautics and Astronautics and is the DoD's Computational Technology Area Leader for Fluid Dynamics.
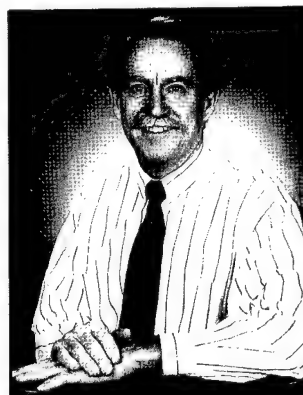
WILLIAM C. SANDBERG received his B.S. degree in physics from Boston College (1967) and M.Sc. in naval architecture from M.I.T (1970). He joined the Naval Ship Engineering Center (later NAVSEA) and was involved in hull form design and hydrodynamic performance assessments for submarines and surface ships. He received a Ph.D. in physics from the Catholic University of America (1987) and joined NRL later that year. His research area is nonequilibrium molecular dynamics of atomic and molecular liquids, focusing primarily on shear-induced structural dynamics and transport processes. He is also involved in computational fluid dynamics for a variety of naval applications.

Acoustics

Influence of Internal Gravity Waves on Acoustic Propagation

S. Finette, S. Wolf, and M. Orr
Acoustics Division

D. Tielbuerger
Forschungsanstalt der Bundeswehr fuer
Wasserschall-und Geophysik
Kiel, Germany

Overview: Acoustic propagation in a shallow ocean is strongly influenced by spatial and temporal variations in the sound speed in the water. The spatial structure of the water sound speed is primarily determined by the vertical and horizontal temperature and salinity (T&S) distributions. This T&S structure is often vertically stratified and, as a result, the water density and sound-speed profile have vertical stratification, which can be significantly changed by the energetic ocean dynamics. Shelf-slope frontal zones, currents caused by wind shear and tidal flow, bubbles injected by breaking waves, fresh water intrusions, and daily and seasonal changes in the heat flux are among the physical processes that continuously alter the shallow-water acoustic environment.

The stratified density structure can support internal waves that displace the density structure and associated sound-speed profile, thus causing temporal and spatial variability in acoustic signal properties. Shallow-water internal gravity waves can vertically displace the density structure in the water column by 10 to 30 m in 5 to 10 min, have spatial wavelengths as short as a few tens of meters, and cause shear instabilities, which mix the water column. As a result, Navy acoustic system performance may change markedly over short time periods (minutes) and spatial intervals (hundreds of meters). The Acoustics Signal Processing Branch has been studying the effects that internal waves can have on the characteristics (for example, amplitude, phase, and coherence) of acoustic signals. Our objective is to improve the Navy's capability to predict and model the performance bounds of existing sonar systems in shallow-water operating environments and develop new signal-processing approaches for improved sonar performance.

Random Shallow Oceans: The internal wave field in shallow water can be modeled as a background wave field, which can be statistically described, and a deterministic soliton wave packet, which is generated on each diurnal tidal cycle. Our statistical model of the shallow ocean density structure was obtained by modifying the well-known Garrett-Munk deep-water internal wave model to account for the proximity of the ocean bottom. This model describes a continuous, spatially isotropic, background sound-speed oscillation. To this background component, we added a directional, tidally induced component, which consists of a pulse packet of internal solitary waves. The soliton component can be generated by a tidal flow across bathymetric features such as the continental shelf edge. We use a Monte-Carlo technique to calculate the properties of acoustic signals modified by the shallow-water internal wavefield by generating individual realizations of the sound-speed structure and then numerically calculating the acoustic signal which propagates through each sound channel realization. Figure 1 shows a single realization of the sound-speed structure as a function of range and depth.
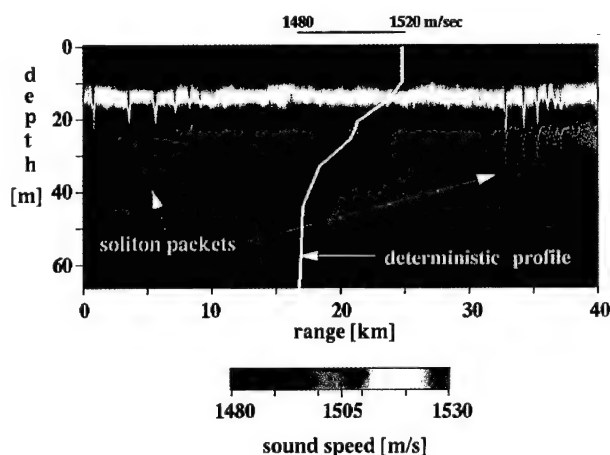
Fig. 1 — Deterministic and random contributions to the sound-speed distribution.

Acoustic Propagation Theory: Previous research addressing the propagation of acoustic signals through the random ocean led to the prediction that the scintillation index—a measure of the fluctuations in acoustic intensity—would approach a value of unity in the so-called saturation limit. The studies leading to this prediction assumed either that there was no medium absorption or that the acoustic modes of propagation were absorbed at the same rate. Recent

analytic work in the Acoustics Division [1] extended this result to the more realistic case in which the acoustic modes have different absorption coefficients. This work made a general prediction that, at long range, the scintillation index would grow exponentially rather than saturate at a limiting value. Part of the objective of the numerical calculations performed in our group was to test the analytic prediction with a realistic model of a random ocean.

Simulation of Acoustic Fields: The Monte-Carlo calculations produced an ensemble of acoustic fields from which acoustic signal statistics such as the scintillation index can be estimated. Figure 2 shows a typical result for the scintillation index as a function of depth and range from the source. The upper portion of the figure is the result obtained when the source is at depth 45 m; the lower portion corresponds to a source depth of 15 m. It is apparent that, at least at some depths, the scintillation index

increases with range to values larger than 1, thus supporting the analytic work. The differences in the source-depth dependence of the scintillation index may be attributed to differences in the normal-mode content of the field near the source and the energy transfer between modes.

Summary: We have developed a method for simulating the influence of a random shallow-water waveguide on a propagating acoustic field, thereby allowing us to calculate statistical properties of the field under realistic ocean conditions. The results obtained to date are consistent with a recently developed analytic theory. The theory predicts that if random medium properties induce energy exchange among modes which propagate with different attenuation rates, then the scintillation index increases to large values with increasing range, rather than assuming a limiting value of unity.

Reference

1. D. Creamer, "Scintillating Shallow-Water Waveguides," submitted to *J. Acoust. Soc. Am.*, to appear in 1996. ∎

(a)

(b)

SI

Fig. 2 — Scintillation indices (400 Hz) as a function of depth and range from the source: (a) depth - 45 m; (b) depth - 15 m.

High-Frequency Shallow-Water Signal Fluctuations

S. Stanic, C. Mire, and E. Kennedy
Acoustics Division

Shallow-water, high-frequency synthetic aperture sonar (SAS) systems being developed for the Navy require data and models that can relate the decorrelating effects of the ocean environment to SAS processing gains. High-frequency SAS systems will be affected by internal waves, turbulence, thermal fluctuations, and bubbles. Low-frequency variabilities produced by internal waves can usually be accounted for by signal processing algorithms. Acoustic phase fluctuations produced by turbulence and small-scale temporal thermal fluctuations will be random across an SAS aperture and are more difficult to remove. Bubbles can cause extensive scattering, attenuation, and dispersion of complex waveforms. The importance of these rapid, small-scale phenomena on high-frequency acoustic amplitude and phase fluctuations in shallow water are not currently known.

Experimental Measurements: During the Spring of 1995, NRL conducted a series of very shallow-water (25 to 40 ft), high-frequency (10 to 200 kHz) acoustic signal propagation measurements in an area 1200 ft off the beach in Panama City, Florida. These experiments were designed to determine the limits that the shallow-water environment places on SAS processing gains. Figure 3 is a schematic of the experimental configuration. Because of the very shallow-water environment, highly directional source and receiving arrays were designed. They were mounted on 13-ft high towers and deployed in the shallow coastal area off Panama City. To eliminate surface and bottom multipaths, these arrays were designed to have very narrow vertical beams (1° to 2°). These arrays also had broad horizontal beams (60° to 125°) enabling both receiving systems to be simultaneously insonified. In this configuration, the distance between the receiving systems formed part of a simulated synthetic aperture. The distances between the receivers ranged from 40 to 120 ft. The source-to-receiver ranges varied between 85 and 300 ft. Figure 4 shows the source arrays and the two receiving systems. Measurements of both the temporal and spatial small-scale thermal fluctuations, currents, and sound velocity profiles were made and are being used to relate the high-frequency acoustic phase and amplitude fluctuations to environmental parameters.
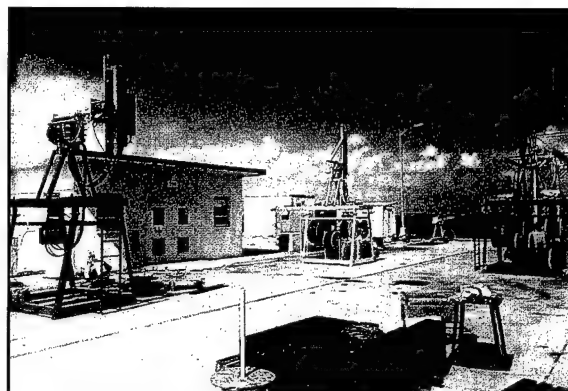
Fig. 4 — Source and receiving systems.

Acoustic Phase Variability: Measurements were made of the instantaneous phase differences between signals transmitted from the source to the receivers and replicas of the transmitted signals. Figure 5(a) shows instantaneous temporal phase variations for 300 acoustic pulses transmitted to one of the receivers 85 ft away. The frequencies were 20 kHz and 110 kHz, the pulse length was 1 ms, and the pulse repetition frequency was 1 Hz. During the time of these measurements, the instantaneous phase variations at 20 kHz were between −20° and +20°, and the phase variations at 110 kHz ranged from −110° to +100°. Figures 5(b) and (c) show the histograms of these phase variations. In these cases,
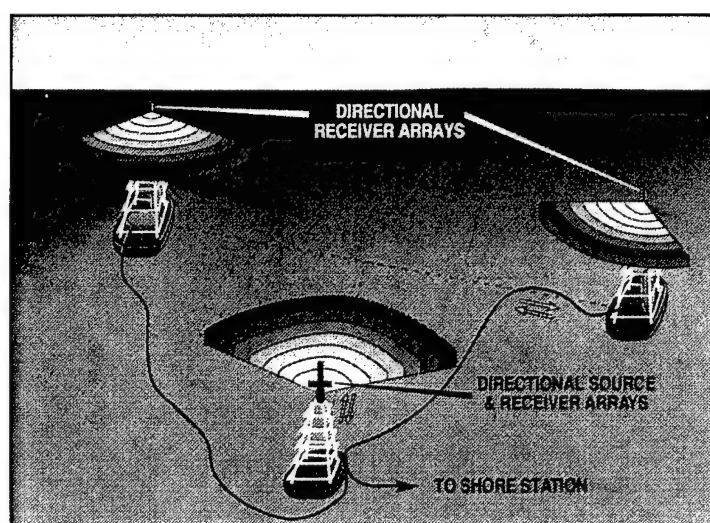
Fig. 3 — Experimental configuration.
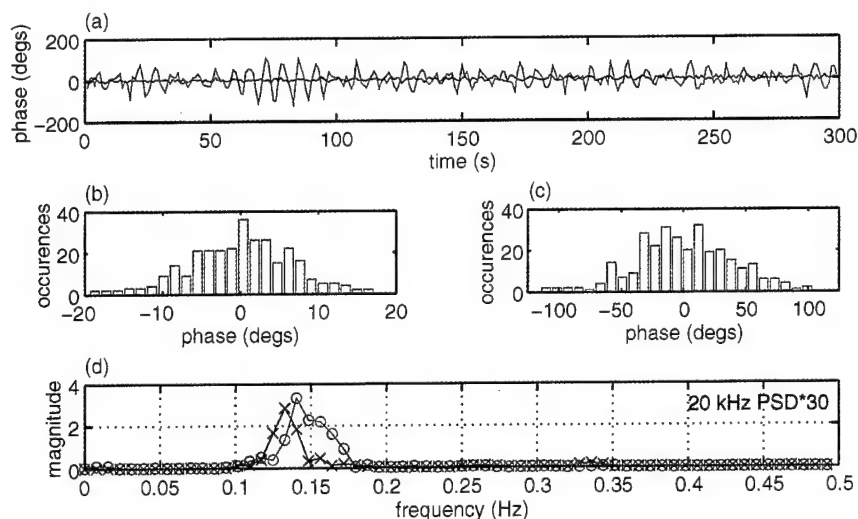
Fig. 5 — (a) Ping-to-ping phase variations for 20 kHz (blue) and 110 kHz (red), (b,c) histogram of ping-to-ping phase variations for 20 and 110 kHz respectively, and (d) the power spectral density of the phase differences for each frequency.

the phase distribution functions appeared to be Gaussian. Measurements were made of the small-scale variations of the ocean's thermal structure using a fast response (15 ms) spatial thermistor system. These measurements suggest that the magnitude of these phase differences could be correlated with small-scale variabilities in the thermal microstructure of the water column [1]. The larger the thermal fluctuations, the greater the acoustic phase changes. A spectral analysis of the 20 kHz and 110 kHz instantaneous phase variations revealed a spectral peak at about 0.14 Hz (Fig. 5(d)). During the acoustic experiments, a wave rider buoy recorded data on the sea surface characteristics. These data also showed a spectral peak at about 0.14 Hz. While the acoustic phase changes are due to thermal variations, they are also modulated by the ocean swell. The areas of thermal variability move between the source and receive towers with a frequency that is coincident with the period of the ocean swell. A high-resolution SAS system requires about 30 s to synthesize a large aperture array. Current motion compensation algorithms can correct for about a tenth of a wavelength in signal phase variabilities. Environment variabilities that cause signal phase shifts greater than 36° and occur at time scales less than 30 s will increase the sidelobe levels of the synthesized aperture and result in a decrease of SAS system resolution.

Summary: NRL is conducting high-frequency shallow-water acoustic propagation measurements to determine the limits that the ocean's small-scale variabilities place on the performance of high-frequency SAS systems. We have found that the phase variabilities of high-frequency acoustic signals are a result of small-scale variations in the ocean's thermal microstructure, that they increase with acoustic frequency, and occur with a period that corresponds to the ocean swell. These data will be used to predict temporal coherence and to predict SAS processing gains based on selected environment parameters.

Reference

1. R. Smith, S. Stanic, and E. Kennedy, "High-Frequency Acoustic Phase Stability Measurement System," *Proc. IEEE Ocean's 95* **2**, 1311-1318 (1995). ∎

Fiber-Optic, Noise-Filtering Acoustic Velocity Sensors

J.A. Bucaro, N. Lagakos, and B.H. Houston
Acoustics Division

The Navy has become increasingly interested in submarine sensor technologies that would permit the implementation of thousands of hull-

mounted acoustic sensors virtually over the entire submarine surface. Such large-aperture sensor arrays are seen as enabling technologies for high-performance sonar receivers (with an aperture the dimensions of the submarine), for new systems to actively control the submarine's own acoustic echoes, and for self-monitoring of what acoustic signals the submarine might inadvertently be sending to distant enemy receivers.

Why Acoustic Velocity Sensors?: In addition to the obvious requirements that such devices be inexpensive and lightweight (we want to use thousands), the sensors must be able to perform two important structural-acoustic functions. The first is to be able not only to sensitively detect acoustic energy near the hull but also to separate the acoustic velocity signal from the acoustic pressure signal. Sensors that detect the dynamic pressure in an acoustic wave have been around for a long time, and that technology has reached a certain level of maturity. Velocity-sensing techniques, however, have only recently been addressed. The availability of velocity sensors is

crucial because they would allow the decomposition of the acoustic field into backward- and forward-propagating waves. (Sonars want to detect incoming signals only.) Even more importantly, the sensors would permit acoustic detection on the hull even at positions and frequencies where hull impedance is low (pressure sensors would generate no signal) and where conventional acoustic sensors require heavy signal-conditioning mechanical systems. The second important function is that the sensor be able to detect the low-level-radiating (low-wavenumber) acoustic signal in the presence of high energy, spatially fluctuating (high-wavenumber) hull vibration fields (Fig. 6).

The Need for Special Optical Fibers: We have been exploring the development of fiber-optic sensor technologies that have the potential for performing these two acoustic "processing" functions. The sensor concepts of most interest involve the design of special fibers tailored to respond to accelerating force vs "hydrostatic" pressure and the subsequent embedding of long

Fig. 6 — Typical (numerically calculated) hull-motion decomposed into radiating and nonradiating components. Acoustic velocity sensors (accelerometers) distributed over the hull will sense both radiating hull modes (signal of interest) and nonradiating motions (noise). If the sensor has a large enough area and can perform an exact spatial integration, the large area sensor can filter out the higher wavenumber noise field and provide the normal motion associated with the acoustic wavenumber.

ENABLING TECHNOLOGY:
- Next Generation Hull-mounted Sensors

Vibrational Hull Modes

Radiating (Signal)	&	Non-Radiating (Noise)
• Low Energy		• High Energy
• Acoustic Wavenumbers		• High Wavenumbers

We would like:

$$\text{Accelerometer Output} = c\int_A a_\perp(\omega,\vec{r})dA \Rightarrow \text{Signal}$$

lengths of such fiber in large area polymer layers. Our philosophy is this: if we can arrive at embedded fibers that respond primarily to normal acceleration (acceleration is related to velocity by a single time derivative), then we can use the spatially integrating property of the large area sensor to suppress the vibrational noise field by (in essence) filtering out the higher wavenumber noise. We are attempting to achieve this performance by appropriate fiber, composition, and sensor design.

This is not a trivial goal since, typically, optical fibers respond more readily to acoustic pressure than to uniaxial accelerating forces. Consider that if one places an ideal segment of glass fiber in a fluid through which is passing a plane acoustic wave, the fiber's phase response due to acceleration is a factor $10^{-5} \times$ frequency smaller than that due to acoustic pressure. Good signal to noise would require that the acceleration-to-pressure response ratio be at least 10^2. For example, at 1 kHz, the glass fiber would have to be modified in such a way so as to preferentially increase its acceleration response by 10^4.

A New Sensor Concept: Figure 7 shows one such design [1]. In this sensor, a typical communication-grade single-mode glass fiber is first coated with a hard polymer material. A soft elastomer gel-like material is then deposited, and finally a thin, stainless-steel jacket is formed around the entire fiber. Long lengths of this composite fiber (tens of meters) are then shaped into a flat spiral coil and encapsulated in a thin, flexible elastomer layer—typically a polyurethane material. Sensors made in this way have been subjected to a variety of tests, including response to broadband normal-acceleration forces (the signal of interest) and to the pressure component of an acoustic field (an unwanted, contaminating signal). For the former, we find a strong, frequency-independent response up to 1.5 kHz while the latter is found to be, as required, extremely low. In addition, nearfield acoustic holography measurements performed with the sensor mounted on a vibrating-hull simulator structure demonstrate the sensor's ability to correctly spatially integrate the local acceleration (or velocity) of the hull over this band of frequencies [2]. This is a crucial step because it means that the sensor can indeed filter out the unwanted vibrational noise field (high wavenumber flexural motion).

These results are very encouraging. Indeed, at low frequencies (< ~1 kHz), this sensor technology appears ready for transition to system applications. Large numbers of these sensors would be inexpensive and directly compatible with optical fiber multiplexing and distribution systems. Current efforts are focused on extending the frequency range. A challenging goal in this regard would be to reach the tactical sonar frequency bands. This requires increasing the normal acceleration response of the embedded fiber
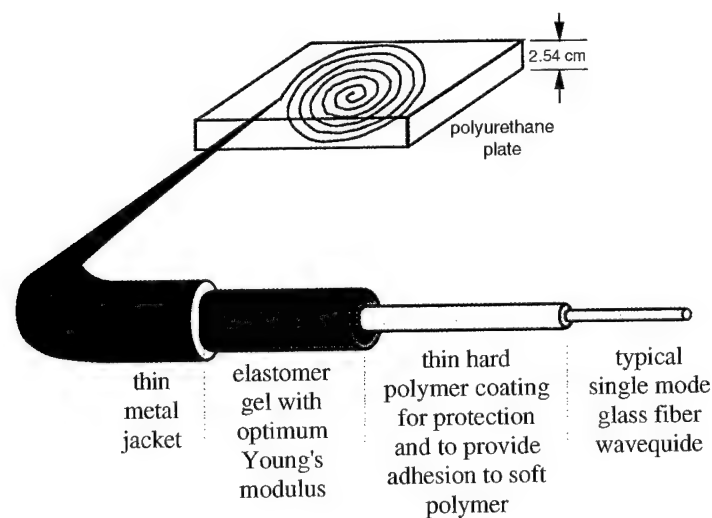
Fig. 7 — A recently developed large-area fiber-optic acoustic velocity sensor for hull-mounted applications. The sensor uses a specially designed optical fiber to respond to acceleration vs acoustic pressure.
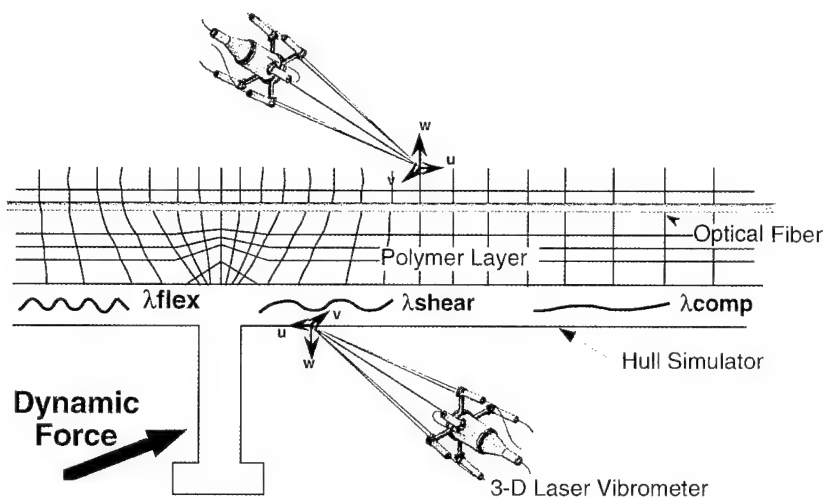
Fig. 8 — Dual 3-D laser vibrometer scanning system. The system provides the three dynamic displacement (velocity or acceleration) components on the interior and exterior of a vibrating structure.

structure at the higher frequencies and decreasing the sensor's response to in-plane structural strains and transverse acceleration. To accomplish this, finite element numerical modeling and advanced experimental measurement techniques are now being used. The latter includes interior/exterior 3-D laser-vibrometer scanning technologies recently developed at NRL (Fig. 8), which allow the mapping of all hull-vibration wave types and the resulting displacement and strains of the polymer layer.

[Sponsored by ONR]

References

1. N. Lagakos and J.A. Bucaro, "Planar Fiber Optic Acoustic Velocity Sensor," *J. Acoust. Soc. Am.* **97**, 1660 (1995).

2. J.A. Bucaro, N. Lagakos, B.H. Houston, and L. Kraus, "Large Area Planar Fiber Optic Accelerometers for Measurement of Acoustic Velocity," *Proceedings of Acoustic Velocity Sensor Focused Workshop*, Sept. 1995, Mystic, Connecticut. ∎

Chemical/
Biochemical
Research

Cubane Chemistry: A Source of New Energetic Materials

R.D. Gilardi
Laboratory for the Structure of Matter

The chemistry for making highly substituted cubane derivatives has advanced tremendously in recent years, stimulated by basic research funding from Departments of the Army and Navy's Energetic Materials Programs and from the Strategic Defense Initiative Office.

Cubane Stability: Cubane is an exotic synthetic hydrocarbon that has eight carbon atoms arranged at the corners of a cube (Fig. l); its carbon-carbon chemical bonds all meet at angles of 90°. In contrast, unconstrained carbon compounds of this type (that is, saturated hydrocarbons) contain much larger bond angles, measuring, on the average, 109.5°. The large bond angle deformations in cubane make it, in theory, a powerhouse of stored energy. It is chemically analogous to a mechanical device built to contain stressed components—bent beams, compressed springs—such as a common mouse-trap. All eight of cubane's C-C bonds are stressed. The mere possibility of its existence was debated until it was made in 1964 and found to be quite a stable compound, with a shelf life of years.

Are cubane and its derivatives really stable? In a strictly thermodynamic sense, no. A relatively unstrained isomer of cubane exists, known as cyclo-octatetraene (Fig. 1), and cubane could rearrange its bonds and convert to it, with the release of energy [1]. However, like many common organic compounds, cubane is resting in a metastable arrangement, and energy is required to activate it. Four fairly strong C-C bonds must be broken before the even stronger bonds of the cyclo-octatetraene can be formed. A similar relationship exists between diamond and graphite. Within our lifetimes, no sign of deterioration to graphite is likely to be seen in any of the diamonds we might hoard, although graphite is the thermodynamically favored form for pure carbon (as raising the temperature to 1000° C would soon prove).

Synthesis of Energetic Cubanes: As early as 1979, researchers in Army and Navy propellant programs recognized that cubane might provide
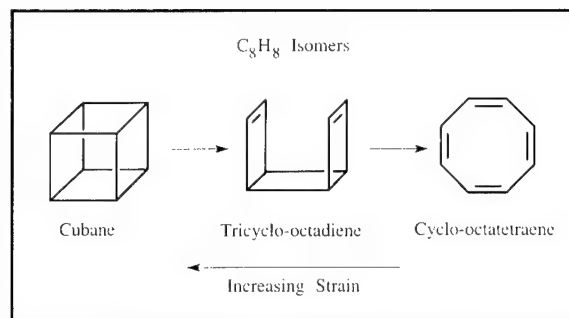
Fig. 1 — Structural formulae for three isomers of C_8H_8. Each vertex represents a carbon atom, and each carbon atom bears one hydrogen atom substituent. (By convention, H atoms on carbon are not explicitly shown in organic structural formulae.)

propellants and explosives of the future if its chemistry were mastered. At the time, just a few mono- and di-substituted cubanes were known, and most were made by forming the cubane from a precursor that already contained the final substituent groups. A long, multistep synthesis sequence was needed to look at the properties of each new compound. Under the stimulus of Defense programs, a body of substitution methodology for cubanes was developed; that is, chemical reaction schemes were developed that can transform a cubane compound by changing its pendant groups or adding new ones, without disturbing the cube.

At NRL, in the Laboratory for the Structure of Matter, more than 40 new cubanes have been analyzed since 1987 by means of single-crystal X-ray diffraction analysis. X-rays scattered by a single crystal, grown by slow evaporation of a solution containing just a milligram (more or less) of pure material, reveal the molecular structure of the compound, its density, and how its molecules pack in the solid state. If the cubic backbone of the molecule has rearranged, it is immediately apparent, and research along that pathway can be halted or modified. Density was specifically mentioned, for it plays an important role in assessing new explosives and propellants. The pressure in a shock wave produced by an explosive is correlated with the square of its density, and similar relationships favor dense propellants. Unless an energetic material is dense (1.8 g/cc or more), it is unlikely to be useful. In 1989/90, using newly developed syntheses, the target energetic molecules 1,3,5-trinitro- and 1,3,5,7-tetranitrocubane were made at the University of Chicago. Analyses

93

at NRL [2] reported quite high densities (1.74 and 1.81 g/cc for the tri- and tetra-nitro cubanes, respectively) and indicated no structural instabilities in the molecules, such as extra-long C-C bonds, a sign of incipient weakness. But direct attempts to add more than four nitro groups to the cube failed, and there was speculation that the placement of nitro groups on two adjacent carbons might inevitably destroy the cube.

Recent Progress in Cubane Syntheses: The tetra-nitro barrier was broken twice in 1995; pentanitrocubane (Fig. 2) and hexanitrocubane (Fig. 3) were made (again, at the University of Chicago) and studied at NRL. In addition, a new method was found to add nonnitro substituents to all four unsubstituted corners of 1,3,5,7-

tetranitrocubane, and two such octa-substituted cubanes were corroborated by analyses at NRL. The density of pentanitrocubane is 1.96, higher than was expected from extrapolation of previous nitrocubane results. The hexanitrocubane crystals contain a solvent—acetonitrile—in the crystal, so its density (1.65 g/cc) is not comparable to the other nitrocubanes, and it has not been made in sufficient quantity to see if a nonsolvated form can be grown.

Outlook: Recent performance tests on tetranitrocubane indicate that the combustion of energetic cubane compounds does indeed deliver all of the extra bond-deformation energy predicted by calculations, so these materials may soon boost the performance of Navy propel-
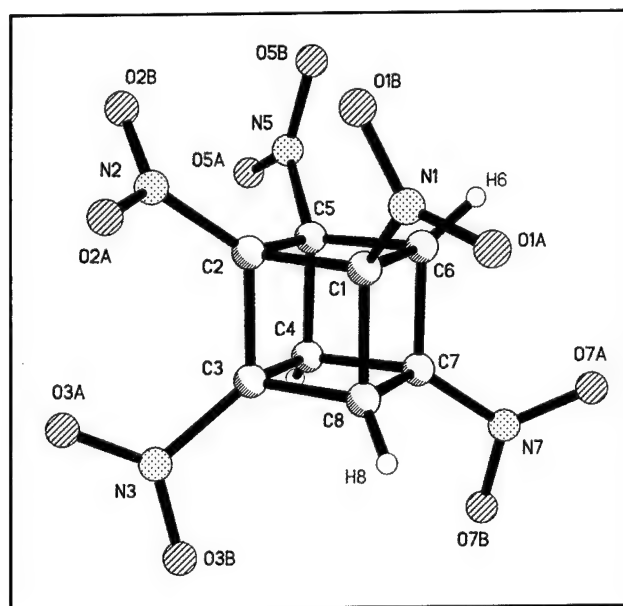
Fig. 2 — A computer drawing of the X-ray-observed structure of 1,2,3,5,7-pentanitrocubane. At 1.96 g/cc, this is one of the 10 densest compounds ever made from C, H, N, and O atoms.

Fig. 3 — The molecular structure of 1,2,3,4,5,7-hexanitrocubane as it occurs in a 2:1 acetonitrile solvate crystal. The two acetonitrile molecules are closely associated to the two remaining CH regions of the molecule and may help to stabilize the compound.
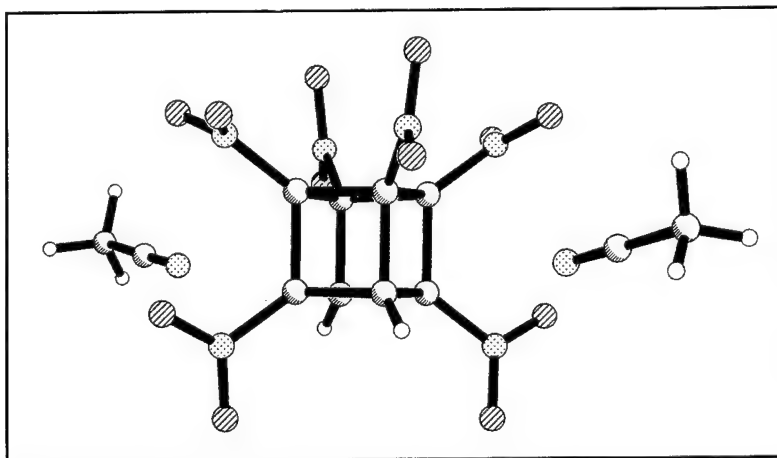
lants and explosives. One ultimate target—octanitrocubane—was once scoffed at by many chemists, but the thermal stability of penta- and hexanitrocubane and of octa-substituted nitrocubanes has changed the outlook; it is now considered highly likely that it will be made, and that it will be stable.

[Sponsored by ONR]

References

1. P.E. Eaton and D. Stossel, "Synthesis of Alkynylcyclooctatetraenes and Alkynylcubanes," *J. Org. Chem.* **56**, 5138 (1991).

2. P.E. Eaton, Y. Xiong, and R. Gilardi, "Systematic Substitution on the Cubane Nucleus. Synthesis and Properties of 1,3,5-Trinitrocubane and 1,3,5,7-Tetranitrocubane," *J. Am. Chem. Soc.* **115**, 10195 (1993).

3. K. Lukin, J. Li, P.E. Eaton, and R. Gilardi, "Penta- and Hexanitrocubanes. N_2O_4 Nitration of Group I-A Organometallics," *Angewandte Chemie*, submitted October 1995. ∎

The Many Faces of Silicon

L.J. Whitman
Chemistry Division

S.C. Erwin
Condensed Matter and Radiation Sciences Division

A.A. Baski
NRC/NRL Cooperative Research Associate

What are the stable surfaces of silicon and what determines their stability? Given that the fabrication of almost every electronic device begins with a clean surface of crystalline silicon, this question is of more than esoteric importance—the answer has implications for technologies of the future.

When a crystal is truncated to expose a surface, the surface atoms are left with uncoordinated chemical bonds. In an effort to reduce the density of these dangling bonds, the atoms in the top few layers rearrange—a process known

as surface reconstruction. Every different slice through a crystal exposes a surface with a different periodic arrangement of atoms (referred to as the unit cell), with each surface described by a set of indices, (x y z) (Fig. 4). The low-index surfaces have the smallest unit cells and simplest surface structures. More complicated surfaces are created when crystals are sliced to high indices, exposing unit cells that are large and composed of many atoms. Such complex faces are usually unstable and reconstruct into facets of low-index planes (like the facets on a gemstone).
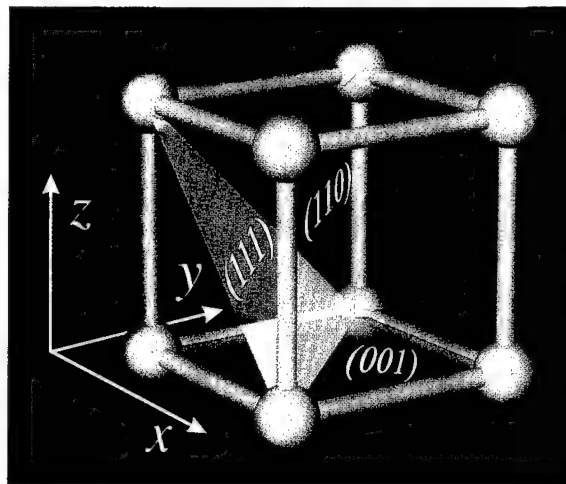
Fig. 4 — The low-index planes of a simple cubic crystal. Each plane can be described by indices (x y z) associated with the vector perpendicular to that plane, as defined by the axes of the crystal; for example, the (111) plane is perpendicular to the vector $1\hat{x} + 1\hat{y} + 1\hat{z}$. Note that silicon has a more complex crystal structure than shown (it has the diamond structure).

The surfaces of silicon, the basis for the multibillion-dollar electronics industry, may be the most widely studied of all. Despite such scrutiny, only a few stable silicon surfaces are known, of which only three have known structures: (001), (111), and (113). Although most electronic devices are fabricated on Si(001), high-index surfaces are being considered as possible substrates for future applications. To date, a general understanding of the structure and stability of high-index silicon surfaces does not exist.

Approach: We have used scanning tunneling microscopy (STM) in combination with first-principles electronic-structure calculations to determine the atomic-scale structure of silicon surfaces

CHEMICAL/BIOCHEMICAL RESEARCH

oriented between (001) and (111). Samples with known orientations were heated to a very high temperature (~1050° C) in ultrahigh vacuum in order to remove surface contaminants and allow the resulting atomically clean surfaces to reach their equilibrium structure. The samples were then cooled to room temperature and imaged with STM, a powerful technique that enables the topography of a surface to be determined with atomic-scale resolution. Proposed structural models were verified by comparing experimental with theoretical images.

A New, Stable Surface: Prior to our investigations, only one stable surface of silicon was known to exist between the low index (001) and (111) planes: Si(113). We have discovered, however, that Si(5 5 12) is also a stable surface. Surfaces oriented very close to this plane consist of wide (5 5 12)-oriented terraces separated by small, jagged steps (Fig. 5, middle image). (It is difficult to exactly slice a crystal through a specified plane).

Our observation that Si(5 5 12) is stable is surprising given its large, complex unit cell (Fig. 6). Truncating a silicon crystal at this face would produce a complicated arrangement of atom rows with 34 surface atoms-per-unit cell. Atomic-resolution STM images reveal that the actual equilibrium surface has a row-like structure that has reconstructed. The reconstructed unit cell is twice as large along the rows as expected, incorporating 68 atoms in a unit cell measuring 0.77 nm by 5.35 nm. Our proposed model for the reconstructed surface produces a theoretical image in excellent agreement with experiment. It was the synergy between theory and experiment that enabled us to confidently determine the structure of the (5 5 12) surface—one of the most complex ever observed.

Quasi-periodic Faceting: If a silicon crystal is sliced a few degrees off the (5 5 12) plane, surfaces with sawtoothlike grooves are observed (Fig. 5, top and bottom images). The grooves are composed of alternating facets of the nearest stable surfaces, (5 5 12) and (111) or (5 5 12) and (113), depending on the direction of the slice. A novel aspect of these surfaces is the nearly periodic structure of the grooves. The period of the grooves depends on the structures of the nearby surfaces and can be varied from ~10 nm to
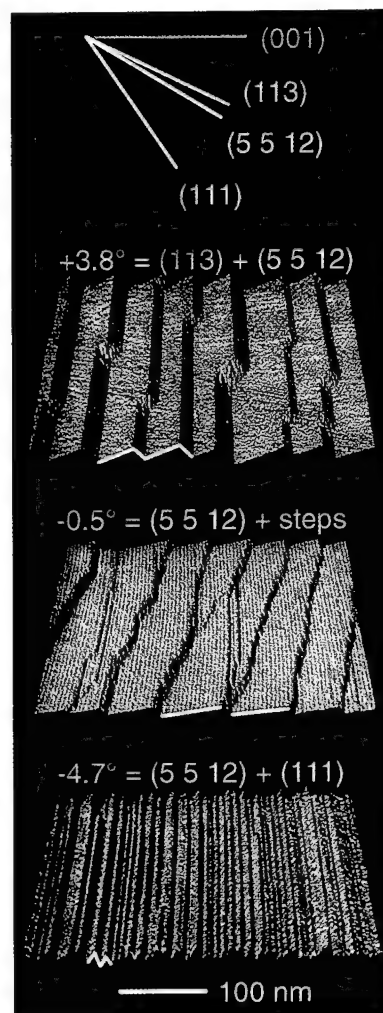
Fig. 5 — Three-dimensionally rendered STM images revealing the topography of silicon surfaces oriented near (5 5 12) (the relief has been magnified about 10 times). The angles refer to the orientation of the substrate with respect to the (5 5 12) plane, with positive angles tilted towards (001). The planes between (001) and (111) are illustrated to scale at the top of the figure.

~100 nm, depending on the orientation of the substrate.

Impact: Our studies of the structure and stability of high-index silicon surfaces may contribute to a variety of electronics applications within the DoD. The grooved or row-like structure of these surfaces should make them good substrates on which to grow films of other semiconductor materials. For example, we are currently working with Army researchers who are
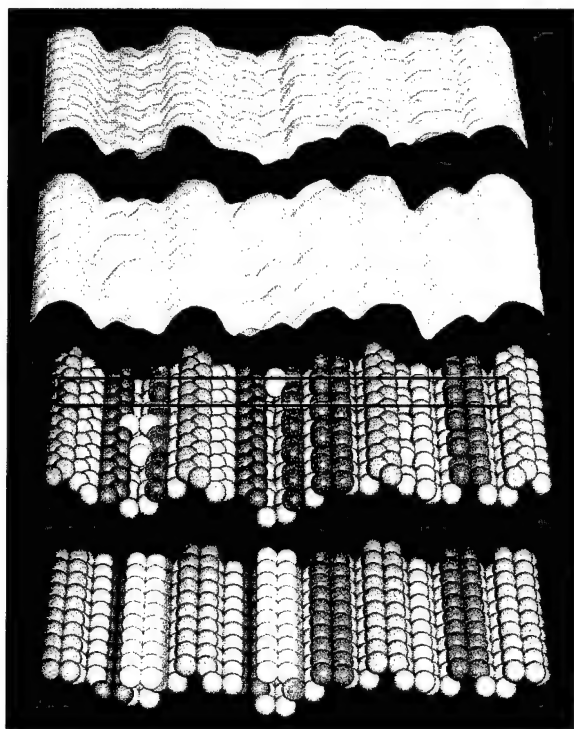
Fig. 6 — The atomic-scale structure of Si(5 5 12). Bottom: models of the bulk-truncated (very bottom) and reconstructed surfaces. The atoms are colored to highlight their proposed rearrangement within the reconstruction. Extra dimers of silicon occasionally observed on the surface are included in the reconstructed model (yellow atom pairs) for comparison with experiment. The unit cell on the reconstructed surface is indicated (black box). Top: Experimental (pink) and theoretical (blue) STM images of the surface. The theoretical image is based on the reconstructed model without extra dimers.

using high-index silicon substrates in HgCdTe-based night vision devices. Periodically grooved silicon surfaces may also be natural templates for the fabrication of nanometer-scale, one-dimensional semiconductor structures; the novel properties expected for such structures make them promising candidates for future electronic devices. Beyond these direct applications, our new understanding of silicon surface structure should become ever more important as the ongoing miniaturization of silicon-based electronics shrinks feature sizes to the nanometer scale.

[Sponsored by ONR]

References

1. A.A. Baski and L.J. Whitman, "Quasiperiodic Nanoscale Faceting on High-Index Si Surfaces," *Phys. Rev. Lett.* **74**, 956 (1995).

2. A.A. Baski, S.C. Erwin, and L.J. Whitman, "A Stable High-Index Surface of Silicon: Si(5 5 12)," *Science* **269**, 1556 (1995). ∎

Field Testing of Environmental Immunosensors

A.W. Kusterbeck and L.C. Shriver-Lake
Center for Bio/Molecular Science and Engineering

Approximately 50 DoD installations have been identified as Superfund Cleanup Sites by the Environmental Protection Agency (EPA). Two such sites—Umatilla Army Depot in Hermiston, Oregon, and Subase Bangor in Washington—were heavily contaminated by explosives disposal over the past 30 to 40 years. The soils in the former washout lagoons and aquifers in the surrounding regions contain parts-per-million concentrations of explosives, as well as other pollutants. Remediation is currently underway at these sites and is expected to take between 10 and 30 years to complete. To assist in monitoring remediation efforts, two NRL environmental sensors—the flow immunosensor and the fiber-optic biosensor—were used during two weeks of field trials to check for the presence of the explosives TNT and RDX in ground-water and lagoon leachate samples.

Background: Both biosensors were demonstrated to detect explosives in laboratory samples [1,2]. The instruments are sensitive, easy to operate, and have a rapid response time. The first sensor, the flow immunosensor, is based on antigen displacement of fluorescently labeled antigen from antibodies immobilized on beads. For each assay, antigen is injected into a flow stream that passes over a column of antibody-coated beads saturated with fluorescently labeled antigen. The displacement of the labeled antigen causes a proportional increase in fluorescence observed downstream. The other sensor, the fiber-optic biosensor, uses long, partially clad optical fibers. Antibodies are immobilized onto the fiber core in the unclad region of the probe. For explosives, competitive immunoassays are performed in which a decrease in fluorescence signal is proportional to the antigen concentration.

On-site testing: For the field trials, groundwater from 20 monitoring wells was pumped directly into 10- to 20-liter containers. Thirty-five samples, including well dilutions, were run on-site by NRL personnel without extractions or prior filtering. Figure 7 shows the test site at Umatilla. To calibrate the sensors, EPA standards were also tested on-site. For the flow immunosensor, a 100-µl test sample was injected onto individual columns that measured either TNT or RDX, and the instrument response was recorded. Analysis times were between 2 and 5 min per sample. In the fiber-optic biosensor, 500-µl test samples containing 75 µl of a fluorescently labeled antigen in buffer were injected over the antibody-coated fiber-optic probe. Assay times, including regeneration of the fiber-optic probe, were approximately 10 min per sample. Triplicate samples were run simultaneously on the fiber-optic biosensor. The results from the two sensors were compared to EPA values obtained from independent, high-performance liquid chromatography (HPLC) analyses of identical splits taken from the original samples. Tables 1 and 2 represent the results for the primary test wells at both sites. Figure 8 demonstrates the accuracy and precision of the NRL immunosensors over a large concentration range to the accepted EPA method for explosives determinations in water samples. From analysis of the data, NRL methods give an overall view of groundwater contamination that is analogous to the HPLC method.
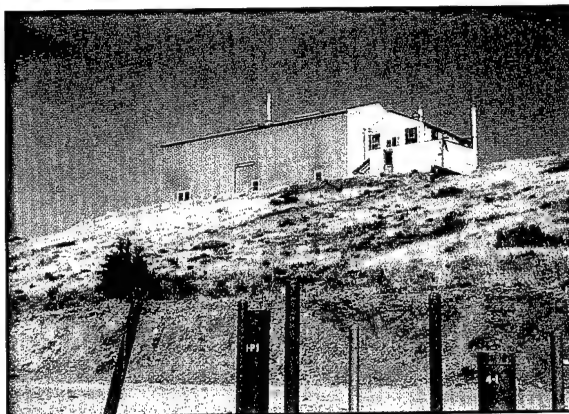
Fig. 7 — Field trial test site, Umatilla Army Depot. The extent of explosives contamination in groundwater was determined using samples obtained from monitoring (foreground) located in waste lagoons. The former munitions washout plant is shown in the background.

Conclusions: Environmental cleanup and pollution control have become high-priority issues for the Navy and DoD. In particular, levels of important pollutants—including explosives—must be accurately monitored during site characterization and remediation. Initial field trials with two NRL immunosensors have demonstrated detection and quantitation of groundwater contamination comparable to EPA analyses. However, the NRL methods can be used on-site, with no sample pretreatment and minimal technical training. Many of the difficulties encountered with sample

Table 1 — TNT Detection (µg/L)

UMATILLA			
Well #	EPA	Flow Immunosensor	Fiber Optic Sensor
Well 4-1-2	198	276	208
Well 4-P-2	3155	3522	3401
Well 4-18-2	299	368	366
Well 4-2	nd	nd	nd
BANGOR			
BEW-1	317	1916	1435
BEW-2	30	56	30
BEW-3	65	62	185
BEW-4	nd	nd	nd

Table 2 — RDX Detection* (µg/L)

UMATILLA		
Well #	EPA	Flow Immunosensor
Well 4-1-2	160	194
Well 4-18-0	1700	1693
Well 4-18-2	170	150
Well 4-2	0.16	nd
Well 4-P-4	4000	4439
Well 4-101	1700	1683
BANGOR		
BEW-1	260	325
BEW-2	640	543
BEW-3	290	263
BEW-4	13	33
BEW-5	56	66
BEW-6	710	770

*RDX measurements were performed only in the flow immunosensor due to limited antibody availability.
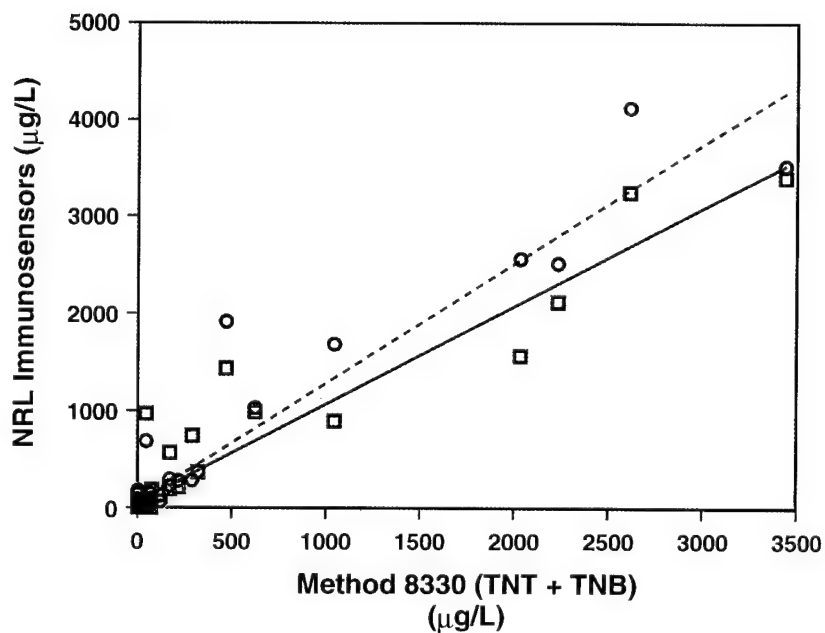
Fig. 8 — Comparison of NRL Immunosensors to EPA Method 8330 (HPLC). Both the flow immunosensor (O) and the fiber-optic biosensor (□) were compared to the HPLC method for explosives detection. From the linear regression analysis, the slope and correlation (r²) values for the flow immunosensor are 1.23 and 0.91. The values for the fiber-optic biosensor are 1.01 and 0.90.

shipping, use of solvents, and laboratory reporting times (typically 2 to 4 weeks) can also be avoided. Application of these systems to the environmental problem should provide improved, cost-effective alternatives to traditional laboratory methods.

References

1. J.P. Whelan, A.W. Kusterbeck, G.A. Wemhoff, R. Bredehorst, and F.S. Ligler, "Continuous-Flow Immunosensor for Detection of Explosives," *Analy. Chem.* **65**, 3561-3565 (1993).

2. L.C. Shriver-Lake, K.A. Breslin, P.T. Charles, D.W. Conrad, J.P. Golden, and F.S. Ligler, "Detection of TNT in Water Using an Evanescent Wave Fiber-Optic Biosensor," *Analy. Chem.* **67**, 2431-2435 (1995). ∎

Electronics
and
Electromagnetics

AN/SPQ-9B ADM Radar

L.M. Leibowitz, L.M. Schaus, and D.J. Cardiel
Radar Division

Sea-skimming missiles are a major threat to U.S. naval ships. NRL, supported by the Program Executive Office, Theater Air Defense (PEO(TAD)), has developed an important new concept for anti-ship missile defense (ASMD). The AN/SPQ-9B radar concept maintains AN/SPQ-9A radar Gun Fire Control System (GFCS) MK 86 support while adding a new, low-cost, quality sea-skimmer detection capability to the Fleet. The AN/SPQ-9B provides significantly increased sensitivity and improved ability to detect targets in clutter. A surface mode maintains or improves performance in support of the GFCS MK 86 and backup navigation. An air mode provides the new sea-skimmer detection capability. An AN/SPQ-9B Advanced Development Model (ADM) radar was successfully land-based tested at Wallops Island, Virginia, and more recently in an at-sea shipboard environment.

ADM Radar: NRL designed and assembled an ADM radar to prove the AN/SPQ-9B concept and reduce development risk [1]. State-of-the-art nondevelopment item and commercial-off-the-shelf (COTS) components were used to obtain significant advances in signal-to-clutter performance on a tight schedule at low cost. The current pedestal was modified, the reflector was replaced by a larger unit with multiple feeds, a new processor and receiver/exciter were developed, and the transmitter was replaced by a USAF AN/APG-68 radar transmitter.

A sensitivity high enough to detect difficult threats is achieved by the larger antenna, increased power from the AN/APG-68 low-phase noise transmitter, receiver noise figure improvement by use of a low-noise amplifier (LNA) at the antenna, and other loss reductions. In the air mode, pulse-Doppler waveforms with appropriate pulse-repetition frequencies (PRFs) provide a velocity notch that allows sea-skimmer detection in clutter. Clutter filtering is sufficient to reduce close-in clutter (competing with weak far-range targets) to near thermal noise. Current surface functions are maintained by a pulse waveform, which is time- and frequency-division multiplexed with the pulse-Doppler waveform to form a composite radar waveform and essentially provide

two radars in one. Surface mode video returns are displayed on a pulse-position indicator (PPI) and are used for GFCS MK 86 functions.

Major units of the ADM radar include antenna, transmitter, receiver/exciter, processor, display, and radome. The current AN/SPQ-9A radar antenna unit was modified under contract to provide a larger reflector having three beam positions controlled by an electronic microwave switch, a new azimuth drive motor to provide a reduced rotation rate, slip rings in the azimuth drive system to furnish control signals to the microwave switch, a circulator and receiver protector, a microwave enclosure housing the LNA, and a COTS radome. An AN/APG-68 radar transmitter was borrowed from the USAF and, under contract, configured for shipboard use. An ultra-low phase-noise signal generator, used for frequency synthesis, was procured. The circulator, receiver protector, and high-power microwave switch were purchased. The processor was configured from COTS 6U-size VME bus boards and supported by COTS software. The track display was implemented by a Sun SPARCstation 2 with NRL-modified Johns Hopkins University/Applied Physics Laboratory AutoID software. Using COTS components, NRL designed and constructed the local oscillation (LO) distribution, exciter, receiver, and baseband waveform generator. NRL wrote the software for the system controller, timing, I/O, signal processing, and tracking functions, performed system integration, testing, and documented the results.

Testing: The AN/SPQ-9B ADM radar was successfully land-based tested at Wallops Island in 1993 using test targets, including Doppler repeaters, Lear jet aircraft, and airborne towed targets. The results demonstrate the ability to provide required firm-track ranges and achieve a major improvement in the detection of targets in clutter. As shown in Fig. 1, the ADM radar was installed on board the PEO(TAD) Self-Defense Test Ship for risk-reduction testing in an at-sea littoral environment in December 1994 and January 1995. Test targets included a BQM-74E sea skimmer, F-16 supersonic fighter aircraft, EA-6B aircraft, and targets of opportunity. Excellent firm-track ranges were obtained in excess of the minimum required thresholds. These results confirm the ability of the AN/SPQ-9B radar concept to achieve firm-track performance thresholds in an at-sea
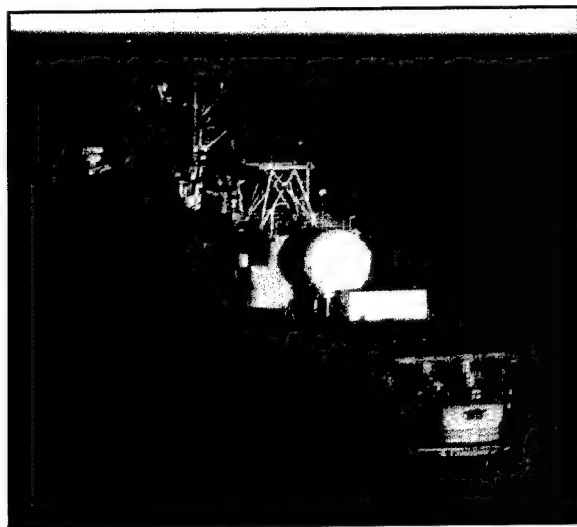
Fig. 1 — The AN/SPQ-9B ADM radar radome and equipment container installed forward of the helo deck on board the Self-Defense Test Ship (ex-USS *Decatur*).

environment and reduce development risk to the Navy.

Preproduction Contract: An AN/SPQ-9B radar prime-item development specification was developed jointly by NRL and the Port Hueneme and Crane Divisions of the Naval Surface Warfare Center. In October 1994, PEO(TAD) awarded a contract to Westinghouse Norden Systems for two AN/SPQ-9B preproduction kits, with an option for six low-rate initial production kits. As an ordnance alteration (ORDALT) kit to the existing GFCS MK 86, the radar is currently planned for installation on DD-963, LHA-1, DDG-993, and CG-47 ship classes and is also being considered for installation as a horizon-search radar on several other ship classes that do not currently host a GFCS MK 86. The AN/SPQ-9B radar, with its unprecedented ability to detect modern, low-altitude air threats in a clutter environment, promises to be a low-cost, effective means of ship self-defense. Successful land-based and at-sea test results significantly reduce the Navy's overall development risk and cost and hasten the introduction of this new, robust, sea-skimmer detection capability to the Fleet.

Science and Technology Base: The AN/SPQ-9B radar development evolved from the science and technology base obtained under the NRL Radar Division research program.

Reference

1. B.H. Cantrell, L.M. Leibowitz, D.J. Cardiel, B. Connolly, S.A. Lessin, M.E. Rachuba, G.C. Tavik, and M.F. Walder, "Advanced Development Model of the AN/SPQ-9(I) Radar," NRL Memorandum Report 7608, 3 October 1994. ∎

Ferroelectric Lens Phased Arrays

J.B.L. Rao, D.P. Patel, and W.R. Pickles
Radar Division

The Navy needs phased array radars for self- and area defense. Phased array antennas can steer transmitted and received signals without mechanically rotating the antenna. Each element of a phased array is connected to a phase shifter, which determines the phase of the signal at each element to form a beam at the desired angle. The most commonly used are ferrite and diode phase shifters. A typical phased array may have several thousand elements and requires that many phase shifters; hence, it is very expensive. Therefore, reducing the cost and complexity of the phase shifters and their controls are important considerations in the design of phased arrays. A new lens phased array reported here (for which a Navy patent application is pending) uniquely incorporates bulk phase shifting—the array does not contain individual phase shifters—using ferroelectric material with applied bias voltage to control the amount of phase shift in a phased array [1]. Bulk phase shifting using diodes has been proposed and reasonably developed in the Radant lens [2]. The lens described here uses a voltage-controlled ferroelectric dielectric, which introduces analog rather than digital phase shift, as in the Radant lens. The ferroelectric lens has further advantages of smaller lens thickness, higher power handling,

and simpler beam steering controls, and it uses less power to control the phase shift compared to the Radant lens. Thus it can potentially lead to affordable phased arrays that are also compact and lightweight.

Lens Description: Figure 2(a) shows the dielectric lens, which is made up of dielectric slabs sandwiched between conducting plates. The dielectric slabs are a ferroelectric material whose dielectric constant can be changed by applying and varying a dc bias voltage. If a plane wave is incident on one side of the lens with an RF electric field E normal to the conducting plates, the beam that is formed on the other side of the lens can be scanned in the E plane, if a linear phase gradient is introduced along the E-plane direction by adjusting the applied bias voltage. An individual section between two conducting parallel plates of the lens can be considered as one column of a phased array. The top view of a column is shown in Fig. 2(b). The separation between the plates is decreased using a step to eliminate higher order modes and to reduce the bias voltage necessary to create a certain amount of dc electric field intensity in the ferroelectric. Quarter-wave dielectric transformers are used for impedance matching of the air region to the ferroelectric region.

The lens proposed here can be fed by a planar array—like a slotted waveguide array. A slotted waveguide array with phase shifters in combination with the lens can be used as an antenna that can scan in two planes. A space feed can also be used with the combination of two lenses proposed here (with a polarizer in between) to scan the beam in two planes [1].

Theoretical and Experimental Results: For the initial theoretical studies of the ferroelectric lens, only one column of the lens is analyzed. The column height is assumed infinite in extent, and hence it becomes a two-dimensional parallel plate waveguide with the electric field normal to the plates as shown in Fig. 2(b). Theoretical analysis was also performed using Touchstone, a commonly available software, for a rectangular waveguide, with the cross section shown in Fig. 2(b). The analysis was done assuming different column heights (waveguide widths). For practical reasons, most of the initial measurements were performed in a WR90 waveguide. So the results included here are for the rectangular waveguide configura-

(a)

(b)
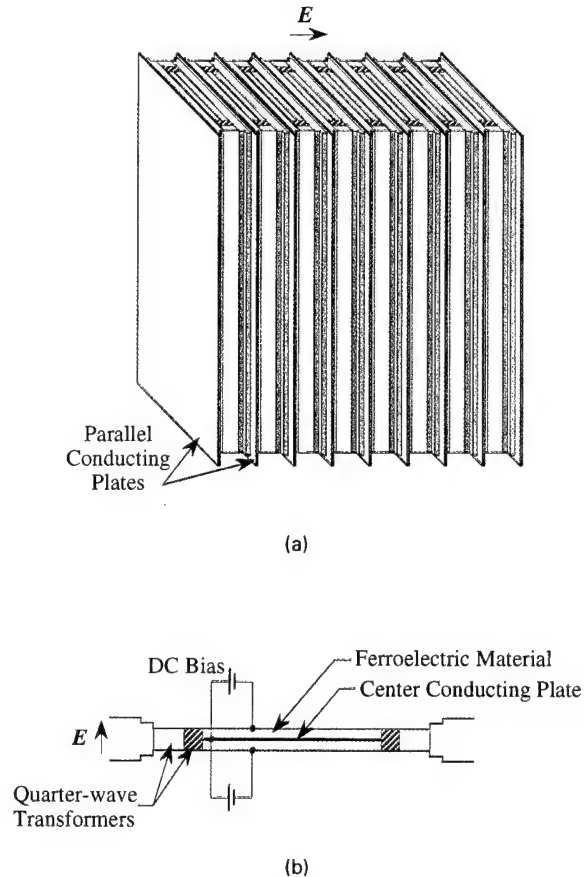
Fig. 2 — Configuration of: (a) ferroelectric lens; (b) top view of one column.

tion only. Figure 3 shows the theoretical voltage reflection coefficient as a function of frequency for a ferroelectric material with a dielectric constant $\epsilon_r \approx 110$. The impedance match was optimized for the frequency range of 8 to 12 GHz. The results indicate that the ferroelectric lens can be matched well to free space. Figure 3 also shows the experimental results for reflection coefficient for a ferroelectric dielectric with $\epsilon_r \approx 110$. The results are comparable to the theoretical predictions. Figure 4 shows the change in insertion phase with applied bias voltage; the results are as expected.

Conclusions: A new concept for a low-cost phased array radar using a voltage-controlled ferroelectric lens antenna was proposed. Theoretical analysis indicated that the ferroelectric lens concept is viable and sound. The initial experimental results are very encouraging.
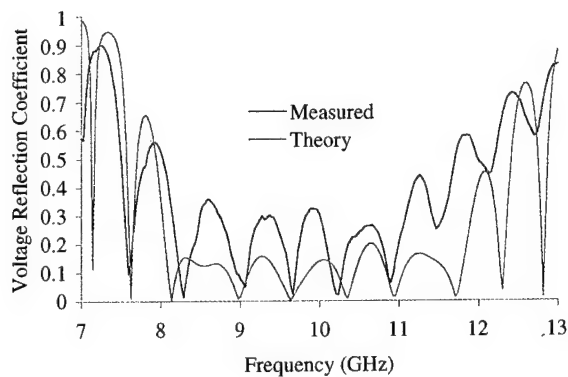
Fig. 3 — Theoretical and experimental voltage reflection coefficient.
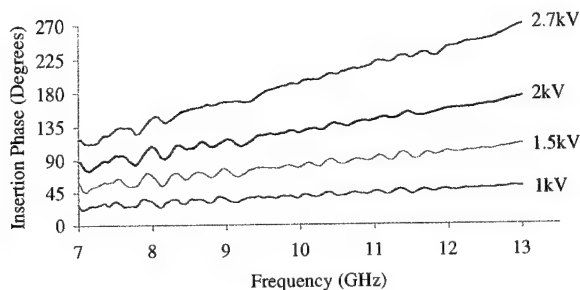
Fig. 4 — Measured change in insertion phase of ferroelectric for various dc bias voltages.

Acknowledgment: Thanks are given to Dr. Louise Sengupta, of the U. S. Army Research Laboratory, for collaborating with us by providing suitable ferroelectric materials.

[Sponsored by ONR]

References

1. J.B.L. Rao, "Low Cost Phased Arrays," NRL Memorandum Report 7793, Nov. 1995.

2. J. Leibinger, "Demonstration of Two-Axis Electronic Scanning by a Hybrid Radant-TM Lens Array," Rome Laboratory, Final Technical Report No. RL-TR-91-201, Sept. 1991. ■

Small Ship ESM System

J.J. Briguglio
Tactical Electronic Warfare Division

Requirement: The need has arisen for the passive intercept, location, identification, and tracking of friendly, neutral, and hostile emitters in near real time, for immediate situational awareness and targeting information aboard U.S. Navy ships in operational situations. The Tactical Electronic Warfare (TEW) Division has developed a low-cost and lightweight system that meets these needs of ship commanders for providing timely and accurate information. This system is an innovative application of commercially available, high-technology computing and NRL-pioneered RF and signal processing technology, coupled with the application of recent advances in lightweight composite materials to produce this highly capable, versatile, and low-cost system.

System Implementation: The Small Ship Electronic Support Measures (ESM) System (Fig. 5) uses several technologies developed by NRL for naval applications. This system is composed of a lightweight antenna/receiver pedestal, an antenna/receiver controller, and an advanced ESM signal processor. The antenna/receiver pedestal is a complete receiving subsystem consisting of a dual-aperture directed antenna, an omnidirectional antenna, and a monolithic microwave integrated circuit (MMIC) superheterodyne receiver. Narrow, wide, and omnidirectional antenna selection and receiver operation are provided over the frequency range of 0.5 to 18 GHz. The antenna/receiver pedestal is constructed for ship topside mounting and weighs < 50 lbs. This processor, housed in a standard ATR chassis, is constructed to withstand extreme environmental conditions, including carrier takeoff and landing.

Key Technologies: Several technologies developed by NRL contribute to the lightweight, compact size, low cost, and significant capability afforded by this system.

NRL directed research into the application of composite materials and unique fabrication techniques for the development of the antenna reflector assembly. Problems that had to be overcome included metal-to-composite adherence and dimensional stability of the parabolic reflecting surface. These problems were corrected by special etching of the reflecting surface and controlled curing of the adhesives. The payoffs were improved antenna performance, low cost, and significant weight reductions of the antenna housing.
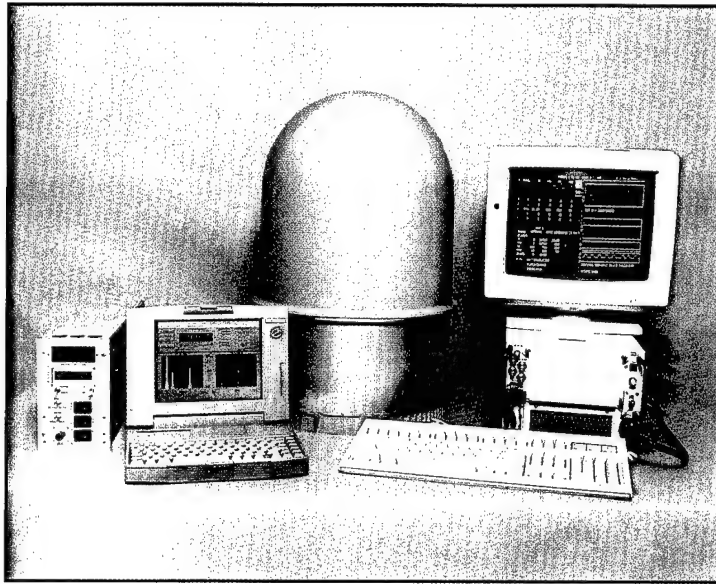
Fig. 5 — Small ship ESM system.

The NRL-developed compact wideband MMIC receiver (Fig. 6) also contributes to size, weight, and cost reduction while improving overall system performance. To accomplish the production of the compact, wideband receiver, NRL developed several custom MMIC components specifically for this application, pushing MMIC technology to new limits. These and commercially available components were combined with power management logic to form the current Phase II MMIC EW receiver.

The advanced signal processor uses the latest technology in analog-to-digital signal sampling and digital signal processing techniques to separate and identify simple and complex emitters. A key component is a complete baseband digital receiver. High-speed digital sampling allows accurate timing and signal parameters to be measured. The processing techniques include several novel and unique algorithms pioneered by NRL for identification and tracking purposes. These processing techniques have proven to be operationally imperative for certain missions and useful on all platforms.

Operational Uses: This system can be easily installed on small and large ships to intercept, locate, and identify emitters and associated platforms based on platform RF emissions. These systems and variants are presently in use by
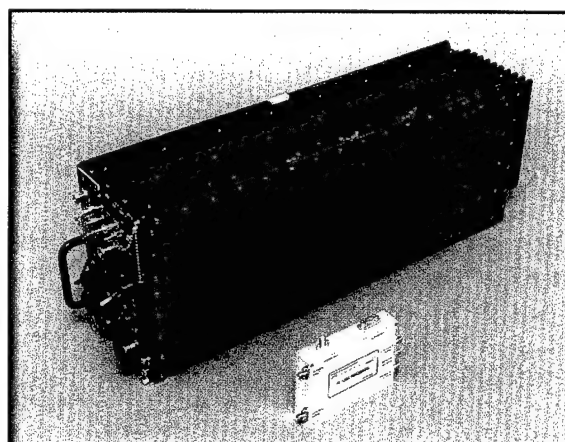
Fig. 6 — Conventional EW receiver (top) vs MMIC EW receiver.

operational forces to collect and identify signals. The operational effectiveness of these systems has been demonstrated in both field exercises and by deployed forces.

References

1. L.W. Lemley, "The Microwave Monolithic Integrated Circuit/Electronic Warfare Receiver," *1994 NRL Review*, Naval Research Laboratory, Washington, D.C., pp. 141-144. ■

Missile Radar Performance Characterization

D.W. Kahl
Tactical Electronic Warfare Division

Background: All tracking radar systems have characteristics that define their ability to detect and track targets. In addition to quantitative characteristics, such as transmitted power, antenna gain, and operating frequency, the performance of many radar systems is also significantly affected by the ability of the operator who interprets and reacts to the data displayed on the radar screen. Missile radar guidance systems are quite different, however, since they generally operate autonomously after launch. The missile radar seeker scans the environment for potential targets, selects a target to track, and then provides guidance data to the missile autopilot. All of these functions are performed without human intervention. If the logic programmed into the seeker performs as designed and the seeker does not encounter any unexpected conditions, the missile will ultimately intercept the target.

Radar Characteristics and EW: For NRL's Tactical Electronic Warfare Division (TEWD), knowledge of the performance characteristics of missile radar guidance systems is essential to

fulfilling its mission of developing and testing electronic warfare (EW) tactics and techniques for the U.S. Navy. Although developing EW techniques is somewhat of an art, the technique developer begins the process with the knowledge of the missile radar system's operational characteristics and weaknesses. Since much of these data are typically not available outside the manufacturing environment, they must be determined by the EW community prior to developing and deploying an effective countermeasure. The Integrated EW Simulations (IEWS) Branch of the TEWD has developed a set of automated tests for characterizing the performance of RF-guided missile seekers in the Central Target Simulator (CTS) facility. The tests quantify numerous tracking radar characteristics, and the test data aid division personnel with the development and optimization of both passive and active countermeasures.

CTS Characterization: The CTS facility consists of a large RF anechoic chamber which, under computer control, generates and radiates realistic radar returns for the missile seeker to receive and process. IEWS engineers have developed characterization test software for CTS using the Visual Basic programming language. Visual Basic provides the tools necessary to develop a user-friendly graphical interface that runs on a standard PC under the familiar Windows environment. Engineers use the software's main window, shown in Fig. 7, to select the characterization test, data acquisition system, and target generation system interface. A second-level window is used to establish the required target and test parameters. Default values allow tests to be performed without entering information. The third-level window, shown in Fig. 8, is used to view seeker data while the test is being performed. This feature allows the test operator to visually verify the results prior to saving the data. The intuitive design of the graphical interface makes it a valuable tool for accessing the numerous capabilities of CTS, including those not required for characterization testing. The interface has also simplified the process of training new CTS operations personnel.

The characterization software currently runs on a 66 MHz 80486 computer. During test periods, this computer communicates with three other PCs in the facility to set up the required test conditions and acquire data from the missile seeker being evaluated. The software initially
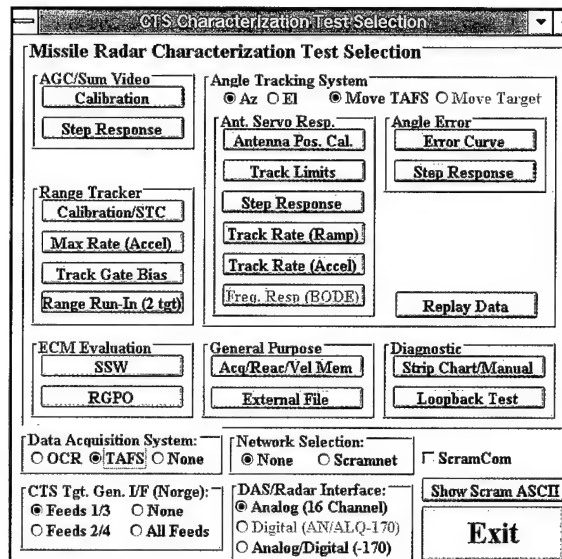
Fig. 7 — Main characterization window.
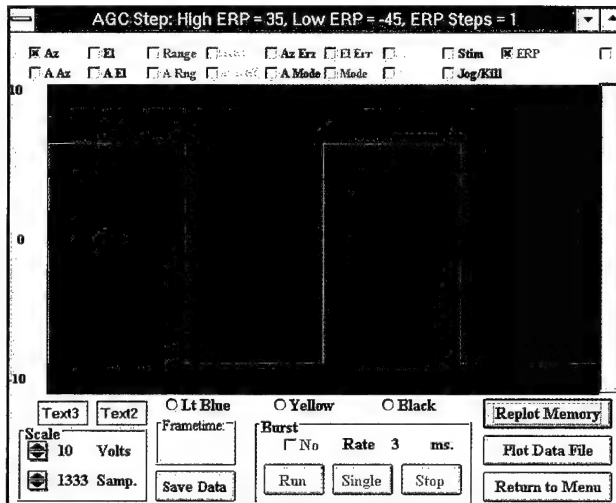
Fig. 8 — Typical characterization data display window.

used real-time Ethernet communications made possible by custom drivers written by IEWS personnel. This configuration allowed tests to be performed at frame rates of up to 100 Hz. Although this frame rate was adequate for many of the tests, several key tests required frame rates of at least 250 Hz. A reflective memory fiber-optic network was recently added to the facility; tests are now performed at frame rates of up to 500 Hz.

At the present time, approximately 75 different characterization tests can be performed. The majority of these tests stress one particular aspect of the seeker to determine its performance limit. Typical parameters obtained from the testing are maximum range tracking rate, maximum angle tracking rate, angle step response, and Automatic Gain Control step response.

Summary: The missile radar characterization performed in the CTS facility is a vital and necessary first step in the process of developing and deploying effective antiship missile countermeasures for the U.S. Navy. The test environment and capabilities developed by NRL are easy to use and provide accurate and repeatable results. The recent improvements to the characterization process allow the test and evaluation capabilities to keep pace with today's generation of threat hardware.

∎

A Novel Coaxial Free-Electron Laser

M. Blank, R.H. Jackson, and H.P. Freund
Electronics Science and Technology Division

Millimeter-wave systems offer substantial performance improvements over microwave systems for many Navy applications, including high-resolution fire-control radars, target-identification radars, advanced missile seekers, and broadband jammers. Specific system needs and platform constraints impose a wide array of demands on the performance and packaging of the coherent electromagnetic wave source. The free-electron maser (FEM) is a promising radiation source for future millimeter wave systems. However, typical FEMs require electron beams with voltages ranging from hundreds of kilovolts to megavolts. For Navy applications, operation below 100 kV is critical. Current research in the Vacuum Electronics Branch is aimed at designing and demonstrating high-power, broadband FEMs with operating voltages that are compatible with airborne and shipboard radar systems.

The FEM is a versatile electromagnetic source that can produce coherent radiation over virtually the entire spectrum—from microwaves to visible light. The FEM interaction occurs when an electron beam traverses a periodic magnetic field produced by a wiggler, which imparts an undulatory motion to the beam. The undulating beam then loses its energy to a resonant electromagnetic wave and the wave is amplified. The resonant frequency is proportional to the axial velocity of the electron beam and inversely proportional to the wiggler period. High-frequency, low-voltage operation can be achieved by reducing the wiggler period. Unfortunately, decreasing the period results in a decreased wiggler field amplitude, which leads to a reduction in the gain and efficiency. Coaxial wiggler configurations, wherein the inner structure aids in maintaining the field strength as the wiggler period is decreased, can be used to design high-frequency, low-voltage FEMs.

Wiggler Concept: The wiggler under consideration (Fig. 9) consists of two bifilar helical current windings arranged in a coaxial configuration. The outer winding produces a helical magnetic field whose amplitude increases as the radius increases from a to b. The inner winding pro-
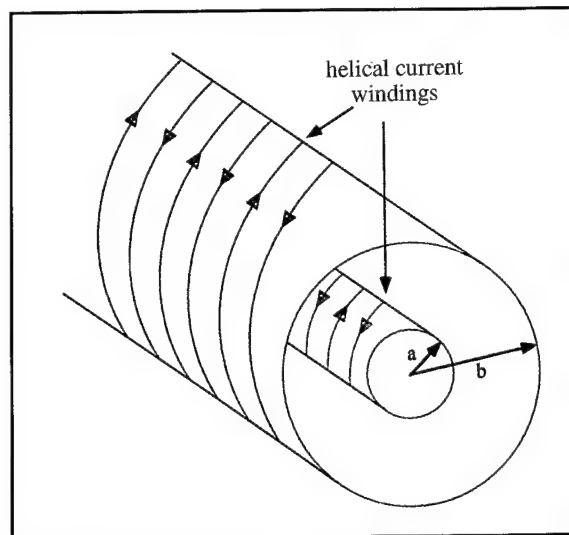
Fig. 9 — A coaxial wiggler with inner and outer bifilar helical current windings. The inner and outer windings are located at $r = a$ and $r = b$, respectively.

duces a second helical field which decreases as the radius increases from a to b. The combined field will have a minimum near the center of the radial gap, which tends to focus the electron beam against spread due to self-fields. This configuration is also advantageous in that large wiggler fields can be achieved by running moderate currents through the inner and outer wigglers. In contrast, for a typical bifilar helical wiggler consisting of only the outer winding, the currents required for strong wiggler fields become prohibitively high as the wiggler period is reduced.

Nonlinear Simulations: The ARACHNE [1] nonlinear simulation code was used to examine the FEM interaction between an annular electron beam and the 17 GHz TE_{11} coaxial waveguide mode in the presence of a coaxial bifilar helical wiggler. Performance predictions for the annular beam device are compared to simulations for a solid beam, undulated by a single (outer) helical wiggler, interacting with the TE_{11} cylindrical waveguide mode at 17 GHz. Figure 10 plots the results. The beam current, beam voltage, wiggler period, and transverse wiggler field at the beam location are constant for the two cases. Figure 10 also shows that use of the annular beam and coaxial wiggler results in dramatic performance improvements over the solid beam, single-wiggler FEM. The saturated power for the annular beam case is more than twice that of the solid beam. In
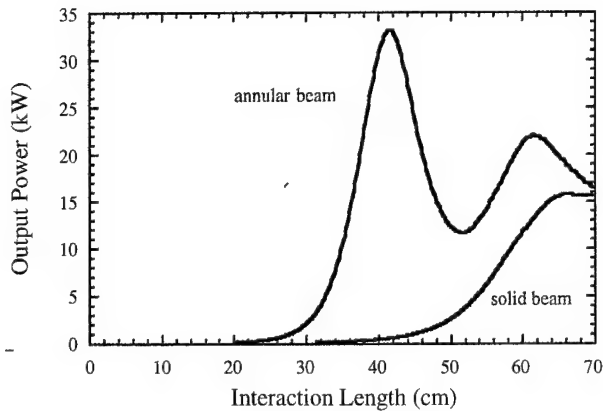
Fig. 10 — Nonlinear theory predictions of output power for a solid beam in a single bifilar helical wiggler field (red) and an annular beam in a coaxial wiggler (blue). The beam voltage, beam current, wiggler period, and wiggler field at the beam location were held constant for the two cases.

Fig. 11 — Nonlinear theory predictions of efficiency for the coaxial FEM.

addition, the saturation length is significantly reduced for the hollow beam, indicating that a reduction in device length is possible.

The nonlinear code was next used to examine the theoretical efficiency vs frequency for the coaxial FEM; Fig. 11 plots the results. The simulations were made for a 55 kV, 5 Å annular electron beam. The wiggler period is 0.9 cm and the currents in the inner and outer windings are 275 Å and 450 Å, respectively. The combined radial wiggler field at the center of the gap is approximately 1 kG. In addition, a 3 kG constant amplitude axial guide field is applied. The input power is 1 W in the coaxial TE_{11} mode.

As Fig. 11 shows, the maximum efficiency is 11.8%, corresponding to an output power of 33 kW and 45 dB saturated gain. The 3 dB instantaneous bandwidth is greater than 20%. These simulated results can be compared to the results of a K_u-band FEM experiment recently completed in the branch [2]. In the experiment, a 255 kV, 94 Å solid electron beam interacted with the TE_{11} cylindrical waveguide mode in K_a band. A single outer helical wiggler was used. The measured efficiency was 17.5%, and the instantaneous band-

width was greater than 22%. The simulations show that a 55 kV coaxial K_u-band FEM achieves an efficiency and bandwidth that are comparable to those of a 255 kV cylindrical waveguide FEM. Thus, the novel coaxial wiggler can be used to maintain device performance while reducing the beam kinetic energy by more than a factor of four. With high output power, large instantaneous bandwidth, and reduced operating voltage, the coaxial FEM is a promising source for future millimeter wave systems.

References

1. H.P. Freund and T.M. Antonsen, Jr., in *Principles of Free-Electron Lasers* (Chapman & Hall, London, 1992).

2. D.E. Pershing, R.D. Seeley, R.H. Jackson, H.P. Freund, "Amplifier Performance of the NRL Ubitron," *Nucl. Instr. and Meth. Phys. Res. A,* **358**, 104-107 (1995). ∎

Energetic Particles, Plasmas, and Beams

In Situ Monitoring of the Absorption of Deuterium into Palladium Using Synchrotron-Wiggler Radiation

E.F. Skelton and S.B. Qadri
Condensed Matter and Radiation Sciences Division

P.L. Hagans and D.D. Dominguez
Chemistry Division

Palladium-hydrogen(deuterium) [Pd-H(D)] is probably the most extensively investigated of all metal-hydride(deuteride) systems. Nevertheless, some of its properties at high hydrogen (deuterium) concentration still remain unexplained. Claims have been made of possible anomalous power production in this system. Therefore, it is important to understand the mechanisms involved in the absorption or desorption of hydrogen or deuterium, especially at high concentration levels. This work was initiated in order to provide crystallographic structural information from regions inaccessible with standard X-ray diffraction methods.

X-ray diffraction is the technique most commonly used for crystallographic structural studies. It can detect changes in the Pd-lattice as hydrogen (or deuterium) is loaded into the Pd. However, because of the absorption of energy from the X-ray beam, principally by the Pd, this information is limited to the first few microns from the surface. Whether changes in this region are representative of changes taking place in the interior is an open question. One way to answer this question is by increasing the energy of the X-ray photons. Typically an increase of an order of magnitude in the X-ray energy corresponds to an increase of two orders of magnitude in the absorption length. Therefore, this experiment was performed at one of the most intense sources of high energy X-rays in the world, namely, NRL's synchrotron-wiggler beam line (X17C) at the National Synchrotron Light Source (NSLS), Brookhaven National Laboratory. In contrast to the 8 keV photons available from a Cu X-ray tube, photons up to 80 keV are used on X17C.

Structural Changes: As x in PdH_x (or PdD_x) is increased at room temperature, there are three distinct crystallographic regions: for x < 0.02, the material is in the α-phase; for x > 0.7, the sample is in the β-phase; and for 0.02 < x < 0.7, a mixture of both phases exists. All three phases—pure-Pd, α, and β—are face-centered cubic (FCC). Neutron diffraction studies have shown that the H(or D)-atoms are located in the octahedral interstitial sites of the Pd-lattice [1]. The unit cell parameter for the α-phase is very close to that of pure Pd (3.8898 Å), but there is about a 10% volume increase associated with the α-to-β phase transition.

Experimental Procedure: A 1-mm diameter Pd wire is rigidly mounted and centered in a polyethylene electrochemical cell. The wire serves as the cathode and is surrounded by a 0.254-mm thick graphite foil, the anode. The cell is filled with an electrolyte of 0.1 M LiOD in D_2O, and deuterium is electrochemically driven into the wire. Figure 1 is a schematic drawing of the experimental set-up. The entire electrochemical cell can be translated in either of the three orthogonal directions shown (x,y,z).

White X-rays from the superconducting wiggler on beamline X17 at NSLS are reduced to a narrow pencil of radiation, 28 × 28 μm^2 in cross-section. The scattered radiation is measured at an adjustable angle (2θ) with an intrinsic Ge energy-sensitive detector. Any portion of the Pd wire can be studied by appropriate adjustment of the x,y,z settings. Data are collected from a microspot 18 × 10^{-12} m^3 in volume.

The penetrating power of the higher energy X-ray photons is demonstrated by the two diffraction spectra shown in Fig. 2. Both are recorded from the same amount of volume of PdD_x and show several diffraction peaks. The left spectrum is recorded from the edge of the wire and shows all possible diffraction peaks within the energy range covered. The right spectrum is recorded from the core of the wire, and all but the highest diffraction peaks are lost due to the absorption of the Pd. There also is a precipitous decrease in the lower energy background intensity. It is further noted that in situ experiments (such as performed here) would not be possible with Cu Kα radiation, for example, because of the absorption by the polyethylene electrochemical cell, the graphite anode, and the electrolyte.

Results: Spectra were recorded from the edge of the wire in 100-μm steps to the core. This was done as a function of time of electrolysis and current density. Each of the phases involved in this study are cubic. Therefore, any
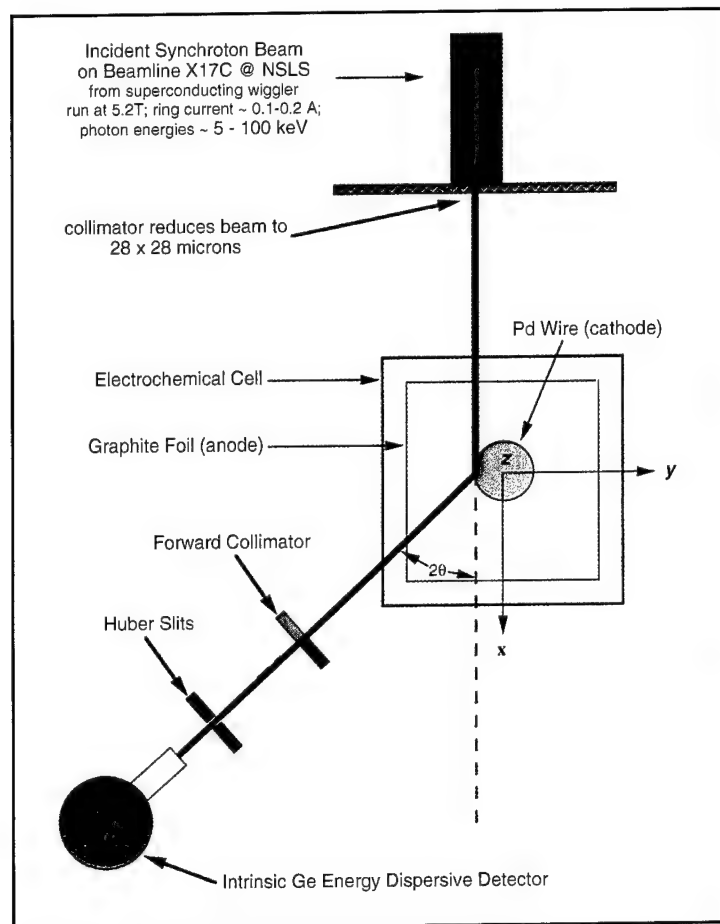
Fig. 1 — The experimental setup.
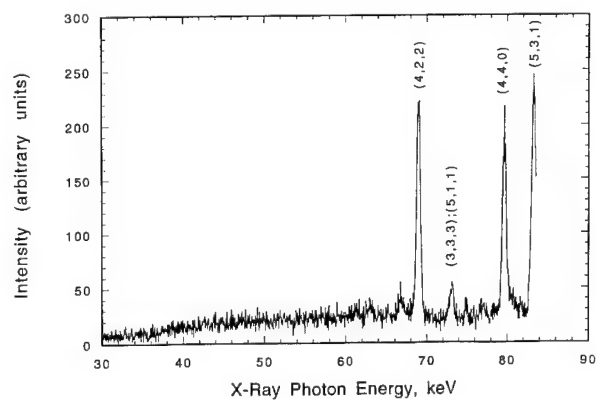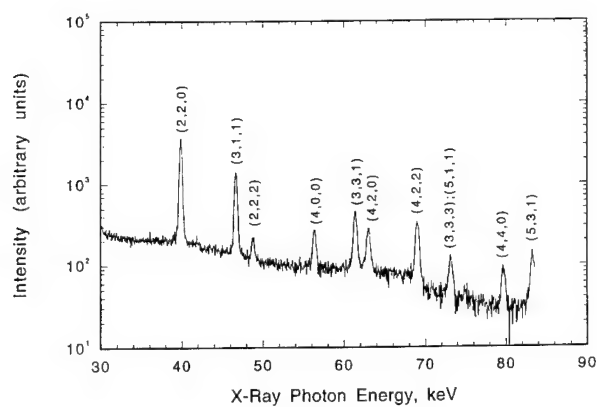
Fig. 2 — Energy dispersive diffraction pattern taken from a 18×10^{-12} m^3 volume of PdD$_x$ from the edge (left curve) and from the core (right curve).

of the diffraction peaks can be used to monitor the crystallographic changes. The (4,2,2)-peak was used. Based on a comparison of the volume change measured from the spectra, the transition from the mixed phase region ($\alpha + \beta$) to the pure β-phase takes place at the same time at the edge and the core. This suggests that all of the octahedral sites of the α-phase must be filled before transition to the pure β-phase occurs. Results also show that, although the α-phase forms rapidly at both the surface and the core, there is considerable delay in the initiation of the β-phase at the core compared to that at the surface.

Work continues on this project, focusing on simultaneous measurements of the resistivity of the wire and the structure. This will permit a more detailed comparison of the lattice and volume changes as a function of loading. These details may lead to an improved understanding of this system, especially at high concentration levels and could shed light on claims made for anomalous power production mechanisms in this system.

[Sponsored by ONR]

Reference

1. Y. Fukai and N. Okuma, *Phys. Rev. Lett.* **73**, 1640 (1994) and references therein. ∎

Laboratory Research in Space Plasma Physics

D.N. Walker, W.E. Amatucci (NRC/NRL Cooperative Research Associate), and J.A. Antoniades
Plasma Physics Division

An understanding of the origin of the energy source responsible for observations of auroral ions with more energy than typical has been hampered by a lack of experimental work concentrating on various possible candidates. An experimental effort underway in the NRL Space Physics Simulation Chamber (SPSC) has concentrated on one of the most promising of these candidates: localized electric-field regions that lead to plasma instability wave growth. Theoretical groups at NRL have done seminal work in this area which suggests that these shear-generated waves can be responsible for the ion energization [1]. In this view, the plasma waves arise from a spatial varia-

tion in energy density caused by sheared plasma flow; the instability responsible for this wave growth is termed the inhomogeneous energy-density driven (IEDD) instability. Such shears, the associated intense wave activity, and ion heating have, for example, been observed by the Swedish satellite *Freja*. The upcoming Fast Auroral Snapshot Explorer satellite is expected to investigate electric fields with scale sizes sufficiently small to uncover such shear regions. In addition, the possibility that these structures are associated with black aurora is today considered a topic of intense theoretical and experimental interest. In addition, a clear understanding of the physics of the wave generation, which can influence detectable large-scale phenomena, is necessary for the success of ionospheric applications such as ground-to-satellite and satellite-to-satellite communications. This article describes the experimental investigation underway to understand the coupling between velocity shear driven instabilities and ion heating. The first phase, which is described here, concerns the generation of plasma waves by the shear; the second, which is in progress, is related to the coupling of this wave energy into ion heating.

Approach: The basis of this study is the production of an electric field that is nonuniform in space (that is, has a shear) but is contained within a 1-m cylindrical plasma column in the SPSC. Multiple concentric rings to which different potentials are applied—when placed in a plasma—produce an electric field, which is a function of radius from the center of the ring structure.

Figure 3 shows a schematic diagram of the experimental setup in the SPSC. Sheared transverse plasma flow is induced by a controllable, transverse, localized, dc electric field within the column. This is accomplished with a highly transparent grid structure made from concentric, coplanar, conducting ring electrodes. This multiringed electrode (MRE), which is pictured as a blow-up to the right in the Fig. 3, consists of eleven circular rings constructed from 3-mm outer-diameter brass rods. The innermost and outermost rings have diameters of 10 cm and 30 cm, respectively, and the inter-ring spacing is 1 cm. The MRE diameter is several ion gyroradii smaller than the plasma column diameter and is centered on the column axis 2 m axially
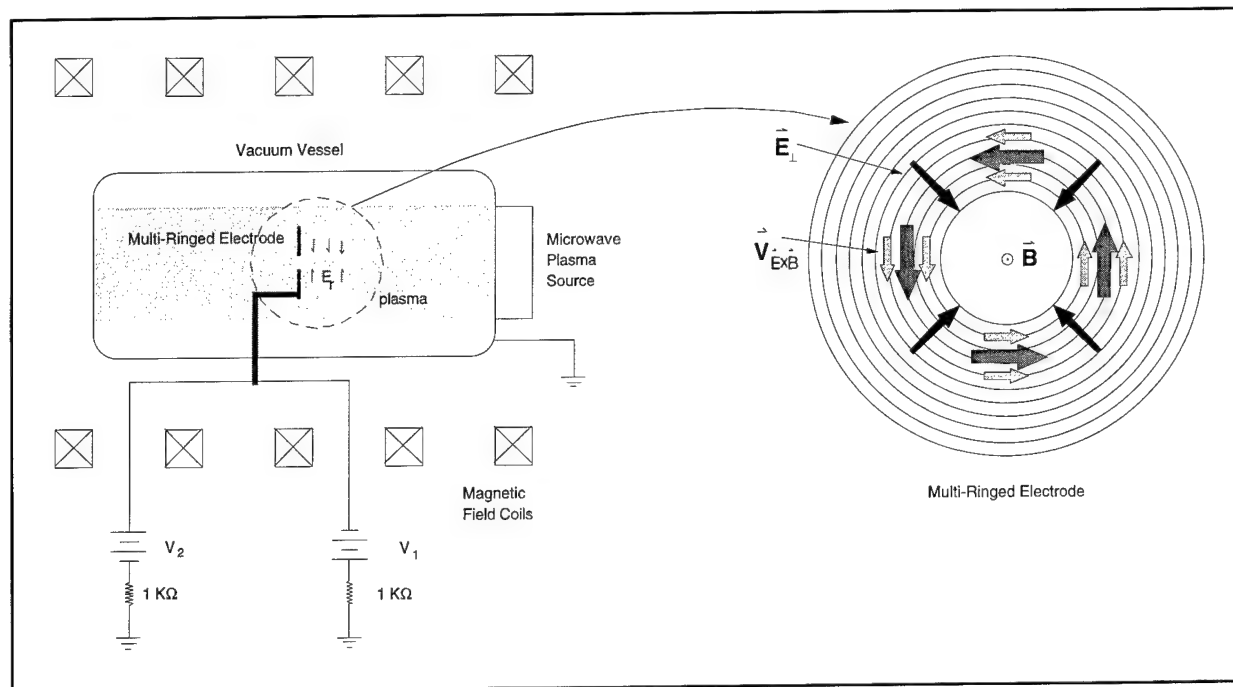
Fig. 3 — The multiple-ring electrode (MRE) and its position in the space physics simulation chamber.

from the microwave plasma source. In the simplest mode of operation, the MRE rings are divided into inner and outer groups by electrically connecting each ring within a group. Application of different potentials to the inner and outer groups modifies the radial structure of the plasma potential, creating a localized, dc electric field, which is shown pointing radially inward in Fig. 3. The presence of this electric field oriented perpendicular to the magnetic field results in a plasma drift with velocity $V_E = (E \times B)/B^2$, as shown in the figure. Emissive probe measurements along the axis between the plasma source and the MRE show that this field extends as far as 20 λ_D into the plasma column, where λ_D is the plasma Debye length.

Figure 4 shows a typical plasma potential profile and the associated electric field produced by the MRE. In this illustration, the plasma potential (solid line) and the electric field (dashed line) are plotted as a function of radial position with $r = 0$ corresponding to the plasma column cylindrical axis. Plasma potential is measured with an emissive probe, which is located 10 cm axially in front of the MRE. For this example, the seven outermost rings are grouped together and biased to +20 V with respect to chamber ground, while the four innermost rings are held
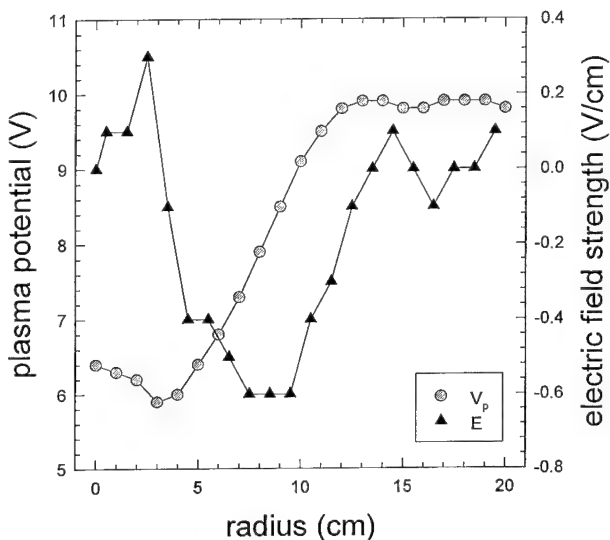
Fig. 4 — Electric field and plasma potential profiles produced by the MRE.

at a potential of −10 V. The radial gradient induced in the plasma potential generates a dc electric field that is spatially localized to the annular region $4 < r < 11$ cm and has a maximum amplitude of 60 V/m. With an axial magnetic field strength of 40 G, the peak value of V_E ($\approx 1.5 \times 10^6$ cm/s) is approximately 30 times

the ion thermal velocity. The electric field strength can be increased to a maximum of approximately 100 V/m (peak $V_E \approx 2.5 \times 10^6$ cm/s). At radii less than 4 cm or larger than 11 cm, the plasma potential is relatively uniform, indicating little electric field. In the cylindrical plasma column geometry, radial shear in the azimuthal plasma flow is induced within the boundary layers separating these regions. The scale length of the electric field gradient $L_E \approx 5$ cm, which is approximately equal to one ion gyroradius, indicates that the ions are magnetized within the velocity shear layer.

Fig. 5 — MRE inside the SPSC with three azimuthally separated probes.

Results: When an electric field of sufficient magnitude (as described above) is imposed, plasma waves in the ion-cyclotron frequency range can be detected with Langmuir probes or from fluctuations in dc current collected by the MRE sections. The transverse and field-aligned wavevector components $k_\theta = 2\pi/\lambda_\theta$ and $k_z = 2\pi/\lambda_z$

have been determined using cross-correlation techniques to measure the phase differences between ion saturation current fluctuations simultaneously obtained from pairs of Langmuir probes. For the measurement of azimuthal wavelength, three Langmuir probes with identical tips are positioned at the same radial and axial positions but are separated in azimuth. A photograph of the actual arrangement is shown in Fig. 5 and schematically in Fig. 3. The probes are placed at identical radial and axial coordinates to measure only azimuthal contributions to the phase difference $\Delta\phi$. Unequal azimuthal spacing is used to reduce the possibility of aliased azimuthal mode numbers. The measured phase difference between the simultaneously acquired signal of the various possible probe separations is compared to the measured angular separation of the probes. The measured values of $\Delta\phi$ are consistent with an $m = 1$ mode with $k_\theta = 0.11 \pm 0.01$ cm^{-1} propagating azimuthally in the ExB direction. The axial wavenumber k_z is determined in a similar fashion. These measurements indicate axial propagation away from the plasma source with wave number $k_z = 1.32 \times 10^{-2} \pm 1 \times 10^{-3}$ cm^{-1}. The mode has been identified as the IEDD instability based upon excellent agreement between experimentally observed mode characteristics and those predicted by theory.

[Sponsored by ONR].

References

1. G. Ganguli, Y.C. Lee, and P.J. Palmadesso, "Kinetic Theory for Electrostatic Waves Due to Transverse Velocity Shear," *Phys. Fluids*, **31**, 823 (1988). ∎

Kinetic Limitations to Molecular Beam Epitaxy

M.E. Twigg,[1] B.R. Bennett,[1] P.M. Thibado,[2] B.V. Shanabrook,[1] and L.J. Whitman[3]
[1]*Electronics Science and Technology Division*
[2]*NRC/NRL Cooperative Research Associate, Chemistry Division*
[3]*Chemistry Division*

The novel properties of many modern semiconductor devices depend on the ability to grow

thin layers with thickness and composition controlled on an atomic scale. This degree of control can be achieved by molecular beam epitaxy (MBE), a form of vapor phase growth in that molecular or atomic beams deposit a thin film onto a substrate surface which is maintained at an elevated temperature in ultrahigh vacuum. Although under thermodynamic equilibrium the deposited atoms (that is, adatoms) may form a smooth and uniform surface, kinetic limitations may dictate otherwise. When the diffusing adatoms do not have the opportunity to seek out their equilibrium positions, the resulting surface may not be smooth. Instead, the adatoms may find themselves bunched together in clusters or may leave clusters of unfilled (vacancy) sites. These clusters give the surface a jagged morphology so that when a layer of different composition is deposited onto such a surface, the resulting interface is rough as well.

Interface Roughness: For advanced optoelectronic devices, such as infrared detectors based on a sandwich of alternating semiconducting InAs and GaSb layers (that is, an InAs/GaSb superlattice), the deleterious effects of interface roughness are particularly important. In these device structures, each layer of the superlattice may consist of as few as 10 InAs or GaSb monolayers (ML) [1]. Here, a monolayer is defined as a single layer of compound semiconductor atoms — for example, 1 ML of InAs consists of one atomic layer of In joined to one of As, with a total thickness of 0.3 nm.

An atomic-scale view of the interface is provided by High-Resolution Transmission Electron Microscopy (HRTEM). In HRTEM, high-energy electrons passing through a thin (20-nm) sample form a projected image of the individual atomic columns. A superlattice sample can be mounted so that it is viewed in the microscope edge-on, providing a cross-sectional view of the interfaces. In addition, the coherent electron scattering mechanism that gives rise to HRTEM imaging also allows the observer to identify the chemical difference between adjacent atomic columns.

As can be seen in the cross-sectional HRTEM image in Fig. 6, in an InAs/GaSb superlattice, the interfaces make up a significant volume fraction of the material. Therefore, any degree of interfacial roughness will have a profound effect on the material properties. Image analysis marks the
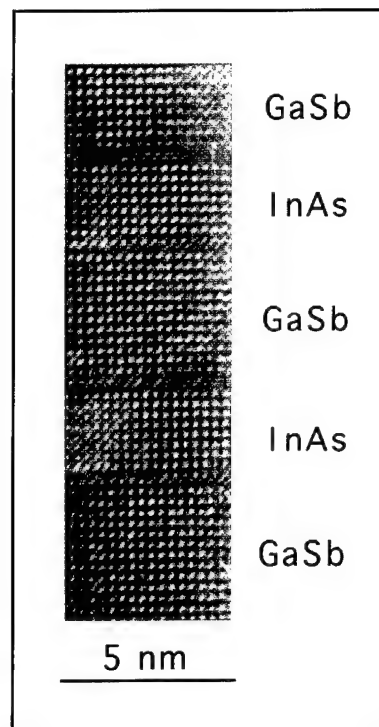
Fig. 6 — Cross-sectional HRTEM image of InAs/GaSb superlattice. White dots in InAs layers corresponds to columns of As atoms; white dots in GaSb layers correspond to In atoms. Note how the registry of the image changes at each interface.

chemical transition at the interface and thereby determines the degree of interfacial roughness, as Fig. 7 shows [2]. As one follows the interface from left to right, it is seen to wander up and down by as much as 0.3 nm so that the interface roughness amounts to 1 ML. Because the HRTEM sample is 20-nm thick, this roughness indicates that over a 20-nm region of the interfacial surface, one is likely to encounter either a vacancy (filled by the next layer) or an adatom cluster (inserted into the next layer).

Control of Surface Topography: A complementary view of the interface is afforded by scanning tunneling microscopy (STM) performed in situ immediately after MBE growth. STM provides a planar view of the surface topography with atomic-scale resolution. An STM image of a single InAs monolayer on GaSb is displayed in Fig. 8 (left), revealing large, atomically smooth terraces (~ 50-nm wide) separated by monolayer-height steps with a few adatom and vacancy clusters.

Fig. 7 — (Left) HRTEM image taken from a portion of a HRTEM micrograph; (right) the same portion of the HRTEM image after image processing. The dark regions denote the interfacial region and allow the determination of interfacial roughness.
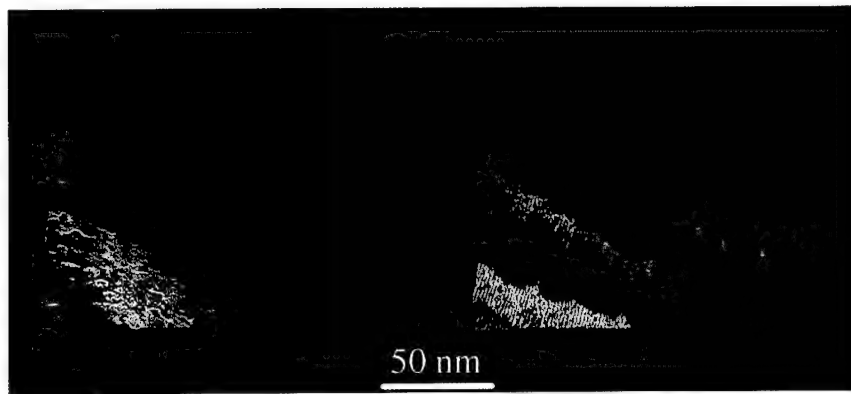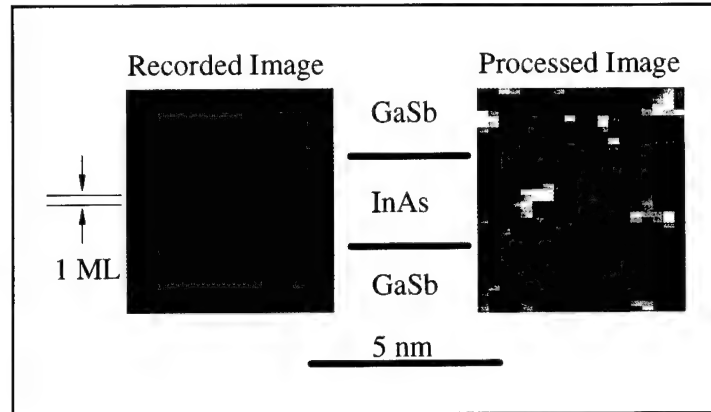
Fig. 8 — STM images of a single monolayer of InAs grown by MBE on GaSb at 400° C. (Left) grown without interruption; (right) grown with 100-s delays between deposition steps.

This surface corresponds to one of the interfaces seen in the HRTEM images. On the 20-nm length scale relevant to the HRTEM results, the surface roughness is also 1 ML, indicating that the degree of roughness on the initial surface is the same as that at the interface [3]. Whereas the terraces are part of the original structure of the substrate surface, the surface roughness associated with the adatom and vacancy clusters indicates that the InAs-covered surface has not achieved equilibrium. This observation presents us with an opportunity to improve on the growth of the interface. InAs/GaSb superlattices are grown at a relatively low temperature of 400° C in order to minimize intermixing at the interfaces. We find that by halting the growth for 100 s between deposition steps and thereby allowing the adatoms more time to find their equilibrium positions, a significantly smoother interfacial surface can be produced (Fig. 8, right).

Towards Device Optimization: From our complementary use of HRTEM and in-situ STM, we have learned that there is a close correspondence between the InAs/GaSb interface and the initial surface consisting of a single monolayer of InAs grown on GaSb. Because this surface serves as a precursor to interface formation, the study of surface morphology provides an understanding of the origin of the resulting interface. The ability to relate the effects of different growth conditions with the morphology of the interfacial surface should allow the optimization of device structures requiring atomic-scale control of the interface.

[Sponsored by ONR]

References

1. D.L Smith and C. Mailhiot, "Proposal for Strained Typed II Superlattice Infrared Detector," *J. Appl. Phys.* **62**, 2545 (1987).

2. M.E. Twigg, B.R. Bennett, and B.V. Shana-brook, "Influence of Interface and Buffer Layer on the Structure of InAs/GaSb Super-lattices," *Appl. Phys. Lett.* **67**, 1609 (1995).

3. P.M Thibado, B.R. Bennett, M.E. Twigg, B.V. Shanabrook, and L.J. Whitman, "Origins of Interfacial Disorder in GaSb/InAs Superlat-tices," *Appl. Phys. Lett.* **67** (1995). ∎

Information Technology and Communication

Rejection with Multilayer Neural Networks: Screening Image Data

B. Kamgar-Parsi and B. Kamgar-Parsi
Information Technology Division

Existing neural networks are unable to reject unfamiliar patterns and thus misclassify them as members of classes of patterns with which they are familiar. Indeed, other classifiers in the fields of computer vision, statistical pattern recognition, etc., also suffer from a similar shortcoming, as they can only find the closest class—which may or may not be the correct class. Hence, the use of neural networks and other classifiers for pattern recognition have been limited to controlled environments, that is, environments that only involve a limited number of known classes of patterns (classes used in the design of the classifier), for example, optical character recognition. In uncontrolled environments encompassing many real-life problems, however, there is no guarantee that all the patterns that will be presented to the network (or other classifiers) would actually belong to one of the classes on which the network has been trained. For application in such environments, current pattern recognition and computer vision techniques resort to some ad hoc thresholds in order to decide whether to accept or reject the unknown pattern as belonging to a certain class. This often produces unreliable results. We have developed a method to construct multilayer perceptrons with rejection capabilities for visual patterns that are meaningful to humans. The method is potentially applicable to a variety of problems that are of interest both to the Navy and the commercial sector.

Approach: We develop rejection capability assuming that there is only one acceptable class. The extension to more classes is straightforward. Consider the following problem. Assuming that P is a visual pattern which has a meaning to humans, we want to develop a neural network to determine whether an unknown pattern is a correct match of P or not. We make the following observation. If we subject P to deformation, but the magnitude of deformation is sufficiently small, then the resulting pattern will still be recognized as P by humans. However, if we deform P more and more, in a fixed manner, the resulting pattern will eventually lose its similarity to P. Moreover, further deformation will never make it look similar to P again. This implies that in the pattern space, the manifold of borderline patterns encloses P and its acceptable matches. Thus, to define the acceptable decision region which will be learned by the network, we need to know how to construct the manifold of borderline patterns M. We do this by generating a large training set composed of two classes of patterns—those which are close to M but still acceptable and those which are close to M but unacceptable. This is done by deforming P. The magnitude of deformation is determined by the human eye, more precisely by an expert or trained eye, depending on the domain of application. Patterns that are projected just inside the decision boundaries are those which are fairly deformed, yet—judging by eye—they still possess sufficient resemblance to pattern P. And patterns that are projected just outside the decision boundaries are those whose resemblance to P, judging by eye, is somewhat less than acceptable. If a sufficiently large training set of such patterns is composed, then the decision boundaries defined by the network will be expected to be sufficiently close to M. Note that one may interpret P as a prototype of the class of interest. Also, to represent a class adequately, it may be necessary to use more than one prototype pattern per class.

The number of required patterns is generally very large, to the extent that collecting sufficient real (and borderline) data is generally beyond one's resources or time constraints. The reason is as follows: if a network is designed to distinguish members of several classes of patterns *from each other* and is guaranteed to encounter only members of those limited classes, then decision boundaries may not need to be defined very tightly. This is because, in general, different classes are separate from each other. But, a network that is designed to distinguish members of one class—say class A—from members of *all other classes of patterns in the universe*, requires far more accurately defined decision boundaries because the rest of the patterns will include (false) lookalikes of class A. In other words, the decision region belonging to class A will be surrounded in every direction by borderline patterns not belonging to A. In our approach, we use real data to train the eye but not to (directly) train the network. After training the eye on real data, we use

the eye's enormous generalization power (captured by a random deformation technique (RDT)) to generate a sufficiently large data set to train the network. Once the network learns such a training set, in our experience, the network will be able to generalize as well as the eye.

An Application: In certain applications, the exact type of landing aircraft must be determined without communicating with them. The recognition is done from the shape of the approaching aircraft by trained personnel. To automate this process, an infrared camera continuously takes images of the sky in front of the runway. However, when analyzing an image, the question cannot simply be the type of the aircraft because a given frame may not contain any. By using image-processing techniques, the most prominent signal in the image is extracted. The signal, however, may not necessarily be an aircraft, as it could be a cloud (or just noise). Therefore, the first question is whether the signal that has been picked up is an aircraft. For clarity and brevity, suppose we have only one class of aircraft to distinguish from all other objects or patterns. A prototype image for this class was taken to be the model. (Soon after appearing on the horizon until almost landing, the pose of no aircraft changes significantly.) Applying the RDT to this model, we composed a set of 2300 automatically generated borderline patterns. By placing a 10 × 20 window on each pattern, we developed for the network an input representation and translation invariant.

Evaluation of the Network: To test the network, we used both real and synthetic data. Real data included 132 images of the skies, of which 86 contained approaching aircraft while 46 did not. For a given image, the input to the network was the most prominent signal in that image. The network's answers were correct on all 132 images (two aircraft examples are given in Fig. 1). All aircraft in real images were within 2 min of landing. We note that no real images were used in the training set. Since most of the real data were easy examples, for example, clear aircraft, or the skies void of any object having any resemblance to aircraft, we felt a need for more challenging data. By adjusting the parameters of the RDT, we generated hundreds of examples which appeared highly borderline and thus very challenging. We found it very difficult (if at all possible) to find
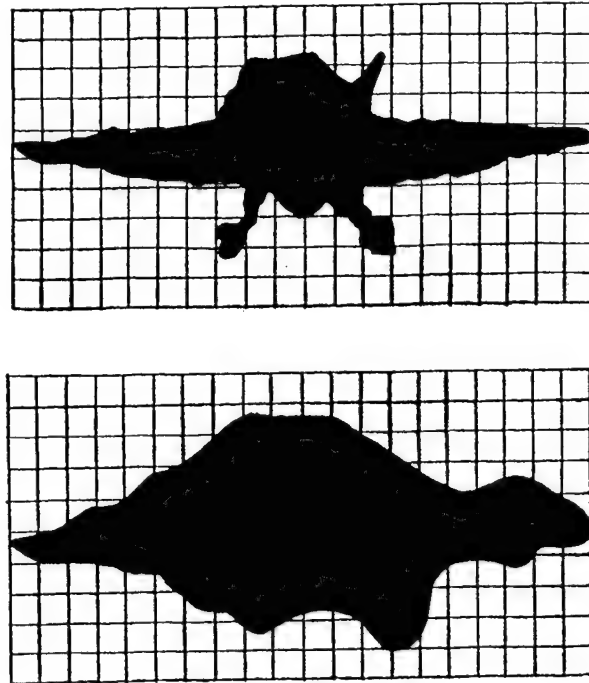
Fig. 1 — Extracted aircraft from real IR images scaled to the same size: top—an aircraft within 15 s of landing; bottom—the same aircraft almost 2 min before landing. Due to low signal-to-noise ratio, the distant aircraft appears fairly deformed, yet the network classifies it correctly.

examples where we can be confident that there is disagreement between the network and the eye—that is, the eye of the composer. The fact that it is possible to develop a network that can apparently be trusted as much as the eye is very important in developing powerful vision systems for pattern or object recognition. Two different person's eyes may not agree with each other completely, but even so, the eye of each of them is far more dependable than existing pattern recognition systems.

Discussion: If we wish to develop a vision system with humanlike performance, then we need to pay attention to how humans decide whether two patterns match or not. The human visual system makes such decisions based on the meanings of the patterns in question. Popular distance measures such as Euclidian, Mahalanobis distance, etc., in conjunction with a cut-off for deciding whether the match is correct, completely ignore any meaning that humans attach to visual patterns or object views. On the other hand, the approach we have proposed attempts to construct decision boundaries at places where the

human eye appears to "draw" the line between acceptable and unacceptable patterns. Based on our technique, we have developed a network that screens images of the skies and discards those not containing approaching aircraft. The discriminating power of the network is comparable to that of the human eye.

[Sponsored by ONR] ∎

Scalable Real-time Networking for Distributed Computing

S. Batsell, R. Cole, and B. Root
Information Technology Division

Introduction: Building a distributed computing environment for military war-gaming has been an on-going effort at the Advanced Research Projects Agency (ARPA) over the last decade. Under the current Synthetic Theater of War (STOW) Advanced Concept and Technology Demonstration, ARPA's goal is to demonstrate that distributed interactive simulation (DIS) is capable of simulating an entire theater of war, with participating sites networked together over large distances. In order to achieve this, a network solution is required that can meet the demands of a highly dynamic simulation environment, provide both the required scalability and bandwidth, and yet minimize end-to-end latency. ARPA initiated

the Real-time Information and Networking (RITN) program to support STOW network requirements (Fig. 2). Under RITN, NRL has developed an integrated effort of research, advanced development, and test and evaluation leading to a solution for implementation of the underlying network and communications for the STOW 97 Demonstration.

The Multicast Paradigm for Distributed Computing: Current DIS applications broadcast all information to all of the participating sites. This is an inefficient use of the network bandwidth because not all receiving sites require the information. Further, the broadcast nature of the current DIS will not scale to support a very large number of entities (tanks, missiles, aircraft, etc.) in a theater-size simulation. DIS simulations in the RITN program are based on a distributed computing paradigm that uses multicast to organize information so that only those hosts that need the information receive it. As a result, network bandwidth demands are minimized, and the offered load to the simulation hosts is reduced. The battle space is divided into a grid with each grid square representing a multicast group. Each square is then assigned an internet protocol (IP) multicast address. In addition to receiving information from their own geographic grid square, entities in the battle space receive data for other multicast groups depending on direction of movement for the entity, velocity, line-of-site visibility, and other factors. Multicast groups may be short-lived, and
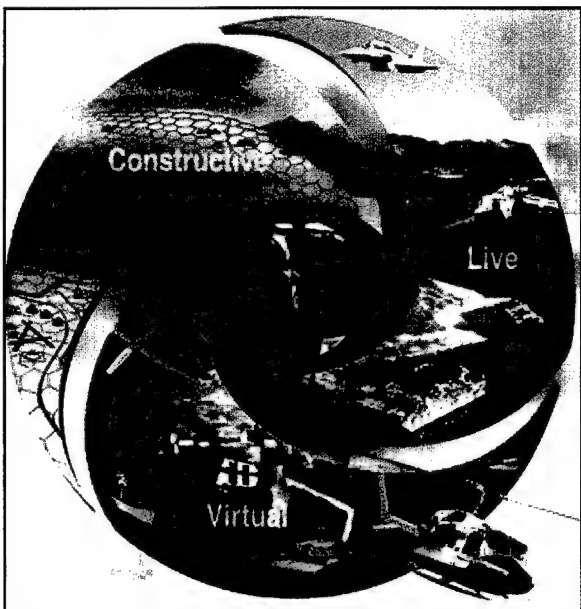
Fig. 2 — Plot showing how ARPA's Real-time Information Networking (RITN) program supports the Synthetic Theater of War (STOW) network requirements.

participants in the multicast group can join and leave the group quite rapidly. In addition, all members of a STOW-like multicast group act as both a source and receiver. Current multicast protocols were not developed with this paradigm in mind. Rather, they were developed for a lecture paradigm where there are a few (usually one) senders and many receivers or for video conferencing where there are only a few sites.

Improving IP Multicast: Initial work in the RITN program has already demonstrated improved scaling to larger exercises using multicast techniques. However, current IP multicast protocols themselves have limited scaling properties [1] due in part to designs based on the lecture paradigm. NRL is participating in the development and integration of several new IP multicast technologies to support STOW scalability requirements.

IP multicast operates by using the Internet Group Management Protocol (IGMP) to communicate between a workstation and a router when an application needs to join or leave a particular multicast group. In IGMP version 1, there is an explicit join message sent to the router but not an explicit leave message. The router periodically sends a message asking who wants to participate in the group, and if no response is received by the router, it will assume no workstations on the LAN want to participate and then leave the multicast group. The period between queries can be on the order of several minutes, over which time the local area network (LAN) will receive data that no workstation wants, resulting in inefficient use the LAN bandwidth. Based on testing conducted at NRL, a new version of IGMP, IGMP version 2, has been developed that has explicit leave messages. This version of IGMP will be an important feature in the STOW network. NRL has successfully coordinated IGMPv2 implementations with router vendors to ensure that STOW-required technology is available in commercial products.

Routers in a multicast group interact using a multicast routing protocol. As the number of processes or tasks in distributed computing increases, the multicast routing method must scale to accommodate this increase. Current techniques implement shortest path trees (SPTs) that use a (source, group) pair state in the on-tree routers. This state contains the forwarding information for datagrams corresponding to that (source, group) pair. Therefore, there is a routing table entry for each (source, group) combination and a concomitant explosion in table size in large distributed simulations. In the lecture and conferencing paradigms, it is assumed that only one multicast group is required. However, in the distributed simulation cause, there are many (typically hundreds or thousands) of groups for one exercise. In addition, all entities in a simulation are sources. The result is a very large number of source-group pairs that severely limits scalability. An alternative to the SPT is a shared tree, which generally contains forwarding information based only on the group. Under the direction of NRL, Bellcore and Bay Networks are implementing a shared tree protocol called Core-Based Trees (CBT). CBT was originally developed at University College, London. Simulation results have shown that it is more scalable than SPT protocols currently being used [2,3] and has the potential of providing the scaling needed for STOW 97.

Real-time Requirements: While IP multicast provides the high dynamic robust behavior required for a multicast distributed interactive simulation, the entities must also interact in real time. To provide minimum end-to-end latency over the wide-area network (WAN), acrosyncronous transfer mode (ATM) will be used as the WAN protocol. In the ATM Forum's user-to-network interface standard (UNI 3.1), ATM has a point-to-multipoint capability that will be integrated with IP-multicast on the STOW LANs. NRL, with the assistance of Bellcore and Bay Networks, is currently working on integrating both the multicast and quality of service capabilities of IP and ATM [4]. Bellcore is developing a multicast address resolution server (MARS) (Fig. 3) to allow translation of IP multicast addresses to ATM virtual circuit identifiers.

Future Work: Future work includes further integration of IP local area and ATM wide area services. The next major milestone will be the integration of secure cryptographic devices in the ATM portion of the STOW environment to allow classified exercises and training. The results of the RITN effort will provide important baseline information to support the Defense Information Systems Agency's Leading Edge Services deployment of next generation communications services to DoD.

[Sponsored by ARPA]
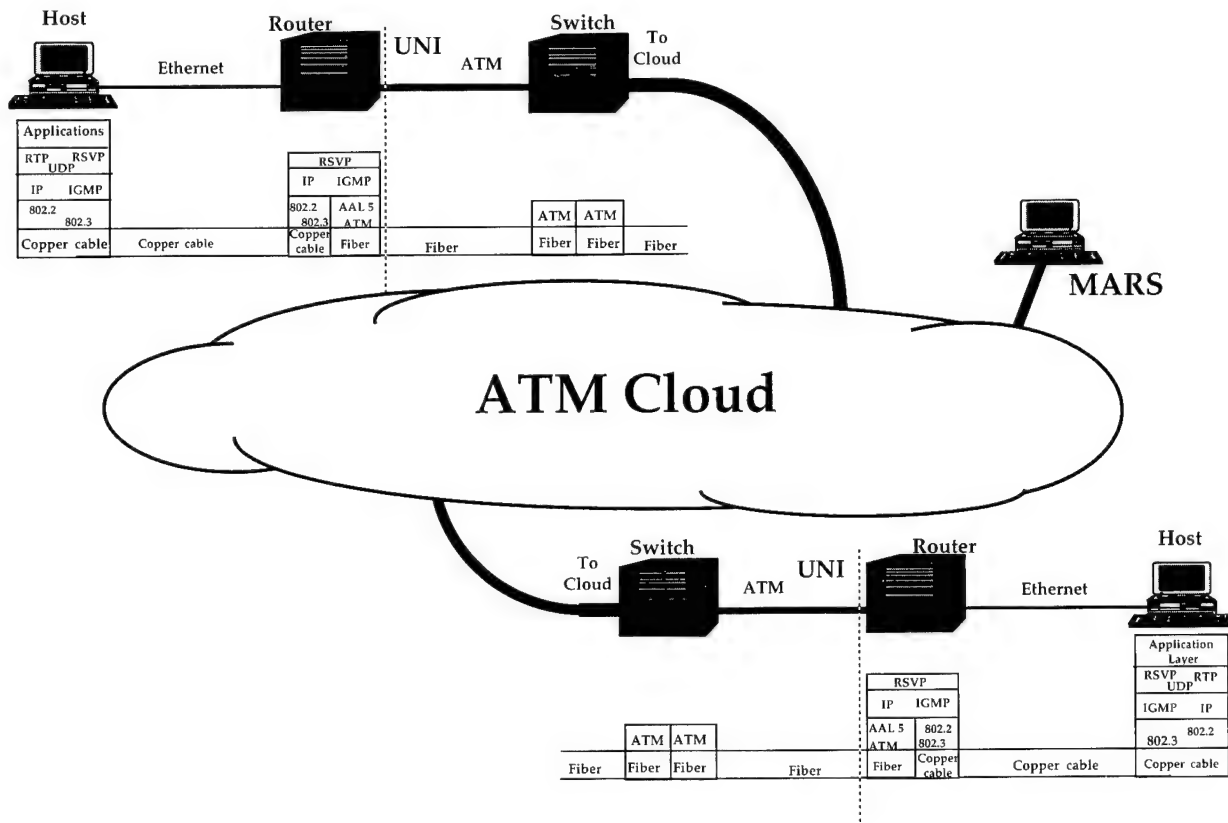
Fig. 3 — A multicast address resolution server (MARS) is being implemented to allow translation of IP multicast addresses to ATM virtual circuit identifiers.

References

1. S.G. Batsell and J.E. Klinker, "The Implications of a Distributed Computing Paradigm on Multicast Routing," *Proceeding of MILCOM 95* (IEEE Press, Piscataway, NJ, November 1995).

2. T. Billhartz, J. Cain, E. Farrey-Goudreau, D. Fieg, and S. Batsell, "Performance and Resource Cost Comparisons of CBT and PIM Multicasting for DIS Environment," accepted for the 1996 Infocom to be held in San Francisco, CA, in March 1996.

3. T. Billhartz, J. Cain, E. Farrey-Goudreau, D. Fieg, and S. Batsell, "Simulation Comparison of CBT and PIM Multicasting for Distributed Interactive Simulation (DIS)," *Proceedings of the 1996 SCS Western Multiconference*, January 1996.

4. M. Borden, E. Crawley, B. Davie, and S. Batsell, "Integration of Real-time Services in an IP-ATM Network Architecture, IETF RFC 1821," available from fttp://ds.Internic.net/rfc, August 1995.

Key Management Support Inside 4.4 BSD UNIX

D.L. McDonald, B.G. Phan, and R.J. Atkinson
Information Technology Division

As the global Internet continues its exponential growth, many concerns once disregarded now fall under the scrutiny of the Internet community. Security is a top area of concern for the Internet Engineering Task Force (IETF)—the primary Internet standards body. NRL has driven the effort to extend the Internet Protocol (IP) and its successor, version 6 of IP (IPv6), so that IP datagrams can be encrypted or strongly authenticated. The presence of these security mechanisms in the IP does not, by itself, ensure good security. The

establishment and maintenance of cryptographic keys and related security information, also known as *key management*, is also crucial to effective security. Key management for the IP is a subject of much experimentation and debate. NRL has implemented IPv6 inside the 4.4 BSD UNIX operating system. To allow experimentation with different key management solutions, the implementation includes a general purpose mechanism to allow management of security associations. A security association (Fig. 4) specifies the cryptographic key, as well as the security service and which parties are using it.

Key
Security service and algorithm
Source IPv6 address
Destination IPv6 address
Lifetime
Sensitivity level of association

Fig. 4 — A security association

History: The Internet Protocol suite has gained popularity largely because of its availability in the Berkeley Software Distribution (BSD) versions of the UNIX operating system. Even though many commercial operating systems no longer use the BSD networking implementation, they still support BSD abstractions for application programmers, such as the sockets application programming interface (API). The sockets interface allows applications in BSD to communicate with other applications, or sometimes, even with the operating system itself. One of the recent developments in BSD was the *routing socket*, allowing a privileged application to alter a machine's routing tables, which influences the path an IP datagram takes to reach its destination. This abstraction allows a BSD computer to implement whatever routing policy the administrator sees fit. When confronted with the task of placing security associations inside the operating system for use by the IP security services, the authors chose to use a *key* socket to allow privileged applications to alter the operating system's security associations. The similarity between the

operating system's routing tables and the security association table was strong enough to merit an analogous solution. This key socket, known as *PF_KEY* after the symbolic name of this type of socket (other examples include PF_ROUTE, for routing sockets, and PF_INET6 for IPv6 network sockets), is how key management can be separated out for purposes of experimentation and high-assurance implementation. Different key management strategies can be implemented in different applications, all of which use PF_KEY to affect changes in the operating system's security association table.

Security Association Table Mechanisms: The security association table resides inside the operating system and is actually modified by a *key engine* that handles requests from either applications or other operating system services. PF_KEY is the interface to the key engine presented to applications. Key management software uses the PF_KEY interface to maintain the security associations that will be used by services inside the operating system. Key management applications send PF_KEY messages to the operating system to add, delete, get, or update security associations. The operating system sends a PF_KEY message to key management programs to signal the need for more keys.

A different interface to the key engine is presented to other parts of the operating system—in particular, the networking services. For example, consider an IPv6 datagram arriving with an encrypted data payload. Using a cleartext portion of the datagram, the IPv6 engine will access the security association table to obtain a decryption key or authentication key for this datagram. On outgoing datagrams, the IPv6 engine queries the security association table based on the destination IPv6 address. The outgoing datagram is then authenticated or encrypted with the key obtained from the table.

A Framework for Experimentation: Figure 5 shows the interactions among the networking portions of the kernel, the key engine, and user applications that use network services and those that perform key management. Experimenting with different key management strategies is
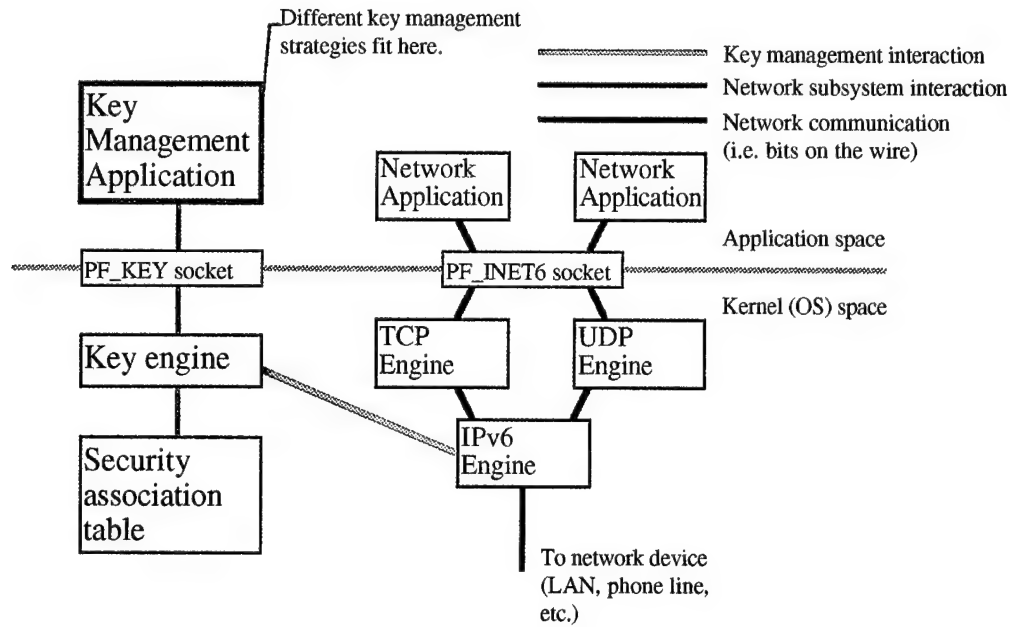
Fig. 5 — Interactions of key management and networking.

straight-forward, because different key management programs can be compiled and run without having to rebuild the operating system. Also, other operating system modules can be modified to use the security association table; both original IP and IPv6 use the key management table for IP-layer security. This flexibility allows commercial interests to adapt their security technology to the demands of the marketplace, as well as allowing the Navy to use state-of-the-art methods of key management.

■

Materials
Science
and
Technology

Magnetic Metal/Semiconductor Heterostructure Studies in the EPICENTER Facility

B.T. Jonker[1], P.M. Thibado,[2,3] E. Kneedler,[1,3] B.R. Bennett,[4] B.V. Shanabrook,[4] R.J. Wagner,[4] and L.J. Whitman[2]

[1]*Materials Science and Technology Division*
[2]*Chemistry Division*
[3]*NRC/NRL Cooperative Research Associate*
[4]*Electronics Science and Technology Division*

Magnetic metal films on semiconductor substrates form the basis for a new class of magneto-electronic and magneto-optic devices [1]. In these devices, the magnetic moment or carrier spin allow one to produce and control new electrical or optical properties in novel ways. For very thin films, the magnetic and electronic properties of the heterostructure may depend strongly on the nature of the metal/semiconductor interface. This is particularly true in the case of magnetic over-layer growth on compound semiconductor substrates whose surfaces exhibit a plethora of atomic terminations which may have a significant impact on the structure and subsequent magnetic properties of the overlayer [2]. Before magnetic heterostructure devices can be widely realized, the characteristics of the metal/semiconductor interface must be well understood.

One magnetic system of special interest is Fe on GaAs, which is considered to have one of the most well-ordered and abrupt metal-semiconductor interfaces. Fe grows epitaxially (bcc) on the (110) and (001) crystallographic surfaces of GaAs, due in part to the fact that the bcc Fe lattice constant is approximately half that of zinc-blende GaAs ($2a_{Fe}/a_{GaAs} = 1.013$). Previous studies of this epitaxial system have used poorly characterized bulk single crystal GaAs substrates, despite the fact that most GaAs-based device structures are grown by molecular beam epitaxy (MBE) under carefully controlled conditions to optimize final device performance. The surface stoichiometry at the growth front is particularly important, with optimum results achieved for a surface terminated by one-half monolayer of As atoms in the form of atom pairs—called dimers. The arrangement of these dimers on the surface leads to a rectangular repeating unit, or unit cell, which is twice as long as the bulk-terminated surface atom spacing in one direction and four times as long in the other. Hence this rearrangement of surface atoms is referred to as the "2×4" surface reconstruction and is shown schematically in Fig. 1(a).

Approach: The thin film growth and surface analysis capabilities of the recently dedicated NRL EPICENTER Facility have allowed the first detailed investigation of the epitaxial growth of Fe films on the technologically important GaAs(001)-2×4 reconstructed surface. The EPICENTER is a multi-chamber ultrahigh vacuum (UHV) facility that consists of two MBE chambers (one for metals and one for III-V semiconductors), a chamber for photoelectron diffraction (PED), and a chamber for scanning tunneling microscopy (STM)—all connected via a UHV sample transfer system. These combined capabilities enable us to obtain an atomic-scale picture of the metal/semiconductor interface as it is formed. A typical experiment begins in the III-V MBE chamber where the GaAs(001) surface is prepared using a growth procedure that optimizes the atomic order of the As-dimer terminated 2×4 surface. The sample is transferred to the second MBE chamber where Fe is deposited using a specialized high temperature evaporation source developed at NRL and then transferred further to either the STM or PED chamber for study. Great care is taken at each step to ensure that the sample surface is not contaminated, which would otherwise compromise the results of the experiment.

Initial Nucleation: Figure 1(b) shows an STM image of the surface with an Fe coverage of 0.1 monolayers (ML). At this coverage, most of the surface is unperturbed GaAs(001)-2×4, and the alternating light and dark vertical rows correspond to rows of As-dimer pairs separated by Ga-terminated rows where the dimer pairs are missing, as shown in Fig. 1(a). The light vertical rows are spaced 16 Å apart. The deposited Fe gives rise to the bright "bumps" that appear almost exclusively on the As-dimer rows, typically covering one dimer pair. We therefore are able for the first time to directly observe that the Fe adatoms preferentially adsorb on the As-dimer sites—forming 2-D islands containing a few Fe atoms—with little, if any, disruption of the 2×4 reconstruction on adjacent uncovered dimer sites. As Fe growth continues, both the Fe island

(a) o 1st layer As
  • 2nd layer Ga
  o 3rd layer As
  • 4th layer Ga

[$\bar{1}$10]

[110]
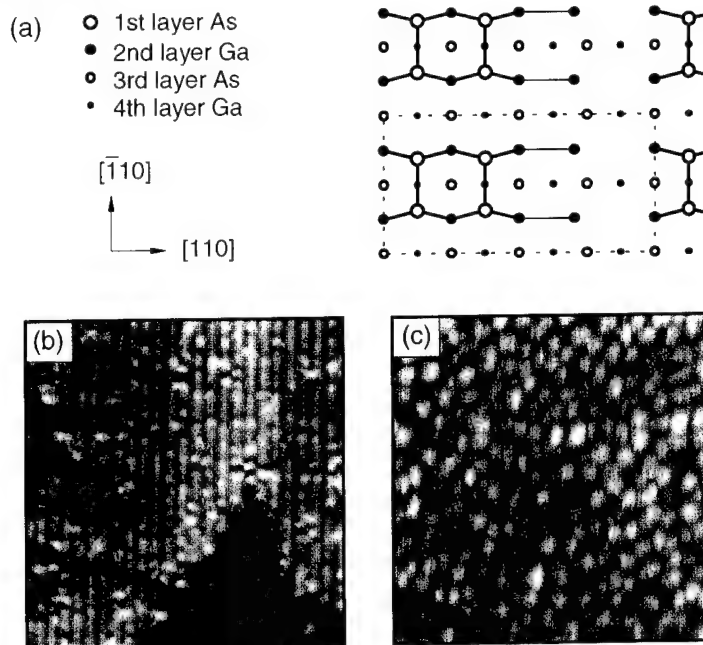
Fig. 1(a) — Model of the As-dimer terminated GaAs(001)-2×4 recon-
structed surface. The dashed rectangle indicates the 2×4 unit cell.
STM images (40 nm × 40 nm) of the surface after deposition of (b)
0.1 ML and (c) 0.5 ML of Fe.

density along the dimer rows and the average
island size increase, as seen in Fig. 1(c) where an
image of a 0.5-ML-thick film is shown. Although
the surface is almost completely covered by Fe
islands, the rowlike structure of the (2×4) sub-
strate reconstruction is still evident in the general
alignment of the islands. The islands are now
typically wider than the As dimer rows, indicating
that Fe adsorption, initially confined to the dimer
rows, has now taken place on the missing dimer
rows.

Layer Formation: Whereas STM provides an
excellent view of the atomic-scale surface topog-
raphy following Fe deposition, PED provides com-
plementary information regarding the structure
and composition of the Fe overlayers. In this
technique, an incident X-ray photon from a mono-
chromatic source is absorbed by an atom in the
sample, resulting in the emission of an electron
(called a photoelectron) from one of the electron-
ic levels with an energy characteristic of that
atom. At sufficiently high energy (> 300 eV), the
photoelectrons are focused along the directions
of neighboring atoms, which act as electronic
lenses. This focusing effect results in peaks in
photoelectron emission intensity along the princi-

ple crystallographic axes of the crystal. If one
measures the angles at which these intensity
maxima occur with an appropriate electron detec-
tor as a function of coverage, one can determine
the early growth morphology since the appear-
ance of intensity maxima at angles characteristic
of the structure signals the occupation of second,
third, or fourth layer sites, as seen in Fig. 2(a).

The photoelectron emission intensity from
the Fe $2p$ core level is plotted as a function of
emission angle in Fig. 2(b) for a range of Fe
coverages on the GaAs(001)-2×4 surface. The
polar scan for 0.5 ML of Fe clearly shows a maxi-
mum in the [111] direction, which by comparison
with Fig. 2(a), indicates that some second layer
sites are already occupied. These results, together
with the STM data, reveal that as the Fe covers
the Ga atoms in the missing dimer rows, bilayer
growth occurs between the dimer rows to main-
tain a flat surface. The PED spectrum at 1.25 ML
exhibits a strong [111] peak, as expected as the
second layer forms. In addition, a much weaker
peak along [001] (the surface normal) indicates
that some third layer sites are occupied, as well.
As the third equivalent monolayer of Fe is depos-
ited, the PED polar scan at 2.5 ML shows strong
[001] and [111] features as anticipated but, in

(a)

(b)
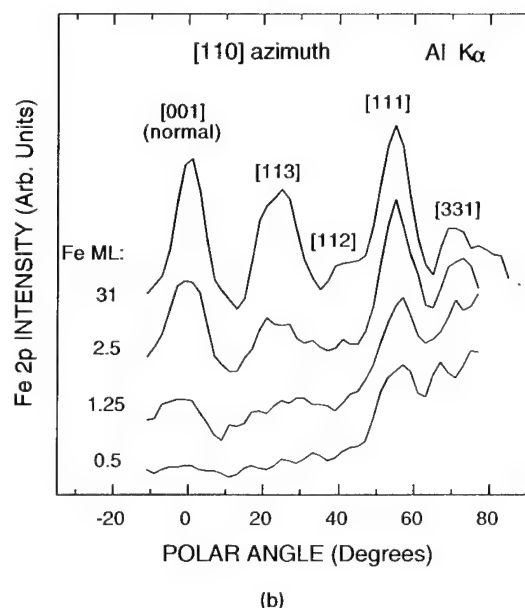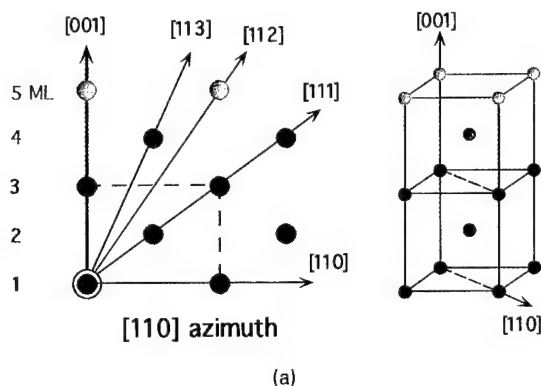
Fig. 2(a) — Schematic of the (110) cross section of the bcc Fe lattice, indicating the directions along which the photoelectrons are expected to be focused; (b) the photoelectron emission intensity as a function of emission angle for several coverages of Fe on the GaAs(001)-2 × 4 surface (Fe $2p$ level, Al $K\alpha$ radiation, KE = 772 eV).

addition, shows a weak peak along the [113] direction indicative of modest fourth layer site occupation. Scans for thicker films exhibit most of the features typical of bulklike films, as can be seen by comparing the 2.5 ML and 31 ML data of Fig. 2. We thus observe that Fe grows in a predominantly layer-by-layer fashion, with the growth front for the nth deposited layer limited to the $(n+1)$th layer, forming flat islands with no initial disruption of the substrate. As the growth proceeds, the islands become elongated along the dimer rows.

The information obtained from these studies provides the first detailed atomic-scale picture of the formation of this technologically important interface. This information will enable researchers to interpret and understand the macroscopic magnetic and electronic properties in light of the nanoscale structure of the film and interface and provides a basis for the optimization of hybrid magnetic metal/semiconductor spin-polarized device structures.

[Sponsored by ONR]

References

1. G.A. Prinz, "Spin Polarized Transport," *Phys. Today* **48**, 58 (1995).

2. B.T. Jonker, "Interfacial Contributions to Magnetic Thin Film Anistrophy Arising from Epitaxial Growth Processes in Metal/Semiconductor Structures," *Soc. Photo-Opt. Instrum. Eng. Proc.* **2140**, 118 (1994). ∎

Hydrogen Exchange Reactions within Density-Functional Theory

M.R. Pederson
Condensed Matter and Radiation Sciences Division

A long-range goal of theoretical materials research and molecular design is the ability to understand and predict, at an atomistic level, how materials grow and react in different environments. Requisite to such an understanding is the ability to determine reaction surfaces, pathways, and barriers from first principles. This article discusses the calculation of several different low-energy phenomena that are important for understanding hydrogen exchange reactions [1,2]. The calculation of reaction barriers relates to such problems as crystal growth, catalysis, cluster-cluster reaction energies, and other DoD and naval technologies.

Figure 3 shows a hydrogen exchange reaction that is of specific interest to the problem of chemical vapor deposition. As pictured, transfer of the active hydrogen atom (red) from the methane molecule to the methyl radical is accomplished by allowing the two carbon atoms (green) to come into close proximity of one another. The lowest energy pathway is determined by allowing all of the electronic and hydrogenic degrees of

TRANSITION STATE

REACTANTS   PRODUCTS
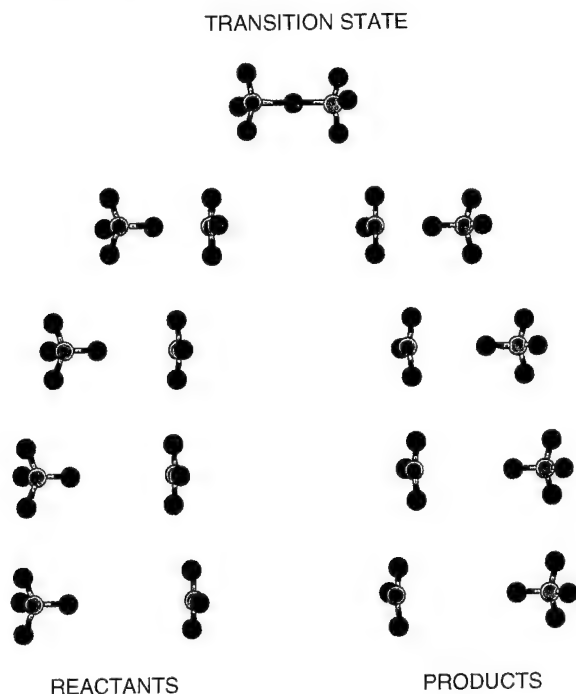
Fig 3 — Reaction pathway followed during a methyl-methane hydrogen exchange reaction.

freedom to relax as a function of the C-C separation. In nature, the energy barrier for this reaction is known to be approximately 0.6 eV. Also, in this class of reactions, is the transfer of a hydrogen from a methane molecule to a gas-phase hydrogen atom. Related reactions are responsible for abstraction of hydrogen atoms from diamond surfaces. The latter reaction also governs the production of gas-phase methyl radicals, which are then exothermically attached to vacant sites on the diamond surface.

Theory and Computation: The underlying theory on which these calculations are based is the density-functional formalism. This formalism allows for a quantum-mechanical solution of the electronic motion and a semiclassical treatment of the motion of the nuclei. To solve quantum-mechanically for the electronic wavefunctions, a local-orbital cluster code developed at NRL by the author and coworkers, has been used. The charge densities from the electronic wavefunctions are used to determine interatomic forces. The information obtained from the interatomic forces at many different atomic configurations allows the determination of molecular geometries, transition states, and vibrational modes. The calculations

have been performed on the DoD CEWES (Corps of Engineers Waterway Experimental Station) and NAVO (Naval Oceanographic Office) computers, as well as local workstations. A recent theoretical development of importance to reaction barriers is the Perdew-Wang generalized-gradient approximation (GGA) to the density-functional theory. Personnel within the Complex-Systems Theory Branch participated in the first comprehensive numerical test of this theory in 1991 [3]. In contrast to older versions of the density-functional theory that overestimated bonding energies by approximately 0.7 eV/atom, the GGA predicts hydrocarbon formation energies with an accuracy of approximately 0.1 eV/atom [3]. Since typical reaction barriers are in the 0.2-1.0 eV energy range and reaction rates depend exponentially on such barriers, the improvements realized from GGA are an absolute necessity.

Results: We have determined the lowest energy pathway for the methyl-methane hydrogen exchange reaction (Fig. 3). Within the GGA, we predict a classical reaction barrier of 0.44 eV [2]. As the two reactants proceed to the transition-state geometry, general arguments suggest that effects due to zero-point vibration will slightly enhance the barrier. To estimate the effects due to zero-point motion, vibrational modes and displacement vectors associated with each atomic configuration are calculated within the harmonic approximation. Figure 4 shows the resulting frequencies. In addition to the frequencies in Fig. 4, it is necessary to account for the very large anharmonic effects observed by the transition state mode to calculate enhancements due to zero-point motion. Following this prescription, we estimate the reaction barrier to be 0.47 eV [1,2]. For comparison, we note that the experimental barrier is approximately 0.61 eV.

The CH_3-H_2 hydrogen exchange reaction has also been studied within the GGA [2]. Figure 5 summarizes the transition-state geometry and the *classical* reaction surface. Neglecting zero-point effects, we predict that the [H,CH_4] products are more stable than the [H_2,CH_3] reactants by 0.22 eV. Inclusion of zero-point effects decreases the enthalpy of reaction to 0.108 eV, which is in excellent agreement with the experimentally determined value of 0.113 eV. While the net enthalpy of reaction is only 0.108 eV, the reaction energy is determined by the barrier
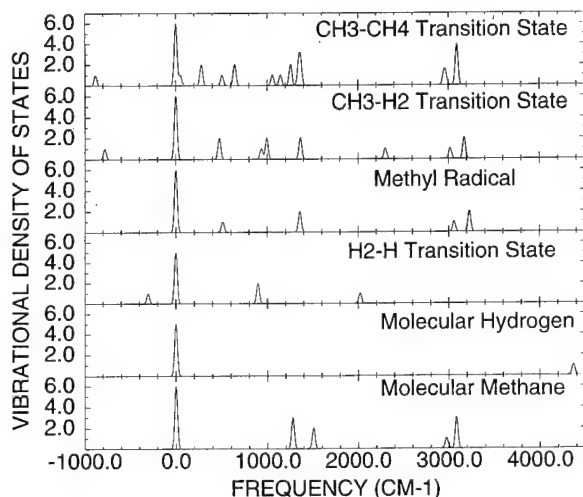
Fig 4 — Vibrational modes of CH_4, H_2, CH_3 and the CH_3-CH_4, CH_3-H_2, and H_2-H transition states. Since the transition-state corresponds to a saddle-point, each transition state has one imaginary frequency that is represented above as a negative frequency. The calculation of frequencies allows for an accounting of zero-point energies and is required for efficient determination of transition-state geometries.
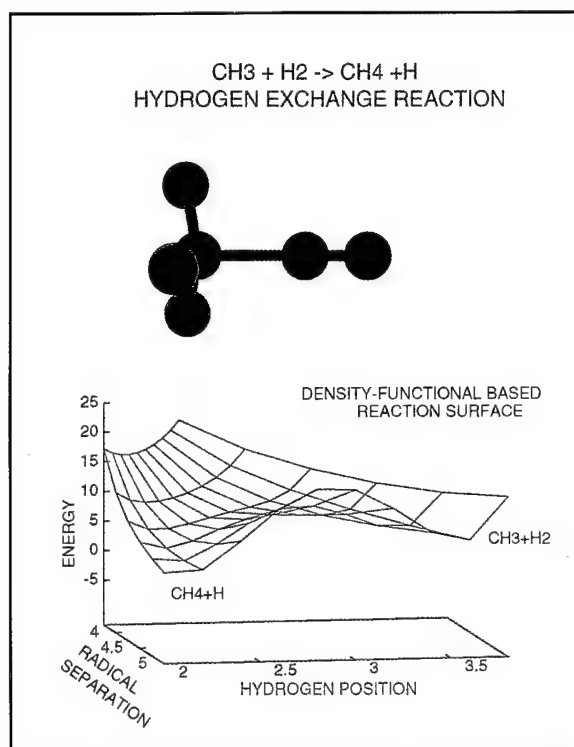
Fig. 5 — Representation of CH_3-H_2 transition-state and associated reaction surface.

encountered during the hydrogen transfer. We predict a reaction barrier of 0.42 eV, which is in good agreement with the experimental value of 0.51 eV.

Significance: While we have only discussed two reactions here, a total of four different hydrogen-exchange mechanisms have been calculated [1,2]. On average, the theoretical reaction barriers yielded approximately 68% of the experimental values. The average underestimate of 0.14 eV is in accord with earlier results that suggested the GGA tends to overestimate bond energies by a similar amount. While there is still room for improvement of the theory, we note that these results represent a large improvement over the older local version of density-functional theory. The results of this work show that it is now possible to predict reaction rates with qualitative-to-quantitative accuracy with modern supercomputers and computational methods. Further, transition states determined from density functional theory are expected to be very accurate. Future work will include porting these routines to DoD parallel platforms, implementing hill-climbing algorithms, and understanding surface reactions and catalysis applications. Some of this work was performed in collaboration with D.V. Porezag during his visit to the Naval Research Laboratory.

[Sponsored by ONR]

References

1. M.R. Pederson, "Density-Functional-based Determination of the CH_3-CH_4 Hydrogen Exchange Reaction Barrier," *Chem. Phys. Lett.* **230**, 54 (1994).

2. D.V. Porezag and M.R. Pederson, "Density Functional Studies of Transition States and Barriers for Hydrogen Exchange and Abstraction Reactions," *J. Chem. Phys.* **102**, 9345 (1995).

3. J.P. Perdew, J.A. Chevary, S.H. Vosko, K.A. Jackson, M.R. Pederson, and C. Fiolhais, "Atoms, Molecules, Solids, and Surfaces: Applications of the Generalized Gradient Approximations for Exchange and Correlation," *Phys. Rev. B* **46**, 6671 (1992). ∎

Optical Spectroscopy of Single GaAs Quantum Dots

D.G. Gammon, E.S. Snow, and B.V. Shanabrook
Electronics Science and Technology Division

Semiconductor quantum dots are electronic structures in which the electron is localized in all three spatial dimensions. This spatial confinement imposes a complete quantization of the electron energy spectrum that is analogous to the confined energy states of an atom. However, in quantum dots, the presence of the crystalline lattice introduces new physical phenomena that affect both the energetics and the kinetics of the confined electrons. Until recently, optical experiments designed to probe such phenomena have suffered from the dominance of extrinsic effects, most notably dot-size variations resulting in inhomogeneous broadening of the spectral features and surface defects that decrease carrier lifetimes. Measurements of the intrinsic optical properties are important because such properties ultimately determine the feasibility of potential applications.

Near-Field Optical Spectroscopy: Recently, we have overcome these problems and are now able to probe the intrinsic optical properties of quantum dots. Inhomogeneous broadening has been eliminated by using near-field optical spectroscopy, a technique with extremely high spatial resolution that allows us to measure the optical spectrum of a single quantum dot. Surface states have been eliminated by studying naturally occurring quantum dot structures that do not rely on lithographically defined electron confinement. These improvements have allowed us to obtain the first detailed optical spectrum of a single quantum dot.

The quantum dots we have studied are GaAs dots that are formed naturally during molecular beam epitaxy (MBE) growth from the lateral potential fluctuations caused by monolayer-sized interface fluctuations in thin GaAs/AlGaAs quantum wells (Fig. 6). Such samples form a model system for investigating the intrinsic optical properties of quantum dots because the confinement of the electron is achieved in a defect-free manner. In order to isolate a single quantum dot, we perform photoluminescence (PL) and PL excitation (PLE) measurements through a submicron-diameter metal aperture that is deposited on the sam-
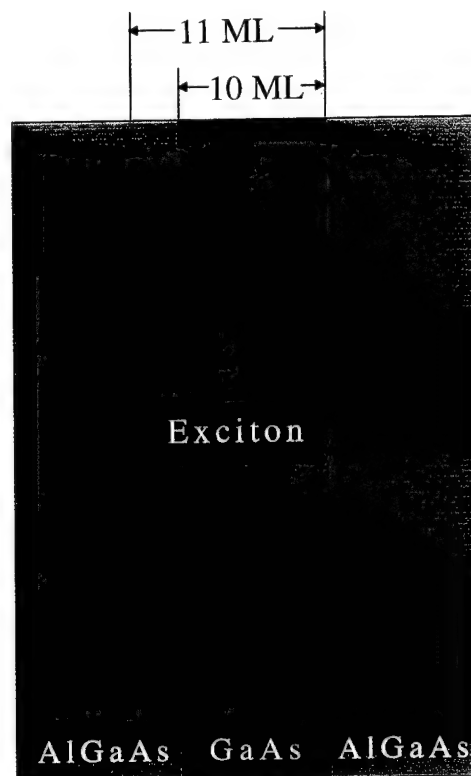
Fig. 6 — An exciton laterally confined by monolayer-sized thickness variations in a quantum well interface. The exciton is confined to the 11 monolayer region because of the larger confinement energy in the 10 monolayer regions.

ple (Fig. 7). Such measurements probe the ground and excited states of excitons (electrostatically bound electron-hole pairs) confined in single quantum dots. The measurements reveal the discrete atomiclike spectra expected for quantum dots and also reveal that the low-temperature PL linewidths are approximately a factor of 10 smaller than typically measured in 2- or 3-dimensional samples [1]. Such narrow lines result not only from the elimination of nonradiative recombination and inhomogeneous broadening but also from the absence of elastic scattering in zero-dimensional systems.

Optical Fine Structure: The narrow linewidths permit detailed investigation of the confined exciton energy spectrum. Figure 8 plots the PL and PLE spectra from one particular quantum dot. The PL arises from the ground state of the quantum dot and the PLE measures absorption into the excited states. Polarization studies reveal that each of the spectral features is composed of
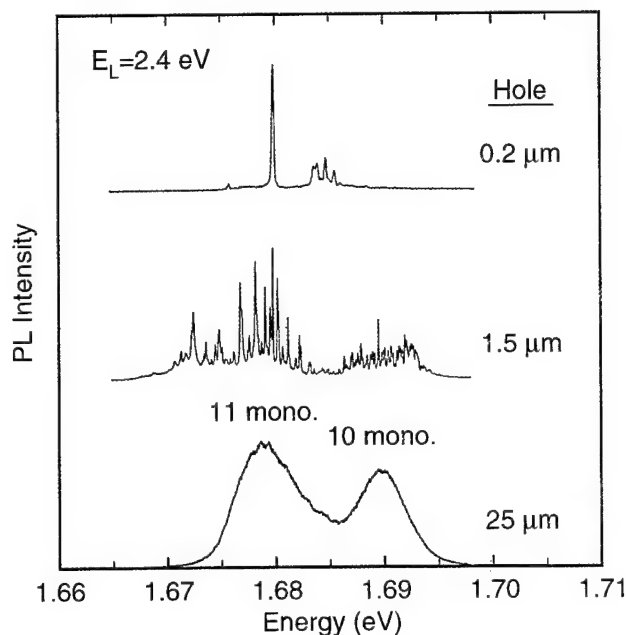
Fig. 7 — PL spectra from a 25, 1.5 and 0.2 µm diameter aperture. The two peaks in the 25 µm spectrum arise from the inhomogeneously broadened PL in the 10 and 11 monolayer-wide regions of the quantum well. The much sharper homogeneous PL peaks from the individual quantum dots are resolved by using the smaller apertures.
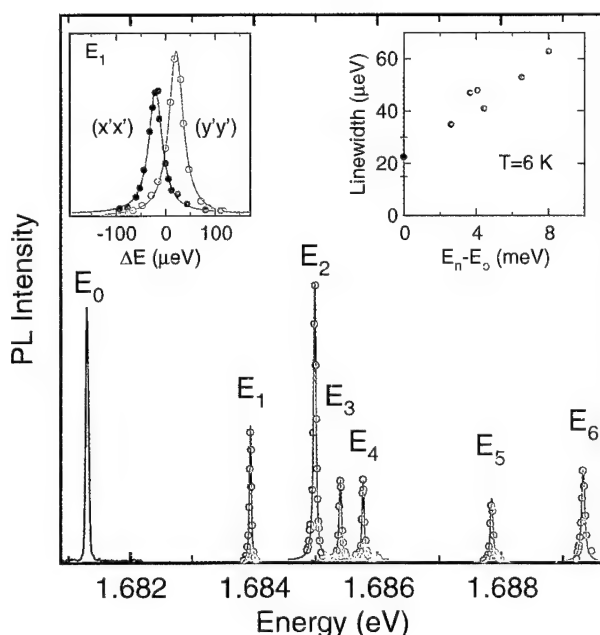
Fig. 8 — The ground state PL line and the PLE spectrum from the excited states of a single GaAs quantum dot. Each spectral feature is actually composed of a linearly polarized doublet (top left insert). The top right insert shows the linewidth of each of the states as a function of its energy relative to the ground state.

a doublet (separated by ~ 40 µeV) that is linearly polarized along the (110) and the ($\bar{1}$10 crystallographic axes (top left insert, Fig. 8). Although this fine structure was not predicted by theory, it most likely arises from a spatial asymmetry in the confining potential. Such an asymmetry has been observed by scanning tunneling microscopy and arises from the elongation of the interface fluctuations along the ($\bar{1}$10) direction. We propose that the excitation of the quantum dot gives rise to depolarization fields that cause a small shift of the quantized exciton energy states. The observed splitting arises from the different depolarization shifts for excitons polarized along the elongated ($\bar{1}$10) axis relative to the shorter (110) direction.

Homogeneous Linewidths: Additional information is gleaned from the homogeneous linewidths of the ground and excited states. Our measurements indicate that the ground state linewidth (~ 25 µeV) is consistent (via the uncertainty relationship) with theoretical predictions of the radiative exciton lifetime in a quantum dot. We also observe a systematic increase in linewidth with increasing energy of the excited states (top right insert, Fig. 8) that indicates an increase in phonon emission rate. Such lifetime information is critical to applications like quantum dot lasers that depend on the details of the exciton kinetics. This vital information can be obtained only from experiments such as these that probe the intrinsic optical properties of single quantum dots.

[Sponsored by ONR]

Reference

1.	D. Gammon, E.S. Snow, and D.S. Katzer, *Appl. Phys. Lett.* **67**, 2391 (1995). ∎

Dynamics and Control of Spatio-Temporal Systems

I.B. Schwartz
Plasma Physics Division

I. Triandaf
Science Applications International Corporation
McLean, Virginia

A great deal of interest has been devoted recently to the study of complex spatio-temporal

Chaotic Bursting in a Reaction Diffusion System
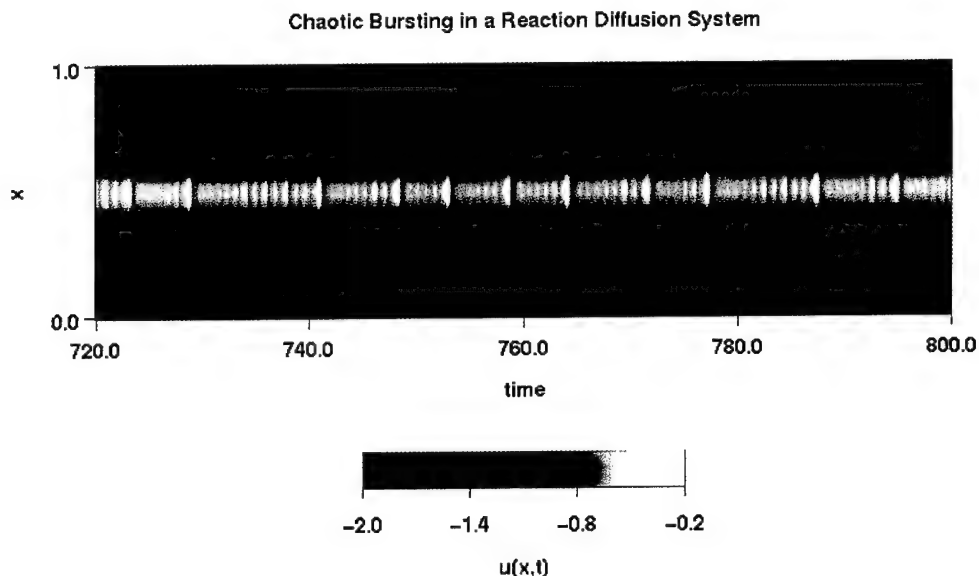
Fig 9 — One species (scaled) of the chemical reaction is shown as a function of space and time. The underlying dynamics is one of chaotic bursting. The reaction dominant regime is in the middle red region. Bursting occurs at the peak near white intensity. The diffusion dominant regime is in the blue region.

dynamics that occur as nonlinear systems are driven away from thermal equilibrium. Such systems play important roles in technological fields such as classical mechanics and materials (buckling of plate, piezoelectric materials), hydrodynamics (thermal convection, liquid crystal instabilities, turbulence), chemistry (corrosion, nonlinear waves, Turing patterns), and solid-state physics (solidification, melting, growth). In this paper, we show how powerful new tools [1] can be applied to control the dynamics of such systems in an experimental system. To exemplify the new methods, we study the dynamics of a particular chemical reaction that is used in open flow systems such as annular gel and tubular reactors. We demonstrate how to improve dramatically the reaction by using control and tracking methods.

Introduction: Recent developments in the theory of nonlinear dynamical systems have provided experimentalists with new tools for exploring a wide range of aspects in the dynamics of real systems based on analyzing a single time series [2]. Methods such as embedding techniques allow one to reconstruct a geometric model of an attractor and recover all its essential properties from time series measurements alone. Employing embedding methods for attractor reconstruction has led to a new, highly adaptive control and tracking algorithm for stabilizing orbits inside a

chaotic attractor and tracking (or following) these orbits as functions of parameters. Because of the generality of the method, the application of tracking and control has been applied to many problems in different fields such as chemistry, mechanics, smart materials, and excitable biological media, to name just a few. In this article, we illustrate the control for a reaction-diffusion system used in modeling a class of annular gel reactors that exhibit chaotic dynamics [3].

Nonlinear Dynamics of a Reaction-Diffusion System: The model we consider is one that approximates the experimental conditions and requirements of chemical kinetics laws in many types of processes, such as electrochemical reactions, corrosion, gas-solid, and gas-liquid interfacial reactions. The following equations model the qualitative behavior in the Couette flow reactor associated with the observed front patterns in achlorite-iodide reaction and have been used for investigating the formation and dynamics of sustained front patterns:

$$\frac{\partial u}{\partial t} = D\frac{\partial^2 u}{\partial x^2} + \frac{1}{\varepsilon}\,[v - f(u)]$$

RD

$$\frac{\partial v}{\partial t} = D\frac{\partial^2 v}{\partial x^2} - u + \alpha$$

142

Here D is the diffusion coefficient, and the form of the nonlinear reaction term f is not important. The boundary conditions are of Dirichlet type; that is, the concentrations are held fixed at the boundary. The reaction term is a two-variable equation that accounts for much of the bursting behavior observed in chemical and biological dynamics. Without diffusion, the model cannot simulate the observed chaos found in many of these experiments. The interaction of reaction and diffusion terms gives rise to a variety of sustained patterns such as stationary periodic structures, nonlinear waves, or chaotic spatio-temporal structures of large amplitude. An example of chaotic dynamics of the model RD is depicted in Fig. 9, where the variable $u(x,t)$ is plotted as a function of space and time. Notice that there are two basic regions: the middle region, which supports the large scale bursting, is where the dynamics is reaction dominated. The outer quiescent regions near the boundaries are where the dynamics is diffusion dominated. These two regions exhibit vastly different time-scaled behavior, where the reaction-dominant region operates on time scales that are orders of magnitude greater than those in the diffusion-dominant region.

Controlling the Reaction at the Boundary: It is important in many cases of chemical engineering interest to improve the performance of the reactions by either adjusting the operating ranges or adaptively varying the parameters. Recent progress has shown that a wide variety of applications in chemical engineering are amenable to adaptive control. Moreover, control may be implemented based on studying the dynamics at a single spatial point. In many cases, it is observed that there exists extreme sensitivity of the solution with respect to parameters, such as diffusion, which do not allow the use of these parameters for control. One way to circumvent the sensitivity is to control the solution from the boundary. By sampling a spatial point in the reaction-dominant regime, it is possible to determine where an unstable but desirable orbit to be controlled is located. The desired orbit is maintained by adjusting an external system parameter, which will be fluctuations of one component at one boundary. Figure 10 exhibits the results of such a procedure to control an unstable periodic solution. Notice that control fluctuations are evident at one of the boundaries. Reaction and diffusion stabilize the entire profile by propagating the

Spatio–Temporal Control
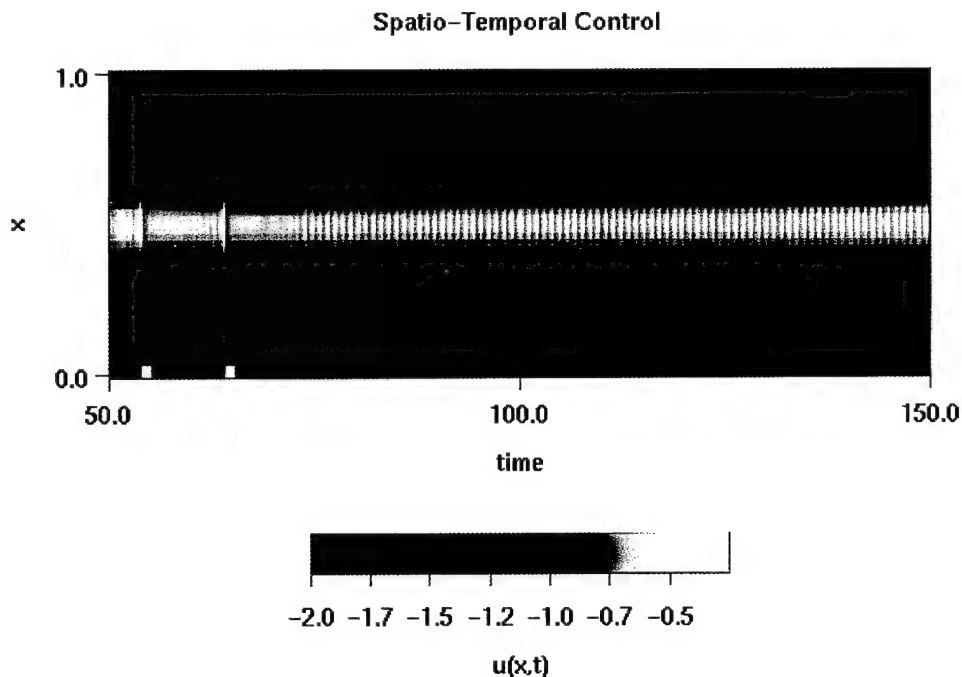
Fig. 10 — Control is applied at the boundary to the chaotic bursting regime to generate regular periodic behavior. Although perturbed at the boundary only, diffusion forces the control to act spatially as well as temporally.

Fig 11 — Two species sampled in the middle of the reaction-dominant region are plotted in a projected phase portrait. The uncontrolled dynamics of chaotic bursting is shown in green. The controlled dynamics is shown in red, which exhibits no bursting.
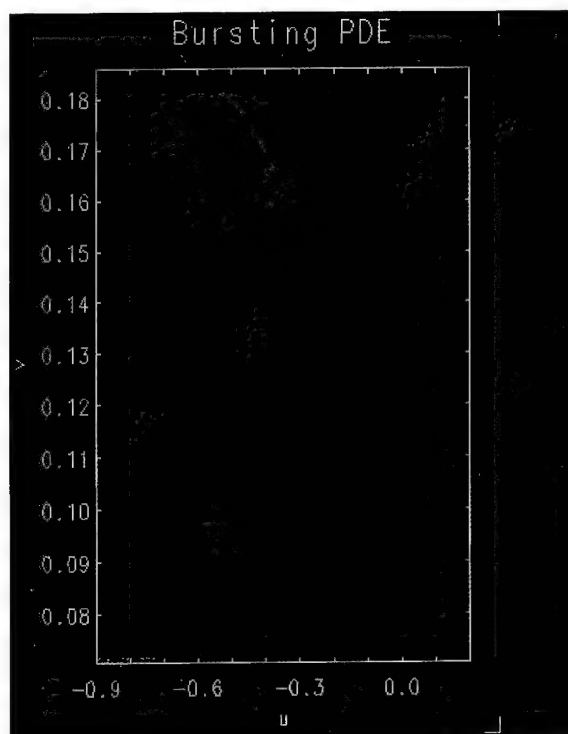
excited control signal through the spatial domain. Figure 11 shows a projection in phase space of u plotted against v for both the uncontrolled and controlled time series in the reaction-dominant region. Notice that the large bursts of the uncontrolled chaotic oscillations (green) are not present in the controlled orbits (red).

Conclusions: We have introduced boundary control methods designed from nonlinear time series that stabilize unstable states of spatio-temporal processes occurring in reaction-diffusion processes. Compared to similar techniques, it has the advantage that it achieves control spatially as well as temporally. Since it applies to time series samples in the reaction-dominant regime directly, the method is suitable for experimentalists. By coupling control with tracking [2], certain regimes

previously not seen in chemical engineering experiments can be now realized.

References

1. United States Patent 5,442,510, Control System for Tracking Nonlinear Systems, Aug. 15, 1995.

2. I.B. Schwartz and I. Triandaf, "Tracking Unstable Orbits in Experiments: A New Continuation Method," *Phys. Rev. A* **46**, 7439 (1992).

3. I.B. Schwartz and I. Triandaf, "Controlling Unstable States in Reaction-Diffusion Systems Modelled by Time Series," *Phys. Rev. E* **50**, 2548-2552, 1994. ■

Ocean
and
Atmospheric
Science
and
Technology

Polarimetric SAR Remote Sensing of Topography

D.L. Schuler and J.S. Lee
Remote Sensing Division

A new technique for terrain measurement using polarimetric synthetic aperture radar (SAR) data has been developed. It produces profiles of terrain slopes and elevations in the azimuthal (or along-track) direction. The technique estimates the average shift in the polarization orientation angle of copolarization backscatter caused by azimuthal tilts in the scattering plane. The first test of this technique was made using data from a forested area near Freiburg, Germany. Subsequent tests of the algorithm have been conducted using polarimetric SAR data in a mountainous, nonforested region of the Mojave Desert. The radar-measured slope and elevation profiles have low rms errors (and high correlation values), when compared with digital-elevation model (DEM) values for the two areas. The algorithm is capable of adaptively making a transition from forested areas to regions having open terrain. Using this technique, spaceborne and airborne polarimetric SAR will be capable of providing topographic information over wide areas.

Terrain slope maps in the along-track direction can be produced by the technique without any prior knowledge of the terrain. Terrain elevations can be derived from the polarimetric SAR slope measurements by integrating the slopes in the azimuthal direction. To obtain absolute (rather than relative) elevation values, at least one elevation "tie point" must be independently known somewhere along each slope profile. Complete elevation and slope mapping of the terrain in two dimensions is possible using this technique when azimuthal elevation profiles are produced throughout the range extent of the SAR image.

Concept: Figure 1 illustrates the concept by showing that physical terrain tilts in the azimuthal direction produce significant shifts in the orientation angle of the copolarization maximum in P-band polarimetric SAR data. This observation is supported by other comparisons of signature peak displacements and DEM-derived surface tilts throughout the datasets [1]. A search-based algorithm has been developed to accurately and effi-
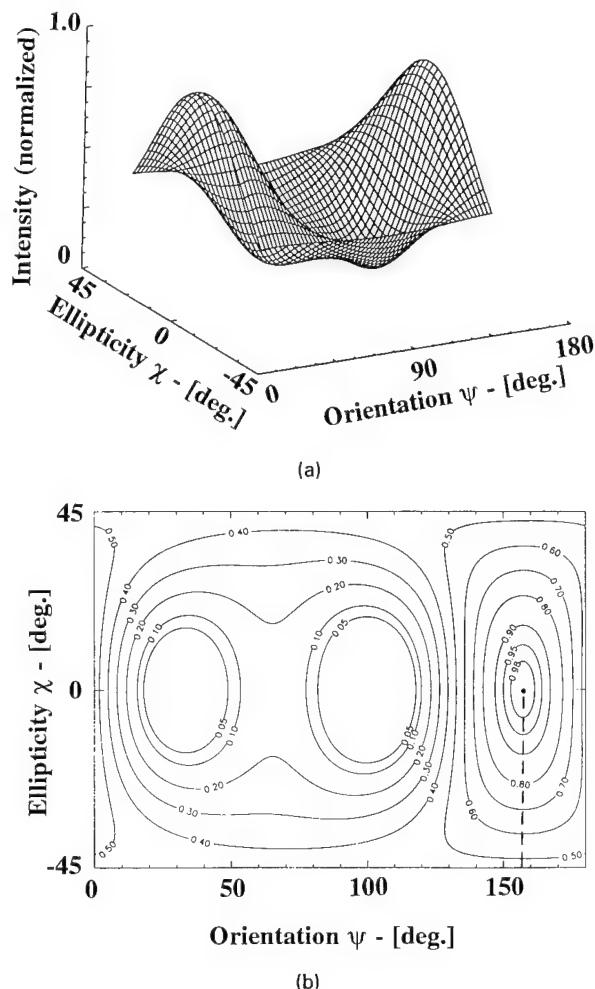
Fig. 1 — (a) Co-pol signature of P-band scatter in the Black Forest and (b) a contour plot of a forest signature from terrain having an azimuthal tilt of 22°. Note: The horizontal-transmit/receive peak (normally at (ψ = 0°/180°) has shifted to ψ = 158°).

ciently measure the location of the maximum of polarization signatures in (ψ,χ) space, where ψ is the orientation angle and χ is the ellipticity angle. In the algorithm, the location of the maximum is determined for each SAR slant-range resolution cell. Changes in position of the maximum ($\Delta\psi$) parallel to the orientation axis are related to topography, while values (χ) in the orthogonal direction measure the ellipticity. Both physical parameters yield useful information. The algorithm adapts automatically to changing open or forested terrain conditions throughout the image.

Forested Terrain Studies: The effect of topography on P-band (68-cm wavelength) backscatter from forested areas was studied [1] using

147

a 1989 data set acquired by the National Aeronautics and Space Administration/Jet Propulsion Laboratory's (NASA/JPL) polarimetric AIRSAR. The technique, implemented at P-band, allows sensing of topography for forested areas directly at the ground plane. The topography of the Black Forest region that was studied consisted of a forested, gently rising (3° to 4° slope) plateau bounded on either side by indented river valleys. Forested terrain slopes leading down to rivers often reached slope values of 25° to 30°. Study results indicate that the overall rms slope/elevation accuracies (relative to a conventional stereo-photo DEM) were 2°/8.4 m (inter-river terrain) and 3.2°/18 m (river-valley terrain). The correlation coefficients for all slopes was 0.8 and for all elevations was 0.92.

Open-Terrain Studies: A second polarimetric SAR dataset has been analyzed where the scattering was from mountainous desert terrain on the National Training Center near Ft. Irwin, in southeastern California. The purpose of this study was to show that this new polarimetric SAR technique will also work in open terrain. The L-band (28-cm wavelength) data used were from a NASA/JPL

AIRSAR flight of 26 May 1994. Figure 2 shows an image produced from the dataset and a 3-D plot of the polarimetric SAR-generated DEM of the Tiefort Mountain Range, Drinkwater Lake, and the surrounding Mojave Desert basins. In general, the mountains in the image are rugged and devoid of trees or other large vegetation. Topographic slopes of up to ± 50° and elevation differences of 487 m exist in the imaged area. This study location was selected because of the existence of a very accurate DEM covering the area. This DEM is constructed on a 5-m spacing with an accuracy of 0.3 m. Azimuthal profiles of polarimetric SAR DEM and conventional DEM elevations were made. Figure 3 shows the agreement between these profiles in determining elevations. The overall rms slope/elevation accuracies for 44 such profiles were 2.4°/5.6 m (moderate terrain) and 3.5°/23.5 m (rugged terrain). The correlation coefficient for all slopes was 0.85 and for all elevations was 0.88.

Significance: This new polarimetric technique is capable of measuring terrain slopes and elevations directly at the ground plane for forested, open, and coastal terrain. Measurements made
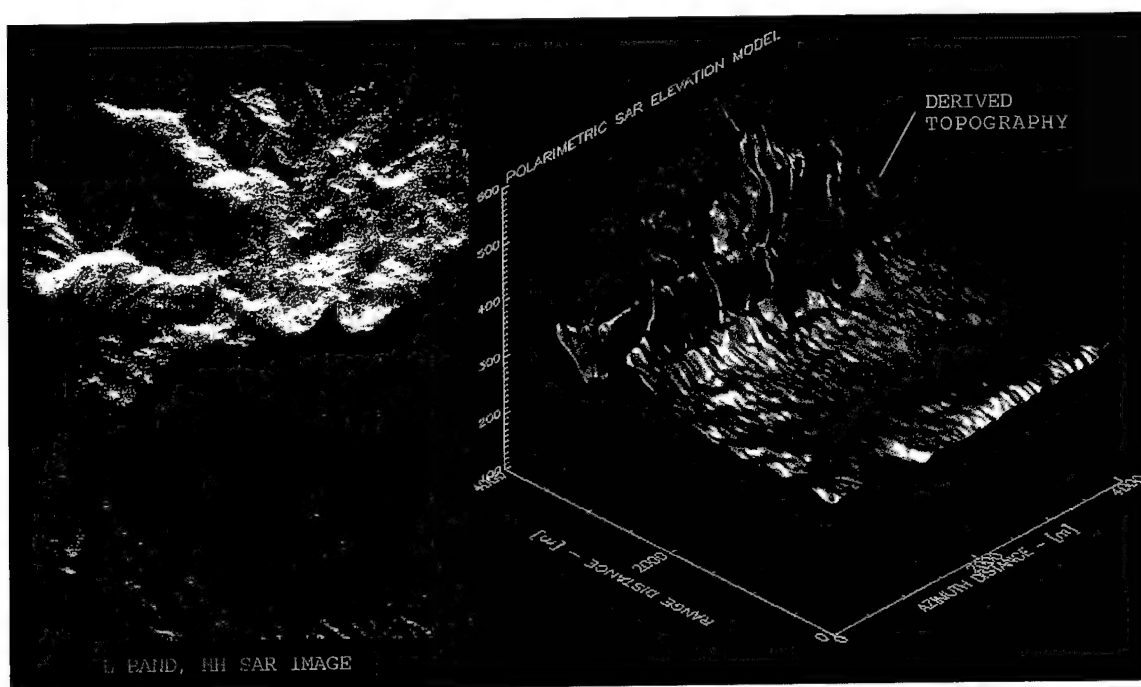
Fig. 2 — A polarimetric SAR DEM surface generated for the Ft. Irwin data. The Tiefort Mountains are in the background and Drinkwater Lake (dry) is the shallow basin in the foreground. The insert (left) is the original data processed conventionally as an L-band HH-polarization image.
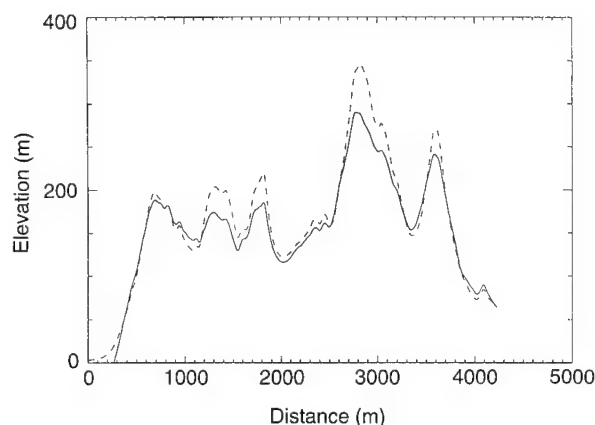
Fig. 3 — Comparison of elevations derived for an azimuthal transect of the Tiefort Mountains (1) from polarimetric SAR data (solid line) and (2) from the Ft. Irwin DEM (dashed line). The polarimetric SAR elevation profile is initialized to the DEM value at the right side.

from aircraft and (potentially) from satellites will provide topographic information over wide areas of the Earth.

[Sponsored by ONR and ARPA]

References

1. D.L. Schuler, J.S. Lee, and G. De Grandi, "The Remote Sensing of Topography Using Polarimetric SAR," *Proc. Geosci. Remote Sens. Symp. (IGARSS'95)*, Vol. III, 10-14 July 1995, Florence, Italy, pp. 1789-1791.

2. D.L. Schuler, J.S. Lee, and G. De Grandi, "The Measurement of Topography Using Polarimetric SAR Images," submitted to *IEEE Trans. Geosci. Remote Sens.*, March 1995.   ∎

Biophysical Interactions in the Arabian Sea

J.C. Kindle,[1] D.K. Young,[1] R.A. Arnone,[2] and A.W. Green[1]
[1]*Oceanography Division*
[2]*Remote Sensing Division*

Background: The Arabian Sea is an area with steady wind-forcing during the regularly alternating southwest (June-September) and northeast (December-February) monsoons (Fig. 4), with wind lulls in Spring and Fall. These regular wind reversals make the region one of the few where one encounters a complete switch in wind-forcing and ocean-current response on a regular basis. The switch is associated with plankton blooms and extremely high production during the southwest (SW) monsoon and with reduced productivity in the other monsoon and impoverishment during the Spring transition. These cycles of high productivity, alternating with impoverishment, are so extreme that they represent end members in the range of open-ocean productivity values. This wide range makes the region especially appealing for investigating the response of the ecosystem to changes in the physical environment, which is the primary goal of the Accelerated Research Initiative, "Forced Upper Ocean Dynamics."

Approach: NRL scientists used a combination of numerical modeling, remote sensing, and field work to examine the source of nutrients for the 300- to 400-km wide phytoplankton bloom in the northern Arabian Sea during the SW monsoon. The intense southwesterly winds during the Summer monsoon are conducive to coastal upwelling along the coasts of Somalia and Oman. Coastal filaments, which are formed by the interaction of the northeastward-flowing Omani Coastal Current with the prominent capes along the coast, extend offshore as jets, with width scales of up to 100 km and surface velocities as large as 100 cm/s.

The potential importance of the coastal filaments to the large-scale bio-optical response to the SW monsoon in the northern Arabian Sea was hypothesized in the modeling work of Young and Kindle [1] and the follow-on study of Gallacher and Rochford [2]; Fig. 5 depicts the offshore advection of nitrate (an essential nutrient for phytoplankton growth) by the coastal filaments as represented by the coupled biophysical model of the Arabian Sea. Subsequently, images from historical-advanced very-high-resolution radiometer (AVHRR) databases at NRL provided information about the timing and horizontal scales of the jets. Use of the modeling results, together with the IR imagery, permitted the definition of an optimum sampling scheme for an observational field program during both monsoon seasons. The field work, consisting of four cruises jointly funded by NRL and ONR, was in collaboration with the National Science Foundation's Joint Global Ocean
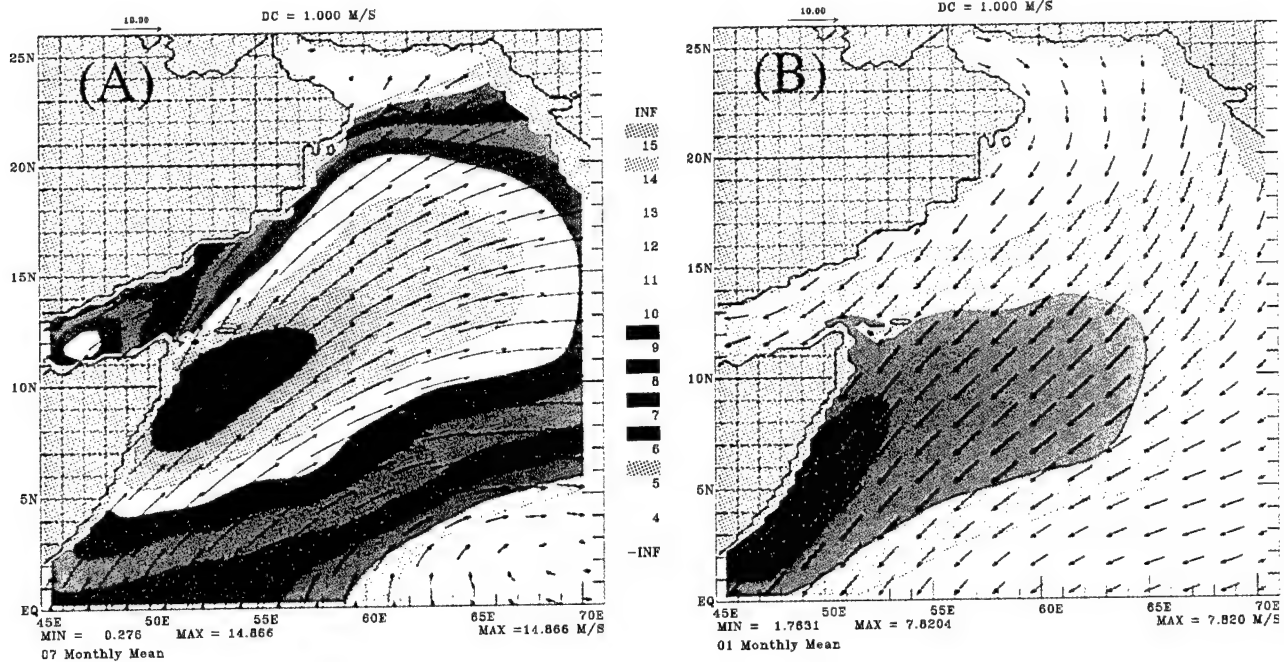
Fig. 4 — Average surface winds in the Arabian Sea from the Naval Operational Global Atmospheric Prediction System (NOGAPS) model for the months of (A) July and (B) January. The arrows indicate direction of flow, and color contours represent magnitude in m/s. The contour interval is 1 m/s.
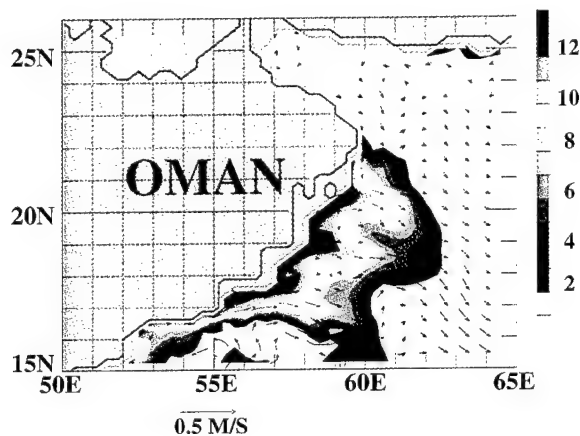
Fig. 5 — Surface current vectors superimposed with contours of nitrate concentration for September 2 from a coupled biological-physical of the Indian Ocean. The model is forced with climatological winds. The contour interval is 1 mg/m***3. The nitrate, brought to the surface by coastal upwelling, is advected offshore by the filaments.

Flux Study (JGOFS) Arabian Sea Expedition—a 16-month field program from 1994 to 1996. An AVHRR receiving station, installed by NRL scientists onboard the RV *Thomas G. Thompson,* permitted real-time identification of intensified upwelling regions and the filaments (Fig. 6). The real-time IR analysis allowed short-term alterations of the sampling plan; the subsequent measurements of the physical, biological, chemical, and optical properties of the coastal upwelling centers and the offshore-directed filaments yielded the most detailed observations yet conducted

of these features. Preliminary analysis of these data fully support the hypothesis that offshore advection by the filaments is the primary mechanism that supplies nutrients for the large-scale phytoplankton bloom during the SW monsoon.

Conclusion: This result provides an exciting example of the dynamic coupling between a coastal regime and the adjacent off-shore environment. The work presents an alternative hypothesis to that of open-ocean upwelling as the primary mechanism for the supply of nutrients to
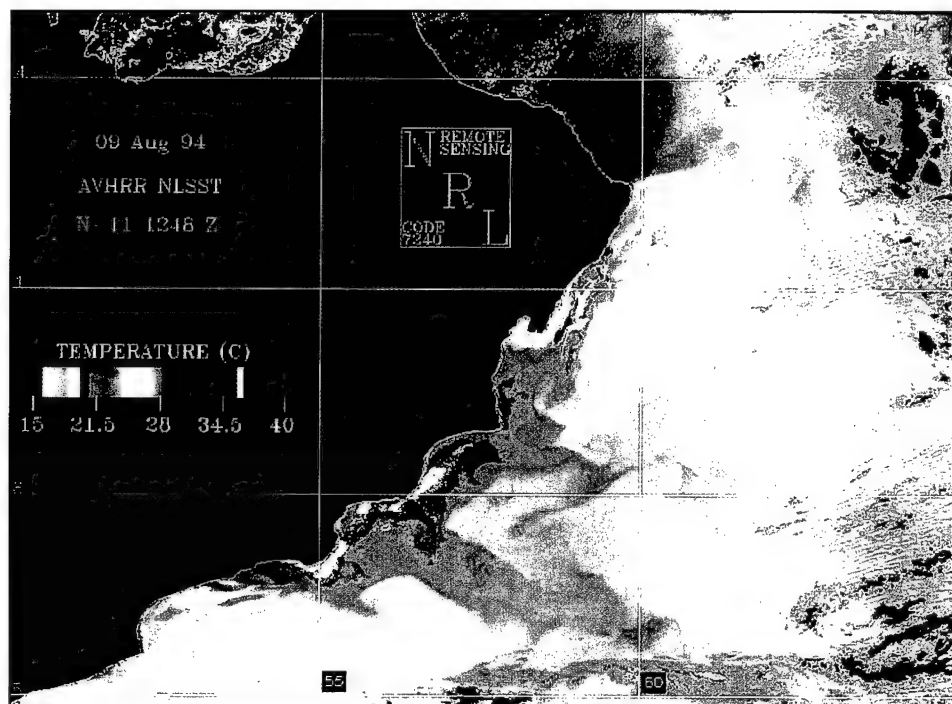
Fig. 6 — This AVHRR image of sea surface temperature collected on August 9, 1994, illustrates cold upwelling (blue) occurring along the Oman coast. These high-nutrient cold waters form filaments that emanate from the Capes and extend approximately 150 km offshore. They are observed from May through September.

the large plankton bloom during the SW monsoon. Ongoing modeling studies and analyses of the remotely sensed and in-situ observations, together with collaborative work with ONR-funded scientists, will provide a fuller understanding of the complex biophysical processes of the northern Arabian Sea.

[Sponsored by ONR]

References

1. D.K. Young and J.C. Kindle, "Physical Processes Affecting the Availability of Dissolved Silicate for Diatom Production in the Arabian Sea," *J. Geophys. Res.* **99**, 22619-22632 (1994).

2. P.C. Gallacher, and P. Rochford, "Numerical Simulations of the Arabian Sea Using Tracers as Proxies for Phytoplankton Biomass," *J. Geophys. Res.* **100**, 18565-18580 (1995). ∎

An Investigation of the Southerly Surge

W.T. Thompson, T. Haack, and J.D. Doyle
Marine Meteorology Division

During the Summer months, the California coast is under the influence of persistent northwesterly flow. Several times each Summer, the northwesterly flow weakens, and an abrupt shift to southerly winds occurs in a narrow zone along the coast, accompanied by significant cooling and development of a low-level overcast. Visible satellite imagery of these events is quite striking, showing a narrow tongue of stratus surging rapidly northward along the coast. The genesis of these events is controversial and may involve Kelvin waves, coastal gravity currents, and/or an ageostrophic response to synoptic scale forcing.

In the present study, we use NRL's coupled mesoscale model (the Coupled Ocean/Atmosphere Mesoscale Prediction System (COAMPS)) to simulate a southerly surge event and attempt to determine the mechanism(s) responsible for its initiation.

Model Description: COAMPS [1] is a triply nested, nonhydrostatic mesoscale model with detailed parameterizations of moist processes, radiation, and boundary layer turbulence. A sophisticated data assimilation procedure is also used to provide initial conditions. Lateral boundary conditions are supplied by the Navy's global model. In the present study, simulations were performed with horizontal resolutions of 45 km, 15 km, and 5 km on the three nests with 30 vertical levels.

Case Description: We performed simulations of the 10-11 June 1994 surge event [2]. This event begins with weak southerly flow just south of Pt. Conception at 0600 UTC 10 June. The northward extent of the southerly flow reaches Monterey Bay at 1700 UTC 10 June and Pt. Reyes (just north of the Golden Gate) by 0900 UTC 11 June. Southerly flow extends along the coast over 850 km and peaks at 8 m/s. The "surging" of coastal stratus northward along the coast is clearly evident in satellite imagery for this period, although the southerly flow precedes the clouds by up to 3 h in some locations. Figure 7 is a visible satellite image for 18:10 UTC 10 June.

Model Results: The model is able to capture this evolution quite realistically. Figure 8 shows a model 19-h forecast valid at 1900 UTC of cloud
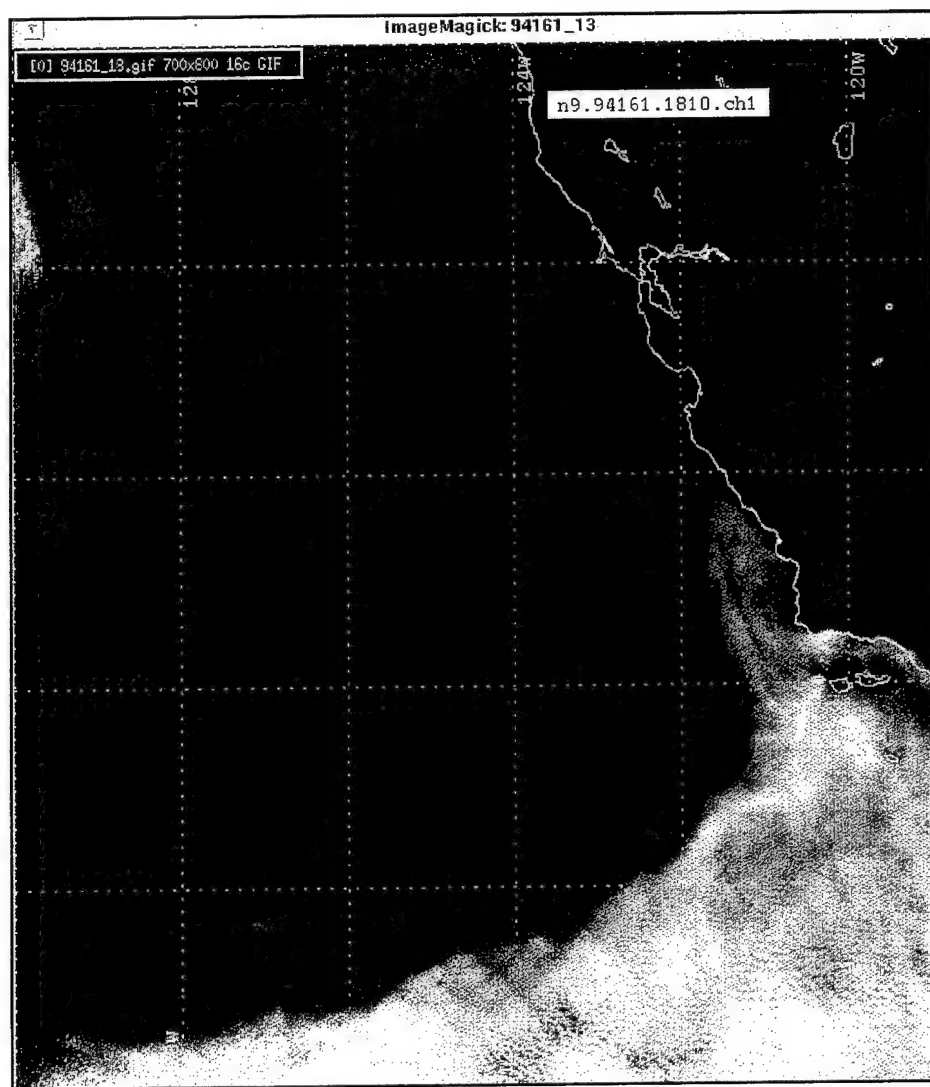
Fig. 7 — Visible satellite image valid at 1810 UTC 10 June 1994.
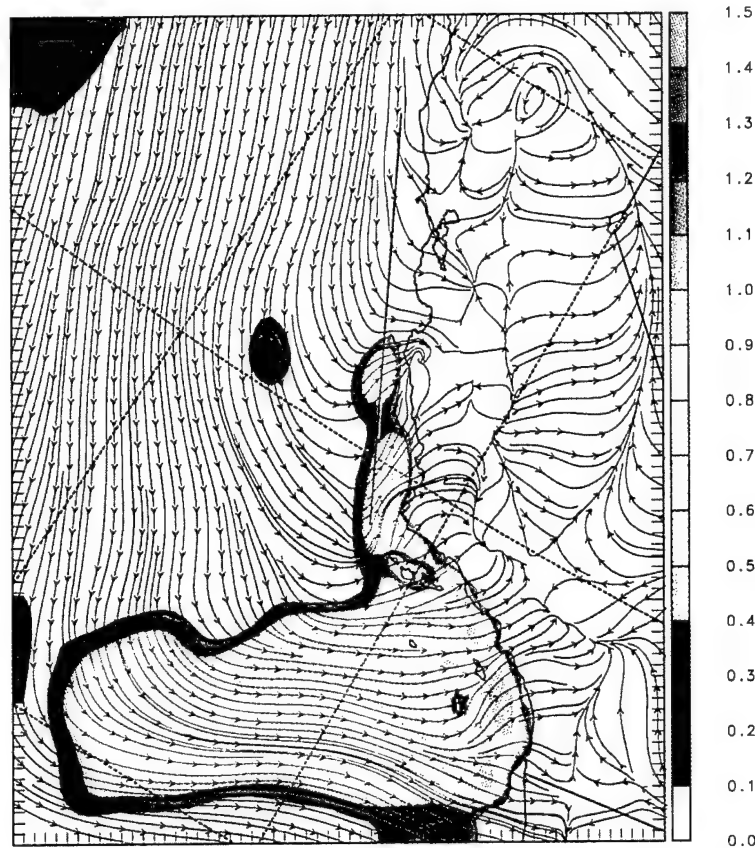
Fig. 8 — COAMPS 19-h forecast cloud liquid water mixing ratio (gm/kg)
and wind streamlines at the lowest model level valid at 1900 UTC
10 June 1994.

liquid water mixing ratio and wind streamlines at the lowest model level (~10 m). The model cloud position agrees well with the satellite image, although the cloud edge is slightly to the north of the position shown in the image.

In an effort to examine the characteristics of the surge, a vertical cross section was constructed in a plane through the center of the stratus tongue along the coast (Fig. 8). Figure 9 shows the cross section of cloud liquid water (g/kg, shaded) and potential temperature (contoured in degrees Kelvin) at hour 30. The boundary layer deepens as the southerly flow and stratus move north along the coast, and the leading edge of the cloud tongue takes on an appearance of a linear Kelvin wave response. At this time, southerly flow and the deepening of the boundary layer precede the leading edge of the clouds, just as in the observations.

Conclusions: Early work [3] associated these orographically trapped phenomena with linear Kelvin waves. The theory assumes that two fluid layers exist separated by an elevated interface adjacent to a lateral boundary. The Kelvin wave response has the phase speed of the shallow-water wave solution, and the width of the response scales as the ratio of the phase speed to the Coriolis parameter. Computations of the Kelvin wave response phase speed and width associated with the 10-11 June 1994 surge event are in excellent agreement with the COAMPS simulation results. However, some inconsistencies exist between linear Kelvin wave theory and the model simulation. Further investigation of this mechanism and others is thus required. In the future, we plan to perform numerical experiments designed to identify the physical mechanisms responsible for initiation of the surge.

[Sponsored by ONR]

153
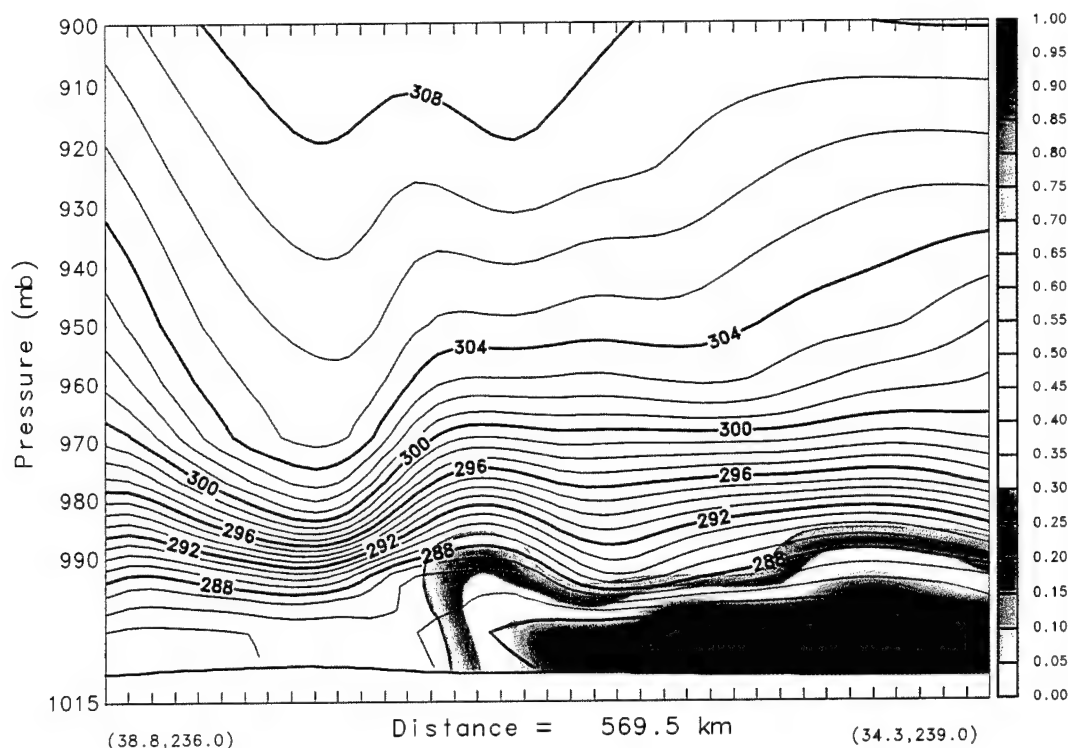
Fig. 9 — Vertical cross-section of COAMPS 30-h forecast cloud liquid water mixing ratio (gm/kg; shaded) and potential temperature (K) valid at 0600 UTC 11 June 1994. Figure 8 shows the plane of the cross section.

References

1. R.M. Hodur, "Numerical Modeling of the Atmosphere and Ocean," *1993 NRL Review*, Naval Research Laboratory, Washington, D.C., pp. 190-193.
2. F.M. Ralph, P.J. Neiman, P.O.G. Persson, W.D. Neff, J. Miletta, L. Armi, and J.M. Bane, "Observations of an Orographically Trapped Disturbance along the California Coast on 10-11 June 1994," Preprints, *7th Conference on Mountain Meteorology*, 17-21 July, Breckenridge, Colorado.
3. C.E. Dorman, "Evidence of Kelvin Waves in California's Marine Layer and Related Eddy Generation," *Mon. Wea. Rev.* **113**, 827-839 (1985). ■

Solar Irradiance Variability Models

J.T. Mariska, H.P. Warren, and J. Lean
Space Science Division

Over the Sun's 11-year activity cycle, short wavelength solar radiation varies by more than an order of magnitude. These changes dramatically alter the temperature, density, and composition of the Earth's upper atmosphere (Fig. 10), impacting spacecraft operation and communication. For example, atmospheric density fluctuations modulate the drag on artificial satellites, leading to orbit changes that must be accounted for to keep track of the large number of objects currently orbiting the Earth.

Presently, most modeling of the interaction of solar radiation with the Earth's atmosphere uses proxies for the actual values of the solar irradiance (the energy emitted from the entire Sun at a specified wavelength that reaches the Earth). This is necessitated by the lack of continuous satellite-based measurements of solar irradiances. As a substitute, investigators have taken the limited available satellite irradiance data and correlated them with easily measured quantities, such as the solar radio flux at a wavelength of 10.7 cm. While these proxies are easy to measure, they are only indirectly related to the solar short-wavelength radiation they are supposed to represent. Thus, large uncertainties exist in
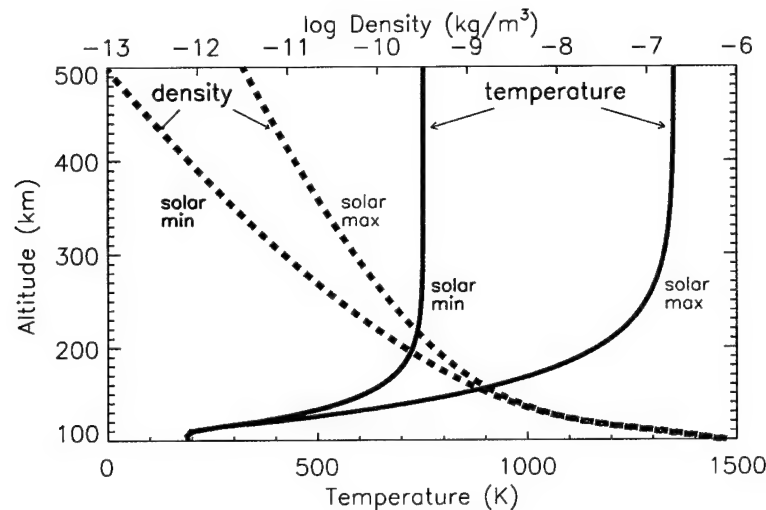
Fig. 10 — Temperature and density distribution in the Earth's upper atmosphere at maximum and minimum levels of solar activity.

specifying the Sun's irradiance for any given level of solar activity.

A Physics-based Model: Since the early days of space research, solar physicists in the Space Science Division and elsewhere have been studying extreme ultraviolet and soft X-ray radiation from the Sun's outer atmosphere under different conditions of solar activity. These studies provide a detailed semi-empirical physical picture of the ever-changing physical conditions in the outer layers of the solar atmosphere (Fig. 11). Using this understanding and drawing on NRL's leadership position in both solar physics and extreme ultraviolet and soft X-ray spectroscopy, we have developed a physics-based solar irradiance variability model [1, 2].

Our model combines three key ingredients. First, we employ the extensive solar ultraviolet and X-ray data available at NRL and elsewhere to produce descriptions of the average physical properties of the primary features of the outer solar atmosphere. Second, we have assembled a database of the atomic physics parameters necessary to compute the emission from the Sun's high-temperature plasma for any spectral line or continuum in the extreme ultraviolet and soft X-ray wavelength region. These two ingredients permit us to compute the radiance (energy emitted from a small region of the Sun at a specified wavelength at the Earth).
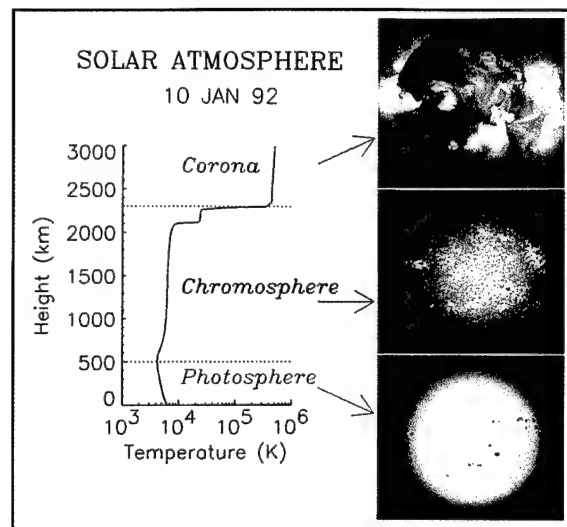
Fig. 11 — Average temperature structure of the solar atmosphere together with images showing how the Sun appears at different levels of the atmosphere. The solar photosphere is imaged in broad-band visible light, the chromosphere in the light of singly ionized Ca, and the corona in soft X-rays. Extreme ultraviolet and soft X-ray radiation comes from the upper chromosphere and corona.

Finally, we have developed algorithms for using ground-based visible light images and space-based X-ray images to estimate the fraction of the Sun covered by each kind of emitting structure. Combining this last ingredient with the radiances produces an irradiance at any selected wavelength for any level of solar activity.
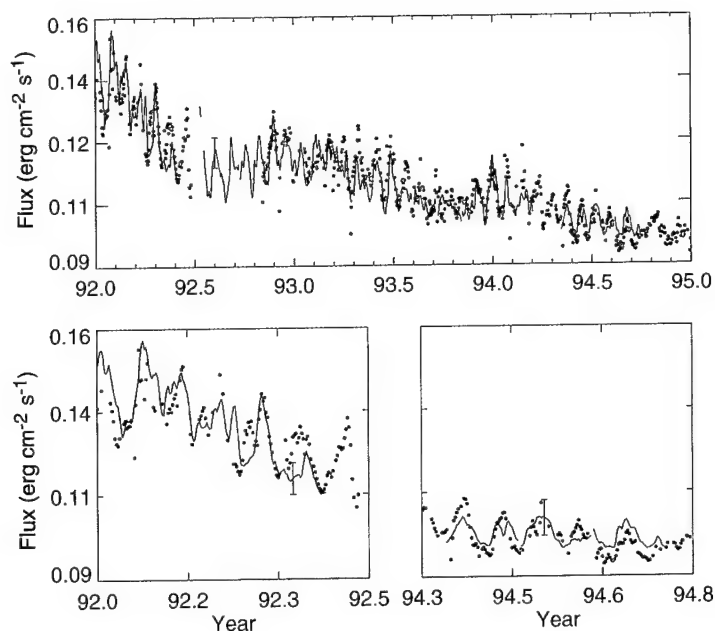
Fig. 12 — Comparison of physics-based model predictions for the C IV 154.8 nm emission line (red filled circles) with observations from the SOLSTICE experiment on the Upper Atmosphere Research Satellite. The two bottom graphs show details of the comparison at times of high and low solar activity.

Comparison with Observations: Figure 12 shows an example of the results of this physics-based model. Here we synthesize the irradiance in the 154.8-nm emission line of C IV (three times ionized C) using ionized Ca K-line solar images (such as the one shown in Fig. 11) taken from a ground-based observatory to decompose the solar disk into its primary emitting components. Our synthesized C IV irradiances agree very well with recent direct observations. Our model successfully accounts for both the 27-day modulation due to solar rotation and the longer term declining trend as the current solar cycle decays toward minimum in 1996.

Future Directions: We are currently validating our physics-based model against available solar observations at other wavelengths. We plan to provide simplified versions of the validated model to spacecraft designers at NASA for use in satellite design and to the space weather community to provide improved solar irradiance data to models describing neutral and ionized upper-atmospheric chemistry and dynamics.

[Sponsored by ONR, NASA, and SERDP]

References

1. H.P. Warren, J.T. Mariska, and J. Lean, "A Physics-based Model of Solar Irradiance Variability from 1-300 Å," *EOS*, (1995), in press.

2. J.T. Mariska and J. Lean, "Radiative Influences," in K. S. Balasubramaniam, S. L. Keil, and R. N. Smartt (eds.), Proceedings of the 16th NSO/SP International Workshop, San Francisco: Astronomical Society of the Pacific, (1996), in press. ∎

Optical
Science

Change Detection Using Multispectral Invariants

A. Schaum
Optical Sciences Division

A. Stocker
Space Computer Corporation

Progress in achieving worldwide remote sensing capabilities for Earth resources management, environmental monitoring, and surveillance applications has been limited by the need to cover enormous ground areas and by the requirement for a human analyst to interpret individual images. Autonomous detection methods could make effective wide-area coverage feasible for crop management, pollution control, treaty verification, and many other remote-sensing applications. The feature common to many of the activities that need to be monitored is some type of localized change. NRL has developed new algorithms for change detection that promise to make wide-area coverage feasible, by screening large volumes of imagery and efficiently selecting areas for human intervention. The new signal-processing methods incorporate spectroscopic analysis into a target-detection formalism.

If digitized imagery can be collected often enough, then simple image subtraction can make any changes prominent by removing neighboring clutter from the background. But a requirement for frequent revisits conflicts with many wide-area operational concepts. Realistic intervals between data collections are often many hours or even months. During such periods, natural background evolution causes undesired changes to dominate subtracted images, making discrimination between targets and background impossible with conventional techniques.

Spectral Methods: Continuing advances in electro-optical sensor technologies have made the simultaneous collection of images in many different wavebands possible. The extra spectral dimension can often be used to identify subpixel-scale objects or tenuous gases in cases where spatial discrimination is impossible. But certain targets of interest can have color signatures that are too weak to be detected in a single multispectral image. Nevertheless, although static detection of a dim target's presence might prove infeasible, spectral-temporal information can often be exploited to detect its *appearance*.

The principle behind this form of change detection is the use of color information to find temporally invariant features in the background. If, for example, each scene pixel can be modeled as a mixture of a few primary constituents, then spectral measurements can be used to generate estimates of their concentrations. In the simplest cases, these concentrations can supplant the measured radiances as the appropriate background descriptors. Furthermore, they should be conserved over time, in the absence of a real change. In an ideal sensing environment, one could expect to detect novel features, even after long intervals, by examining changes in constituent concentrations.

In practice, the estimation of constituent concentrations in remotely sensed data is a somewhat immature art. Figure 1 shows the apparent fractional concentrations of a particular background constituent in several pixels of a multiband thermal infrared image. The data are derived from measurements collected by the Joint Multispectral Program, a tri-service effort to explore spectral techniques of image exploitation. The concentration estimates in the figure are based on a simple additive model of constituent contributions to the total background. Although these estimates are not perfectly conserved, the plots for different pixels seldom cross, indicating correlated behavior over time. Strong correlation in background descriptors is an invaluable tool for detecting anomalies like local changes.

The use of intrinsic spectral-temporal correlations to detect a real subpixel target in multiband infrared data is illustrated by the two-band spectral scatter plots shown in Fig. 2. The target clearly cannot be separated from its local background using a single dual-band observation. However, in this case, the same background pixels were imaged several hours prior to target insertion, and these correlated reference data were processed to predict the dual-band scene containing the target. The pixel prediction errors shown in Fig. 2 are variable but correlated *except* at the target pixel, thus allowing it to be readily discriminated. This two-look multispectral procedure has been successfully applied to locate extremely small changes, most notably a camouflaged target in a desert background that filled only 1.6% of a pixel and was not detectable
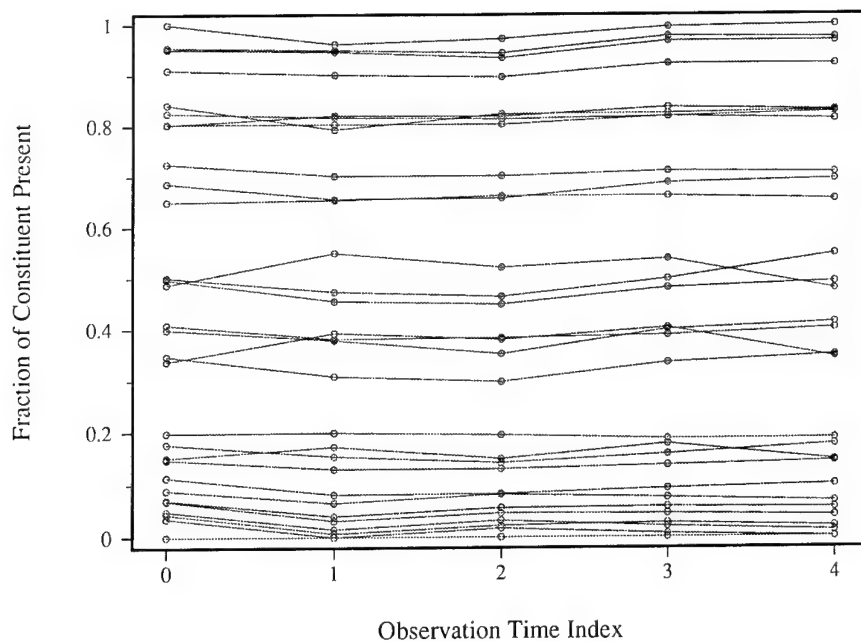
Fig. 1 — Fractional concentrations of a background constituent vs time in 30 pixels of a multiband thermal infrared image, estimated by means of a linear spectral mixture model. Although the estimated fractions are not perfectly conserved, their temporal trajectories are highly correlated over time. This provides a physical basis for background clutter suppression in change detection applications.
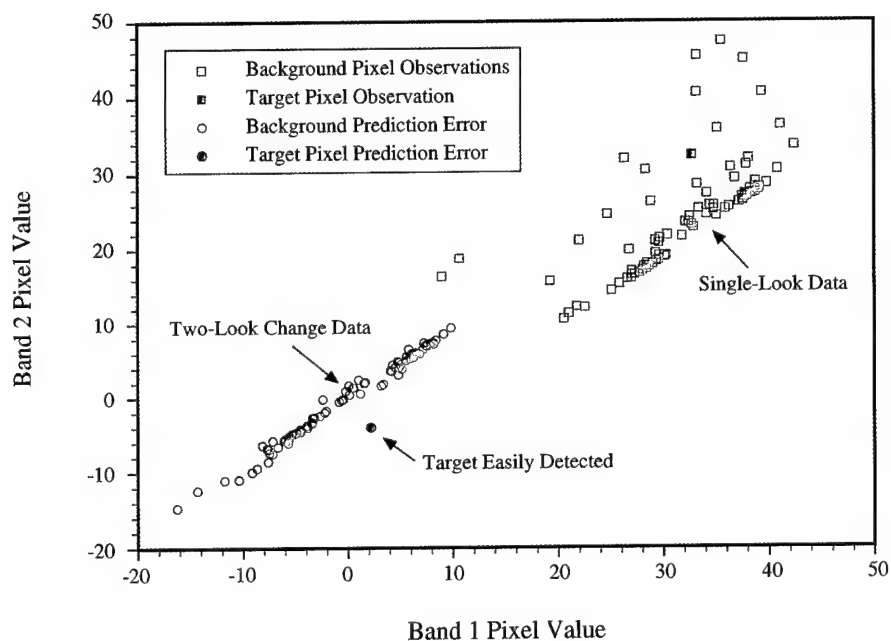
Fig. 2 — Dual-band spectral scatter plots of pixels in a thermal infrared image containing a heterogeneous background and an M60 tank target that fills only 25% of a single pixel. The unresolved target cannot be separated from the background in the original single-look image observations. However, if spectral invariants are used to predict the scene containing the tank from one collected prior to target insertion, discrimination becomes easy in the prediction error image.

by purely spectral or purely temporal methods. Furthermore, the interval between the looks was 27 h, which allowed many natural background changes to occur.

Hidden Correlations: To achieve even higher sensitivity, spectral images from more than two times can be processed. All spectral and temporal correlations can be estimated from these data and used to construct a multidimensional filter that minimizes the background clutter in a particular scene being tested for change events. This approach captures and exploits any hidden correlations that might exist in the spectral component time histories because of background invariants, even ones that cannot be specified in advance. If a sufficient number of such observations are processed, then the physically unchanged part of the background can be completely removed, and the detection of changes becomes limited only by sensor noise.

Figure 3 shows how the detectability of the subpixel target can be improved if additional dual-band reference scenes are made available

(the zero reference and one reference cases were illustrated in Fig. 2). Optimal processing of the target scene, in combination with reference scenes from six different times, increases the target's signal-to-clutter ratio by a factor of 26 with respect to single-look operation. Figure 3 also shows that the fluctuation in the scene background can be suppressed to the sensor noise floor if five reference times are used. This remarkable result is obtained even though the measurements span a time period of 27 days. It shows that there is no fundamental reason for change detection performance to be limited by environmental evolution.

Prospects: Intrinsic spectral invariants provide a powerful new tool for automated change analysis in multispectral imagery. Successful development of this technology is expected to remove a major barrier to achieving autonomous worldwide change monitoring for both Navy and civilian applications.

[Sponsored by ONR] ■
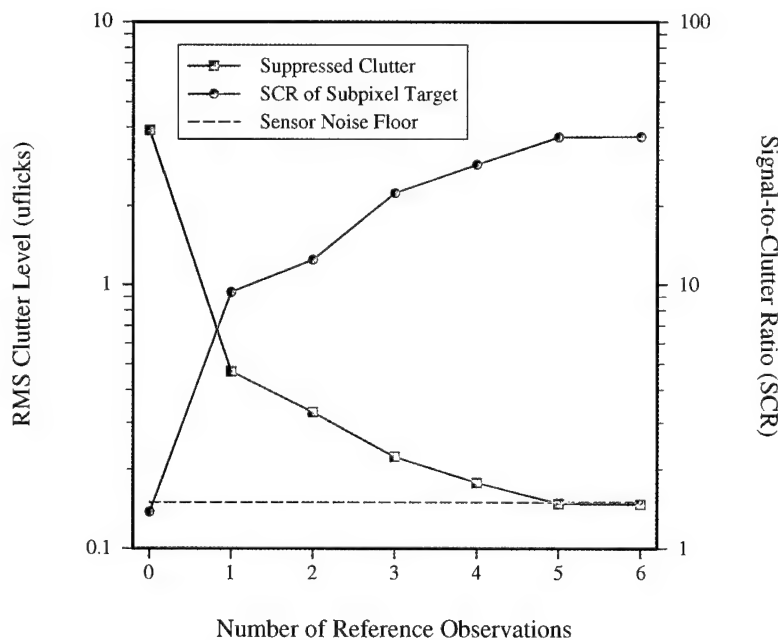
Fig. 3 — Change detection performance improves if additional observations of the same scene are processed. For the subpixel tank target of Fig. 2, the signal-to-clutter ratio for detection stabilizes after five of six dual-band reference images taken over a 27-day time period is used to remove background clutter. By reaching the sensor noise floor, the method converts a clutter-limited detection problem into a noise-limited one.

Nanochannel Glass Replica Membrane Technology

D.H. Pearson and R.J. Tonucci
Optical Sciences Division

Nanochannel Glass Replica Membranes:
Nanochannel glass replica membranes are thin, metallic films containing uniform, nanometer-scale voids whose sizes, positions, geometric patterns, and packing densities may be controlled to a high degree [1]. They are readily prepared from a variety of metals, including noble and refractory metals such as platinum, gold, palladium, tungsten, and molybdenum. The membranes typically contain approximately 10^6 voids and have been prepared thus far with void diameters as small as 40 nm at packing densities greater than 3×10^9 voids/cm^2. We have prepared these membranes by a replication technique using thin-film deposition onto wafers of nanochannel glass (NCG), a patterned glass material containing uniform, nanometer-scale capillaries recently developed at NRL [2]. The fabrication of NCG replica membranes begins by sputtering or evaporating a thin-film bilayer onto the surface of a polished NCG wafer containing capillaries of a desired size. The thin-film layer in contact with the NCG wafer is an easily dissolved buffer layer, and the outer layer is the NCG replica membrane. Typical choices for the buffer layer and replica membrane layer include aluminum and platinum, respectively. Dissolving the buffer layer in an appropriate chemical solution, such as a warm sodium hydroxide solution for dissolving aluminum, releases the NCG replica membrane, which may be rinsed and placed on a substrate for a desired patterning application, as in Fig. 4. Figure 5 shows a platinum NCG replica membrane 110 nm in thickness with 115-nm diameter voids. These NCG replica membranes are well suited for use as low-aspect-ratio shadow masks in substrate patterning applications such as materials deposition, reactive ion-etching, and ion implantation. Their utility is due, in part, to the fact that their thicknesses and the aspect ratios may be controlled to a high degree. In fact, we have successfully prepared these membranes with thicknesses ranging from a few hundred to a few thousand angstroms and aspect ratios ranging from 0.06:1 to approximately 2:1. Another factor which contributes to their usefulness is flexibility in the

Deposition Source
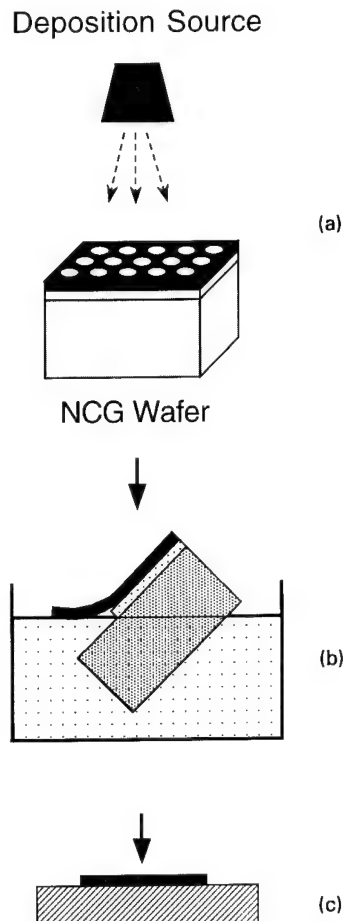
Fig. 4 — The preparation of NCG replica membranes: (a) an easily dissolved buffer layer and a desired membrane layer are deposited onto the surface of an NCG wafer; (b) the membrane is released by dissolving the buffer layer in an appropriate chemical solution; and (c) after rinsing, the membrane is placed on a substrate for a desired patterning application.

choice of materials. NCG replica membranes may be prepared from a variety of metals, alloys, and perhaps ceramics and other refractory materials. As a result, their properties may be engineered to suit particular tasks. The membranes we have prepared from noble and refractory metals possess high-temperature stability, good chemical resistance, and high mass density, making them well suited for use in a variety of patterning applications at the nanometer size scale.

Research Efforts and Applications: The development and fabrication of NCG replica membranes have been carried out in the Optical Sciences Division at NRL. We are currently investi-
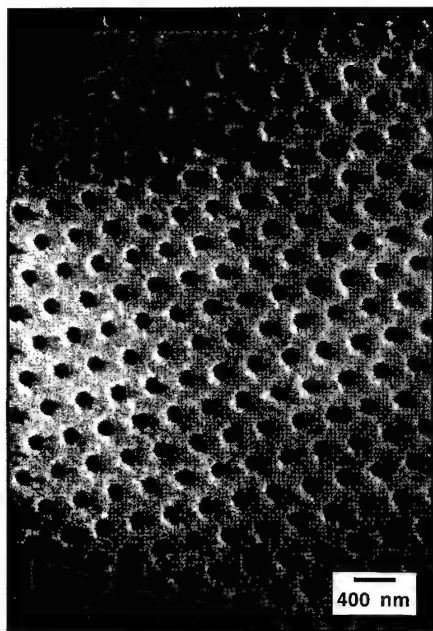
Fig. 5 — Scanning electron microscopy micrograph of a platinum NCG replica membrane with a thickness of 110 nm and voids 115 nm in diameter.

gating numerous patterning applications of NCG replica membranes involving materials growth, reactive-ion etching (RIE), and ion implantation in collaboration with NRL researchers through the Nanostructure Array Advanced Research Initiative begun in FY 95. This research is carried out by the Chemistry, Electronics Science and Technology, Materials Science and Technology, and Condensed Matter and Radiation Sciences Divisions at NRL. Work is also being carried out in conjunction with NRL's Nanoelectronics Processing Facility, the National Institute of Standards and Technology, and several universities including Caltech, the University of Illinois, and the University of Houston.

One of our ongoing studies involves the use of NCG replica membranes as deposition masks for the first-ever in-situ growth of submicron, laterally patterned metallic and semiconductor structures by molecular beam epitaxy (MBE). The use of NCG replica membranes that are compatible with the high-temperature, ultrahigh vacuum environments encountered in MBE provides an opportunity to prepare nanometer-scale structures in a single-step process with a potential reduction in growth defects. Other current studies involve the use of NCG replica membranes as

shadow masks to laterally pattern semiconductor materials and diamond on a nanometer scale by RIE and ion implantation. Patterned semiconductor materials provide an opportunity for optical and electronic studies of quantum-confinement effects. In addition, patterned diamond is potentially useful through enhanced thermal transfer properties in device applications.

[Sponsored by ONR and ARPA]

References

1. D.H. Pearson and R.J. Tonucci, "Nanochannel Glass Replica Membranes," *Science* **270**, 68 (1995).

2. R.J. Tonucci, B.L. Justus, A.J. Campillo, and C.E. Ford, "Nanochannel Array Glass," *Science* **258**, 783 (1992). ∎

Infrared Color Vision

D.A. Scribner, M.P. Satyshur, and M.R. Kruer
Optical Sciences Division

The development of infrared (IR) focal plane arrays [1] (IRFPA) and associated IRFPA sensors have led to a new generation of IR imaging systems for defense applications. However, the probability of detecting military targets in background clutter can be very poor, even when the sensor is performing near its ideal limit of sensitivity. The probability of detection is poorest when the contrast between the background and the target is low or when the target is partially obscured. Intuitively, it is expected that the use of information from multiple bands should improve performance. In human vision, color is sometimes as important as intensity or shape for overcoming the effects of camouflage. An infrared color vision system combines multiple bands and creates a composite color image in a manner such that all the information in each of the bands is contained in a single composite color image. In order to take advantage of the multidimensional color space that is created, algorithms need to be developed to enhance the color contrast between man-made objects and natural backgrounds and display these differences in a color scheme that is synergistic with that of the human eye-brain color processing system.

Approach: Initial investigations in this area have involved two basic efforts. First, composite IR color images have been generated from previously recorded multispectral data. Visualization was performed to analyze the general color phenomenology of the scene. Second, spatio-spectral matched filters were derived and used to perform processing based on form and color combined.

A three-band IR system with wide individual spectral bands is of special interest for several reasons. First, implementation of three bands on an IRFPA is conceivable in a staring mode. A multispectral IR system with a large number of narrow sub-bands (for example 10 or even 1000) could probably be implemented only as a scanning system. Compared to staring systems, scanning systems generally have very short integration times and, thus, lower sensitivity as well as being more mechanically complex and unreliable. Second, studies of human color vision in general have shown that three basis functions give near-optimum performance; that is, more than three bands add only marginal performance compared to a three-band system [2]. Finally, because the human observer's eye/brain cognitive system is essentially a three-band system, it would be a natural choice to transform multispectral IR images into a color display.

The starting approach was to construct a composite color image by normalizing and scaling each IR band to correspond to the red, green, and blue bands of a visible image. The normalizing and scaling can be done in either a global or local manner. A composite IR color image is formed using the three-band images. Computer visualization is achieved by assigning eight bits of color to the intensities of each band — red for LWIR, green for MWIR, and blue for SWIR. Combining these colors on a pixel-by-pixel basis creates a composite color image that can be immediately examined — all the information from the three bands is contained in the composite color image.

In an IR color vision system, an important performance concern is the amount of color contrast between the target and the background. If the three bands are highly correlated, the contrast enhancement can be performed to allow better target-background discrimination when viewing the display. In the visible color domain,

this would be equivalent to saying that all three color bands are highly correlated, resulting in a background that is comprised of nearly equal ratios of red, green, and blue. The image would then appear in various shades of grey. If the target color component were uncorrelated, then it would have a unique color. The degree of target-background correlation in the visible/IR spectral region is an area of ongoing study.

Performance: In order to make a quantitative comparison of target-background discrimination between single-band and composite color systems, multidimensional matched-filtering operations were performed. For the color images, a spatio-spectral matched filter (3-D) was derived. For the single-band case, a spatial-only filter (2-D) was derived. The derivation of the filters considered a generic aircraft target and the background statistics of specific scenes. In the case of the 3-D spatio-spectral filter, the third dimension was based on the spectral values.

Figure 6 shows two test images that were created using three bands each. The top image used three IR bands (SWIR, MWIR, and LWIR). The bottom image used three visible bands, roughly corresponding to the spectral response functions of the red, green, and blue cones of the human retina. One method of analyzing the target detection performance of the filtered results is to plot a receiver-operator curve (ROC) in which misdetections and false alarms are compiled and plotted for varying threshold settings. ROC curves are shown for both the visible and IR cases. For each spectral region, ROC curves are exhibited for three single-band results, as well as the composite color result. For the visible case, when the threshold is set for an equal number of misdetections and false alarms, the composite color results are over an order of magnitude better than any of the single band results. For the IR case, the composite color results are over two orders of magnitude better than the single bands results.

References

1. D.A. Scribner, M.R. Kruer, and J.M. Killiany, "Infrared Focal Plane Array Technology," *IEEE Proc.* **79**, 66 (1961).
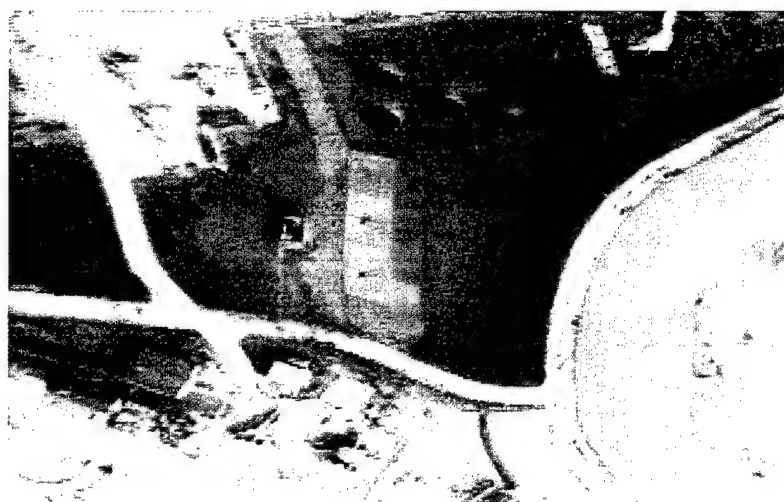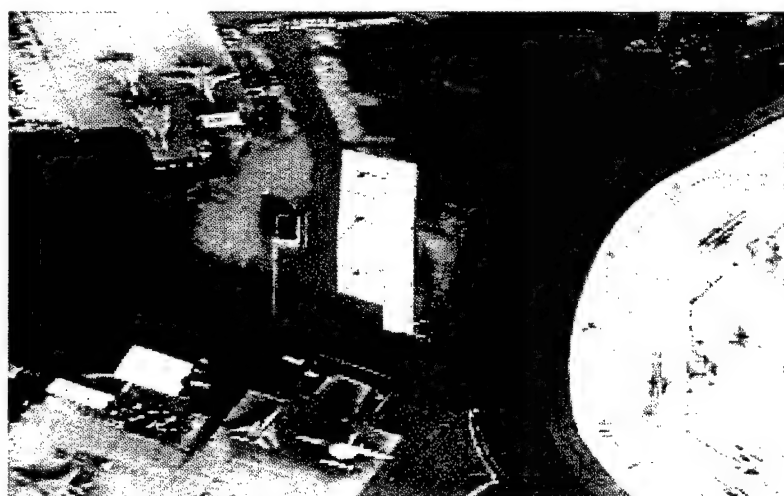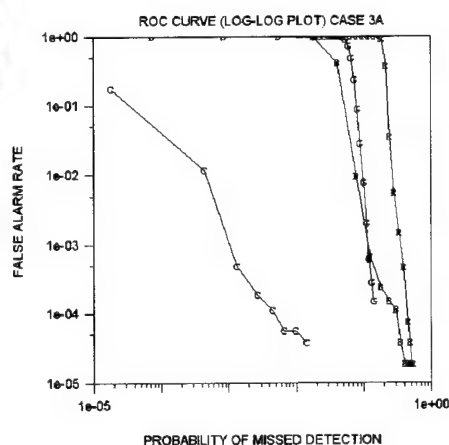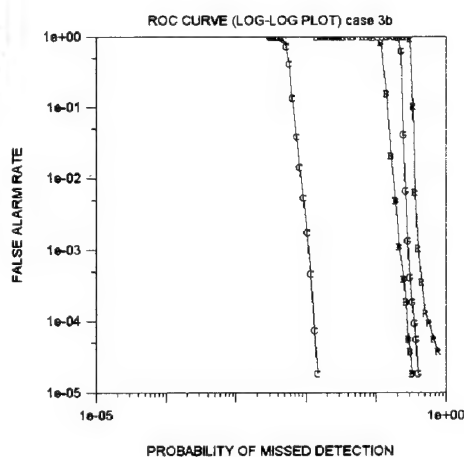
Fig. 6 — Left side, test images; right side, ROC curves: (a) three-color IR image and (b) visible image.

2. J.L. Dannemiller, "Spectral Reflectance of Natural Objects: How Many Basis Functions are Necessary?" *J. Opt. Soc. Am. A* **9**, 507 (1992). ∎

Fiber Bragg Grating Laser Sensors

A.D. Kersey and K.P. Koo
Optical Sciences Division

Substantial progress has been made since the pioneering work from NRL in 1977 [1] to use optical fiber for sensing acoustic fields. Today, optical fiber sensors can be used to detect a variety of parameters such as temperature, magnetic field, electrical field, acoustic field, rotation, displacement, and many others [2]. With the introduction of fabrication techniques that allow Bragg gratings to be written directly in the core of optical fiber, new types of intrinsic fiber-optical sensors are emerging. Recently, passive fiber Bragg grating sensors have become the focus of many smart structure systems development. These fiber Bragg grating devices are attractive

due to their small size (on the order of 1 cm), their ease of fabrication, the potential for affordable mass production, and relatively high sensitivity. Another area associated with the in-line fiber Bragg grating is the emergence of active fiber Bragg grating devices such as fiber Bragg grating laser sensors. The fiber Bragg grating laser sensors offer many attractive features, including small size, more power per bandwidth than passive grating sensors, single frequency lasing capability, remote optical pumping (remote activation), remote interrogation, and ultrahigh sensitivity.

Operation Principle: In sensings parameters using the fiber laser sensor approach, the sensed parameter is encoded onto the emission wavelength of a single frequency fiber laser via a parameter-induced optical path length change in the fiber laser cavity. In our system, minute changes in the laser wavelength are detected with ultrahigh resolution using a read-out, two-arm interferometer with an optical path difference [3] that is large compared to the laser cavity length. This read-out interferometer transposes the wavelength shift to relatively large phase shifts, which can easily be detected.

Sensor Description: Figure 7 is a schematic of a single-frequency fiber Bragg grating laser sensor system. The fiber laser is made up of a short piece of Erbium-doped fiber with two fiber Bragg gratings written directly in the Erbium fiber. For single frequency operation, the laser cavity defined by the two Bragg gratings is chosen to be approximately 2.5-cm long. The Erbium fiber forms the active medium and can be optical pumped by a laser operating at either the wavelength of 980 nm or 1480 nm, using a wavelength selective coupler. When the pump power is strong enough to achieve lasing threshold, the Erbium fiber laser will lase at the wavelength determined by the Bragg grating wavelength of the fiber grating. The laser output is extracted from the return port of the wavelength selective coupler. Measurand fields that cause a strain or an optical path length change in the fiber laser cavity will induce a wavelength shift at the laser output. Because of the long coherence length of this type of fiber laser, a two-arm fiber read-out interferometer with a large optical path difference (OPD) on the order of 100 m can be used. The ratio of the OPD of the read-out interferometer to the laser cavity length effectively enhances the detectability of small frequency or wavelength
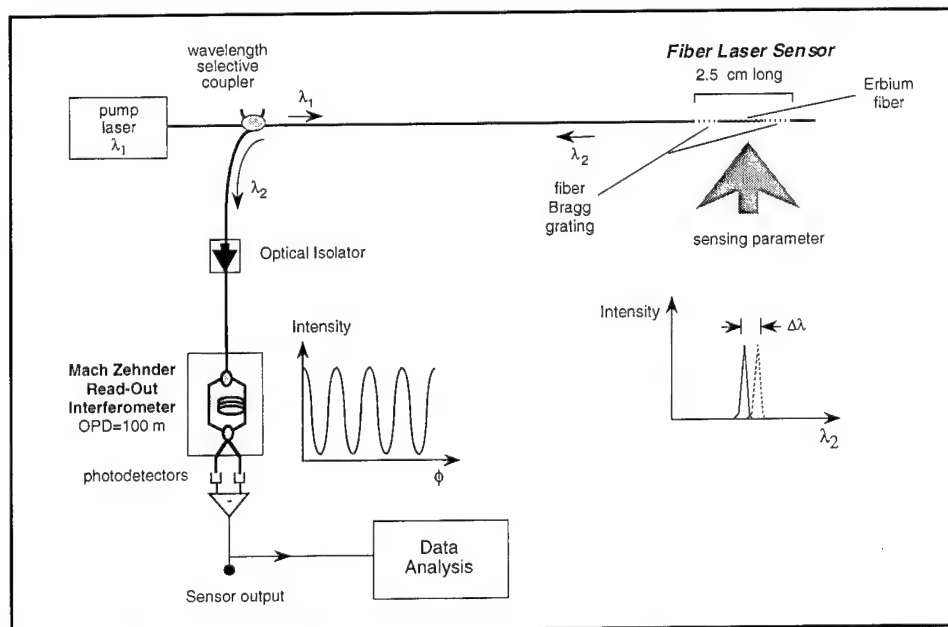
Fig. 7 — Fiber Bragg grating-based laser arrangement with interferometric readout.

Single-Mode FBG Laser Sensor

(L_{FL}=2.5 cm, phase gain=1920)

Read-out Interferometer Phase (Rad. RMS) / **Laser Cavity RMS Strain**

BW=18.7 Hz

Test Signal

Phase res.=26 μRad RMS/$\sqrt{Hz}$

(strain res.=5.6×10^{-14} RMS/$\sqrt{Hz}$)

Frequency   (kHz)
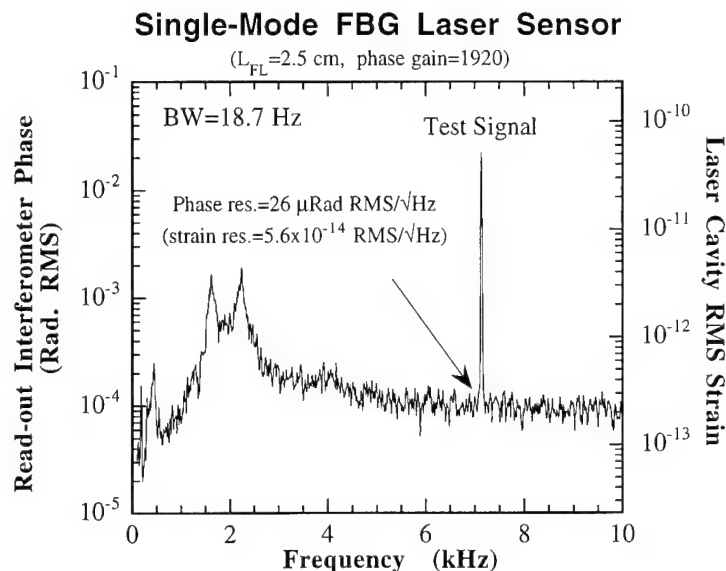
Fig. 8 — Dynamic strain sensitivity over the 0 to 10 kHz range.

changes in the fiber laser sensor output. Ultrahigh strain resolution on the order of $10^{-14}/\sqrt{HZ}$ for dynamic strains at frequencies greater than 3 kHz have been demonstrated in our laboratory [3] (Fig. 8). This kind of resolution is limited by thermally induced fluctuations of the fiber laser cavity length.

Applications: Using the approach described here, fiber laser sensors can serve as compact sensor heads with high performance commensurate to more traditional but less-compact interferometric optical fiber sensors that use much longer lengths of sensing fiber. In addition, fiber laser sensors are readily adaptable to wavelength multiplexing [3] for the integration of an array of these sensors for multipoint sensing in system applications. Furthermore, a given sensor array can be configured to sense different types of parameters by incorporating the proper trans-

ducer onto the different laser cavity fibers. Research related to various applications of this compact, high-sensitivity fiber laser sensor are currently being evaluated.

References

1. J.A. Bucaro, H.D. Dardy, and E. Carome, "Fiber Optic Hydrophone," *J. Acoust. Soc. Amer.* **62**, 1302-1304 (1977).

2. For example, *Fiber Optic Sensors*, Eric Udd, ed. (John Wiley & Sons, Inc., New York, 1991).

3. K.P. Koo and A.D. Kersy, "Bragg Grating-based Laser Sensors Systems with Interferometric Interrogation and Wavelength Division Multiplexing," *J. Lightwave Technol.* **13**, 1243-1249 (1995).   ∎

Remote Sensing

Radar Imaging of Underwater Sand Dunes

T.F. Donato, F. Askari, C.L. Trump, and
G.O. Marmorino
Remote Sensing Division

Introduction: Understanding the variability of shallow water bathymetry is critically important to commercial, environmental, and military interests. Traditional bathymetric surveys are often expensive, time consuming, and do not accurately resolve the topography in a dynamic littoral environment. Imaging radars, such as real aperture radar (RAR) and synthetic aperture radar (SAR), under certain environmental conditions, can provide an extensive, rapid, and cost-effective description of shallow submarine topography. Underwater sand dunes (sand waves) are among the features imaged by these radars. We note that bathymetric features are not imaged directly by radars. Instead, the imaging mechanism involves the interaction of topography with the overlying flow which perturbs the surface current. In turn, surface current perturbations induce variations in the surface wave-field through wave-current interactions. It is these variations in the wind-generated surface wave field that appear as intensity modulations in radar imagery. However, the ability to image submarine topography is limited by surface current velocity and the wind speed. Previous studies suggest that sand waves and other bottom-related features are observed in radar imagery at current speeds greater than 0.5 m/s^{-1} and at wind speeds between 3 and 12 m/s^{-1} [1,2].

In this study, we show that sand wave signatures appear in RAR imagery under low current and wind speeds and when the water column is strongly stratified. Furthermore, we show that contrary to past studies, the radar modulations lead the sand wave crest by as much as 150 m. We attribute this to hydrodynamic effects associated with strong stratification.

Methods and Results: RAR imagery and shipboard data were collected during an investigation of submesoscale oceanographic phenomena off Cape Hatteras, North Carolina. This is a region subjected to strong stratification and where historical bathymetry does not adequately resolve small-scale bottom features. To compare the radar imagery with bathymetry, we developed a novel method for extracting bottom profile data from a shipboard acoustic Doppler current profiler (ADCP). The extracted information yielded sand wave height, length, and orientation.

Currents measured just prior to the RAR observations indicated northeastward flow at 30 cm/s^{-1}. Hydrographic measurements showed salinity differences of 7 psu and density differences of 3.3 kg/m^{-3} between 2 and 15 m. This shows the presence of a relatively fresh water lens overlying a saltier, denser water mass. Winds were light and less than 5 m/s^{-1}, from the southwest.

Sand wave signatures appear as groups of bright east-west trending features in the radar data (Fig. 1). These features are approximately 5 km in length and spaced about 250 m apart. Red line segments, overlain on the image, indicate the position and orientation of the sand wave crests resolved in the ADCP data. Immediately apparent is the fact that the signatures in the RAR image are parallel to but offset from the sand wave crest. A detailed comparison between the RAR imagery and ADCP bottom profile (Fig. 2) shows that the peaks in the RAR modulations lead the sand wave crests by 135 m (the mapping uncertainty is 35 m). Also, the peak modulations, emphasized by the shading, remain stationary while others progress consistently northward. (These latter signals depict a front that was repeatedly sampled by a second research ship).

Summary: In this study, we have demonstrated that a georeferenced time-series of radar images can distinguish between stationary and dynamically evolving submesocale features, such as sand waves and fronts. We showed the utility of radar in mapping the general location and the aerial extent of a sand wave field in continental shelf waters. Previous studies have demonstrated that, under highly idealized conditions, the peak radar intensity is well correlated with the sand wave height and slope. Furthermore, past research has shown that in moderately strong tidal flow and in the absence of stratification, the peak radar modulation occurs either directly over the sand wave crest or to its lee. However, we have shown that there can be spatial differences of several tens of meters between the radar modulations and the location of the sand wave crest. A plausible explanation for this spatial separation
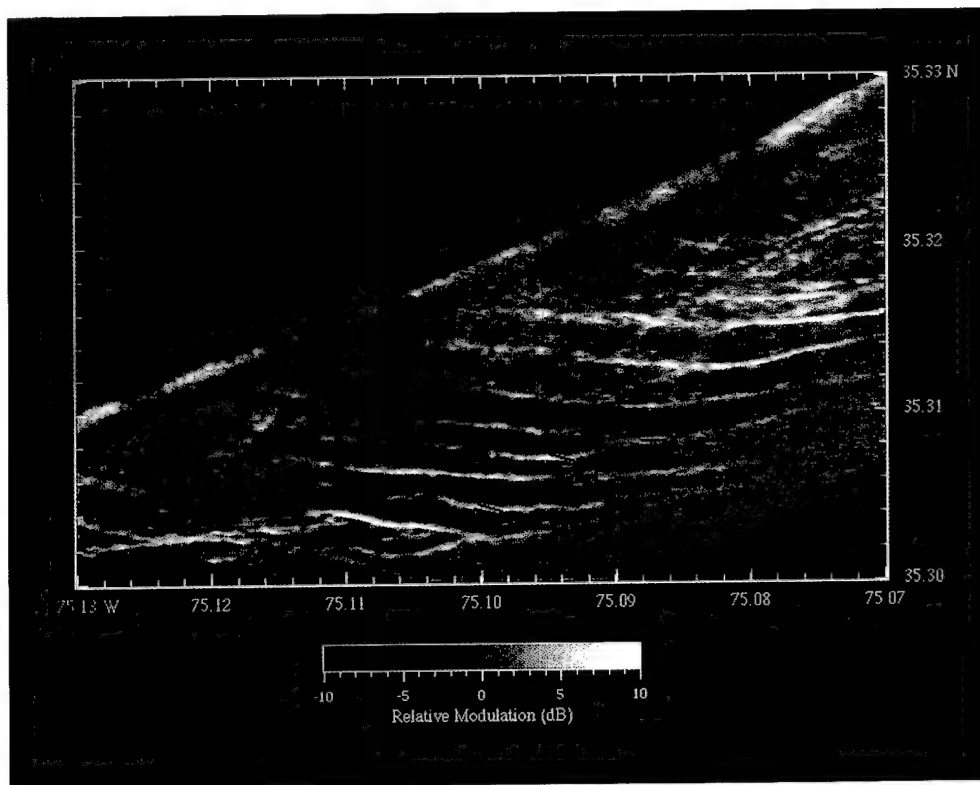
Fig. 1 — This is an example of a radar image depicting sand waves. The sand waves appear as bright linear features. The red line segments denote the position and orientation of sand wave crests as extracted from shipboard ADCP data. This image was taken from a RAR flown aboard one of NRL's P-3 aircraft on 18 June 1993.
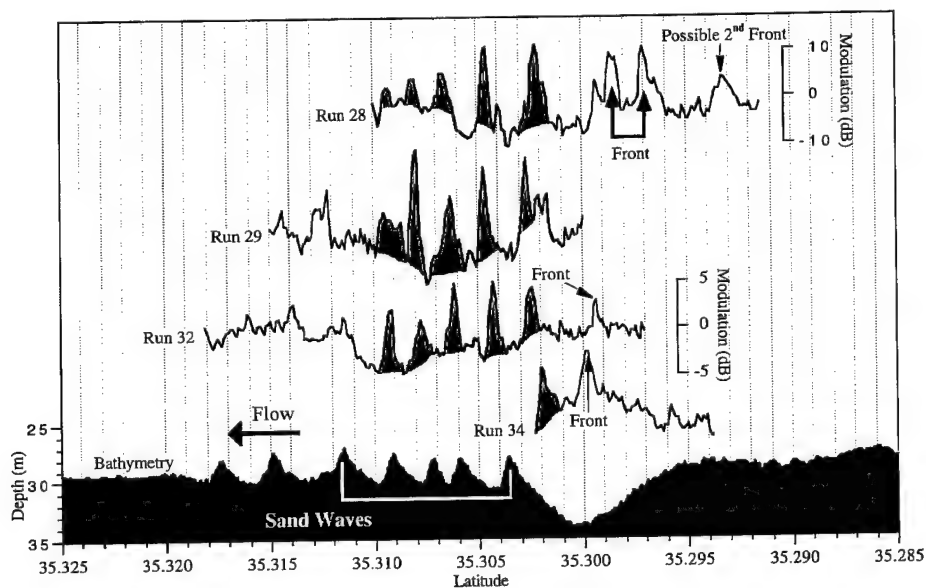
Fig. 2 — A comparison of radar modulation and ADCP bottom profile for four RAR passes. A latitude cut centered at 75.10° W, corresponding with the ADCP tract, was extracted from each pass. The shaded regions in the RAR profiles and the white bracket in the ADCP profile emphasize a section used for detailed analysis.

is the complex interaction between topography and stratified flow. Additional research is required on the interaction of stratified flow with complex topography and the surface wave field before quantitative information, such as sand wave height and slope, can be derived from radar imagery. Simulation studies are planned to investigate these interactions.

References

1. W. Alpers and I. Hennings, "A Theory of the Imaging Mechanism of Underwater Bottom Topography by Real and Synthetic Aperture Radar," *J. Geophys. Res.* **89**, 10,529-10,546 (1984).

2. J. Vogelzang, G.J. Wensink, G.P. DeLoor, H.C. Peters, and H. Pouwels, "Sea Bottom Topography with X-band SLAR: The Relation Between Radar Imagery and Bathymetry." *Int. J. Remote Sens.* **10**, 1943-1958 (1992). ∎

Hydrodynamic and Radar Modeling of Ocean Currents

R.W. Jansen, S.R. Chubb, and C.Y. Shen
Remote Sensing Division

Introduction: Inferring ocean currents and associated ocean properties from radar measurements are long-standing problems of considerable interest to the Navy. Because microwaves cannot directly probe the subsurface, many aspects of the ocean-current/radar relationship are still poorly understood. To gain a better understanding of this problem, NRL and ONR have cosponsored the High-Resolution Remote Sensing Advanced Research Initiative. Through this program, two field experiments involving in-situ current/ oceanographic measurements and radar data collection have been conducted. Here an "end-to-end" approach [1] that incorporates subsurface and surface hydrodynamics, wave-surface current interaction, and radar backscatter modeling is used to investigate a particularly strong line-shaped radar signature that was observed by real aperture radar over a Gulf Stream boundary region during the first experiment [2]. This is the first time such an "end-to-end" approach has been applied to study the relationship between subsurface currents and radar signatures.

Subsurface Hydrodynamics: The long, line-shaped signature is shown by in-situ measurements to coincide with a surface current convergence or "Rip" at the Gulf Stream/Shelf-water boundary. This convergence front is formed when denser, more saline Gulf Stream water intrudes onto the Shelf, subducts under and flows opposite to the lighter, fresher shelf water. The effect is modeled numerically by using a rigid-lid, 2-D solution of the Navier Stokes hydrodynamic equations for a current/density boundary on a flat shelf. Figure 3 shows the vertical configuration of the density boundary after about an hour of evolution (top) and the formation (bottom), consistent with observation, of a sharp current Rip (where V varies from light to dark blue at zero depth). Additionally, the modeling reveals subsurface wavelike structures and that the influence of the Coriolis force on the along-front current (not shown) significantly increases the rate of frontal formation.

Surface Waves: Since the radar image is essentially a reflectivity map of the ocean surface waves, adequate treatment of the surface-wave characteristics is an integral requirement of the radar modeling. A statistical distribution of surface waves in the vicinity of the Rip was generated using a spectral wave propagation model. The input parameters to the model are the surface currents (taken from the subsurface hydrodynamics model) and surface winds (from shipboard measurements). As the waves propagate over the converging currents at the Rip edge (Gulf Stream/ Shelf-water boundary), their wavelengths and directions are altered as a result of the advective and refractive effects of wave-current interaction. The surface-wave model shows a buildup of 1- to 3-m waves to the north of the Rip and a shift to the north in the propagation direction. The bright line in the radar image is a direct consequence of this shift in the wave distribution.
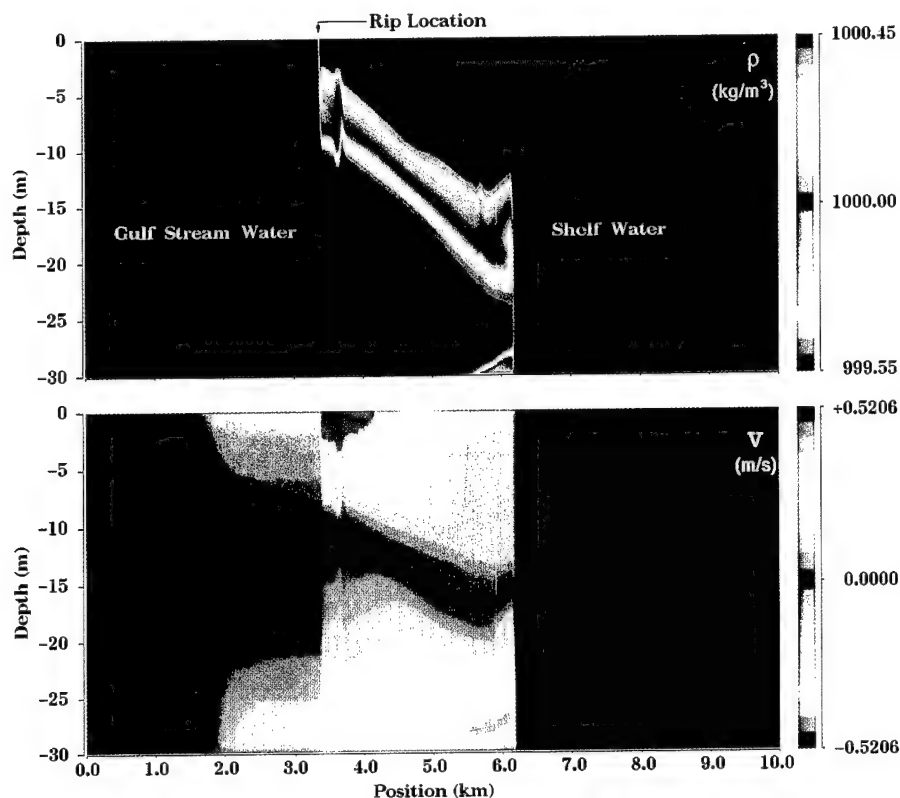
Fig. 3 — Simulated subsurface density ρ (top) and horizontal current component V (bottom) normal to the Rip-surface convergence front. (Provided by T. Evans)

Radar Modeling: Radar cross-section (RCS) is derived from a model that includes (1) mirrorlike (spectral) reflections from ocean wave facets perpendicular to the radar transmission direction, (2) Bragg-like coherent reflections from adjacent sinusoidal centimeter-scale waves that ride on larger waves, and (3) reflections from breaking waves. Figure 4 shows plots of the simulated RCS (bottom panel) that include (solid line) and do not include (dashed line) the effects of wave breaking and (in the top panel) the dominant surface current component that is responsible for the convergence (and down-welling) that leads to the radar signature as a function of position perpendicular to the location of the Rip. As seen from the figure, the position of the signature occurs directly above the location of the strong current convergence associated with the Rip. The magnitude is in good agreement with the experiment only when wave-breaking is included. Our predictions demonstrate the importance of including scattering from breaking waves, which is often neglected in radar modeling.

Summary: By using an end-to-end approach incorporating subsurface and surface hydrodynamics and surface backscattering models, we have predicted the current dynamics and radar signatures associated with a Gulf Stream/Shelf-water convergence front. The hydrodynamics of the subsurface currents were modeled numerically and provide results that are in good agreement with available current and other in situ measurements, including estimates of the width of the resulting convergence, density profiles, and strain rates. Using the surface currents from these hydrodynamic calculations, we have modeled wave spectra and used them as input to our radar backscattering models. These calculations show good agreement for the magnitude and width of the radar signature but only when wave-breaking effects are included.
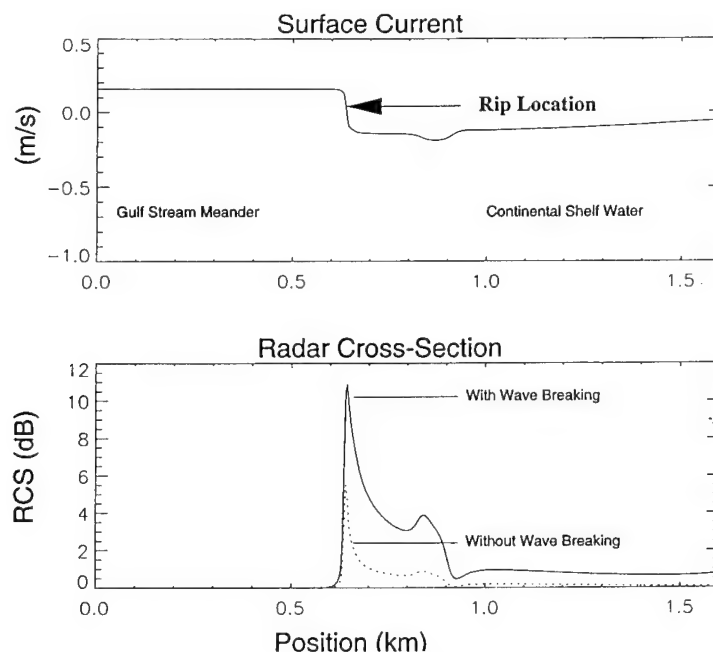
Surface Current

Fig. 4 — Surface current (top) and predicted HH-X-Band radar signatures with and without wave-breaking contributions (bottom) across the front.

References

1. R.W. Jansen, C.Y. Shen, S.R. Chubb, A.L. Cooper, and T.E. Evans, "Subsurface, Surface, and Radar Modeling of a Convergence Front," submitted to *J. Geophys. Res.* (1995).

2. R.P. Mied, F. Askari, G.O. Marmorino, G.R. Valenzuela, and D.B. Trizna, "High-Resolution Remote Sensing," *1992 NRL Review*, Naval Research Laboratory, Washington, D.C., pp. 181-183. ∎

Measurement of Nearshore Dynamics Using Video

K.T. Holland and J.C. Church
Marine Geosciences Division

Traditionally, the study of nearshore dynamics (water depths < 10 m) under natural conditions has been accomplished through the placement of costly instrumentation at a discrete number of locations. This approach becomes prohibitively expensive in the study of certain surf and swash zone processes, such as the development of longshore bars and beach cusps because these features can evolve either gradually or catastrophically. Recently, our ability to measure beach and nearshore processes over a wide range of spatial scales (centimeters to kilometers) and time periods (seconds to years) has been greatly enhanced through innovative techniques that use video imagery. Advantages of using video image processing in nearshore research include sampling of a broad variety of visible processes at low cost, having the instrumentation removed from the flow field to allow measurement during extreme conditions (for example, hurricanes), and the potential for modifying the original sampling design following image acquisition. Here we describe several physical processes and bathymetric features that are measurable using video techniques.

Video Imagery: The basis of video image processing is similar to that of aerial photogrammetry or satellite remote sensing in that the light intensity (illuminance) of individual picture elements (pixels) within a camera view can be quantified, with the extension that temporal variations in pixel intensity (up to 30 Hz) can be digitally sampled as a near continuous sequence of images. Such temporal variability in pixel brightness results from differential reflection
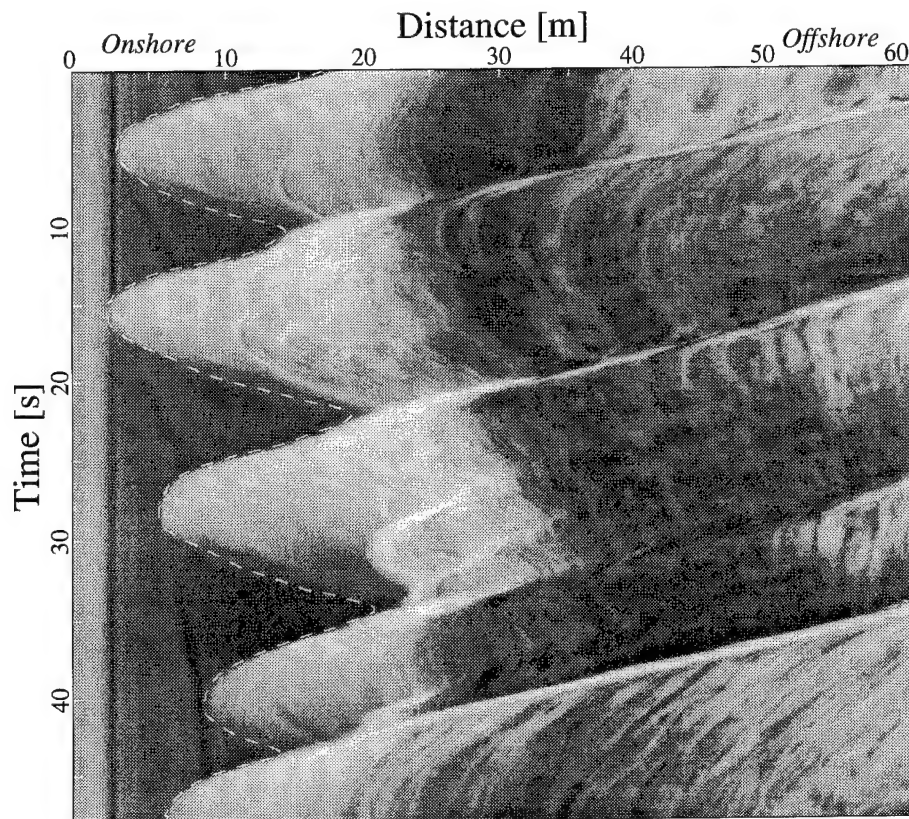
Fig. 5 — Timestack of swash motion showing temporal (down the page) and spatial (across the page) variations in pixel intensity. The cross-shore motion of the water's edge (swash) is indicated by the dashed line. The intensity patterns seaward of the swash edge represent fluid dynamics at greater depths. For example, the slope (Δdistance/Δtime) of the obliquely trending, approximately linear features indicates that the speed of advancing bores is approximately 5 m/s.

over wave surfaces or from foam patterns produced during wave breaking and can be correlated to geophysical processes using the geometric relationship between real-world and pixel coordinates. Numerous applications using this scheme have been developed [1]; an example of the relationship between pixels and processes is shown in Fig. 5.

Nearshore Bathymetry: One of the more useful applications of video imagery involves the estimation of nearshore bathymetry and shoreline topography. For instance, Fig. 6 shows an image constructed by time-averaging the intensity patterns of breaking waves to reveal surf zone bathymetric features. In this example, the association between intensity and morphology results because wave breaking is typically depth dependent; therefore, on average, shallow fea-

tures (such as sand bars and shorelines) appear brighter. These features, evident in time-exposure images, have shown good correspondence with the underlying bathymetry [2], making this technique useful in littoral warfare applications by providing remotely sensed bathymetry information.

While a single, 2-D image is not sufficient alone to profile long-shore, cross-shore, and elevation information, the use of multiple video images from different perspectives permits the recovery of the three-dimensionality of a region. We have developed a fully automated, trinocular (three-view) stereo technique for estimating foreshore topography to an accuracy of approximately 1 cm [3]. Although computationally intensive and limited to fairly small (for example, 10 × 10 m) regions, this technique provides nearly continuous, densely-spaced estimates of beach elevation

Fig. 6 — Ten-min time exposure image of swash and inner-surf-zone intensity patterns at Camp Pendleton. Lighter regions indicate preferential breaking over submerged sand bars and at the shoreline. The darker circular patterns close to shore are depressions of approximately 10-m width and 0.8-m depth.

while simultaneously capturing the forcing due to wave motions. We are using the information provided by the stereo and time-exposure techniques in describing the statistical stability of near-shore morphology and in the development of models of swash zone sediment transport.

Surf-Zone/Mine Interactions: An application involving the use of video-image processing that pertains to a specific Navy need is documentation of the behavior of lightweight antitank mines within the surf and swash zones on sandy beaches. As part of a pilot experiment conducted at Camp Pendleton, California, video measurements of mine motions and wave processes were made. These mines were extremely mobile, with typical cross-shore excursions (linked to large swash motions) on the order of 5 m every few seconds (Fig. 7). Alongshore mine movements appear related to the longshore current, with the largest transports occurring during oblique wave approach. Understanding of such migration behavior is expected to lead to exploitable information affecting mine-countermeasures doctrine.
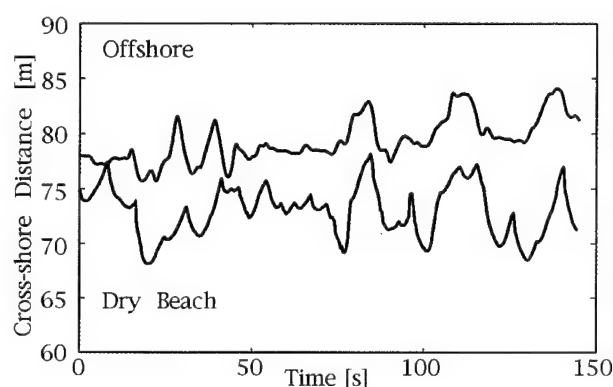
Fig. 7 — Cross-shore mine (blue) and swash (red) motions from the Camp Pendleton experiment. Note the strong correlation between offshore mine movement and large rundown excursions.

From these few examples, one can see how video techniques allow the quantification and comparison of both fluid and morphological processes that could not be as easily sampled using traditional instrumentation. We intend to further use video-image processing to address these and other Navy interests in future research.

[Sponsored by ONR]

References

1. R.A. Holman, A.H. Sallenger, Jr., T.C. Lippmann and J.W. Haines, "The Application of Video-Image Processing to the Study of Nearshore Processes," *Oceanogr.* **6**, 78-85 (1993).

2. T.C. Lippmann and R.A. Holman, "Quantification of Sand-Bar Morphology: A Video Technique Based on Wave Dissipation," *J. Geophys. Res.* **94**, 995-1011 (1989).

3. K.T. Holland and R.A. Holman, "Video Estimation of Fore-shore Topography Using Trinocular Stereo," *J. Coastal Res.* **12**, (1996).   ■

Simulation, Computing, and Modeling

A Hybrid Virtual Environment Interface to C³I Information

R.P. Darken, T.A. Hill, and B.T. Solan
Tactical Electronic Warfare Division

Since the end of World War II and the introduction of the widespread use of radar, sonar, infrared sensors, and other electronic surveillance systems, the task of information processing for military command and control operations has become excessively complex. A primary bottleneck in this scenario is in the use of traditional techniques for visualization and interaction with C³I information. This type of information gathered from the 3-D world is visualized on 2-D displays requiring conscious interpretation by the operator to reconstruct an accurate image of the physical world. Humans are 3-D spatial beings who operate most effectively in 3-D space. The Effectiveness of Naval Electronic Warfare Systems (ENEWS) Program, a part of NRL's Tactical Electronic Warfare Division, is investigating the use of virtual environment technology to provide a more efficient and natural interface between command and control operators and the information on which the success of their mission depends. The approach involves a hybrid interface, merging a top-down maplike view with an immersive, head-coupled display.

Implementation: The hybrid interface has been constructed as an extension to an existing naval simulation system. The ENEWS Program has long been involved in the modeling and simulation community developing systems specializing in electronic warfare (EW) simulation. The cornerstone of this effort is the Interactive Scenario Builder. Builder provides extensive capabilities in electromagnetic simulation and visualization, including a full range of emitter characteristics and scan patterns. It can be used to visualize communication links, networks, spherical-Earth platform motion, and satellite modeling. Builder can show coverage areas that take into account the effects of propagation, terrain masking, jamming, and target characteristics.

The hybrid workstation consists of a map display that is shown on a 40-in. diagonal CRT monitor turned on its back (like a table) and an immersive display, shown in a Fakespace, Inc. BOOM3C™ head-coupled display and tracker

(Fig. 1). The two displays are controlled by different computers operating on a single network and communicating via the distributed interactive simulation (DIS) protocol (Fig. 2). There is also a one-way, special-purpose socket, allowing display parameters selected on the map display to be communicated to the immersive display. The immersive display places the user within the simulated environment. The user is not actually an active participant in the scenario but is able to move about the environment freely without restrictions from the simulation. The position of the viewpoint in the immersive display is communicated to the map display, which presents it as if it were another entity in the simulation. In the example in Fig. 2, the left image shows a typical view of the map display while the right image shows the corresponding immersive view associated with the map display. The yellow triangular symbol on the map display shows that the immersive display viewpoint is looking toward a nearby ship. The immersive display shows the actual ship as it is seen from that perspective.

Fig. 1 — The hybrid immersive/nonimmersive workstation shown with multiple simultaneous users.

Both the map and immersive displays contain the visualization capabilities of Builder. However, those techniques best suited to a global top-down view are shown on the map display while other
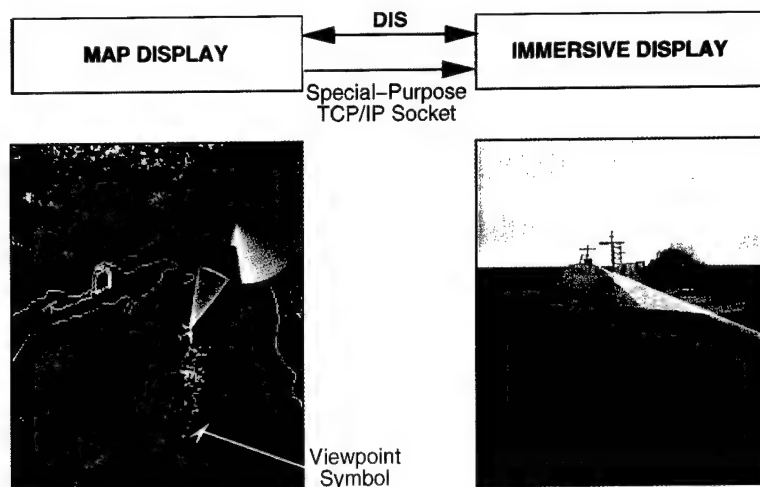
Fig. 2 — The system architecture showing a typical view on the map display and its corresponding view in the immersive display.

techniques requiring a spatial component are shown in the immersive display. The immersive display example in Fig. 2 shows a radar emitter from the ship as a yellow conical beam. Similarly, the aircraft in the map display view shows a 2-D representation of an active radar emitter. The red region on the map display represents a radar coverage volume.

The operator can switch between displays at will. From the map display, an operator can reposition the viewpoint of the immersive display to a specific location of interest. Platforms can be followed by attaching the viewpoint to the platform symbol on the map view. A platform can be visually marked on the map, making it highly visible from a distance in the immersive display. This is done using a flashing column over the platform's location. The scale of the platform models can also be increased to simplify searching tasks.

The hybrid workstation was specifically designed to be usable both by a single user and by a small group of users. If used by a group, any one user can view the immersive display without interrupting the other users. A small external monitor is often used to show the other members of the group what the BOOM operator is seeing. In its single-user mode, the hybrid workstation can be specially configured for navigational purposes. The map display can be centered on the viewpoint marker so that it is always in the center of the screen facing forward. When using the immersive display, the user needs only to glance at the map to determine the absolute position immediately, as well as relative information, such as "What is to my left?".

Operational Implications: In its multiuser mode, the hybrid workstation is a powerful, tactical mission planner and evaluation tool. It retains the best features of traditional map displays while adding the ability to view the spatial components of any part of the environment. As a single-user system, the hybrid workstation could be developed toward an enhanced shipboard tactical display, allowing easy access to spatial information without inhibiting performance on time-critical threat recognition and response tasks.

Future Research: The hybrid workstation is currently in its early stages of research. Much remains undetermined as to how specific information should be visualized and interacted with. The strengths of this approach lie in the seamless nature of the two displays and the ease with which they can be manipulated. However, functionality is currently limited by the interface. We would like to move toward a hand-operated metaphor, much like a touch screen, to operate the map.

An alternative to the BOOM as the immersive display would be lightweight eye-worn goggles with adjustable see-through capability. When this technology becomes available, the immersive display will be available immediately. It will be activated by darkening the lenses and projecting the graphics and will be removed by the reverse procedure. These improvements will greatly increase the practicality of the workstation as a viable operational tool.

[Sponsored by NAVAIR] ∎

Virtual Firefighting

P.A. Tatem
Chemistry Division

D.L. Tate
Information Technology Division

Since World War II, significant technical advances in shipboard firefighting have included the development and deployment of new materials and devices to be used on the scene by damage control/firefighting personnel, such as Aqueous Film-Forming Foam (AFFF), the Naval Firefighter's Thermal Imager (NFTI), and HALON 1301. More recently, the Damage Control System has been under development to integrate communications among all the ship's systems for simultaneous containment and recovery from damage by improving the damage control capability to fight through damage. However, there is room for more innovation in the techniques that the Navy uses to actively and passively protect its platforms against fire and train its personnel.

Readiness is receiving increased focus by emphasizing better preparation through cost-effective training and virtual rather than real danger in training. Environmental issues and constraints are constantly being raised and are becoming severely restrictive. The government is placing higher constraints on insult to the environment and restricting the smoke and water additive release into the atmosphere. The mechanisms for training Navy firefighting personnel have become increasingly difficult and expensive.

An emerging technology—virtual reality—can be used as a means for damage control training without costly live fires. In this application, a human operator can be immersed in a realistic but virtual environment to develop damage control skills without safety and environmental concerns. This technology has been used significantly in training applications for agencies such as NASA and the Department of the Army. It differs from conventional interactive computer simulation found in training simulators in that a virtual environment creates a much stronger illusion of actually being there and being able to interact and generate change. An environment, including a virtual fire, could be created with interactive capabilities to which firefighters can respond and react through optimized sensors attached to the firefighter's suit. Virtual environment (VE) training can bridge the gap very effectively between the classroom and the live trainer. VE can provide the opportunity in individual and team training for exposure to unlimited fires, to study the fire physics of each, and to evaluate the damage control options that can be taken.

Identifying Key Technologies: The Damage Control/Firefighting into the 21st Century Workshop [1] was held at the Naval Research Laboratory in June 1994 to identify all technologies that could make an impact on innovative damage control concepts and systems, specifically firefighting, so the Navy can move out smartly in the 21st century. The key technologies identified were: (a) Fire simulation: What are our current capabilities and limitations? What modeling approach should be taken to adequately describe the fire physics? (b) Computing capability: What hardware/software approaches should be taken to achieve the speed and detail required? (c) Display capability: How should the issues of imagery, object resolution, tracking, and hypermedia integration (video, still, simulations, audio) be resolved to achieve the desired operator/training effects? (d) Virtual reality: What are the human factors and sensors issues that must be resolved to achieve a state of immersion that is as effective for training as real life? How successful have other applications of virtual reality been in other training environments? Based on issues raised in the workshop, an initial effort was undertaken to assess the effectiveness of using immersive VE as a tool for firefighter training and mission rehearsal in firefighting exercises aboard the ex-USS *Shadwell*, NRL's full-scale fire-research ship, located in Mobile Bay, Alabama.

Virtual Environment Feasibility Tests: Feasibility tests of the use of VE for firefighter training were performed aboard the ex-USS *Shadwell* during September 18-22, 1995 [2]. The objectives of these tests were to demonstrate and measure the effectiveness of VE training and mission rehearsal on the navigation and firefighting performance of trained firefighters in unfamiliar ship's spaces. The tests were performed in areas aboard the ex-USS *Shadwell* that had been modeled in VE with simulated smoke and fire. The tests were performed under realistic conditions with real shipboard fires, using Navy firefighting teams.

The feasibility test comprised two phases. Phase 1 was a navigation task in which the participant's task was to traverse a specified path through the ex-USS *Shadwell* while wearing a firefighter's mask with a special faceplate that simulates a smoke-filled environment. Phase 1 required the traversal of three decks, four doors, three passageways, two inclined ladders, and one compartment, with eight possible wrong turns, to achieve a single goal—covering an approximate distance of 80 ft. Phase 2 required the participant to locate and retrieve specific firefighting equipment and lead the firefighting team to extinguish a real shipboard fire. Phase 2 required traversal of two decks, two passageways, one inclined ladder, three compartments, four doors, with nine possible wrong turns, to achieve three goals—for an approximate distance of 70 ft.

Twelve enlisted personnel participated—eight men and four women from the USS *Inchon* and the USS *Puget Sound*. All firefighters were either fire-team or team-leader qualified, but none was familiar with the ex-USS *Shadwell*. The test participants were divided into a traditional training group and a VE training group, with the two groups having the same number of males and females. Both groups were given mission briefings to inform them of their assigned task followed by time to plan their mission using a written mission statement and ship's drawings. The traditional training group then performed their tasks aboard the ex-USS *Shadwell*, and performance measurements were taken and evaluated.

After their mission briefing and mission planning time, the VE training group used VE to familiarize themselves with the layout of the ship and to rehearse their assigned tasks with and without simulated smoke and fire. Figure 3 is a view of the ex-USS *Shadwell*'s VE showing the fire test area with simulated fire and smoke. After completion of their VE training, the VE training group then performed their tasks aboard the ex-USS *Shadwell*, and performance measurements were taken and evaluated. The performance measurements that were (1) collected during both phases of the tests were the time to complete the task and (2) the number of wrong turns taken while performing the task.

Findings: Preliminary results show that there was a measurable improvement in the performance of firefighters that used VE training over
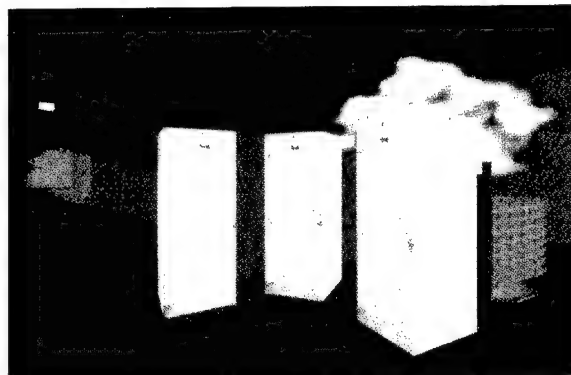
Fig. 3 — A view of the ex-USS *Shadwell*'s virtual environment.

firefighters without VE training in both phases of the tests. In the Phase 1 (navigation) test, the VE training group was an average of 30 s faster over a 2-min run. In addition, all members of the traditional training group made at least one wrong turn, while only one VE training group member made any wrong turns. In Phase 2 (the firefighting test), the majority of the participants in the traditional training group made wrong turns, but no one in the VE training group did. Timing data were recorded in Phase 2, but individual differences in team leadership style and differences in the actions of the firefighting team made those timing measurements inconclusive.

In addition to the quantifiable results obtained during the tests, participants expressed their increased confidence in performing their tasks because of the familiarization of the spaces and situation awareness that they received through VE. Most members of the VE training group used the VE to actively investigate the scene and plan their strategies so that during the fire, they were able to concentrate on fighting the fire instead of finding their way through unfamiliar spaces.

The preliminary results show that virtual environments can be effectively used for training and mission rehearsal for shipboard firefighting. VE provides a flexible environment where a firefighter can learn an unfamiliar part of the ship and practice tactics and procedures for fighting a fire by interacting with simulated smoke and fire without risking life or property.

Remaining Challenges: To achieve the long-term goal of creating a virtual fire in shipboard

VE for firefighter training, there are remaining technological challenges that must be addressed in fire simulation and sensor development, as well as VE. To generate the required sense of realism, computing capability and resolution for a fire/smoke spread model must be improved to assure that the immersion experience effectively transfers to real life. In addition, manual intervention for firefighting tactics must be included, such as active manipulation of ventilation systems for desmoking or active suppression with extinguishers/suppression systems. The requirements for the sensor suite for the firefighter suit in the training environment have not been defined. Questions remain as to how to make the trainer "feel" the hostile environment created by the fire but not be harmed by it. Work is currently being performed under a Small Business Innovative Research effort to investigate the requirements for firefighter sensors to create the realism desired for VE training.

[Sponsored by ONR and OPNAV]

References

1. P.A. Tatem, "Proceedings on the Damage Control/Firefighting into the 21st Century Workshop," NRL Memorandum Report 6180–94-7643, Dec. 21, 1994.

2. D.L. Tate, L. Sibert, F.W. Williams, T. King, and D.H. Hewitt, "Virtual Environment Firefighting/Ship Familiarization Feasibility Tests Aboard the Ex-USS *Shadwell*," NRL Letter Report 6180/0672A.1, Oct. 17, 1995.   ∎

Ultrasonic Tomography of Solids Using Parallel Processing

R.S. Schechter and R.B. Mignogna
Materials Science and Technology Division

P.P. Delsanto
Politecnico di Torino, 10129 Torino, Italy

Using ultrasonic waves, reconstruction of different material properties and their spatial distribution inside solids may be accomplished. Current ultrasonic tomography methods do not properly handle cases involving refraction, mode conversion, scattering, and finite apertures. (These effects are absent with X-ray-based tomography, where the energy travels in straight lines.) To account for these different effects, we have developed a method using a very efficient code to model elastic wave propagation on a massively parallel computer. The wave propagation approach permits improved tomographic reconstructions in cases having large changes in the refractive index ($> 10\%$), where traditional ray-tracing approaches, based on the geometrical acoustics approximation, become numerically unstable. The entire tomography computation required is immense but is feasible because the code is highly parallel and implemented on a parallel supercomputer.

Tomography Algorithms: There are two classes of tomographic reconstruction techniques. One class is based on Fourier transforms and includes such methods as the filtered back-projection and others. These methods are fast but have the restriction that the data be acquired on evenly spaced sets of straight ray paths, called projections.

A second method employs an iterative procedure to reconstruct an image. Iterative techniques are less efficient than transform-based methods, however they have several advantages. They can be used with irregular sampling geometries and may incorporate ray-bending at each iteration.

There are other methods to correct for weak scattering occurring in media in which the velocity changes are small, such as soft biologic tissues. These techniques fall into the category of diffraction tomography and involve using a first-order Born or Rytov approximation in the standard back-projection technique.

Wave Propagation Simulation Approach: The method presented here is intended for specimens with large velocity changes in their interiors ($> 10\%$), commonly encountered in solids in nondestructive evaluation. Using our recently developed local interaction approach (LISA) [1,2], which accurately models sharp interfaces between materials of different physical properties, the processes of radiation from a finite aperture, propagation, and scattering are modeled in detail. In these simulations, all elastic wave effects are captured, including mode conversion. In addition,

we have developed a novel method of using the wave propagation code to determine the path of the first arrival acoustic energy from a receiver back to the source by using the vector field along the wave front [3]. These computed ray paths are used in an iterative tomography algorithm called the algebraic reconstruction technique, or ART. Embedding a forward numerical simulation inside an inverse algorithm allows the faithful modeling of the physics of propagation and scattering needed in ultrasonic tomography.

Simulated Inclusion Case: A simulated case of an 8.45-mm diameter inclusion embedded in a 16.3-mm square piece of plexiglas is considered first. The inclusion has the same density as plexiglas but with the Lamé constants λ and μ being twice those of plexiglas, to give a longitudinal velocity about 40% higher than plexiglas (2.67 mm/μs in the plexiglas and 3.78 mm/μs in the inclusion). This represents a large velocity change—introducing strong refraction and scattering—not handled by other techniques.

Figure 4(a) shows a "snapshot," gray-scale image of the amplitude of the entire displacement field at 3.7 μs into the simulation, obtained from a forward run with the specimen known

beforehand. The leading edge—or in this case, longitudinal wavefront—is used to trace the first arrival acoustic energy through the specimen. The first arrival ray paths, along with the positions of the longitudinal wavefront computed for a source position at the center of one edge of the specimen, are shown in Fig. 4(b). The ray paths are curved near the source because of the finite aperture near the edge of the inclusion due to scattering and inside the inclusion due to refraction. There are 31 such source positions along each side and 63 receivers (not shown).

The resulting velocity tomogram has 31 $\times$ 31 tomography cells (defined by the sources) and is shown in Fig. 5(a). The image shows a well-resolved circular scatterer. Figure 5(b) shows the same tomogram as a surface. In Fig. 5(c), a cut through the center of the tomogram is shown along with the ideal cut, or true profile of the velocity field. The computed profile comes close to the ideal profile, only slightly underestimating the velocity of the inclusion. A second case, identical to the previous one, is done except that now the ray paths are computed for every iteration instead of being known beforehand. The resulting tomograms in Figs. 6(a) and 6(b) show a less spatially resolved scatterer. The computed profile (Fig. 6(c)) is not nearly as square as in Fig. 5(c).
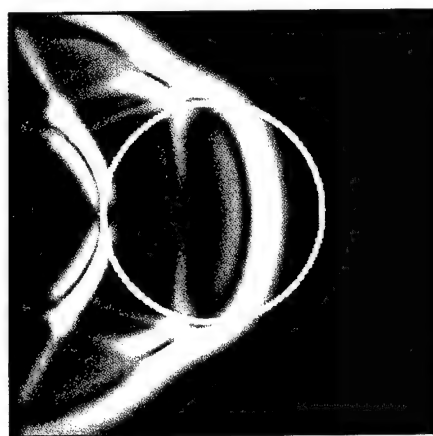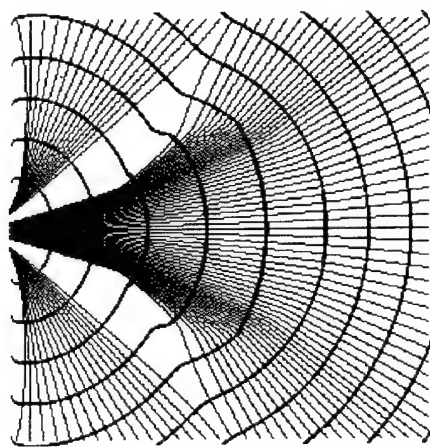
(a)   (b)

Fig. 4 — Snapshot (a) of displacement wavefield after 275 time steps for circular inclusion case and (b) ray-path reconstruction for a source located at center of left edge of specimen.
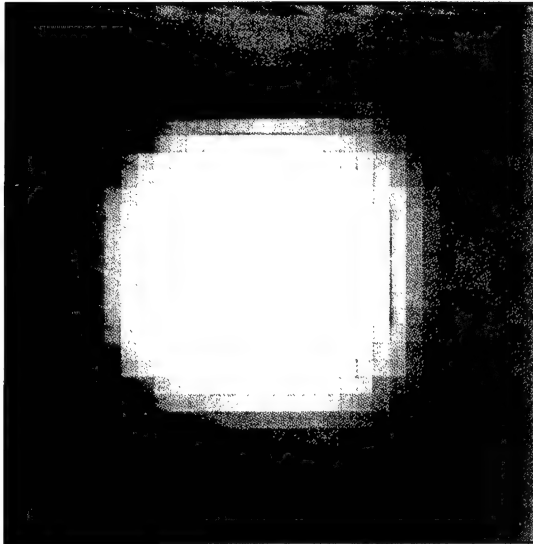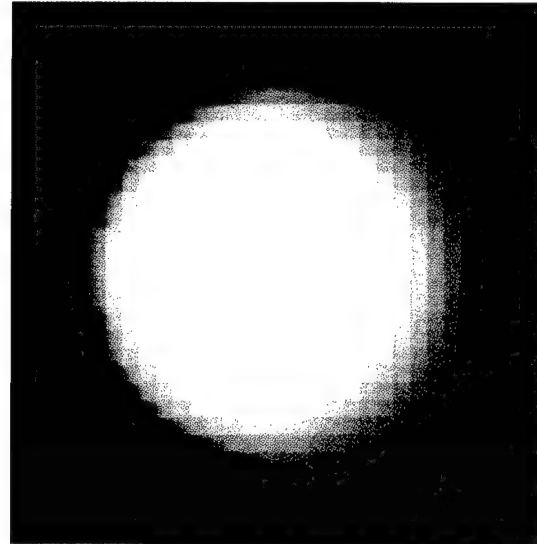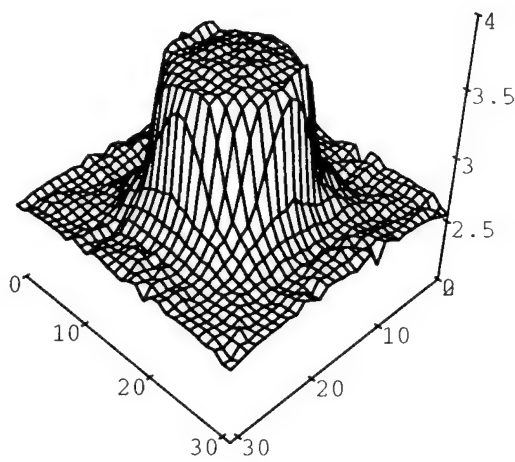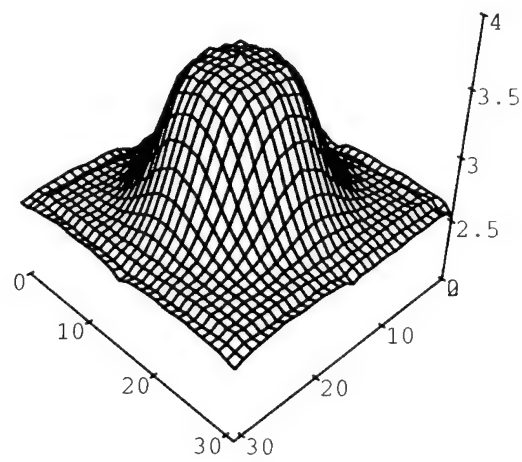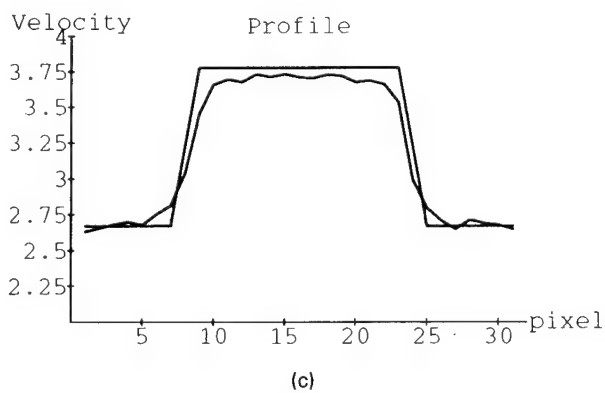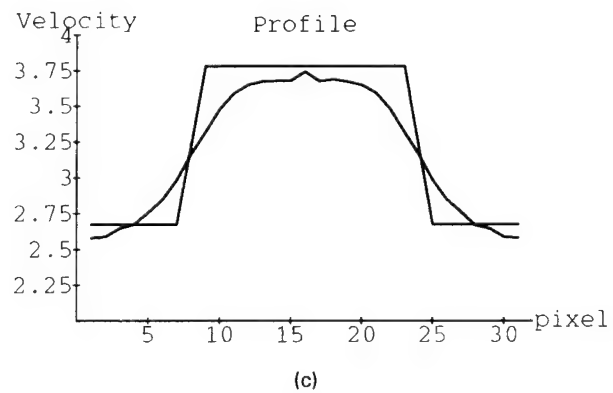
Fig. 5 — Tomogram (a) using known ray-paths for circular inclusion case; (b) shown as surface; and (c) cut through tomogram compared with ideal profile.

Fig. 6 — Tomogram (a) using ray-paths computed at each iteration for circular inclusion case; (b) shown as surface; and (c) cut through tomogram compared with ideal profile.

187
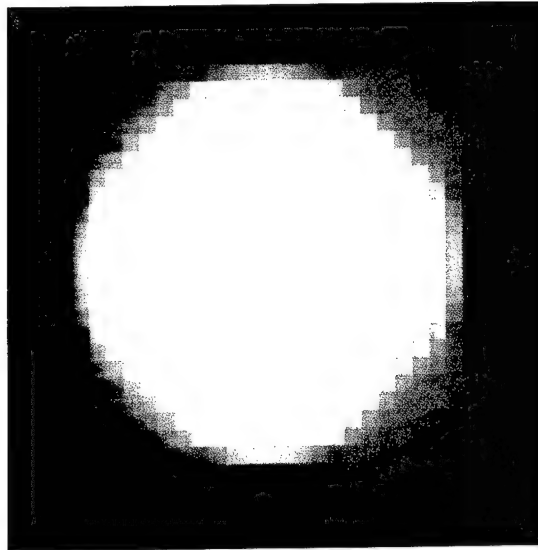
(a)
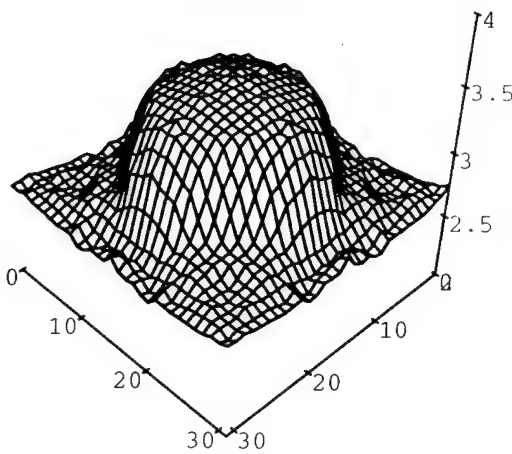
(b)
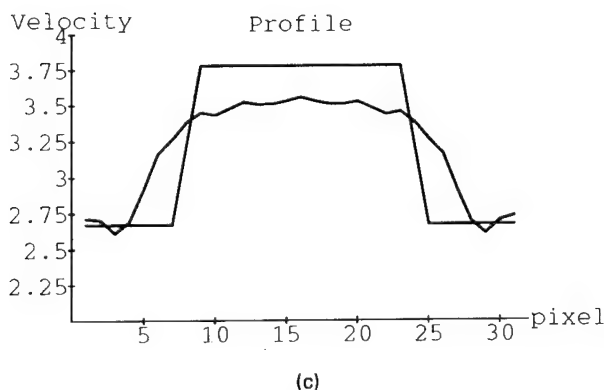
(c)

Fig. 7 — Tomogram (a) using straight ray-paths for circular inclusion case; (b) shown as surface; and (c) cut through tomogram compared with ideal profile.

The computation to obtain Fig. 6 is enormous compared to Fig. 5 since the forward computation needs to be run 124 times (number of sources) for 800 time steps on a 256×256 nodepoint grid, for 8 iterations. This amounts to 52-billion gridpoint updates for the displacement field. In addition, 64,494 rays are traced back and used in the ART algorithm. This entire procedure uses about 1 h of CP time on a 256-processor node CM-5.

Figure 7(a) shows a tomogram assuming straight ray paths. The tomogram appears greatly distorted or smeared out. The surface is shown in Fig. 7(b), and a cut is shown in Fig. 7(c). The tomogram greatly underestimates the velocity since ART is using ray paths that are too short in the interior of the inclusion. Since the assumed rays passing near the edge of the inclusion go through the wrong cells, the tomogram appears spread out.

Other tomographic reconstructions have been simulated using voids, irregular shaped scatterers, and multiple scatterers. Higher resolutions have been used to obtain sharper tomograms. These are not shown here.

[Sponsored by ONR]

References

1. P.P. Delsanto, R.S. Schechter, H.H. Chaskelis, R.B. Mignogna, and R. Kline, "Connection Machine Simulation of Ultrasonic Wave Propagation in Materials II: The Two-Dimensional Case," *Wave Motion* **20**, 295-314 (1994).
2. R.S. Schechter, H.H. Chaskelis, R.B. Mignogna, and P.P. Delsanto, "Real-time Parallel Computation and Visualization of Ultrasonic Pulses in Solids," *Science* **265**, 1188-1192 (1994).
3. R.S. Schechter, R.B. Mignogna, and P.P. Delsanto, "Ultrasonic Tomography Based on Wave Propagation Simulations by Parallel Processing," submitted for publication in the *J. Acoust. Soc. Am.*, 1995. ∎

Laboratory Simulations of the Coupling of Blast Waves into Solid Materials

C.K. Manka, J. Grun, and H.R. Burris
Plasma Physics Division

With the current ban/moratorium on all testing of nuclear weapons and expectations that this

will not eliminate the threat of nuclear weapons, the only means to continue the development of predictive capabilities for nuclear weapons effects are analyses of prior nuclear test data, scalable laboratory experiments, and computer simulations.

Miniature Explosions: Laser-produced millimeter-scale explosions have an energy-to-mass ratio similar to nuclear explosions, which are on a scale of many meters and produce X-rays that can simulate X-ray loading of the surface. Explosions and the accompanying blast waves are produced when NRL's PHAROS III high-energy, short-pulse laser [1] is focused to a small spot on a thin piece of solid material. The material rapidly expands from the initial spot and blast wave pressures equivalent to nuclear explosions are produced within a few millimeters of the explosion. This expanding blast wave then impacts any solid material placed close to the initial spot, simulating the impact of a nuclear blast wave with the ground. The amount and spectrum of X-ray energy reaching the "ground" in a laser experiment can be varied by changing the target material (source), the ambient gas or gas density, and the distance (height of burst) from the "ground" to the explosion point.

Objective: The research effort, designed to simulate the energy coupling to ground material in nuclear explosions, consisted of a series of laser-induced explosions of aluminized mylar above blocks of polymethyl methacrylate (PMMA), a transparent polymer. Use of a transparent material to simulate the ground allowed the shock wave to be followed as it propagated through the ground. A major goal of this work was to perform a well-characterized experiment, including source and materials, that could be modeled by existing sophisticated computer codes. Comparison of code predictions with experimental results will benchmark the validity of those codes and provide a measure of confidence in the code's predictive capabilities. A second goal was to create a set of laboratory-scaled data over a large parameter range and obtain fits to scaling laws that had been derived from actual nuclear tests or large-scale chemical explosions.

Approach: Dark-field (Schlieren) shadowgraphy [2] was used to image the sharp density gradients that characterize the shock front. The PHAROS III four-probe system, shown schematically in Fig. 8, was designed to allow optical probing of shock fronts propagating through a transparent solid at four different times after impact of the blast wave from a single explosion. Thus, measurement of shock position and calculations of shock velocity and shock pressure would not depend on shot-to-shot reproducibility.
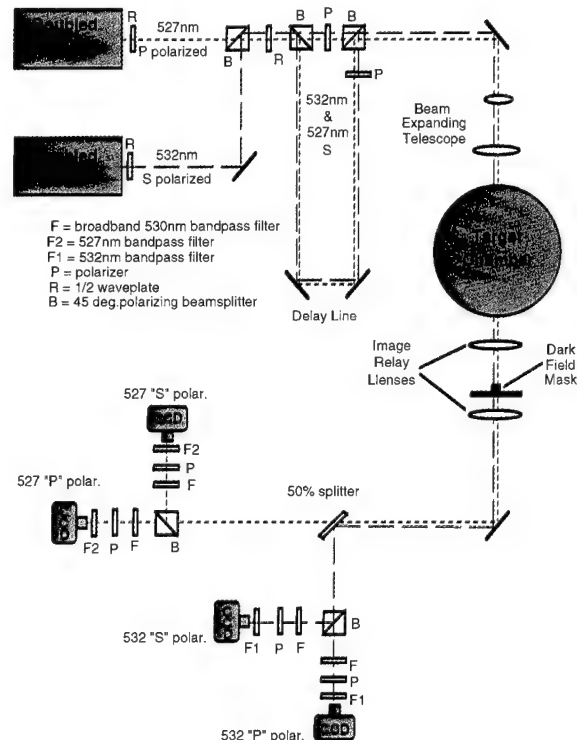
Fig. 8 — The dark field shadowgraphy diagnostic.

This was accomplished using the two orthogonal polarization components of each of two lasers — one Nd:Glass and the other Nd:YAG — operating at the frequency-doubled wavelengths of 527 nm and 532 nm, respectively. The analysis techniques being used required the probing wavelengths to have a common optical axis and have wavelengths within a few nanometers of each other. The time, after blast-wave impact, at which each probe laser emitted a short (0.5 ns) light pulse could be controlled electronically while the time at which each laser's polarization state (S or P) arrived in the test chamber was controlled by adjusting the optical path length it traveled. Thus, the two polarized light pulses from each of the two wavelengths allowed probing at four different times on the same shot.
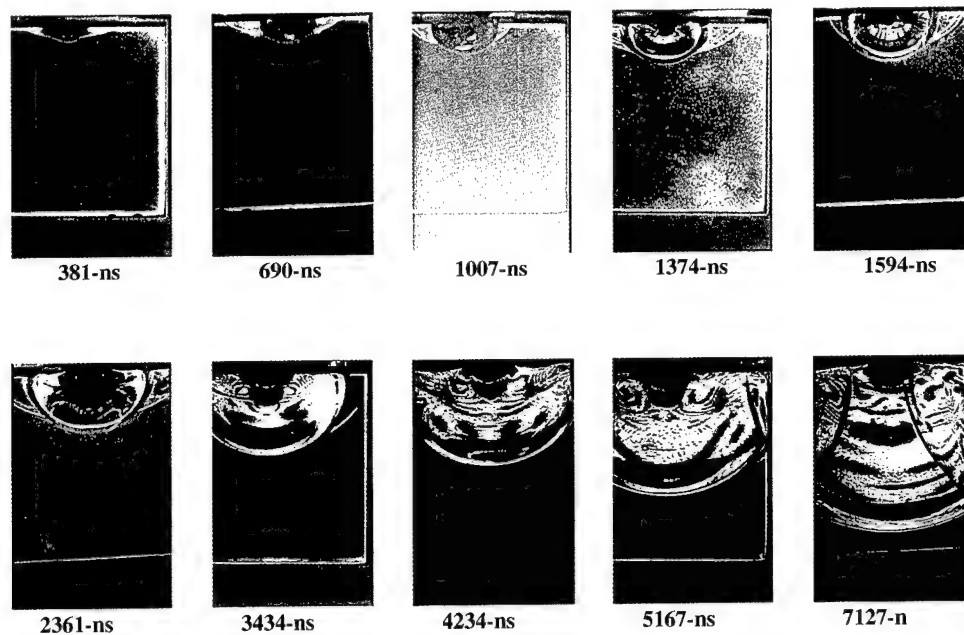
Fig. 9 — Composite of images from several nearly identical shots. PMMA cuve is 1 in. × 1 in.
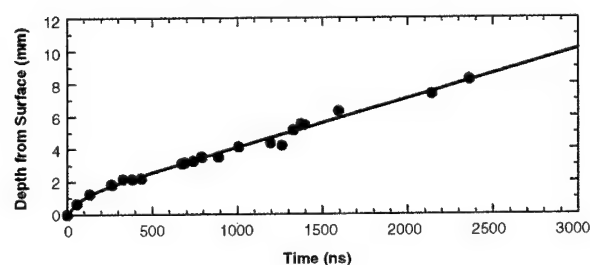
(a)
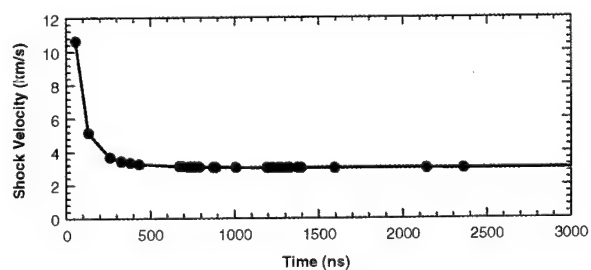
(b)
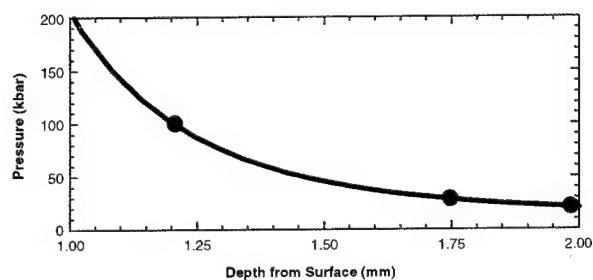
(c)

Fig. 10 — Shock position vs (a) time, (b) velocity, and (c) calculated pressure vs depth from the shock velocity and equation of state.

Images of Blast Waves: A composite of a series of several nearly identical experimental shots illustrates the progress of the shock front (Fig. 9) through the 1-in. PMMA block. Surface interaction, crater formation, and a number of reflected shock fronts are also observed. The main shock front's position, as a function of time, is measured from such an experimental series. An empirical curve fit to the position vs time data is obtained, differentiated to obtain shock velocity vs time, and shock pressure vs time is then calculated using the material's equation of state and the velocities determined from the experiment. Figure 10 shows the position, velocity, and pressure results.

Summary: The multiframe optical-probing technique has been demonstrated to accurately document the propagation of energetic shock waves into transparent materials. These data pro-

vide the foundation for the benchmarking of sophisticated, predictive computer models of nuclear blast waves. Additionally, this work demonstrates a method for calibrating newly developed, ultrafast pressure probes which, in turn, will be able to document the propagation of energetic shock waves into opaque materials such as soils, rocks, and complicated structures or geologic features.

References

1. J.M. McMahon, R.P. Burns, T.H. DeRieux, R.A. Hunsicker, and R.H. Lehmberg, *IEEE J. Quantum Electron.* **QE-17**, 1629 (1981).
2. J.A. Stamper, E.A. McLean, S.P. Obenschain, and B.H. Ripin, "Concepts and Illustrations of Optical Probing Diagnostics for Laser-Produced Plasmas," *Fast Electrical and Optical Measurements*, p. 691, (NATO ASI Series E109, Martinus Nijhoff Publishers, 1986), p. 691. ∎

Observed and Simulated Intraseasonal Circulation Anomalies

C.A. Reynolds and R. Gelaro
Marine Meteorology Division

T. Murphree
Naval Postgraduate School

Observations have shown that there are significant atmospheric circulation anomalies on intraseasonal time scales (20 to 70 days). Previous studies indicate that these circulation anomalies can have a significant impact on medium-range weather forecasting. The ability of the Navy Operational Global Atmospheric Prediction System (NOGAPS) to simulate the observed primary modes of intraseasonal variability in the Northern Hemisphere during boreal winter is examined. The NOGAPS data come from 9 winters of a 10-year integration of the model run at T47 resolution with observed time-varying sea surface temperatures. Atmospheric analyses prepared by the European Centre for Medium-range Weather Forecasts are used to represent observations.

To identify the primary modes of observed and simulated intraseasonal variability, we use rotated empirical orthogonal function (REOF) analysis. The observed and simulated upper-tropospheric zonal and meridional wind fields were first filtered to retain only variations with periods between 20 and 70 days. REOFs were then computed for the North Pacific and North Atlantic regions based on these filtered wind fields. Diagnostic tools such as time-lagged composite analyses and wave activity flux vectors [1] were used to examine the temporal evolution of these modes and their relationship to tropical and extratropical forcing. Diagnostic studies of this type help illuminate the basic mechanisms that force and guide these modes and provide important guidance for diagnosing model errors. One example is given here.

Jet-guided Wave Trains: The upper-tropospheric circulation anomalies associated with an east-west-oriented wave train propagating across the Pacific in the model simulation and observations are shown in Fig. 11. The wave trains appear similar to each other in the western Pacific. However, over the central and eastern Pacific, the observed wave train arcs equatorward and has significant amplitude in the subtropics, while the simulated wave train arcs poleward toward the Gulf of Alaska. These differences may account for the fact that the model is deficient in intraseasonal variability in the subtropical Pacific, yet has excess amounts of intraseasonal variability in the region south of Alaska. The REOFs representing these wave trains account for 18% and 16% of the observed and simulated variance in this region, respectively.

Figure 12 shows the corresponding wave-activity flux vectors for these modes superimposed on the time-mean upper-tropospheric zonal wind. The direction and length of the arrows indicate the direction and strength, respectively, of the stationary wave energy propagation associated with these modes. Over the western Pacific, the flux vectors (and wave trains) are aligned along the axis of maximum wind speed associated with the upper tropospheric jet and are bounded on either side by zones of strong meridional wind shear. In the observations, the

MODEL 200 mb CIRCULATION ANOMALY

OBSERVED 200 mb CIRCULATION ANOMALY
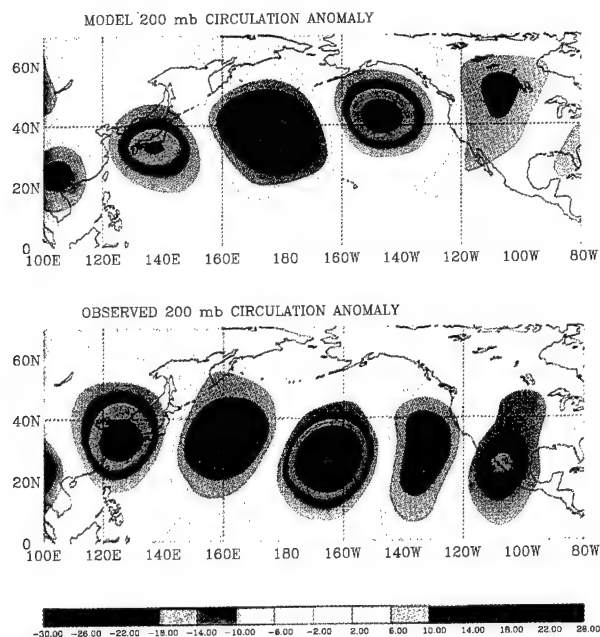
Fig. 11 — The upper-tropospheric circulation anomalies (that is, 200-mb streamfunction anomalies), representing an east-west-oriented wave train across the Pacific, for the model simulation (top) and observations (bottom). Blue colors represent cyclonic (counter-clockwise) anomalies and red colors represent anticyclonic (clockwise) anomalies. Contour interval is 4×10^6 m^2/s^{-1}.

MODEL 200 mb ZONAL WIND

OBSERVED 200 mb ZONAL WIND
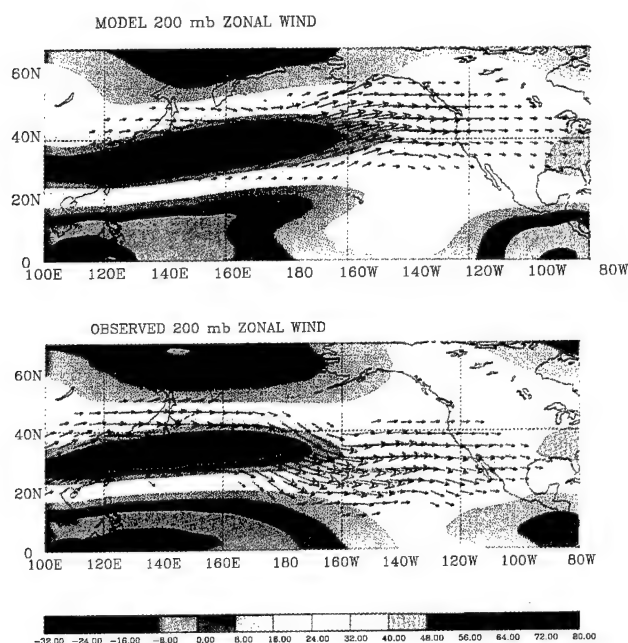
Fig. 12 — The wave activity flux vectors associated with the circulation anomalies shown in Fig. 11, superimposed on the time-mean upper-tropospheric zonal wind for the model simulation (top), and observations (bottom). Blue contours represent easterly winds. Contour interval is 8 m/s^{-1}. A vector length of 10 mm represents 140 m^2/s^{-2}.

meridional shear on the southern flank of the jet in the central Pacific (180°-160° W), along with the jet itself, are weaker than in the model simulation. Where the shear zone weakens, the observed wave train shows a strong equatorward component. In contrast, the simulated wave train shows eastward and poleward propagation as far as North America.

Implications for Forecasting: These results provide observational support for previous theoretical work, which suggests that shear zones along the flanks of jets act as regions of wave reflection because they are regions where the meridional gradient of vorticity vanishes [2]. These and other results not shown indicate that the model captures the basic mechanisms responsible for the generation and propagation of extratropically forced modes of variability. However, biases in the time-mean flow result in a misplacement of these intraseasonal modes. In the above example, this could result in an erroneous northward displacement of storms over the western U.S. in a medium-range forecast. Work in other NRL projects is aimed toward developing improved physical parameterization schemes for NOGAPS. These improvements will have a direct impact on the simulation of the time-mean circulation and should, in turn, allow for a more realistic simulation of the transient structures that directly affect our medium-range forecast skill.

References

1. G. Branstator, "Horizontal Energy Propagation in a Barotropic Atmosphere with Meridional and Zonal Structure," *J. Atmos. Sci.* **40**, 1689-1708 (1983).

2. R.A. Plumb, "On the Three-Dimensional Propagation of Stationary Waves." *J. Atmos. Sci.* **42**, 217-229 (1985). ∎

Space
Research
and
Satellite
Technology

The High-Temperature Superconducting Space Experiment II

T.G. Kawecki, G.E. Price, J.A. Golba, V.S. Rose
Space Systems Development Department

M. Nisenoff
Electronics Science and Technology Division

The HTSSE Program: Since the beginning of spacecraft development history, revolutionary increases in electronic device performance have led to significant increases in satellite performance. For more than 40 years, superconductivity has offered large performance gains for electronic circuits in terms of low noise, wide bandwidth, and low electrical power dissipation. However, prior to 1987, all known superconducting materials had to be cooled to temperatures below 23 K to enter the superconducting state. The complex, heavy, and electrical-power-demanding refrigeration equipment needed to realize these temperatures clearly was not suitable for satellite deployment. In 1987, Y-Ba-Cu-O-based high-T_c materials led to superconductor compounds with T_c's of 90 K or higher. In 1988, realizing the potentially significant benefits to future space systems that high temperature superconducting (HTS) electronics could offer and the attainable goal of providing a long-life, 77 K environment on spacecraft, NRL initiated the High Temperature Superconducting Space Experiment (HTSSE) program. The program goal of HTSSE is to provide a focal point for the industry, academia, and government HTS research and development communities to develop and demonstrate space-qualified HTS technology on a quick development schedule. The NRL HTSSE team consists of engineers and scientists from the Materials Science Division, Condensed Matter and Radiation Sciences Division, Electronics Science and Technology Division, and the Naval Center for Space Technology. A key aspect of HTSSE is that it leverages existing HTS work essentially by paying only for the integration and repackaging of existing devices developed by other potential users for space flight. The first payload developed by this program, HTSSE I, contained 15 simple HTS devices, which were predominantly passive microwave circuit devices cooled to 77 K by a British Aerospace Stirling cycle cryocooler. HTSSE I was launched in 1993.

HTS devices have evolved significantly from HTSSE I to HTSSE II by demonstrating higher device complexity, maturity, and functional capability in experiments that integrate HTS devices together or combine them with semiconductor devices. HTSSE II flight HTS experiments total eight in all and include the following device types: channelized receiver, cueing receiver, digital instantaneous frequency measurement unit, delay lines, rf multiplexer, a digital multiplexer, and a microwave channelizer. Microwave frequency ranges for these devices are in the C and X bands. In March of 1993, HTSSE II was manifested on the Air Force Space Test Program's Advanced Research and Global Observation Satellite (ARGOS), and the flight hardware design portion of HTSSE II began.

In addition to demonstrating HTS devices, an important goal of HTSSE is to develop and demonstrate the unproven critical cryogenic subsystems required to support HTS space systems. HTSSE II is built and awaiting integration on the ARGOS spacecraft in 1996, for a scheduled May 1997 launch.

The HTSSE II Design: The programmatic and design challenges of HTSSE II were significant. The development schedule for HTSSE II flight hardware was a short 20 months. The eight HTSSE II HTS experiments were developed concurrently with the HTSSE II flight system on which they would be mounted, allowing no room for experiment-interface errors. In some cases, the experiment originators had never built space-flight hardware and were unaware of space-flight hardware design and testing practices. There are few design precedents for the cryogenic subsystems required for HTS applications in space. The problems of interfacing a delicate cryocooler to a cryogenic payload and providing 30 thermally efficient cryogenic input/output rf coaxial transmission lines for the HTS experiments had challenging, and in many cases, conflicting requirements that had never been addressed before for long-duration space applications. Figure 1 shows the ARGOS spacecraft with HTSSE II installed and a larger exploded view of the exterior HTSSE II deck without blankets and with some structure removed for clarity.

The heart of the HTSSE II design is the cryogenic subsystem consisting of a central cold bus
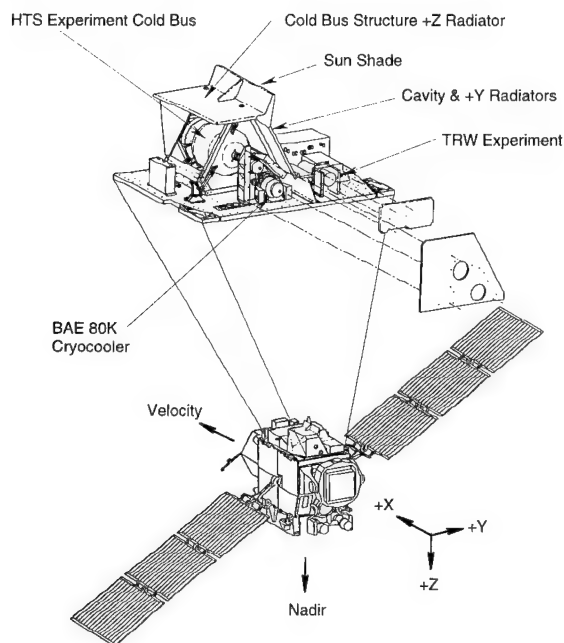
Fig. 1 — ARGOS host spacecraft, with detail of HTSSE II payload deck exploded for illustration.

with seven HTS experiments cooled by a Matra Marconi (formerly British Aerospace) 80 K Stirling cycle cryocooler at a constant 77 K temperature while on orbit. The Matra Marconi cryocooler has less than a 0.8 W of cooling capacity at 77 K, thus requiring a highly efficient cryogenic package. Figure 2 shows the 230-mm-diameter × 240-mm-long cryogenic cold bus and experiments.
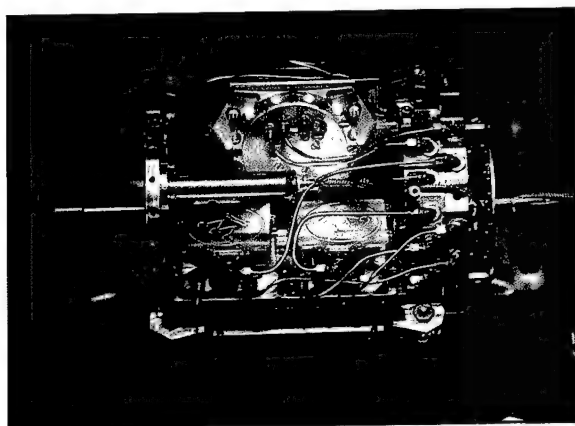
Fig. 2 — HTSSE II flight cryogenic cold bus prior to thermal close-out.

On-orbit measurements of the HTSSE experiments are performed with calibrated signals transmitted from an NRL ground-based facility. Transmissions are received, detected, processed, and stored for later down-link to a receiving site. Experiments are characterized using on-board parameter measurements equipment. Reference channels are used to establish relative received power at the spacecraft. On-board processors record time, pulse width, frequency, and amplitude of the received pulsed rf signals. The data are stored and dumped for subsequent ground-based data reduction and processing.

To characterize an experiment (mux, channelizer, etc.), a received pulse-modulated signal is amplified, and appropriate input levels are applied to the HTS experiment. Simultaneously, the same signal is applied to the reference channel. Both the experiment output and the reference signal are detected and processed (A/D converted), providing comparative measured amplitude outputs. Since the two excitations are from the same antenna and front-end hardware, the pulse amplitude difference in the two paths (HTS vs reference) generates a quantitative response measurement of the experiment.

HTSSE II Performance: The HTS devices of all the experiments worked well on the HTSSE II flight unit. The HTSSE II flight instrumentation measurement system performed very closely to rf industry-standard laboratory instrumentation (HP 8510 network analyzer) and with good repeatability. The performance of two HTSSE II HTS experiments are reported for illustration. The frequency response of the ComDev Multiplexer Experiment is shown in Fig. 3. This is a device with channel bandwidths of less than 1% and extremely selective band edges. Although this is the most challenging measurement that the HTSSE II instrumentation makes, the data demonstrate excellent repeatability of the on-board measurement instrumentation over time.

Figure 4 shows processed data for the Westinghouse Channelizer superimposed on the initial HP 8510 data. It can be seen that the performance is quite similar, especially on the band edges of each channel. Inconsistencies at about the 20 dB levels are understood and known to be the result of the applied fast rise-time pulse modulation to high selectivity filters.
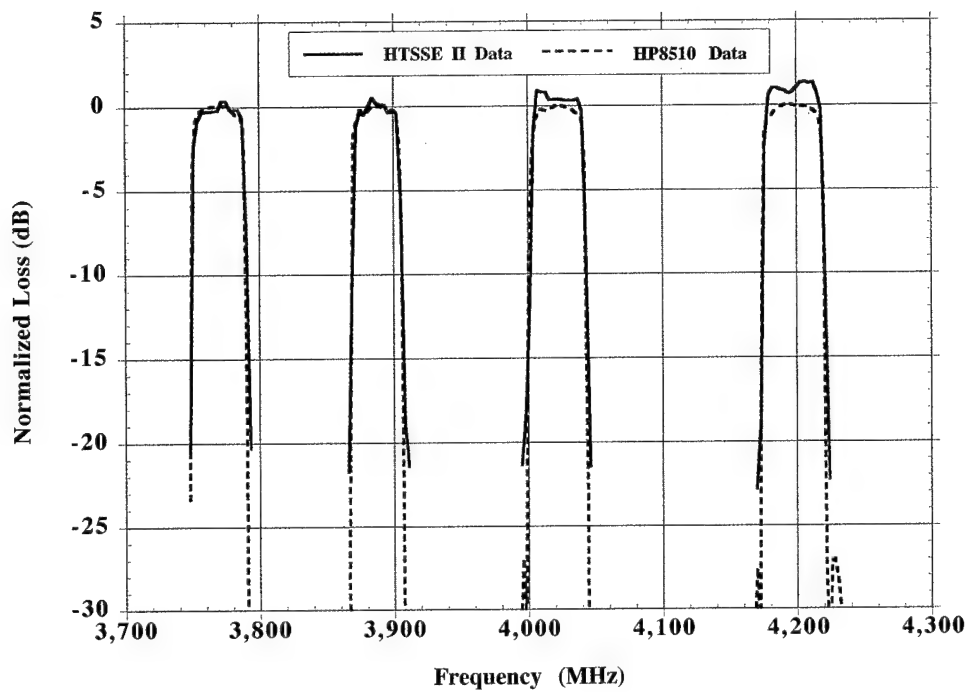
Fig. 3 — ComDev multiplexer data showing the repeatability
of the HTSSE II instrumentation over time.
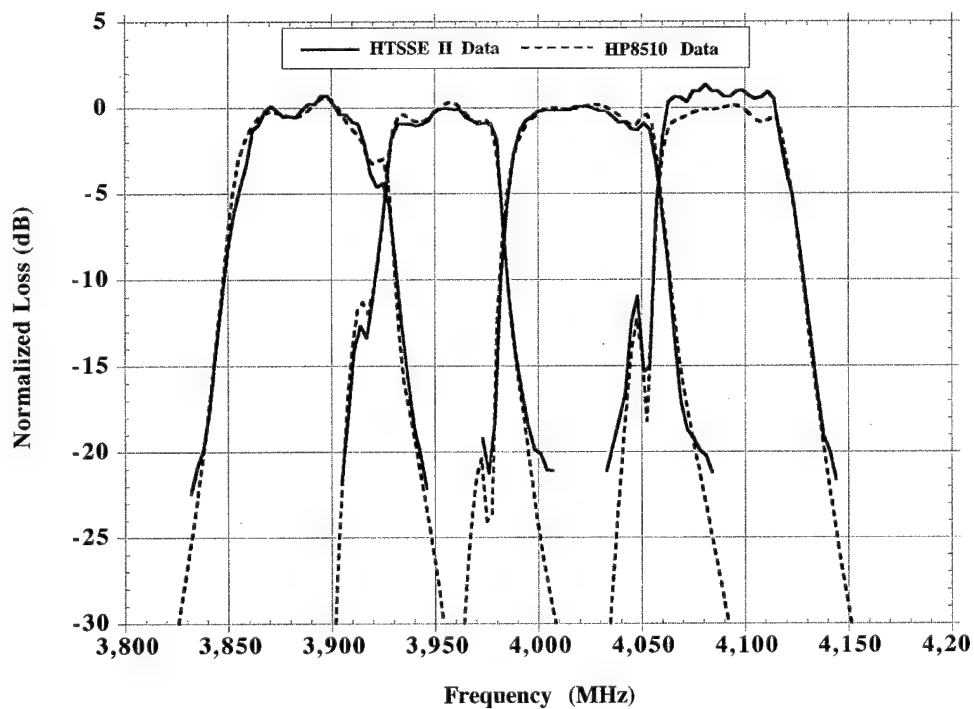
Fig. 4 — The Westinghouse channelizer experiment response showing
HP 8510 data for comparison.

The HTSSE II cryogenic system performed efficiently, requiring only 400 mW of cooling capacity from the Matra Marconi cryocooler in a worst-case flight environment. The cold bus cryogenic temperature was held at 77 K, with 0.1 K temperature stability over a 24-h steady-state environment testing period.

Summary: HTSSE II has integrated eight HTS experiments into a flight package ready for integration on the ARGOS satellite in 1996 and launch in 1997. HTSSE II will demonstrate that HTS devices can offer significant performance gains over conventional metal microwave devices, as well as demonstrate the cryogenic subsystems required to support them in long-term space applications. It is expected that the long-term on-orbit demonstration of these advanced HTS devices and their cryogenic subsystem by HTSSE II will significantly help to expedite the insertion of high-performance HTS devices into future DoD and commercial satellite programs.

[Sponsored by SPAWAR] ∎

Electric Propulsion for Advanced Unmanned Aircraft

R.J. Foch
Tactical Electronic Warfare Division

Electric aircraft propulsion offers advantageous possibilities for small, unmanned air vehicles (UAVs). Small electric motors are inherently quiet, smooth running, reliable, and safe to operate. Their smooth, low vibration characteristics allow power transmission from the motor to propeller with a simple gearbox, each now being able to operate at their maximum efficiency. With little vibration, the airframe can be made appreciably lighter, sensor signal noise is reduced, and the aircraft becomes a more stable sensor platform.

Since the late 1980s, researchers at the Tactical Electronic Warfare Division have been conducting extensive wind tunnel and flight tests of small, electrically propelled decoys and UAVs. Research focused on mission-customizing motors, optimizing airframe structure and aerodynamics, and testing the best available motors and batteries to determine the feasibility of performing useful missions.

Research: The critical electric propulsion technology limitation is the battery. Aircraft propulsion places unique demands on batteries by requiring a high energy density in conjunction with the desirability to drain the stored energy rapidly under high current loads for short periods (takeoff and climb) and moderate loads for longer periods.

There are two readily available battery types practical for small aircraft: lithium sulfur dioxide ($LiSO_2$) and nickel cadmium (NiCad). The lithium batteries have a high energy density when discharged slowly under a low current load. The NiCad batteries have only one-fifth the energy density of lithium but can safely withstand discharge rates 10 to 20 times that of the lithium cells. The limitation of high energy density equating with low discharge rate and vice versa is primarily driven by battery design rather than chemistry. Unfortunately, when a constant current load exceeding the design point is applied, either of these batteries may vent, burn, or explode.

The best dc electric motors for UAVs feature powerful rare-Earth magnets and are a "brushless" design. Brushless motors have their magnets mounted on the rotor around the shaft and have the windings built into the circumference of the case. Power is electronically pulsed to the windings, so the speed of the motor can be precisely controlled by a solid-state current switcher. Brushless motors can operate under water or in a vacuum, but most importantly, have efficiencies over 90%. In comparison, small brush motors have a 35% to 65% efficiency.

With a choice of a lightweight/slow discharge or heavy/fast discharge battery, early electric-powered aircraft were limited to two design approaches. The first—with lithium cells—would be slow, lightweight, and flimsy, with good endurance but no practical payload capacity. The second design—with NiCad batteries—would be conventional looking and performing with a very short flight endurance. Many examples of these two approaches have been developed but few could perform practical missions.

Development and Testing: Developing practical, electrically powered, small UAVs requires taking advantage of low Reynolds number (LRN) aerodynamic and advanced composite structure technologies. By designing the airplane to be aerodynamically "clean" and lightweight, the

power required can be within the capability of lithium batteries. The resulting designs have a long flight endurance and range but at the expense of rate of climb and maneuverability [1].

The Semiautonomous Research Aircraft (SARA) is a radio-controlled testbed designed and fabricated at NRL to investigate and conduct field tests of electric propulsion technologies (Fig. 5). SARA has a mass of 5.0 kg and features a 2.4-m span wing having a high performance LRN airfoil. Recently, SARA was equipped with a 300 W brushless motor produced by Aveox, Inc., and a 12-cell LiSO2 battery. The motor controller was adjusted to limit the current drain for battery safety. The takeoff performance was marginal at that power-setting limit, but on the second attempted takeoff, SARA lifted from the runway at the Naval Surface Weapons Center, Dahlgren, Virginia, and climbed to an altitude of 200 m. The throttle was then set for cruising at minimum power consumption. All systems performed as well or better than planned. SARA was landed 2 h and 47 min after takeoff, having flown an equivalent range of approximately 160 km.
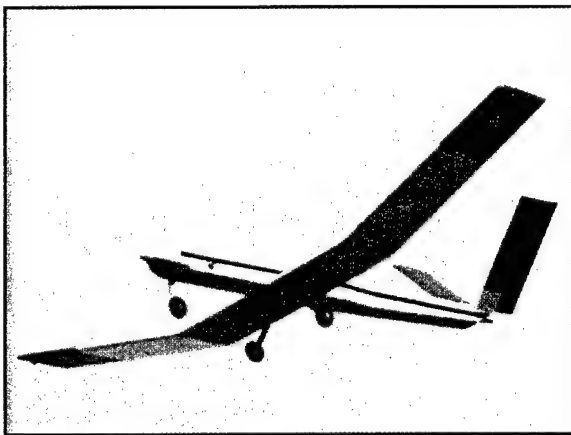
Fig. 5 — The Semiautonomous Research Aircraft (SARA).

The SARA test clearly demonstrated endurance and range that is competitive with small UAVs equipped with fuel-powered engines but without many of their inherent disadvantages. Additional research is now under way at NRL to develop even better performing electric UAVs that will be used for tactical mission demonstrations in the near future.

[Sponsored by ONR]

Reference

1. P.T. Davidson and R.J. Foch, "UAV Development and Test Capabilities at the Naval Research Laboratory," *Proceeding of the Association for Unmanned Vehicle Systems (AUVS) International Conference*, Washington DC, July 10-12, 1995. ∎

Global Maps of OH in the Middle Atmosphere

R.R. Conway and M.E. Summers
Space Science Division

The middle atmosphere is a region of coupling between the upper atmosphere, where the first interaction of the Earth with solar radiation occurs, and the troposphere in which we live. Extending through the altitude region between 10 and 100 km, it includes the stratosphere, where the bulk of the protective ozone layer resides. The discovery and eventual explanation of the ozone hole, which now appears every Spring over Antarctica, focused the attention of the world on the pollution of this region by man-made chlorofluorocarbons and on the physical and chemical processes that shape its behavior. An intensive international research effort—in laboratories (including NRL) and in the field— dramatically confirmed that chemically active gases in tiny concentrations are critical to the chemical balance that allows the ozone layer to endure through the normal daily and seasonal cycles of the atmosphere. In contrast with the troposphere where water is abundant, the middle atmosphere is extremely dry, with water-vapor concentrations of a few parts per million. Yet from this small amount of water, sunlight and atomic oxygen produce the hydroxyl radical, OH, which is the most important oxidizing agent in the atmosphere. Present in concentration of only a few parts per billion (equivalent to 30 ml in an Olympic-size swimming pool), OH plays a pivotal role in much of atmospheric chemistry and is the primary source of natural ozone loss. OH reacts with hundreds of gases—both natural and anthropogenic—and controls the build-up of pollutants and greenhouse gases. Despite its immense

importance, OH has remained one of the most poorly measured constituents of the atmosphere. In the Fall of 1994, NRL took a major step toward correcting this situation by making the first global-scale measurements of OH. This article briefly describes the results of the MAHRSI experiment, which made the measurements from a satellite deployed and retrieved by the space shuttle.

MAHRSI: The Middle Atmosphere High Resolution Spectrograph Investigation (MAHRSI) is a spectrograph experiment designed and built in NRL's Space Science Division to measure the Earth's ultraviolet airglow from space. In collaboration with the University of Wuppertal in Germany, the German Space Agency, and NASA, NRL flew MAHRSI on the CRISTA-SPAS satellite released by the shuttle during its STS-66 mission. With a nearly circular orbit at a height of 304 km, the satellite provided an extremely stable observing platform for 8 days of free flight. When OH in the atmosphere scatters sunlight, it produces a bright emission with a unique spectral signature in the ultraviolet. By accurately measuring the brightness of this glow and how it varies with altitude, we were able to infer the amount of OH at each altitude. A major difficulty with the measurement is the need to discriminate the spectrally narrow lines of the OH emission from the bright Rayleigh scattering of the solar Fraunhofer spectrum. Rayleigh scattering is the process that produces the blue sky. In the MAHRSI data, the complex Rayleigh scattering spectrum is blended with the OH emission. MAHRSI separates these two signals by using very high spectral resolution.

Figure 6 shows the success of that separation. The remarkable agreement achieved between the observed OH spectral signature and the theoretical prediction of its shape was critical to the successful mapping of the OH distribution.

Global OH Images: Figure 7 demonstrates how the MAHRSI data are used to construct OH maps. This image shows the vertical density profile of OH between the altitudes of 50 and 80 km for each latitude between 52° S and 62° N. All of the data were recorded during a single orbital day (about 50 min). The local time for the profiles varied from dawn to dusk due to the satellite's orbital motion. The data taken in southern latitudes represent Spring mornings and the data in the north represent late Fall afternoons. Knowledge of these variations is of immense value in delineating the global structure of OH — a critical element needed for validating atmospheric models. For example, Fig. 8 is a model calculation of the OH abundance profile above the equator but for different local times and fixed to November 5. It shows that OH vanishes below 80 km during the night but reforms rapidly as the sun rises. By 10 A.M., two distinct layers have formed — one at an altitude near 70 km and one near 50 km. Although the observations shown in Fig. 6 also contain the effect of latitudinal and seasonal variability ignored by the model, they clearly show the general features of the predicted behavior. There are however important differences, and the explanation of those will provide the real scientific progress. MAHRSI acquired 75 such orbits of data covering a wide range of latitudes, longitudes, and local times.
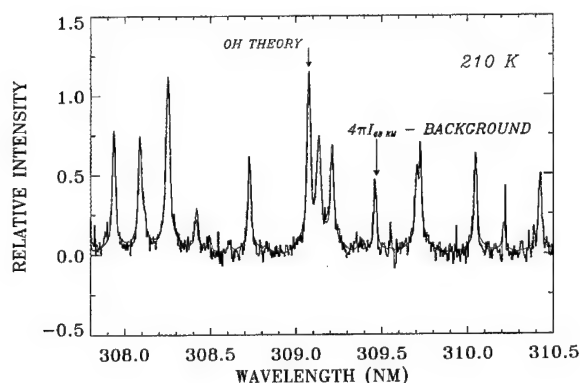
Fig. 6 — The observed OH emission at 70 km. The spectrum was retrieved by subtracting the Rayleigh background spectrum from the observed airglow. The result is compared to the theoretically predicted OH spectrum, which is shown by the red curve.
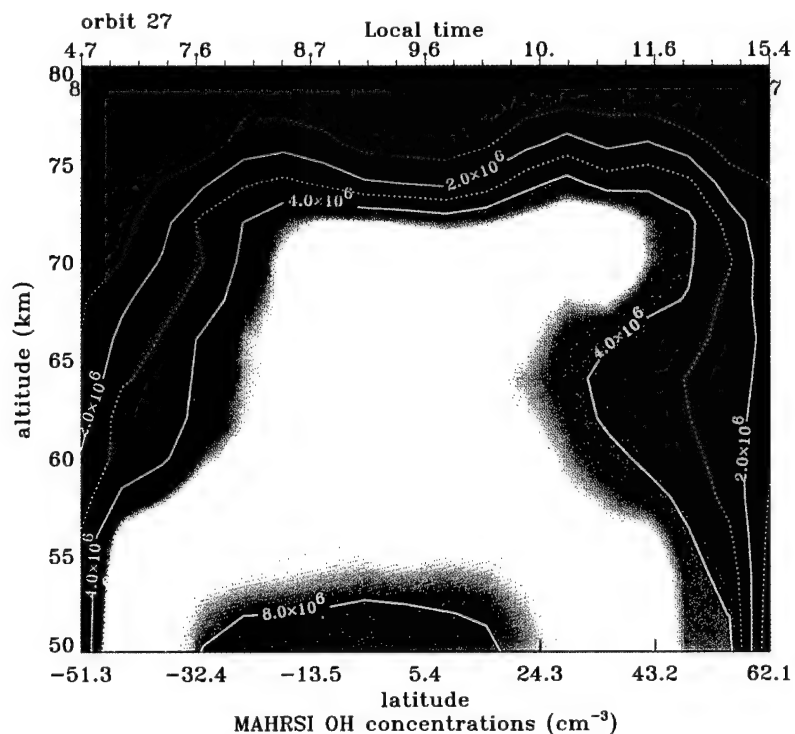
Fig. 7 — OH abundances observed during orbit 27 on 5 November 1994. This figure is the compilation of 13 sequential limb scans. The solar zenith angle and solar local time at the moment the instrument viewed the 60-km tangent height is indicated along the upper border of the figure.
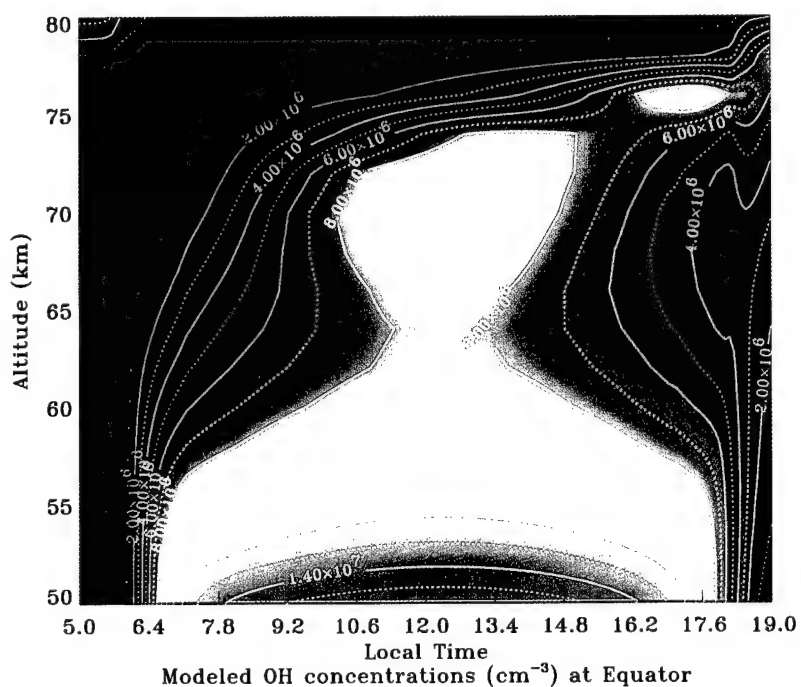
Fig. 8 — A model calculation of the dawn-to-dusk variation of the OH abundance profile above the equator on November 5.

MAHRSI also measured nitric oxide, NO, during its flight. NO is important not only as a catalyst for ozone destruction but also as the primary source of ionization in the D-region ionosphere. The Navy is particularly interested in the ionosphere because it strongly influences both low frequency (VLF and ELF) and high frequency (HF) communications. MAHRSI measurements will begin to provide an observational foundation for the building of a reliable D-region ion chemistry model.

The measurement of OH has been the principal missing element in understanding ozone chemistry in the middle atmosphere. Current theoretical models of atmospheric ozone have difficulty explaining its magnitude and seasonal variations. It is speculated that these discrepancies might be tied to the role of OH, but the lack of *any* global observations have thus far prevented testing the theory. Now from its vantage point on CRISTA-SPAS, MAHRSI has successfully mapped the global distribution of atmospheric OH for the first time. With these first global maps, NRL scientists are poised to incorporate the observations into their comprehensive models of atmospheric chemistry and dynamics. This will lead to the identification of the causes of discrepancies in our understanding of, and ability to detect, global change in ozone. The achievement has identified NRL as a major force in studies of the middle atmosphere.

Acknowledgments: The MAHRSI data analysis team includes M. Stevens of the Upper Atmospheric Physics (UAP) Branch and J. Cardon and S. Zasadil of Computational Physics Incorporated (CPI). The model development team includes J. Bacmeister and D. Siskind of the UAP, S. Eckermann of CPI, and D. Strobel of Johns Hopkins University. The successful flight of MAHRSI was made possible by the dedicated efforts of R. Feldman and J. Moser of ARTEP Incorporated, W. Sawchuck and L. Grove of CPI, R. Dekema, K.-W. Li and A. Kenig of Assurance Technology Corporation, T. Seeley and G. Carruthers of the Ultraviolet Measurements Group, C. Brown of the Solar-Terrestrial Relations Branch, J. Morrill of the Solar Physics Branch, L. Marlin of the Engineering Management Office, the ASTRO-SPAS team at Daimler-Benz Aerospace AG, and the flight crew of the STS-66 space shuttle mission.

[Sponsored by ONR, USAF, and SERDP]

References

1. D. Offermann and R. Conway, "Mission Studies the Composition of Earth's Middle Atmosphere," *EOS Trans. American Geophys. Union* **76**, 337 (1995).

2. R.R. Conway, M.H. Stevens, J.G. Cardon, S.E. Zasadil, C.M. Brown, J.S. Morrill, and G.H. Mount, "Satellite Measurements of Hydroxyl in the Mesosphere," submitted to *Geophys. Res. Let.*

3. M.E. Summers, R.R. Conway, D.E. Siskind, D.F. Strobel, and S.E. Zasadil, "Mesospheric HOx Photochemistry: Constraints from Concurrent Measurements of OH, H_2O and O_3," submitted to *Geophys. Res. Let.* ∎

Sodium Sulfur Battery Cell Space Flight Experiment

J.C. Garner and W.E. Baker
Space Systems Development Department

Aerospace sodium sulfur (NaS) battery cells can be an enabling technology for tomorrow's smaller, faster, cheaper Department of Defense (DoD) satellites. At 150 Wh/kg, NaS battery cells have demonstrated a specific energy three times that of current state-of-the-art nickel hydrogen (NiH_2) battery cells. A spacecraft currently flying a 60-kg NiH_2 battery could now fly a 20-kg NaS battery to perform the same mission and fly 40 more kg of payload mass or save an estimated $800 K (based on an estimated $20 K/kg to orbit). So why aren't NaS batteries in use on DoD and commercial spacecraft? Until recently, most of the tests required to qualify the new aerospace battery technology were not complete. In the last 2 years, the U.S. Air Force's Phillips Laboratory (USAF PL), working through the Sandia National Laboratory, has completed many of the required qualification tests, including random vibration, pyrotechnic shock, freeze-thaw, and safety tests. The remaining qualification test is a demonstration that the space zero-gravity environment will not affect the charge/discharge characteristics of the liquid electrode NaS battery cell. To answer that question, the USAF PL has tasked NRL's Naval

Center for Space Technology to design, fabricate, and integrate a NaS battery cell flight experiment (NaSBE). The NaSBE will fly on the Wake Shield Facility (WSF) Shuttle Cross Bay Carrier mission 03, which is scheduled for launch in late 1996 on STS-80.

NaS Battery Cells: The concept of a secondary NaS battery cell was first announced in 1967. At an operational temperature of 350° C, the system uses a molten sodium anode, a molten sulfur cathode, and a solid material that functions as both a sodium ion-conducting electrolyte and a separator. For the experiment, NaS cells will be manufactured by Eagle Picher Industries Inc., of Joplin, Missouri (Fig. 9). The ceramic β″-Alumina electrolytes are manufactured by Ceramatec.

Experiment Description: The primary purpose of NaSBE is to characterize the performance of the NaS cell's operation in zero gravity (G). Four NaS cells and associated experimental hardware will be mounted in a "smart can" on the WSF Cross Bay Carrier. The experiment will be launched unpowered with the NaS battery cells charged and the electrodes frozen at a temperature of 25° C. After the shuttle is in orbit and the WSF has been removed from the Cross Bay Carrier, the experiment will be powered up and experiment heaters energized to raise the battery cell temperature to 350° C at a rate of 25° C/h. After reaching the operating temperature, the NaS cells will be subjected to the following test

sequence: 2 100% depth-of-discharge (DOD) characterization cycles, 2 60% DOD simulated geosynchronus orbit cycles, and 15 40% DOD simulated low-Earth-orbit (LEO) cycles. Following the conclusion of the last LEO charge cycle, the NaS cells will be discharged to different states of charge, the heaters will be disabled allowing the experiment temperature to drop and the battery electrodes to solidify. After the Shuttle mission is complete, NaSBE will be removed from the WSF Cross Bay Carrier and sent back to the USAF PL. At PL, the NaS cells will be removed and subjected to a destructive physical analysis (DPA). The purpose of the DPA will be to determine what effects the cycling of the cells in zero G have on the cell morphology as a function of state of charge.

Experiment Design: Figure 10 shows a block diagram of the experiment. In order to fit the entire experiment within the smart can, the experiment electronics boxes are mounted to the can lid, and the battery cell safety enclosure is suspended from the lid to a deck in the middle of the can. For safety reasons, the battery cells are contained in a cylindrical 304 stainless steel vessel. By design, the vessel will be capable of withstanding a worst-case cell breach, which could generate internal temperature and pressure in excess of 600° C and 180 psi. The battery vessel is suspended below the mid-deck by a series of kinematic mounts. When the vessel is heated to 350° C, it grows 0.0028 m in the axial
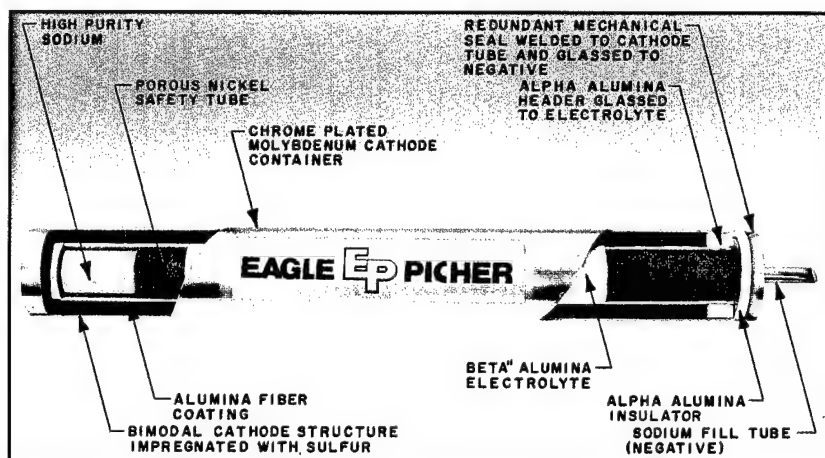
Fig. 9 — Sodium sulfur battery cell design.
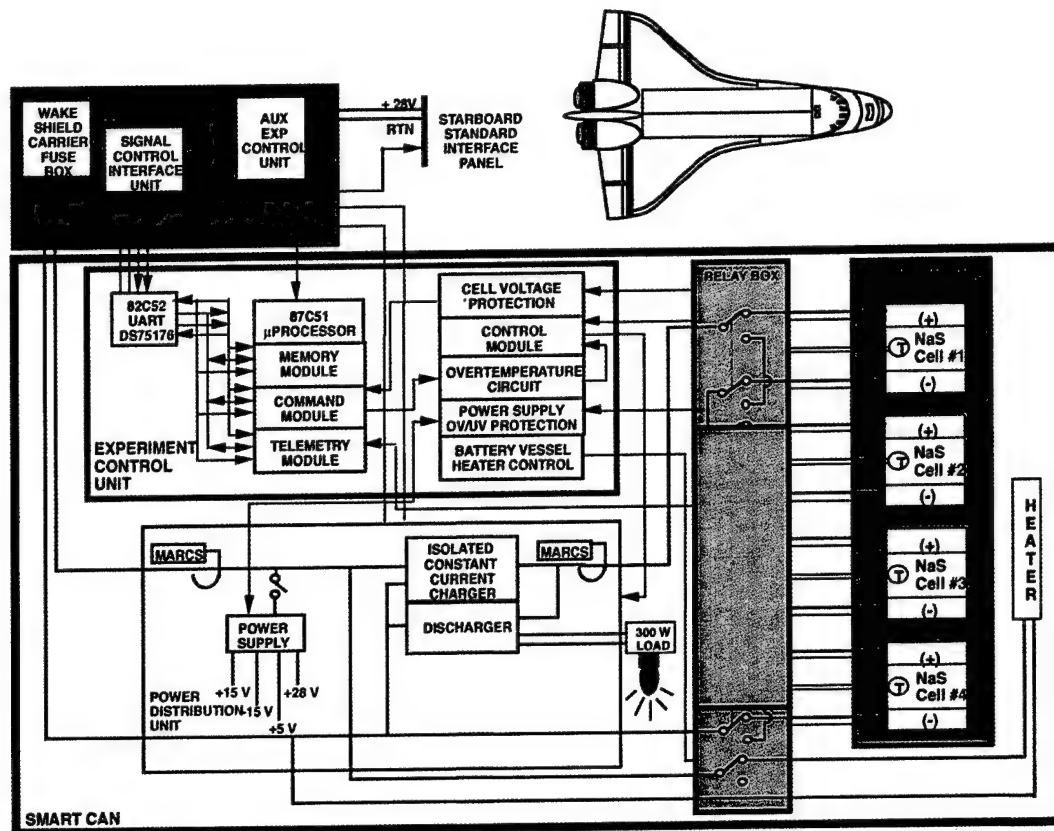
Fig. 10 — Sodium sulfur battery experiment block diagram.

direction and 0.0020 m in the radial direction. The kinematic mounts allow for this expansion and keep the shear stress low on the mounting bolts. Charge and discharge control of the NaS battery cells is driven by the unique electrochemical characteristics of the NaS cell. Unlike NiH_2 or nickel cadmium cells, NaS cells have no inherent overcharge protection mechanism. When fully charged, the NaS cell impedance and voltage rise exponentially. Damage to the ceramic electrolyte can occur if the cell voltage is allowed to exceed 2.50 V. Therefore, charging a battery constructed of a series string of cells requires a method of limiting individual cell voltage or removing fully charged cells from the string. In the experiment, cell removal is accomplished in the relay box (Fig. 10). The relays are controlled by hardware voltage detectors that remove a cell from the circuit when its voltage exceeds 2.35 V (overvoltage) or drops below 1.65 V (undervoltage). In an operational battery, it would be desirable to have voltage limiters or switches capable of operating at 350° C located on the battery to minimize circuit resistance. Constant current charge and dis-

charge of the NaS cells are provided by the experiment power distribution unit (PDU). The PDU charger provides galvanic isolation and conditions the Shuttle's 28-V power supply to supply either a 2, 4, or 16 amps constant current charge to the NaS cells. In order to discharge the cells, the PDU discharger must operate over an input voltage range of 1.8 to 10 V in order to accommodate from one to four NaS cells in various states of charge. The discharger uses three nonisolated boost converters configured to regulate the input current to two selectable discharge rates of 20 and 32 amps. Three halogen "off-road" vehicle lamps will be used as compact, high temperature radiators to dissipate the battery discharge energy to space. The lamps will be mounted on the underside of an extended radiator plate. The radiator plate attaches to the smart can top lid to increase thermal radiator area.

Experiment Command, Control, and Telemetry: The experiment control and telemetry interface functions reside in the experiment control unit (ECU). Software scripts loaded in a 87C51 μ-

processor control the experiment sequences. Scripts may be changed or new scripts may be uploaded from ground control. The μ-processor contains a built-in clock for timing the charge/discharge sequences. In addition, the scripts contain safety-limit checking functions to back up the hardware limit checking. For each battery cell, voltage, current, three temperatures, and on-line/off-line status are recorded along with other experiment data once a minute in a solid state memory bank. RS-485 protocol is used for the interchange of data between NaSBE and the WSF CBC. Plans are to downlink experiment data at least once per orbit and probably more frequently. However, if required, NaSBE can store up to two orbits of data in the solid state memory bank.

To quantify the results against the performance of NaS cells in a 1-G environment, the brassboard experiment hardware and four new NaS cells will be operated in parallel with the flight experiment. The entire test sequence of the flight experiment will be duplicated. Then as an option, the ground test cells may also be subjected to a DPA.

Acknowledgments: This work is overseen by Lt. V. Kennedy and Capt. S. Smellie. In addition, these persons made significant contributions to this effort: M. Adams, W. Barnes, W. Braun, R. Circle, D. Dyer, J. Gauvin, G. Hickman, R. Hobbs, B. Kramer, J. Kim, S. Lam, L. Larson, A. Marderness, R. Ruth, J. Shortt, and R. Skalitzky.
[Sponsored by USAF PL]

Reference

1. D. Linden, *Handbook of Batteries and Fuel Cells*, (McGraw Hill, New York, 1984), pp. 32-1 – 32-3. ∎

HERCULES/MSI: Hand-held Georegistered Multispectral Video

H.M. Pickard, R.F. Higgins, and B. Kaufman
Space Systems Development Department

Overview: HERCULES (Hand-held, Earth-oriented, Real-time, Cooperative, User-friendly, Locating, Targeting, and Environmental System)

is a camera system designed to image and geo-locate Earth targets from space. HERCULES/multi-spectral imagery (MSI) is the third of a sequence of hand-held, shuttle-based, geolocating imaging devices developed jointly by the Navy, Army, and NASA. Its current configuration includes a video camera from the Xybion Corporation, which allows it to produce geolocated MSI from space [1]. By integrating a camera with an attitude reference unit (ARU), HERCULES can geolocate – in real-time – Earth images taken from the space shuttle.

Project History

Phase I: The idea for a geolocating space camera came from a comment made more than a decade ago by Navy astronaut Dave Griggs to Dr. William E. Howard III. Griggs observed that a picture taken from space is often unidentifiable because its location is unknown. Dr. Howard, then technical director of the Naval Space Command, started a cooperative effort between the Navy and NASA to address this need. The first attempt was a NASA-built space sextant, called the Latitude/Longitude Locator (L3), which successfully produced geolocations accurate to 24 km but could not work at high magnification and did not allow on-orbit viewing of the film-based images.

Phase II: HERCULES began to address the deficiencies of L3 and the need for better geolocation accuracy in 1988. NRL's Naval Center for Space Technology (NCST) was tasked with the development of the geolocation system and overall program management. NASA was tasked to develop a megapixel electronic still camera (ESC) to allow pictures taken from space to be viewed instantly on orbit or down-linked to the ground.

HERCULES' Geolocation Hardware: At the core of the geolocation hardware is an ARU developed by the Honeywell Corporation. The ARU consists of three orthogonally mounted helium-neon ring laser gyros and their associated electronics. When attached to the camera, the ARU provides three-axis knowledge of the orientation of the camera to within arc-seconds. NRL developed the electronics and software to integrate the output of the ARU and maintain continuous, precise knowledge of the orientation of the

camera. NRL also developed the user interface to the overall system, the stellar alignment process used to align the ARU to inertial space, and the algorithms to combine the camera orientation and space shuttle orbital position to calculate the latitude and longitude of the captured images [2]. In April 1992, the first HERCULES system was delivered to the Air Force office tasked to integrate it into the Space Shuttle program and train the crew in its use. Meanwhile, the Army provided a night vision lens that could be attached to the ESC. By the time HERCULES flew for the first time in December 1992, it was truly a collaborative effort involving Navy, Army, Air Force, and NASA.

The first flight of HERCULES was in December 1992, on STS-53. A second flight followed shortly after, in April 1993, on STS-56. These missions validated the system concepts. Successful stellar alignments were routinely performed, real-time geolocations were obtained, and digital imagery (including night-time imagery) were stored, viewed on orbit, and down linked to the ground. Geolocation performance averaged 6 km in real-time and 4 km with postmission processing. Imaging operations with lenses having a focal length longer than 300 mm (15-m ground resolution) were largely unsuccessful due to long exposure times causing image smear.

Phase III: An increased need for multispectral and higher resolution imaging products drove a change in the camera system. The Army's Night Vision and Electronic Sensors Directorate, having previously provided the night vision lens, became more actively involved in this phase. They had been working with a multispectral camera from Xybion Corporation, and they were tasked to integrate that camera into HERCULES. The camera, shown in Fig. 11, produces video images of Earth at a rate of 30 images per second. A filter wheel is positioned between the lens and the optical sensor. Because filter wheels can be changed on orbit, several wheels can be flown—each with filters suitable for a specific application. When multispectral images are desired, the wheel spins synchronously with the video image rate so that a new filter is in position for each successive image. Alternately, any of the six filters can be rotated into position for panchromatic imaging. The Xybion camera operates under low light conditions by incorporating a
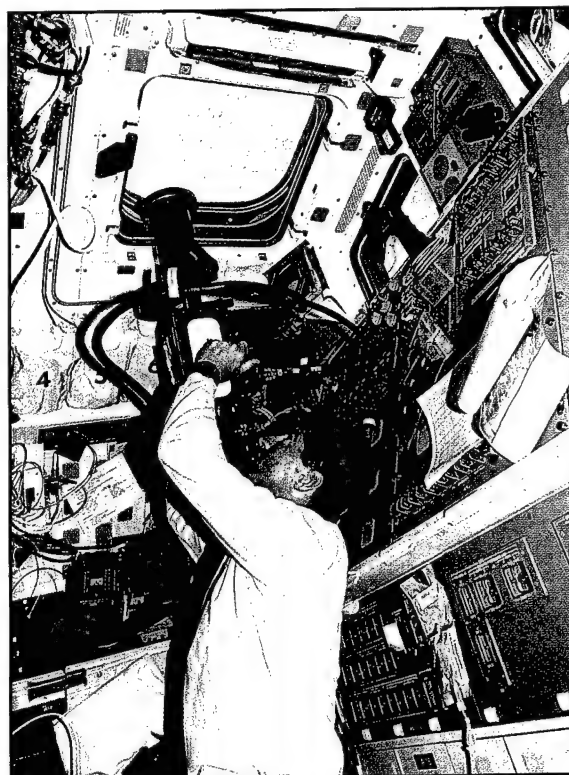
Fig. 11 — STS-70 Commander Tom Henricks is shown here performing preliminary checkout of the HERCULES system in space.

third generation image intensification tube. This can be used to boost the signal from narrow optical filters or to perform imaging operations at dusk or at night. Daytime observations also benefit from the image intensifier because short exposure times can be used, which drastically reduce image smear caused by operator motion and shuttle orbital velocity. Exposure times can be set for each filter anywhere in the range from 50 ns to 33 ms. The location of the center of the image is overlaid onto the image and is accurate in real-time to within 6 km and better than 4 km after postmission correction. This configuration of HERCULES flew on STS-70 in July 1995. The results of this mission show increased resolution imagery, imagery under low-light and night-time conditions, and multispectral imagery. The multispectral images, taken with 310-mm and 520-mm lenses, yield a ground resolution down to about 15 m. Figure 12 is an example of the multispectral output of the system. Panchromatic images were successfully captured with several lenses, the longest having a focal length of 1810 mm and yielding a ground resolution better than 5 m [1].

Filter 1

Filter 2

Filter 3

Filter 4
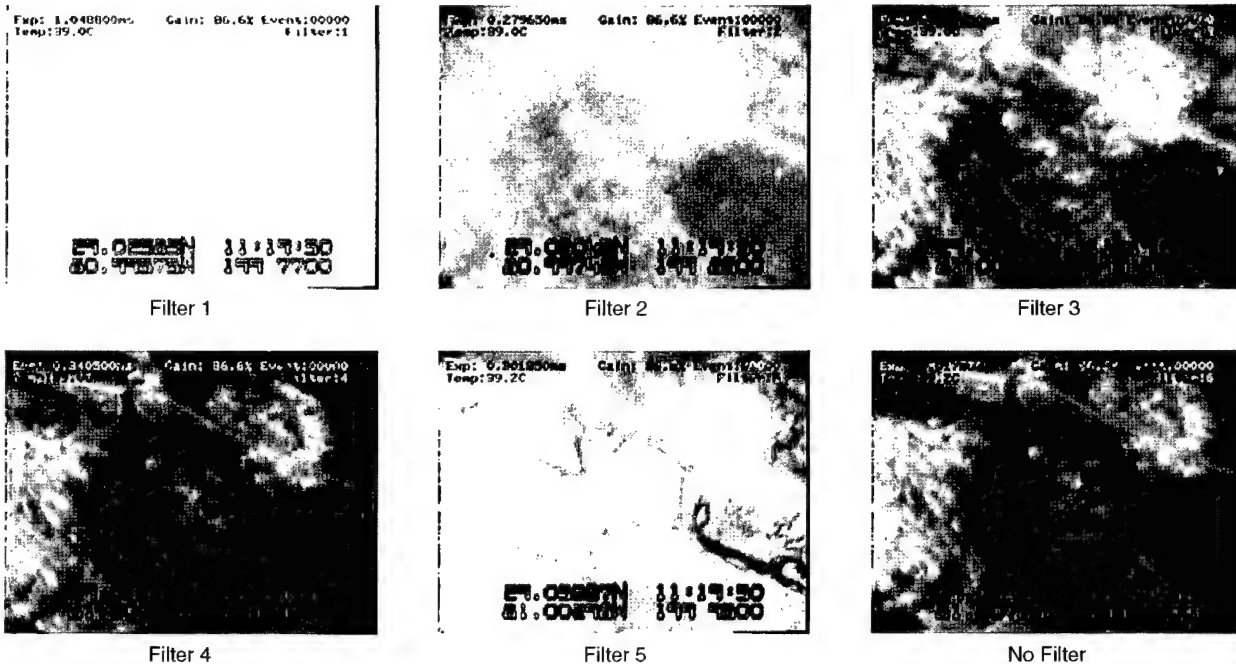
Filter 5

No Filter

Fig. 12 — This sequence of six consecutive frames shows the effects of narrow band filters in imaging this region of Cape Canaveral Air Force Station. A small airport shows up only through filter 5 while the coast line is most apparent in filters 3 and 4. The image taken through filter position 6 (which had no filter in place) does not show any features particularly well. Filter position 1 was overexposed in this sequence.
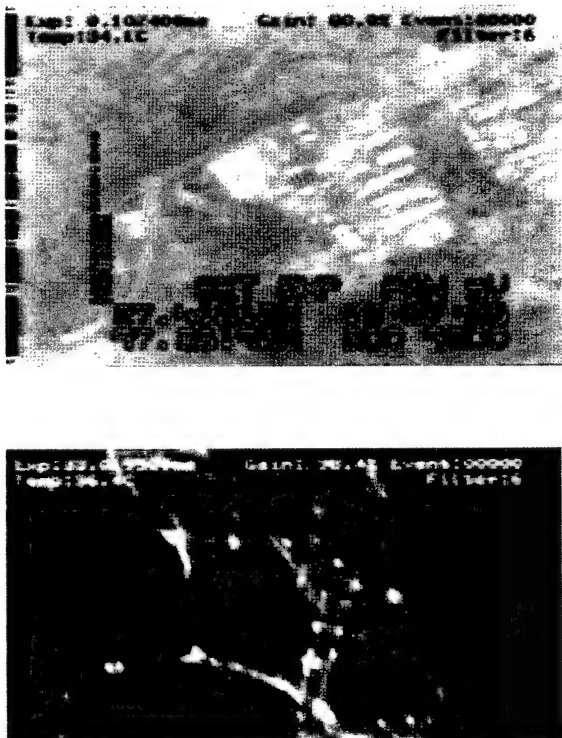
Fig. 13 — HERCULES' high-resolution and night-vision modes are illustrated in these images. Individual buildings in Texas (above) can be seen at a focal length of 1810 nm (5-m resolution). Below, a night shot of a town on the east coast of Australia is shown.

Examples of the long focal length capability and the nighttime capability are shown in Fig. 13.

Future: The next flight of HERCULES will include a newer, simpler user interface. Different combinations of filters will be tested and the resolution limits will be further explored.

Acknowledgments: The extensive efforts provided by the Army's Night Vision and Electronic Sensors Directorate—particularly those of Christopher Simi, Randy Kindsfather, Mark Norton, and Larry Clark—are gratefully acknowledged. CAPT John Hennessey (USAF) and CAPT Jeff Long (USAF) deserve credit for the extensive and critical roles they played in getting HERCULES into space. Equally critical to HERCULES' success were Charles Jones and Mark Soyka at NRL and Doug Holland, Don Harris, and Phyllis Grounds at NASA Johnson Space Center. Finally the continuous support of Navy Tencap during the entire project is deeply appreciated.

[Sponsored by DON, ONR, and DOA]

References

1. H. Pickard, R. Higgins, C. Simi, M. Norton, R. Kindsfather, "HERCULES/MSI: Hand-Held

Georegistered Multispectral Video," (AIAA 95-3759), presented at the AIAA Space Programs and Technologies Conference and Exhibition, Huntsville, Alabama, Sept., 1995.

2. P.J. Melvin, M.T. Soyka, H.M. Pickard, S.N. Lam, K.H. Little, R.R. Dasenbrock, and T.W. Murphy, "Geolocation Accuracy of HERCULES on STS 53," (AAS 93-604), presented at the AAS/AIAA Astrodynamics Specialist Conference, Victoria, British Columbia, August 16-19, 1993. ∎

Active Vibration Suppression in Space Structures

R.S. McClelland and S. Fisher
Spacecraft Engineering Department

A. Bosse
Swales and Associates

Future Navy spacecraft that incorporate flexible appendages can benefit from active suppression of vibrations introduced by dynamic maneuvers, moving parts, and thermal shock. As mission objectives require increasingly complex and large structures—combined with more exacting jitter and pointing requirements, the need for active control of structures grows. Engineers at NRL's Naval Center for Space Technology have developed a Space Truss Simulator Facility and are conducting experiments to address this need. The techniques being explored can be applied to many future spacecraft, including manned platforms such as the international space station, and civil systems, including bridges, buildings, and automobiles.

Space Truss Simulator Facility: The Space Truss Simulator (Fig. 14) is representative of a spacecraft structure that may support solar arrays, scientific instrumentation, or sensor platforms. The piezoelectric active struts and reaction-mass actuators are electromechanical devices that directly substitute for elements of the truss and are used to control vibrations in the structure. The active struts push and pull according to the applied voltage, which causes expansion or contraction of the piezoelectric motor material. The struts are placed in high strain energy locations, which correspond to elements near the base of the truss. The reaction-mass actuator applies a force to the structure in response to the commanded acceleration of its movable reaction mass. This type of actuator is placed at locations near the tip of the truss where the maximum displacement occurs.

Experimental Approach: Two active struts are integrated into the truss to predominantly

PIEZOELECTRIC ACTIVE STRUT

REACTION MASS ACTUATOR
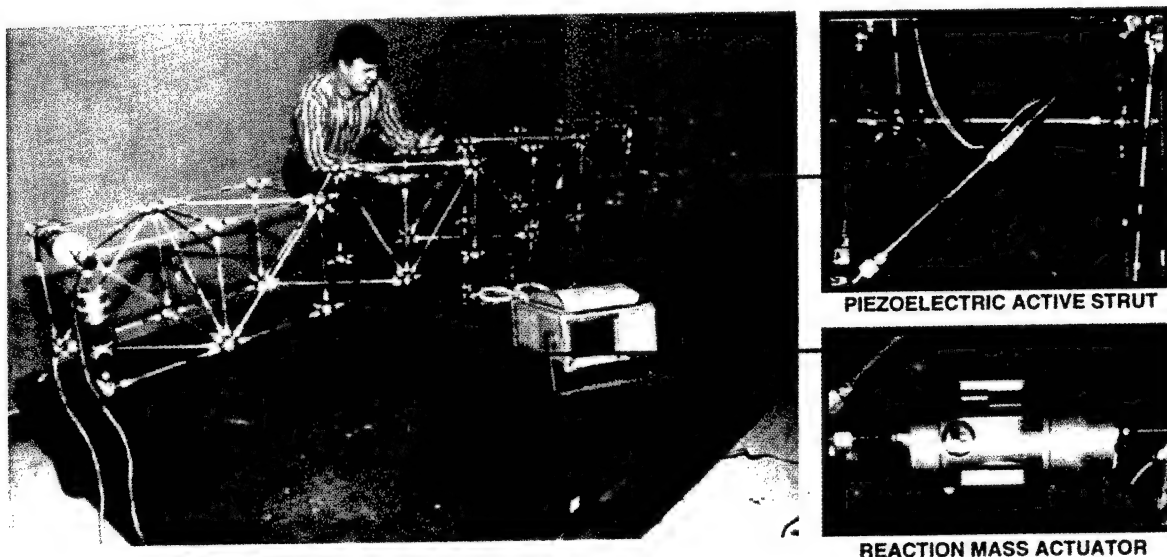
Fig. 14 — Space Truss Simulator Facility

control vibrations at the first and second resonant frequencies of the structure. The optimal locations for controlling these frequencies were determined using a finite element model of the structure. The first and second modes of vibration produce tip motion in the horizontal and vertical planes, respectively. Each active strut includes a force transducer, which is used for feedback. The control algorithm integrates the force signal and applies gains to form a compensating voltage signal with components proportional to both displacement and velocity. Controller gains were selected by measuring the frequency response for each strut, identifying a mathematical model of its input-output behavior, then applying classical control design techniques. Real-time experiment control and data acquisition are accomplished using a high-speed digital signal processor (DSP)-based control computer.

Active Control Results: The performance of the control system was evaluated by measuring the acceleration at the truss tip while subjecting the structure to both impulsive and sinusoidal disturbance forces. Figure 15 shows the frequency response function (FRF), which represents the ratio of the tip acceleration to the impact force applied at a point in the middle of one truss span. Large vibration responses occur at the lightly damped natural frequencies of the structure, as

indicated by the peaks of the FRF. The overlaid closed loop results show nearly complete reduction of the response at the second mode frequency of 17.5 Hz using one piezo-strut, removal of the first mode response at 15.5 Hz with the second strut activated, and significant attenuation at some of the higher modes. Reduction of these resonant peaks indicates that the active control in effect provides an artificial increase in structural damping.

Figure 16 shows the response of the system to sinusoidal forcing at the first two natural frequencies before and after control is applied. The map of horizontal-to-vertical displacement at the truss tip shows a reduction by a factor of 40 in vertical motion and a factor of 110 in horizontal motion.

Summary: Laboratory experiments using local feedback controllers have yielded substantial attenuation of vibration disturbances and effective artificial damping of the structure. Development is proceeding toward the integration of embedded fiber-optic strain sensors (manufactured by NRL's Optical Sciences Division) for feedback control and structural health monitoring, combined with more advanced control laws for improved performance over a wider frequency range. Future plans include the development of a deployable "smart boom" for ground and flight experiments,
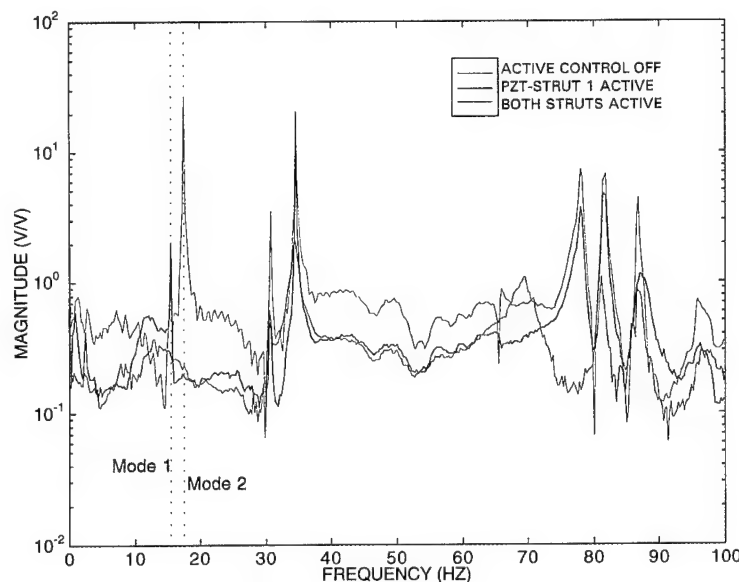
Fig. 15 — Frequency response from hammer input
to acceleration output.
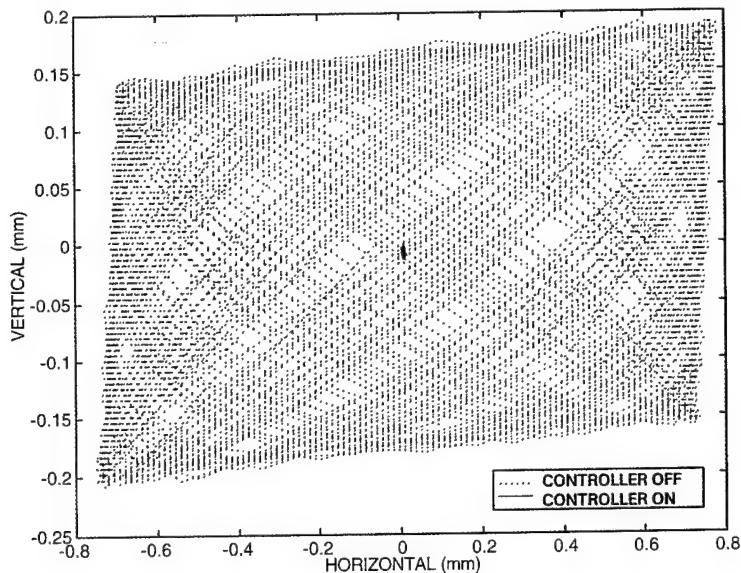
Fig. 16 — Truss tip motion.

which will serve as a prototype for a space-realizable system.

Twenty Years of HRTS Observations

J.W. Cook and G.E. Brueckner
Space Science Division

J. Schultz
Command Support Division

From its first flight on July 21, 1975, to its most recent flight on April 18, 1995, NRL's High Resolution Telescope and Spectrograph (HRTS) has provided a wealth of solar atmospheric data. HRTS has recorded high quality ultraviolet (UV) spectra of the Sun on nine rocket flights and during extended operations on the Space Shuttle *Spacelab 2* mission in July-August 1985. By continual innovations in the instrumentation and by adapting individual flights to specific scientific goals, HRTS has remained a vital research program for 20 years.

HRTS is essentially a space-based telescope that "sees" into the UV spectral region. HRTS has four components: the 30-cm diameter (12-in.) telescope; a slit spectrograph, which obtains UV spectra; a spectroheliograph, which takes images of the Sun in a narrow passband, usually at 1600 Å (Fig. 17), or at 1550 Å, the wavelength of the resonance lines of C IV (Fig. 18); and an H alpha (6563 Å) imaging system, which can transmit images to ground to use in determining the pointing on the solar surface. The instrument is powerful enough to look at very small features on the Sun—down to approximately 700 km—and obtains images on photographic film rapidly enough to observe quickly changing solar structures such as high velocity explosive events. Although the HRTS instrumentation has been modified over the years to fit specific flight scientific objectives, its primary mission has been to obtain UV spectra from the Sun over 1175-1700 Å and accompanying spectroheliograph images with very high spatial resolution.

The data from HRTS observations are used to determine such physical quantities as the temperatures and densities of the plasmas in the different structures of the solar atmosphere, the velocities of moving features, and the relative abundances of the elements that are present. The atmosphere of the Sun is a stormy region of high-speed "winds" of solar gases where temperature roughly changes with altitude, from about

Fig. 17 — A spectroheliograph image from HRTS II of the solar surface seen at 1600 Å in the far UV, showing an active region on the disk with sunspots and another at the solar limb at the top. The image is approximately a solar radius in length and half a solar radius in width (the solar radius is 700,000 km). The smallest features—individual small bright points—are approximately 1500 km in size.
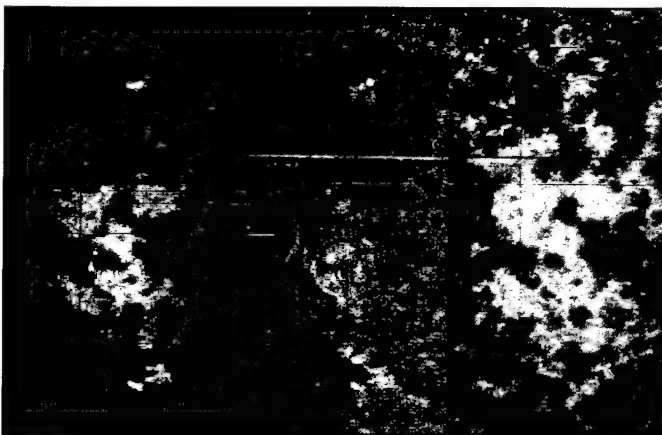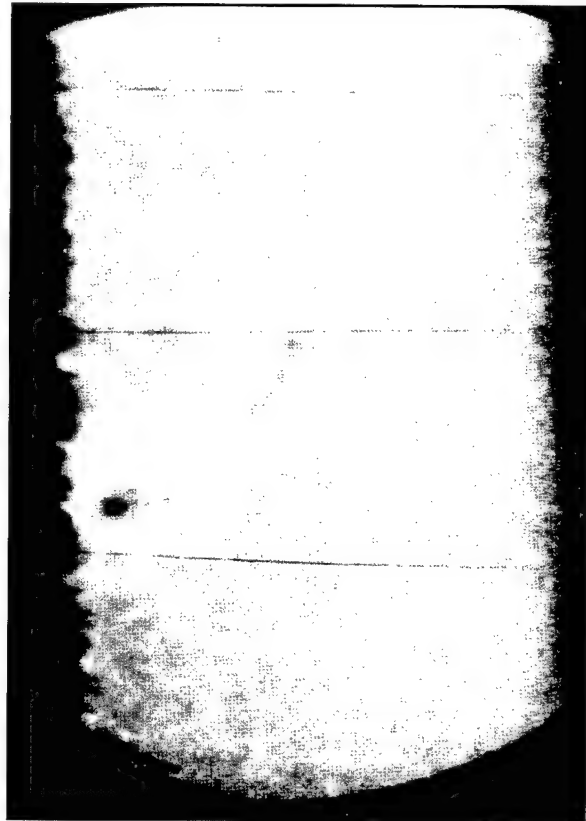
Fig. 18 — Spectroheliograph images from the most recent HRTS IX flight. A 1549 Å image (left), a 1600 Å image (right), and the difference image (center) are shown. The difference image helps to isolate small loops emitting at C IV temperatures (100,000 K) in the solar active region.

6000 K in the visible photosphere to 4500 K in the temperature minimum region. It then reverses and climbs to 8000 K in the chromosphere and upwards through the transition region to a million or more degrees in the corona. Fundamental questions that scientists are hoping to answer to lead to a deeper understanding of the Sun and other stars include: what is the heating mechanism that causes the temperature rise in the outer solar atmosphere?; how are particles accelerat-ed to very high velocities (hundreds of km/s) in structures such as small explosive events, larger sunspot flows, and solar flares?; what is the relationship between the solar magnetic fields and the evolving plasmas which are everywhere observed?

Earlier Results: During its very first flight on a sounding rocket, HRTS made the first observations of a number of supersonic phenomena such

as transition region jets, explosive events, and sunspot downflows. These were only observable because of the great increase in spatial resolution along the spectrograph slit that was possible because of the innovative optical design. Data on the high-velocity outflows from these events led to the suggestion that they were potential sources for the solar wind. This flight also yielded the first observations of solar molecular hydrogen.

In 1985, HRTS flew as one of the instruments on NASA's historic *Spacelab 2* mission, providing the first opportunity for HRTS to make extended observations of the Sun. Solar physicists onboard the shuttle as payload specialists were able to operate several solar instruments, including HRTS, and to point the telescopes at targets of interest. The *Spacelab 2* mission provided new information on UV spicules viewed at the solar limb, the global statistics of the small, high-velocity explosive events, and data on sunspots and prominences. These data led scientists to believe that the study of the plasma-magnetic field interaction producing the explosive events could provide clues to the mechanism for solar flare heating.

Most Recent Flight: For the most recent HRTS flight, the instrument was reconfigured to observe the near-UV lines of Mg II, one of the strongest emitters of radiation from the solar chromosphere, at 2800 Å. By studying the surface variations of the Mg II lines, researchers hope to understand the contribution solar features such as active regions make to observed changes in the solar irradiance (the total brightness of the entire Sun). A second innovation was a modified spectroheliograph, which could obtain images at four different wavelengths instead of only one. Images were obtained at 1600 Å, 1560 Å, 1549 Å, and 1540 Å. The goal was to obtain a subtraction image—a difference image between the 1549 Å image, which is partly but not entirely from the C IV transition region lines and one of the other wavelength images—in order to better show features that are truly from plasmas emitting C IV radiation. In fact, first results show small, bright loops in C IV using the difference images of 1549 Å and 1600 Å, as Fig. 18 shows.

[Sponsored by NASA and ONR] ∎

Special Awards and Recognition

Special Awards and Recognition

NRL is proud of its many distinguished scientists, engineers, and support staff. Here we feature some who have received awards from prestigious institutions, the Department of the Navy, and NRL.
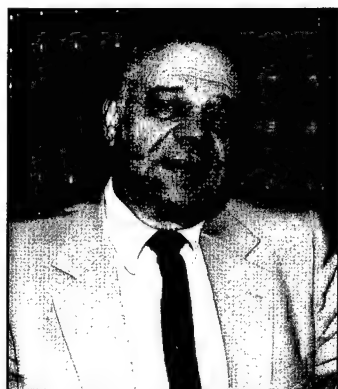
Dr. Jerome Karle
Nobel Laureate
Laboratory for the Structure of Matter

1992 ETTORE MAJORANA—ERICE—SCIENCE FOR PEACE PRIZE

This award is given by the Ettore Majorana Center for Scientific Culture, in Erice, Italy. Dr. Karle, a corecipient, was recognized for his "discoveries relative to the structure of materials with diffractive methods," and for his "engagement to promote international scientific collaboration above any ideological-political-racial barrier giving, in this way, concrete accomplishments to the Spirit of Erice."

Dr. Thomas G. Giallorenzi
Optical Sciences Division

NAVY LEAGUE'S ALBERT A. MICHELSON AWARD

Dr. Giallorenzi was cited "for his significant accomplishments in the development and utilization of fiber optics and electro-optics in the Departments of the Navy and Defense. The award recognizes a civilian scientist, technology innovator, or technical organization...for scientific or technical achievement that results in a significant improvement in the strength of our maritime forces or to the enhancement of our industrial technological base."

Dr. Timothy Coffey
Director of Research

PRESIDENTIAL RANK OF DISTINGUISHED EXECUTIVE IN THE SENIOR EXECUTIVE SERVICE (Second Award)

Dr. Coffey was recognized for his "sustained extraordinary accomplishment in management of programs of the United States Government and for leadership exemplifying the highest standards of service to the public, reflecting credit on the career civil service."
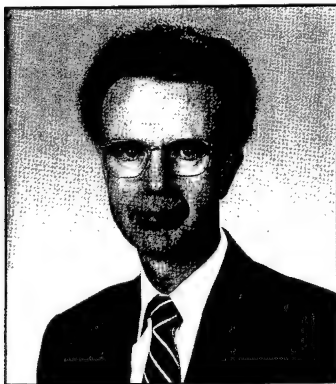
Dr. Thomas L. Reinecke
Electronics Science and Technology Division

1994 HUMBOLDT RESEARCH AWARD

The award is granted by the German Alexander von Humboldt Foundation to "outstanding U.S. scientists in recognition of past accomplishments in research and teaching, and thereby promoting scientific cooperation between institutions in the Federal Republic of Germany and in the U.S.A."

Dr. Homer Carhart
Chemistry Division

JACK BONO ENGINEERING COMMUNICATIONS AWARD

Dr. Carhart was one of three recipients of this inaugural award presented by the Society of Fire Protection Engineering, which is "to be given to the author(s) of the paper that, during the prior year, contributed most to the advancement and application of professional fire-protection engineering. Both technical content and usefulness to the society membership in advancing their competence should be considered." Dr. Carhart's paper was entitled "Extinguishment of Class B Flames by Thermal Mechanisms: Principles Underlying a Comprehensive Theory; Prediction of Flame Extinguishing Effectiveness."

Drs. James Yesinowski, Kenneth McGrath,
and Allen Garroway
(Absent from the photo: Dr. Joel Miller)
Chemistry Division

R&D "BEST" AWARD

This award, presented by *R&D Magazine* to the NRL team and Quantum Magnetics, Inc., of San Diego, California, is called "the Oscar of Inventions" by the *Chicago Tribune*. The award was given for the "package scanner," a novel explosives and contraband detection device, which has a highly sensitive ability to screen postal packages, briefcases, and other small baggage for the presence of explosives and illegal drugs.

Dr. Michael D. Collins
Acoustics Division

A.B. WOOD MEDAL AND PRIZE

Dr. Collins received this distinguished award from the United Kingdom's Institute of Acoustics "for exceptional contributions to numerical modeling of complex acoustical phenomena and nonlinear inversion methods....preference being given to candidates whose work is associated with the sea." The award is made in alternate years to persons residing in the United Kingdom, the United States, and Canada.
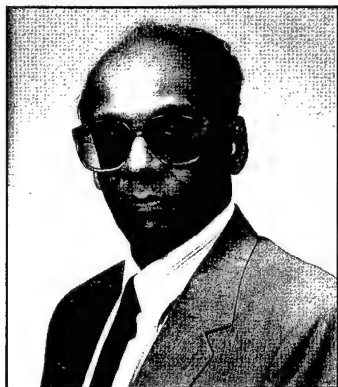
Dr. Attipat K. Rajagopal
*Electronics Science and
Technology Division*

WASHINGTON ACADEMY OF SCIENCES AWARD FOR OUTSTANDING ACHIEVEMENT IN ENGINEERING SCIENCES

Dr. Rajagopal was presented an award "for outstanding achievement in engineering sciences." Dr. Rajagopal conducts theoretical research in condensed matter and statistical physics; lattice vibrations of metals and superconductors; and electron gas theories in 2- and 3-D long-time relaxation phenomena in complex systems, on nanoelectronic structures and devices, and on a new nonequilibrium time-dependent functional theory of condensed matter systems.
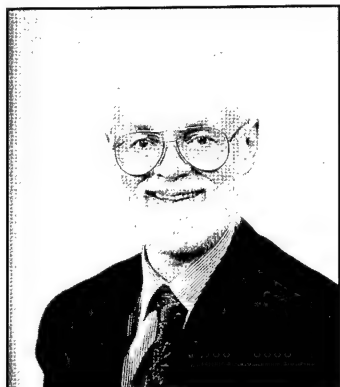
Dr. David L. Griscom
Optical Sciences Division

1995 OTTO SCHOTT RESEARCH AWARD

Dr. Griscom was cited by the Carl-Zeiss-Stiftung, in Germany, "for being among the first to apply the electron-spin resonance techniques to glass materials. He applied lattice defect ideas of solid-state physics to the amorphous state and was able to identify several defects by methods like high-energy radiation, fiber drawing, or compositional additives. All results on defects in silica caused by redox reactions and manufacturing-induced impurities or nonequilibrium structures were highly significant for the emerging technology of optical communication via fiber waveguides."

Dr. Brenda Little
Oceanography Division

1995 WOMEN IN SCIENCE AND ENGINEERING SCIENTIFIC ACHIEVEMENT AWARD

Dr. Little was cited "as being the most outstanding woman scientist in the federal government." This prestigious award is given to women who not only have made important contributions to science but who have also given their time to encourage young women to pursue scientific careers.

Dr. Jimmie L. Mitchell
Oceanography Division

TOPEX/POSEIDON AWARD

The Jet Propulsion Laboratory presented this award to Dr. Mitchell "as a small token of the TOPEX/POSEIDON Project's gratitude and recognition of...significant contributions to the establishment, preparation, and execution of TOPEX/POSEIDON" and for his "research accomplishments in oceanography, and...effective communication of the results to the public, and...personal enthusiasm and knowledge of ocean measurements."

Dr. George A. Doschek
Space Science Division

1994 NAVAL RESEARCH LABORATORY'S
E.O. HULBURT SCIENCE AND ENGINEERING AWARD

Dr. Doschek was cited for "sustained superior performance over a number of years in the research areas of solar physics and astrophysics, laboratory plasma spectroscopy, and atomic physics." He was also recognized for being "the driving force behind the conception and construction of several flight instruments that have revolutionized our understanding of solar flare physics."
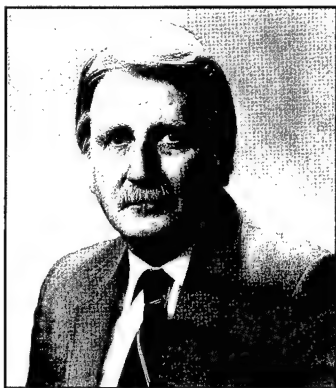
Mr. James W. Gately, Jr.
(Awarded Posthumously)
Command Support Division

NAVY MERITORIOUS CIVILIAN SERVICE AWARD

Mr. Gately was recognized for "his outstanding contributions to the Laboratory and the Navy, particularly in his position as Public Affairs Officer....The public affairs program he developed provides the highest quality of service to the Laboratory, other commands and activities, and the Navy."

Mr. Donald J. DeYoung
Executive Directorate

NAVY MERITORIOUS CIVILIAN SERVICE AWARD

Mr. DeYoung was recognized for his "extraordinary contributions to the Department of the Navy during the period March 1994 through June 1995....Mr. DeYoung has made a substantial and significant contribution to the capabilities and competitiveness of the U.S. Navy of the 21st century. His willingness to take on any assignment and carry it through to completion, and his strong defense of the integrity of the base closure process set an example for other team members to follow. His performance was in the finest tradition of the Navy to 'do it right and do it well.'"

DEPARTMENT OF THE NAVY'S AWARD OF MERIT FOR GROUP ACHIEVEMENT
Members of the Deep Space Program Science Experiment/*Clementine* Team
Space Systems Development Department

This award "is based on the desire to honor all Naval Center for Space Technology (NCST) employees whose skill and dedication contributed to the success of the NRL [Deep Space Science Experiment] Program, also known as the *Clementine* Program. This group provided the scientific, engineering, technical, operations, administrative, and management leadership and coordination to successfully design, build, test, launch, and operate the *Clementine* spacecraft."

Program Management Team

(Left to right) Mark Johnson, Donald Horan, Howard Merk, Patricia Klein, Paul Regeon, Charles Wildermann, and Peter Lynn

Subsystem Technical Leads

(Left to right) Paul Delahunt, Michael Hurley, Ronald Mader, Amy Marderness, Jeffery Cleveland, Renee Mazaheri, Jeong Kim, James Garner, and William Raynor. (Not shown: Alois Kudlach, Kimberly Lyons, and Drew Roberts)

Subsystem Key Technical Personnel

(Kneeling, left to right) Alan Hope, Tim Gross, Robert Haynes, Aaron Chilbert, Christopher Lichtenberg, and David Spencer; (Standing, left to right) Gerald Golba, Joseph Hauser, Susie Lam, Porter Lyon, Julie Kim, William Purdy, Faye Zidek, Hubert Scott, George Flach, Louise McDonald, and Robert Baldauff; (Not shown: Edward Becker, Charles Bird, Paul Cary, Robert Circle, William Collins, Robert Dasenbrock, Joseph Decamp, Frederick Domer, Stephen Gates, Dorothy Harbour, Bernard Kaufman, Stephen Koss, Marvin Levenson, Jay Middour, Russell Mills, Peter Nicholson, Michael Osborn, Robert Perram, Ronald Weakley, and George Wiedemann)

Clementine Support Team

(Bottom row, left to right) Melody Hudson, Angela Hyman, Shirley Herbert, Denise Elliott, Theresa Robison, Kathleen Golba, Sheleen Spencer, and Carla Warner; (Middle row, left to right) Michael Holtery, Morton Frank, Herbert Smathers, Andrew Fox, Joseph Koffley, Mustufa Bahrain, and Robert Patterson; (Top row, left to right) Joseph Inzana, Russell Barnes, Jim Tunney, David Golder, Gilbert Clopper, Larry Burman, James Layher, Daniel Shortt, William Baker, William Braun, Petrina Wynn; (Not shown: Jennifer Altier, Charles Bargerstock, Milton Barrett, Walter Buczek, Christopher Butkiewicz, Junho Choi, Kenneth Clark, Edith Coates, Richard Cooksey, Ann Cox, Michelle Deatley, Tracey Dorsey, Maria Ferrell, Kevin Fick, Joseph Freitas, Kathy Gifford, Cynthia Hartman, Thomas Hayes, Ronald Heflin, Gilbert Herlich, Nelson Hyman, Charles Jones, Juliana Kang, Cory Knudtson, Michael Mardis, Edward McDonald, Charles Morgan, Nancy Peaper, Tiffany Roark, Ralph Ruth, Albert Salvato, David Schriftman, Leo Sentiger, Bob Skalitzky, Josephine Smith, Mark Soyka, Michael Swinney, Tan Tran, and Larry Turner)

Mr. Robert L. Guest
Management Information Systems Staff

1995 NAVAL RESEARCH LABORATORY (NRL) EQUAL EMPLOYMENT OPPORTUNITY AWARD (SUPERVISORY)

Mr. Guest was cited for his "proactive work in supporting initiatives and programs for individuals who are mobility impaired as well as outstanding contributions to the overall NRL EEO Program. Mr. Guest has been active in promoting the rights of individuals with disabilities at NRL. He has been especially concerned for those with mobility impairments and has organized two 'Access Awareness Days' and designed a traverse path across the Lab to illustrate mobility barriers. Mr. Guest continually notes access problem areas, and works with NRL's Research and Development Services to make corrections and/or improvements. He also works throughout the year to remove barriers that impair individuals with disabilities."

Dr. Zakya H. Kafafi
Optical Sciences Division

1995 NAVAL RESEARCH LABORATORY (NRL) EQUAL EMPLOYMENT OPPORTUNITY AWARD (NONSUPERVISORY)

Dr. Kafafi was cited for her "tireless efforts to promote and develop the career of female and male scientists and engineers, and create an environment where work at NRL is a productive and rewarding experience for all. Dr. Kafafi has fostered a new program focused on fulfilling these goals....NRL has now an established Mentor Program available to all employees at all sites."

Ms. Deborah E. Erwin
Human Resources Office

NAVAL RESEARCH LABORATORY'S (NRL) AWARD OF EXCELLENCE IN MISSION SUPPORT

Ms. Erwin was noted "for her outstanding contributions in the areas of NRL equal employment opportunities and prevention of sexual harassment training that has set high marks for others to follow. She was the cornerstone in the development and provision of 'Prevention of Sexual Harassment (POSH)' training for the employees of NRL in response to a mandate from the Secretary of the Navy. Her intuitiveness, dedication, integrity, and willingness to go that extra mile to bring issues to resolution have resulted in the NRL Equal Employment Opportunity Program taking second seat to none in the Navy."

Ms. Joyce Smithwick
Materials Science and Com-
ponent Technology Directorate

NAVAL RESEARCH LABORATORY'S
AWARD FOR EXCELLENCE IN SECRETARIAL SUPPORT

Ms. Smithwick was commended for her "exceptional secretarial support and professionalism in the execution of tasks of the Office of the Materials Science and Component Technology Directorate and for performing a multitude of additional responsibilities for the Laboratory in an exemplary manner."

Ms. Velma Stiverson
Ocean and Atmospheric
Sciences Directorate

NAVAL RESEARCH LABORATORY'S
AWARD FOR EXCELLENCE IN SECRETARIAL SUPPORT

Ms. Stiverson is credited with being "important to the early success of the directorate." She was also chosen for ensuring that all clerical/administrative procedures are well planned, executed, and coordinated.

Ms. Carol Trgina
Space Science Division

NAVAL RESEARCH LABORATORY'S
AWARD FOR EXCELLENCE IN SECRETARIAL SUPPORT

Ms. Trgina was recognized for "demonstrating extraordinary dedication and skill in performing her work...not just the traditional tasks one expects of a secretary, but virtually anything that comes to her attention....Ms. Trgina goes beyond completing work successfully and...she is adept at devising innovative solutions to problems that arise in the division."
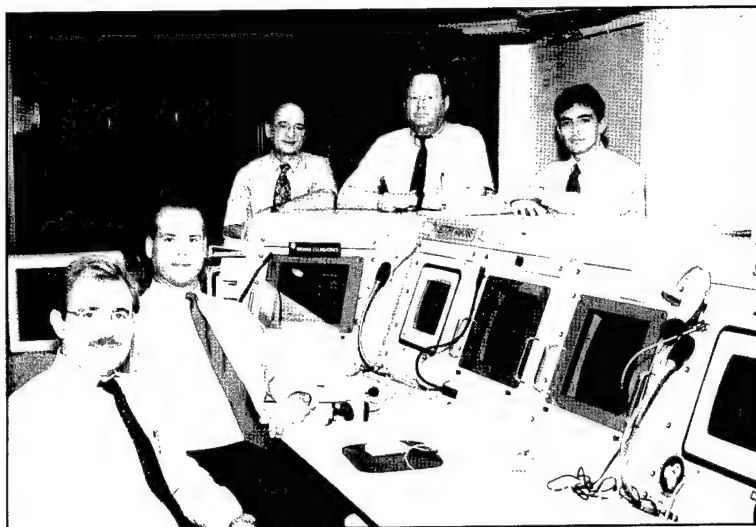
NAVAL RESEARCH LABORATORY'S TECHNOLOGY TRANSFER AWARD
Mr. Jay Middour, Mr. Alan Hope, Mr. Bernard Kaufman,
Dr. Robert Dasenbrock, and Mr. Mark Soyka
Space Systems Development Department

This award was presented for their work in trajectory analysis for the recent *Clementine* mission. The team was responsible for the entire mission, which included the original trajectory design, launch window analysis, maneuver planning and execution, lunar orbit insertion, lunar orbit maintenance, Earth return, lunar gravity assist to the asteroid *Geographos*, and contingency planning.

NAVAL RESEARCH LABORATORY'S AWARD OF EXCELLENCE IN MISSION SUPPORT
Mr. Robert Spragg, Ms. Miriam Oliver, Ms. Judy McKinney, Ms. Angela Allison,
Ms. Brenda Norwood, Mr. Victor Papagno, and Mr. Richard Leadley
Office of Management and Administration

The award was given to the Office for "its exceptional and significant contributions in support of the Laboratory's scientific program." The group's "dedication, skill, and insight have contributed in a major way to the quality of service and productivity of the Laboratory."

224

Alan Berman Research Publication
and Edison Patent Awards

The Annual Research Publication Awards Program was established in 1968 to recognize the authors of the best NRL publications each year. These awards not only honor individuals for superior scientific accomplishments in the field of naval research but also seek to promote continued excellence in research and in its documentation. In 1982, the name of this award was changed to the Alan Berman Research Publication Award, in honor of its founder.

There were 235 separate publications submitted by the divisions in 1995 to be considered for recognition. Of those considered, 38 were selected. These selected publications represent 155 authors, each of whom received a publication awards certificate, a bronze paperweight, and a booklet listing the publications that were chosen for special recognition. In addition, NRL authors share in their respective division's monetary award.

The winning papers and their respective authors are listed below by their research units. Non-Laboratory coauthors are indicated by an asterisk.

NRL also recognizes patents as part of its annual publication awards program. The NRL Edison Patent Award was established in January 1991 to recognize NRL employees for outstanding patents issued to NRL by the U.S. Patent and Trademark Office during the preceding calendar year. The award recognizes significant NRL contributions to science and engineering as demonstrated by the patent process that are perceived to have the greatest potential benefit to the country. Of the 11 patents considered for 1995, 2 were selected and an additional 1 was selected for a special award, representing 6 inventors. They are listed under the NRL Edison Patent Awards.

Command Support Division

Radiation Dosimetry Using Thermoluminescence of Semiconductor-doped Vycor Glass
Tommy L. Johnson, Brian L. Justus, and Alan L. Huston

Radar Division

RADARC Model Comparisons with Amchitka Radar Data
James M. Headrick, Benjamin T. Root, and Joseph F. Thomason

AN/SPQ-9B ADM Radar Test Results
Ben H. Cantrell, Lawrence M. Leibowitz, David J. Cardiel, Win Jou Cheung,
Linda M. Schaus, and Gregory C. Tavik

Information Technology Division

*Standard Clock Simulation and Ordinal Optimization Applied to Admission Control
in Integrated Communication Networks*
Jeffrey E. Wieselthier, Craig M. Barnhart, and Anthony Ephremides*

A Network Version of the Pump
Myong H. Kang, Ira S. Moskowitz, and Daniel C. Lee

Optical Sciences Division

Performance Evaluation of a Staring Two Color MWIR Missile Approach Warning System
Kenneth A. Sarkady, Garry R. Katz, John P. Mateosky, Michael A. Colbert,
Melvin R. Kruer, Ralph A. York,* Stephen P. Michaels,* and Eddie L. Wilder*

*True Time-Delay Fiber-Optic Control of an Ultrawideband Array Transmitter/Receiver
with Multibeam Capability*
Michael Y. Frankel and Ronald D. Esman

Tactical Electronic Warfare Division

Super-resolution Precision Direction-Finding Techniques and Measurements
Hal L. Levitt, Edward M. Alexander, Anthony Y. Tse, and Anthony E. Spezio

Universal Exciter Communications Electronic Attack Applications
William W. Everett, John M. Eardley, and Robert A. Weber

Laboratory for the Structure of Matter

Quantum Crystallography and the Use of Kernel Projector Matrices
Lou Massa,* LuLu Huang,* and Jerome Karle

Chemistry Division

*Results of a Magnetometry Survey at TA-50, MDA-C, Los Alamos National Laboratory,
Los Alamos, New Mexico*
J. R. McDonald and Richard Robertson*

A Stable High-Index Surface of Silicon: Si (5 5 12)
Alison A. Baski,* Steven C. Erwin, and Lloyd J. Whitman

Materials Science and Technology Division

*Characterization of Strain-induced Damage in Composites Based
on the Dissipated Energy Density, Parts I, II, and III*
P. W. Mast, G. E. Nash,* J.G. Michopoulos, R. Thomas,*
R. Badaliance, and I. Wolock*

Corrosion Inhibition of Iron in Acid Solutions by Biological Siderophores
E. McCafferty and J.V. McArdle*

Laboratory for Computational Physics and Fluid Dynamics

Radiating Plasma Structures in Ablating, Laser-Produced Plasmas
J. P. Dahlburg, M. Klapisch,* J. H. Gardner, C. R. DeVore,
A. J. Schmitt, and A. Bar-Shalom*

Condensed Matter and Radiation Sciences Division

Orthogonal Strains and Onset of Plasticity in Shocked LiF Crystals
Robert R. Whitlock and Justin S. Wark*

Vibron Excitations in Solid Hydrogen: A Generalized Binary Random Alloy Problem
Joseph L. Feldman, Jon H. Eggert,* Jan De Kinder,* Russell J. Hemley,*
Ho-kwang Mao,* and Dirk Schoemaker*

Plasma Physics Division

Controlling the Resistive Hose Instability in Relativistic Electron Beams
Richard F. Fernsler, Steven P. Slinker, Martin Lampe, and Richard F. Hubbard

Time-Dependent Asymmetries in Laser-Fusion Hohlraums
Steven E. Bodner

Electronics Science and Technology Division

Optically Detected Magnetic Resonance of GaN Films Grown by
Organometallic Chemical-Vapor Deposition
E. R. Glaser, T. A. Kennedy, K. Doverspike, L. B. Rowland, D. K. Gaskill,
J. A. Freitas, Jr.,* M. Asif Khan,* D. T. Olson,* J. N. Kuznia,* and D. K. Wickenden*

AFM Fabrication of Sub-10 nm Metal-Oxide Devices with In Situ Control
of Electrical Properties
E. S. Snow and P. M. Campbell

Center for Bio/Molecular Science and Engineering

Detection of TNT in Water Using an Evanescent Wave Fiber-Optic Biosensor
Lisa C. Shiver-Lake, Kristen A. Breslin,* Paul T. Charles, David W. Conrad,
Joel P. Golden, and Frances S. Ligler

New Fluctuation Mode in a Chiral Smectic-A Liquid Crystal with a Uniaxial Layer Modulation
Samual N. Sprunt,* Jonathan V. Selinger, Gregory P. Crawford,*
Banahalli R. Ratna, and Ranganathan Shashidhar

Acoustics Division

Supersonic Acoustic Intensity
Earl G. Williams

*Scattering from Collective Modes of Air Bubbles in Water and the
Physical Mechanism of Super-resonances*
Christopher Feuillade

Remote Sensing Division

First Results from POAM II: The Dissipation of the 1993 Antarctic Ozone Hole
Richard M. Bevilacqua, Karl W. Hoppel, John S. Hornstein, Robert L. Lucke, Eric P. Shettle,
Thomas L. Ainsworth,* D. Debrestian,* M. D. Fromm,* S. S. Krigman,* J. Lumpe,* W. Glaccum,*
J. J. Olivero,* R. T. Clancy,* C. E. Randall,* D. W. Rusch,* E. Chassefière,* F. Dalaudier,*
C. Deniel,* C. Brogniez,* and J. Lenoble

A Microwave Technique to Improve the Measurement of Directional Wave Spectra
Dale L. Schuler and Jong-Sen Lee

Oceanography Division

Error in Predicting Hydrosol Backscattering from Remotely Sensed Reflectance
Alan D. Weidemann, Robert H. Stavn,* J. R. V. Zaneveld,* and Michael R. Wilcox*

The Ocean Response to Operational Westerly Wind Bursts During the 1991-1992 El Niño
John C. Kindle and Patricia Phoebus

Marine Geosciences Division

Full Waveform Inversion of Seismic Interface Wave Data
Leonard Dale Bibee and Leroy M. Dorman*

Marine Meteorology Division

Coupled Ocean Wave/Atmosphere Mesoscale Model Simulations of Cyclogenesis
Jim D. Doyle

Numerical Simulations of the Life Cycle of a Baroclinic Wave
William T. Thompson

Space Science Division

The Role of Magnetic Reconnection in Chromospheric Eruptions
Judith T. Karpen, Spiro K. Antiochos, and C. Richard DeVore

The Large Angle Spectroscopic Coronagraph (LASCO)
Guenter E. Brueckner, Russell A. Howard, Clarence M. Korendyke,
Donald J. Michels, J. Daniel Moses, Dennis G. Socker, Kenneth P. Dere,
Martin J. Koomen,* Philippe Lamy,* Antoine Llebaria,* Maurice Bout,* Ranier Schwenn,*
George M. Simnett,* David K. Bedford,* and Christopher J. Eyles*

Space Systems Development Department

The Analysis of GPS Attitude Data from a Slowly Rotating, Symmetrical Gravity Gradient Satellite
Peter J. Melvin, Lisa M. Ward,* and Penina Axelrad*

Determination of the Complex Aperture Distribution of a Planar Spiral Antenna
from 3-D Far-Field Radiation Pattern Data
Wendy L. Lippincott, Michael S. Kluskens, and Mark Kragalott

Spacecraft Engineering Department

Close Conjunction Detection on Parallel Computer
Liam M. Healy

Vibrations of the Low Power Atmospheric Compensation Experiment Satellite
Shalom Fisher, Kenneth I. Schultz,* and Lawrence W. Taylor, Jr.*

NRL Edison Patent Awards

Magnetoresistive Linear Displacement Sensor, Angular Displacement Sensor,
and Variable Resistor
Gary A. Prinz
MATERIALS SCIENCE AND TECHNOLOGY DIVISION

Barry A. Edelberg
OFFICE OF COUNSEL

Nontoxic Antifouling Systems
James R. Griffith
CHEMISTRY DIVISION

George A. Kap
OFFICE OF COUNSEL

Navigation System Using Satellites and Passive Ranging Techniques
Roger L. Easton,* Retired
SPACE SYSTEMS DIVISION

J. Murray
OFFICE OF COUNSEL

Awards for *1995 NRL Review* Articles

Awards for *NRL Review* articles were established in 1990 to recognize authors who submit outstanding research articles for this scientific publication. The articles are judged on the relevance of the work to the Navy and DoD, readability to the college-graduate level, and the use of graphics that are interesting and informative. The following awards were presented for articles that appeared in the *1995 NRL Review*.

FEATURED RESEARCH ARTICLE

Clementine — A Mission to the Moon (and Beyond)
Donald M. Horan and Paul A. Regeon
Space Systems Development Department

Dr. Coffey, NRL's Director of Research, presents the feature article award to Dr. Horan, who accepts for himself and Mr. Regeon.

DIRECTORATE AWARDS FOR SCIENTIFIC ARTICLES

Warfare Systems and Sensors Research Directorate

The Development of Over-The-Horizon Radar at NRL
James M. Headrick and Joseph F. Thomason
Radar Division
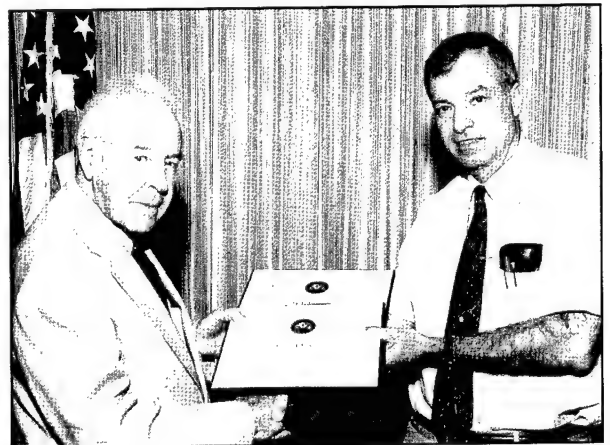
Mr. Headrick receives his and Mr. Thomason's award from Dr. Coffey.

Materials Science and
Component Technology Directorate

Metal-Ion Biosensors for Environmental Studies
Jeffrey R. Deschamps and Keith B. Ward
LABORATORY FOR STRUCTURE OF MATTER

Dr. Coffey presents the Materials Science and Component Technology Directorate award
to Dr. K. Ward (left) and to Dr. J. Deschamps (right).

Ocean and Atmospheric Science and
Technology Directorate

Model Sensitivity Evaluation Using the Adjoint Methods
Rolf H. Langland and Russell L. Elsberry
MARINE METEOROLOGY DIVISION

Mr. Langland accepts the award from
Dr. Coffey for himself and Mr. Elsberry.

Naval Center for Space Technology

Structural Control for Enhanced Space-based Sensing
Shalom Fisher and Albert Bosse
SPACECRAFT ENGINEERING DEPARTMENT
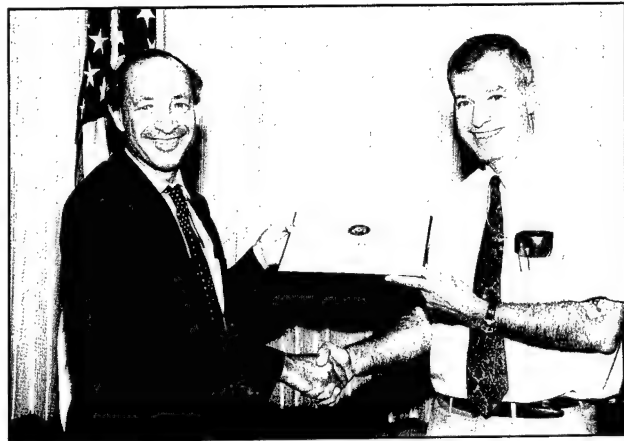
Dr. Shalom Fisher receives the award from Dr. Coffey.

Programs
for
Professional
Development

Programs for NRL Employees

During 1995, under the auspices of the Employee Development Branch, NRL employees participated in 2900 individual training events. Many of these were presented as either video-taped or on-site instructed courses on diverse technical subjects, management techniques, and enhancement of such personal skills as efficient use of time, speed reading, memory improvement, and interpersonal communications. Courses are also available by means of computer-based training (CBT) and live television courses for monitoring nationwide.

One common study procedure is for employees to work full time at the Laboratory while taking job-related scientific courses at universities and schools in the Washington area. The training ranges from a single course to full graduate and postgraduate programs. Tuition for training is paid by NRL. The formal programs offered by NRL are described here.

GRADUATE PROGRAMS

• The **Advanced Graduate Research Program** (formerly the Sabbatical Study Program, which began in 1964) enables selected professional employees to devote full time to research or pursue work in their own or a related field for 1 year at an institution or research facility of their choice without the loss of regular salary, leave, or fringe benefits. NRL pays all educational costs, travel, and moving expenses for the employee and dependents. Criteria for eligibility include professional stature consistent with the applicant's opportunities and experience, a satisfactory program of study, and acceptance by the facility selected by the applicant. The program is open to paraprofessional employees (and above) who have completed 6 years of Federal Service, 4 of which are at NRL.

• The **Edison Memorial Graduate Training Program** enables employees to pursue advanced studies in their fields at local universities. Participants in this program work 24 hours each work-
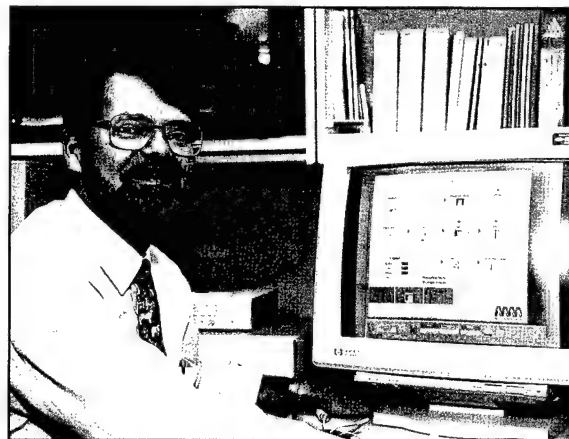
Dr. Robert Jackson, of the Electronics Science and Technology Division, recently participated in the Advanced Graduate Research Program at Culham Laboratory in the United Kingdom.

week and pursue their studies during the other 16 hours. The criteria for eligibility include a minimum of 1 year of service at NRL, a bachelor's or master's degree in an appropriate field, and professional standing in keeping with the candidate's opportunities and experience.

• To be eligible for the **Select Graduate Training Program**, employees must have a college degree in an appropriate field and must have demonstrated ability and aptitude for advanced training. Students accepted in this program devote a full academic year to graduate study. While attending school, they receive one-half of their salary, and NRL pays for tuition, books, and laboratory expenses.

• The **Naval Postgraduate School** (NPS), located in Monterey, California, provides graduate programs to enhance the technical preparation of Naval officers and civilian employees who serve the Navy in the fields of science, engineering, operations analysis, and management. It awards a master of arts degree in national security affairs and a master of science degree in many technical disciplines.

Ms. Laurie Fialkowski, of the Acoustics Division, pursues a Masters Degree at the University of Maryland under the Edison Memorial Graduate Training Program.

NRL employees desiring to pursue graduate studies at NPS may apply for a maximum of six quarters away from NRL, with thesis work accomplished at NRL. Specific programs are described in the NPS catalog. Participants will continue to receive full pay and benefits during the period of study.

• In addition to NRL and university offerings, application may be made to a number of noteworthy programs and fellowships. Examples of such opportunities are the **Alfred P. Sloan Fellows Program, Brookings Institute Advanced Study Program**, the **Fellowship in Congressional Operations**, and the **Women's Executive Leadership Program**. These and other programs are announced from time to time as schedules are published.

• Research conducted at NRL may be used as **thesis material for an advanced degree**. This original research is supervised by a qualified employee of NRL who is approved by the graduate school. The candidate should have completed the required course work and should have satisfied the language, residence, and other requirements of the graduate school from which the degree is sought. NRL provides space, research facilities, and supervision but leaves decisions on academic policy to the cooperating schools.

CONTINUING EDUCATION

• Local colleges and universities offer **undergraduate and graduate courses** at NRL for employees interested in improving their skills and keeping abreast of current developments in their fields. These courses are also available at many other DoD installations in the Washington, D.C. area.

• The Employee Development Branch at NRL offers **short courses** to all employees in a number of fields of interest including technical subjects, computer operation, supervisory and management techniques, and clerical/secretarial skills. Laboratory employees may attend these courses at non-government facilities as well. Interagency courses in management, personnel, finance, supervisory development, and clerical skills are also available.

For further information on any of the above programs, contact the Employee Development Branch (Code 1840) at (202) 767-2956.

TECHNOLOGY TRANSFER

• The **Office of Research and Technology Applications Program** (ORTA) ensures the full use of the results of the Nation's federal investment in research and development by transferring federally owned or originated technology to state and local governments and the private sector. Contact Dr. Richard Rein, Code 1004 at (202) 767-7230, e-mail: techtransfer@nrl.navy.mil. URL: http://infonext.nrl.navy.mil/~techtran/.

TECHNOLOGY BASE

• The **Navy Science Assistance Program** (NSAP) establishes an information loop between the Fleet and the R&D shore establishments to

expedite technology transfer to the user. The program addresses operational problems, focuses resources to solve specific technical problems, and develops a nucleus of senior scientific personnel familiar with the impact of current research and system performance on military operations.

• The **Scientist-to-Sea Program** (STSP) provides increased opportunities for Navy R&D laboratory/center personnel to go to sea to gain first-hand insight into operational factors affecting system design, performance, and operations on a variety of ships.

For further information on the Technology Base Programs, contact Dr. Stephen Sacks, Code 5006, at (202) 767-3666.

PROFESSIONAL DEVELOPMENT

NRL has several programs, professional society chapters, and informal clubs that enhance the professional growth of employees. Some of these are listed below.

• The **Counseling Referral Service** (C/RS) helps employees to achieve optimal job performance through counseling and resolution of problems such as family, stress and anxiety, behavioral, emotional, and alcohol- or drug-related problems that may adversely impact job performance.

C/RS provides confidential assessments and short-term counseling, training workshops, and referrals to additional resources in the community. (Contact Ms. Kelly Kramp at (202) 767-6857.)

• A chartered chapter of **Women in Science and Engineering** (WISE) was established at NRL in 1983. Informal luncheons and seminars are scheduled to inform scientists and engineers of women's research at NRL and to provide an informal environment for members to practice their presentations. WISE also sponsors a colloquium series to feature outstanding women scientists. (Contact Dr. Wendy Fuller-Mora at (202) 767-6207, Dr. Debra Rolison at (202) 767-3617, or Dr. Cha-Mei Tang at (202) 767-4148.)

• **Sigma Xi**, the scientific research society, encourages and acknowledges original investiga-

tion in pure and applied science. As an honor society for research scientists, individuals who have demonstrated the ability to perform original research are elected to membership in local chapters. The NRL Edison Chapter, comprised of approximately 600 members, recognizes original research by presenting awards annually in pure and applied science to outstanding NRL staff members. The chapter also sponsors lectures at NRL on a wide range of scientific topics for the entire NRL community. These lectures are delivered by scientists from all over the nation and the world. The highlight of the Sigma Xi lecture series is the Edison Memorial Lecture, traditionally featuring a Nobel laureate. (Contact Dr. Wendy Fuller-Mora at (202) 767-6207 or Dr. Robert Morris at (202) 767-3845.)

• The **NRL Mentor Program** was established to provide an innovative approach to professional and career training and an environment for personal and professional growth. It is open to permanent NRL employees in all job series and at all sites. Mentorees are matched with successful, experienced colleagues with more technical and/or managerial experience who can provide them with the knowledge and skills needed to maximize their contribution to the success of their immediate organization, to NRL, to the Navy, and to their chosen career fields. The ultimate goal of the program is to increase job productivity, creativity, and satisfaction through better communication, understanding, and training. NRL Instruction 12400.1 established the NRL Mentor Program, and it provides the policy and procedures for the program. (Contact Dr. Pat Tatem at (202) 767-2476.)

• The Charlotte Moore-Sitterly Chapter of **Federally Employed Women, Inc.** (FEW) was chartered at NRL in 1993. FEW is an international organization of federally employed women and men whose purpose is to eliminate sex discrimination and sexual harassment and enhance career opportunities for women in government. FEW works closely with other Federal agencies and organizations, including the Office of Personnel Management, Equal Employment Opportunity Commission, and Federal Women's Program subcommittees. (Contact Ms. Jeanie Osburn at (202) 767-3885.)

237

In the Spring of 1995, the Federal Women's Program (FWP) and the Federally Employed Women's (FEW) Subcommittees sponsored 144 daughters for NRL's third annual "Take Our Daughter's to Work Day."

• Employees interested in developing effective self-expression, listening, thinking, and leadership potential are invited to join either of two NRL chapters of **Toastmasters International**. Members of these clubs, who possess diverse career backgrounds and talents, meet three times a month in an effort to learn to communicate not by rules but by practice in an atmosphere of understanding and helpful fellowship. NRL's commanding officer and director of research endorse Toastmasters, and the Employee Development Branch pays for membership and educational materials for those NRL employees whose supervisors see a need for their active training in public speaking or communication skills. (Contact Ms. Kathleen Parrish at (202) 767-2782.)

• Through the **Women in Science and Technology Program** (WIST), the NRL Stennis Space Center (NRL-SCC) works closely with coordinators from Mississippi Gulf Coast Community College and Pearl River Community College to introduce young high school women to careers in math and science. Conferences held at NRL-SCC and college campuses focus on encouraging young women to take those courses that provide the educational background necessary for developing high-technology skills and promoting their entrance into nontraditional careers. The WIST Program began in 1986 as a Mississippi State Department of Education joint effort between the Department of Vocational Education and the Sex Desegregation Office. (Contact Mr. George Stanford at (601) 688-5211.)

• An agreement between NRL-SSC and **Mississippi's Alliance for Minority Participation** places students whose background and interests match the Laboratory's field of research with NRL mentors in a 10-week research environment. Together with accomplished senior researchers and faculty advisors, students plan, develop, and conduct a summer research project to include challenging, hands-on experiences with research equipment and principles of modern research. (Contact Mr. George Stanford at (601) 688-5211.)

EQUAL EMPLOYMENT OPPORTUNITY (EEO) PROGRAMS

Equal employment opportunity is a fundamental NRL policy for all persons, regardless of race, color, sex, religion, national origin, age, or physical/mental handicap. The EEO Office's major functions include affirmative action in employment, discrimination complaint process, EEO training, advice and guidance to management on EEO policy, and the following special emphasis programs:

• The **Federal Women's Program** (FWP) supports and enhances employment and advancement opportunities for women and addresses issues that affect women in the workplace. It provides counseling and referral services and sponsors a chapter of Women in Science and Engineering to recognize outstanding female scientists and engineers. Distinguished women scientists are guest lecturers at quarterly presentations.

• The **Hispanic Employment Program** (HEP) focuses on working with supervisors, managers, and subcommittees to recruit and place qualified Hispanics. The program is involved with Hispanic community organizations and local schools and provides activities specifically designed to offer employment opportunities to Hispanics. "El Ingeniero" (The Engineer), which encourages Hispanic youth to pursue a career in engineering, is one such program.

The **African-American Employment Program** (AAEP) concentrates on recruiting, placing, developing, and advancing African-American employees throughout NRL. It also encourages them to achieve their maximum potential.

• The **Individuals with Disabilities Program** (IWDP) assists management to improve employment and advancement opportunities for qualified handicapped and disabled veteran employees. It also advises on accommodations necessary for handicapped persons. It recruits handicapped summer students from colleges and universities for technical positions in engineering and science and paraprofessional positions in accounting and administration; it also seeks Student Career Experience Program candidates who are pursuing degrees in engineering, computer sciences, or the physical sciences.

• The **Asian-American/Pacific-Islander Program** (API) identifies areas of concern regarding the recruitment, selection, advancement, and retention of API employees throughout NRL. The program interacts with API professional/community organizations to address employment concerns.
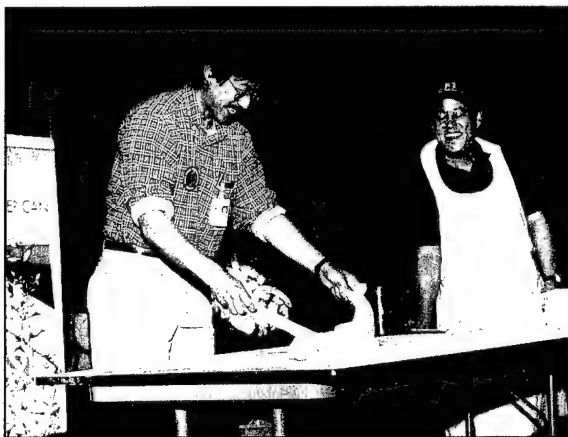
Dr. Eddie Chang attempts to "pull" noodles out of dough—noodles as thin as hair—during NRL's 7th Annual Asian/Pacific American Observance Program.

• The **American-Indian/Alaskan-Native Employment Program** (AI/ANEP) focuses on the employment concerns of AI/ANEP employees. The program provides counseling and referral services on recruitment, hiring, placement, promotion, retention, and other areas of employee interest.

• The **Federal Employment Opportunity Recruitment Program** (FEORP) is designed to establish, maintain, and update targeted recruitment programs to reduce the conspicuous

absence or manifest imbalance categories of NRL employment through innovative internal and external recruitment. In addition, it fosters relationships with minority and women's institutions and organizations.

Special programs are held during the year to promote an awareness of the contributions and capabilities of women and minorities. (Contact the EEO Office at (202) 767-2486 for all EEO programs.)

OTHER ACTIVITIES

• The **Community Outreach Program** traditionally has used its extensive resources to foster programs that provide benefits to students and other community citizens. Volunteer employees assist with and judge science fairs, give lectures, tutor, mentor, coach, and serve as classroom resource teachers. The program also sponsors Black History Month art and essay contests for local schools, student tours of NRL, a student Toastmasters Youth Leadership Program, an annual holiday party for neighborhood children, an annual collection for Children's Hospital, and other programs that support the local community. Also through this program, NRL has active partnerships with four District of Columbia public schools. (Contact the Public Affairs Office at (202) 767-2541.)

CAPT Raymond Leonard accepts the Linda Moody Community Service Award on behalf of the volunteers of NRL's Community Outreach Program. The award was presented by Ms. Linda H. Moody, Ward 8 representative, D.C. Board of Education.

• Other programs that enhance the development of NRL employees include four computer user groups (**IBM PC, Mac, NeXT,** and **Sun**), the **Microcomputer Software Support Center**, and the **Amateur Radio Club**. The **Recreation Club** encourages the wide interest of sports for employees with its many facilities and programs, such as a six-lane heated indoor pool; basketball and volleyball court; weight room with qualified consultant, by appointment; table tennis; hot tub and sauna; five martial arts disciplines; aerobics, ranging from low-low to high and step classes; swimming lessons; water walking and exercise; yoga; swing dance sessions; softball and basketball leagues; and specialized sports clubs (running, skiing, swimming, biking, and golfing). Sportswear, NRL paraphernalia, discount tickets to amusement parks, and film-developing services are available at the Rec Club office. The **Showboaters**, a nonprofit drama group that presents live theater for the enjoyment of NRL and the community, per-

A scene from the Showboaters' production of "Nunsense."

forms two major productions each year in addition to occasional performances at Laboratory functions and benefits for local charities. The most recent productions were "Nunsense" and "Sleuth." Though based at NRL, membership in Showboaters is not limited to NRL employees.

Programs for Non-NRL Employees

Several programs have been established for non-NRL professionals. These programs encourage and support the participation of visiting scientists and engineers in research of interest to the Laboratory. Some of the programs may serve as stepping-stones to federal careers in science and technology. Their objective is to enhance the quality of the Laboratory's research activities through working associations and interchanges with highly capable scientists and engineers and to provide opportunities for outside scientists and engineers to work in the Navy laboratory environment. Along with enhancing the Laboratory's research, these programs acquaint participants with Navy capabilities and concerns.

RECENT PH.D., FACULTY MEMBER, AND COLLEGE GRADUATE PROGRAMS

• The **National Research Council (NRC)/NRL Cooperative Research Associateship Program** selects associates who conduct research at NRL in their chosen fields in collaboration with NRL scientists and engineers. The tenure period is 2 years. The Office of Naval Research offers the associate post-tenure research grants tenable at an academic institution.

• The American Society for Engineering Education (ASEE) administers the **Office of Naval Research (ONR) Postdoctoral Fellowship Program** that aims to increase the involvement of highly trained scientists and engineers in disciplines necessary to meet the evolving needs of naval technology. Appointments are for 1 year (renewable for a second and sometimes a third year). These competitive appointments are made jointly by ONR and ASEE.

• The American Society for Engineering Education also administers the Navy/ASEE **Summer Faculty Research and Sabbatical Leave Program** for university faculty members to work for 10 weeks (or longer for those eligible for sabbatical leave) with professional peers in participating Navy laboratories on research of mutual interest.

• The **NRL/United States Naval Academy (USNA) Cooperative Program for Scientific Interchange** allows faculty members of the U.S. Naval Academy to participate in NRL research. This collaboration benefits the Academy by providing the opportunity for USNA faculty members to work on research of a more practical or applied nature. In turn, NRL's research program

Drs. Isabella and Jerome Karle of the Laboratory for the Structure of Matter sponsored 20 educators representing the National Consortium of Specialized Secondary Schools for mathematics, science, and technology who toured NRL research facilities. The tour introduced educators to the types of research being conducted by the Navy and the practical applications of this research in the Fleet.

is strengthened by the available scientific and engineering expertise of the USNA faculty.

• The **National Defense Science and Engineering Graduate Fellowship Program** helps U.S. citizens obtain advanced training in disciplines of science and engineering critical to the U.S. Navy. The 3-year program awards fellowships to recent outstanding graduates to support their study and research leading to doctoral degrees in specified disciplines such as electrical engineering, computer sciences, material sciences, applied physics, and ocean engineering. Award recipients are encouraged to continue their study and research in a Navy laboratory during the summer.

For further information about the above five programs, please contact Mrs. Jessica Hileman at (202) 767-3865.

• The **Professional Development Program for Ensigns** assigns newly commissioned ensigns, who are awaiting future training, to NRL to work in areas of their own choosing commensurate with their academic qualifications. These young officers provide a fruitful summer of research assistance while gaining valuable experience in the Navy's R&D program. For more information, contact the Military Administrative Office at (202) 767-2103.

PROFESSIONAL APPOINTMENTS

• **Faculty Member Appointments** use the special skills and abilities of faculty members for short periods to fill positions of a scientific, engineering, professional, or analytical nature.

• **Consultants and experts** are employed because they are outstanding in their fields of specialization or because they possess ability of a rare nature and could not normally be employed as regular civil servants.

• **Intergovernmental Personnel Act Appointments** temporarily assign personnel from the state or local government or educational institution to the Federal Government (or vice versa) to improve public services rendered by all levels of government.

STUDENT PROGRAMS

The student programs, tailored to the undergraduate, provide employment and work experience in naval research. These are designed to attract applicants for student and full professional employment in the Laboratory's shortage category positions, such as engineers, physicists, mathematicians, and computer scientists. The student employment programs build an understanding of NRL job opportunities between students and educational personnel so that educators can provide students who will meet NRL's occupational needs. The employment programs for college students include the following:

• The **Student Career Experience Program** (formerly known as Cooperative Education Program) employs students in study-related occupations. The program is conducted in accordance with a planned schedule and a working agreement between NRL, the educational institution, and the student. Primary focus is on students
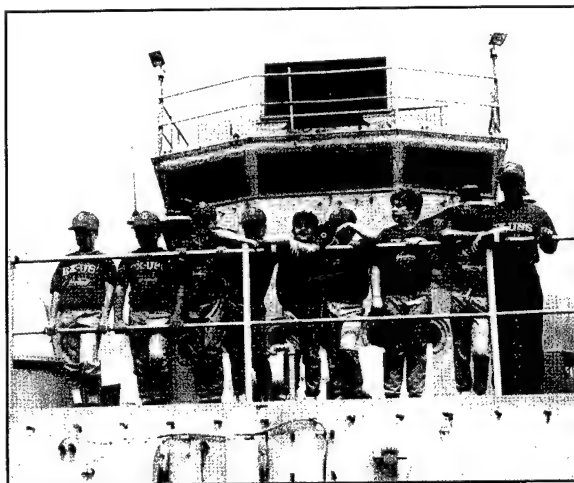
NRL's Navy Technology Center for Safety and Survivability researchers at the ex-USS *Shadwell* in Mobile, Alabama, sponsored the Shadwell Mariners, a local boys' baseball team.

pursuing bachelor degrees in engineering, computer science, or the physical sciences.

• The **Student Temporary Employment Program (STEP)** enables students to earn a salary while continuing their studies and offers them valuable work experience.

• The **Summer Employment Program** employs students for the summer in paraprofessional and technician positions in engineering, physical sciences, computer sciences, and mathematics.

• The **Student Volunteer Program** helps students gain valuable experience by allowing them to voluntarily perform educationally related work at NRL.

For additional information on these undergraduate college student programs, contact Cindy Stiles at (202) 767-8312.

HIGH SCHOOL PROGRAMS

• The **DoD Science & Engineering Apprentice Program** (SEAP) employs high school juniors and seniors to serve for 8 weeks as junior research associates. Under the direction of a mentor, students gain a better understanding of research, its challenges, and its opportunities through participation in scientific programs. Criteria for eligibility are based on science and mathematics courses completed and grades achieved; scientific motivation, curiosity, and capacity for sustained hard work; a desire for a technical career; teacher recommendations; and achievement test scores. The NRL Program is the lead program and the largest in DoD.

For additional information, contact the Employee Development Branch (Code 1840) at (202) 767-2956.

243

General Information

Technical Output

The Navy continues to be a pioneer in initiating new developments and a leader in applying these advancements to military requirements. The primary method of informing the scientific and engineering community of the advances made at NRL is through the Laboratory's technical output—reports, articles in scientific journals, contributions to books, papers presented to scientific societies and topical conferences, patents, and inventions.

The figures for calendar year 1995 presented below represent the output of NRL facilities in Washington, D.C.; Bay St. Louis, Mississippi; and Monterey, California.

In addition to the output listed, NRL scientists made more than 1423 oral presentations during 1995.

A complete listing of the publications by NRL authors appears in the *Bibliography of NRL Publications*, a separate annual publication.

Type of Contribution	Unclassified	Classified	Total
Articles in periodicals, chapters in books, and papers in published proceedings	1041	0	1041
NRL Formal Reports	38	13	51
NRL Memorandum Reports	119	27	146
Other NRL Reports and NRL Publications	21	11	32
Books	0		0
Patents granted			78
Statutory Invention Registrations (SIRs)			10

*This is a provisional total based on information available to the Ruth H. Hooker Research Library and Technical Information Center on January 10, 1996. Additional publications carrying a 1995 publication date are anticipated.

Technology Transfer at NRL

There are many ways for private companies to benefit from the technical resources of NRL. Some of these include: (1) entering into Cooperative Research and Development Agreements (CRADAs), (2) obtaining licenses for Navy-owned patents, and (3) consulting with NRL scientists and engineers.

Entering into a CRADA is an excellent way for U.S. companies to gain access to commercially important NRL research and development (R&D) technology. Authorized under the Federal Technology Transfer Act of 1986, a CRADA is an agreement between one or more federal laboratories and one or more nonfederal parties, such as private companies. Designed to encourage and facilitate cooperative R&D, CRADAs can involve research in any area that is consistent with NRL's mission.

Additionally, the Federal Government can license its own inventions. NRL has developed many new technologies and processes in areas as diverse as advanced materials, chemistry, biotechnology, optics, ocean and atmospheric sciences, and electronics. NRL currently has approximately 500 patents available for license in these fields.

As the Navy's corporate laboratory, NRL draws on the powerful resources of an interdisciplinary combination of scientific expertise and modern facilities. NRL's technical staff is recruited from all disciplines of engineering and the physical sciences and is available to work with private companies to help them solve their technical problems. Many of the staff have received the Award for Excellence in Technology Transfer from the Federal Laboratory Consortium (FLC). This award recognizes employees who have accomplished outstanding work in the process of transferring laboratory-developed technology.

During 1995, new products have been introduced from NRL technology by the private sector. For instance, NRL's Acoustic Seafloor Classification System (ASCS) has been developed into a

The bottoms of these huge Navy fuel tanks, like this one in Hawaii, are being lined with the NRL-21st Century Coatings CRADA materials.

commercially viable system for pipeline location, structure siting surveys, buried object location, and other commercial uses.

A Virginia-based company, 21st Century Coatings, Inc., introduced new paint formulations based on technology licensed from NRL. These new formulations of fluorinated polyurethane resins will be used in petroleum, oil, and lubricant storage tanks that meet or exceed current standards for future implementation.

For additional information, contact NRL's Technology Transfer Office, 4555 Overlook Ave., S.W., Washington, DC 20375-5320, or call (202) 404-7920; e-mail: techtransfer@nrl.navy.mil; URL: http://infonext.nrl.navy.mil/~techtran/.

Key Personnel

Code	Office		Phone Number
		EXECUTIVE DIRECTORATE	
1000	Commanding Officer	CAPT B.W. Buckley, USN	767-3403
1000.1/1002	Inspector General/Chief Staff Officer	CAPT R.E. Leonard, USN	767-3621
1001	Director of Research	Dr. T. Coffey	767-3301
1001.1	Scientific Staff Assistant	Mr. K.W. Lackie	767-2880
1004	Head, Technology Transfer	Dr. R. Rein	767-7230
1006	Head, Office of Program and Administration and Policy Development	Ms. S. Herrin (Acting)	767-3086
1200	Head, Command Support Division	Mr. J.C. Payne	767-3048
1220	Head, Security	Mr. C. Herbert	767-0793
1230	Public Affairs Officer	Mr. R. Baturin	767-2541
1240	Head, Safety Branch	Mr. K.J. King	767-2232
1400	Head, Military Support Division	CDR R. Francisco, USN	767-2271
1600	Officer-in-Charge, Flight Support Detachment	CDR D.R. Dowell, USN	301-863-3751
1800	Director, Human Resources Office	Ms. B. Duffield	767-3421
1803	Deputy EEO Officer	Ms. D. Erwin	767-2486
3204	Deputy for Small Business	Ms. P. Schaefer	767-6263
		BUSINESS OPERATIONS DIRECTORATE	
3000	Associate Director of Research	Mr. R.E. Doak	767-2371
3008	Legal Counsel	Ms. H.J. Halper	767-2244 3030
	Head, Management Information Systems Staff	Mr. R.L. Guest	767-2030
3200	Head, Contracting Division	Mr. J.C. Ely	767-5227
3300	Comptroller, Financial Management Division	Mr. D.T. Green	767-3405
3400	Supply Officer	Ms. C. Hartman	767-3446
3500	Director, Research and Development Services Division	Mr. D.K. Woodington	767-3371
		SYSTEMS DIRECTORATE	
5000	Associate Director of Research	Dr. R.A. LeFande	767-3324
5200	Head, Technical Information Division	Mr. P.H. Imhof	767-2187
5300	Superintendent, Radar Division	Dr. M.I. Skolnik	767-2936
5500	Superintendent, Information Technology Division	Dr. R.P. Shumaker	767-2903
5600	Superintendent, Optical Sciences Division	Dr. T.G. Giallorenzi	767-3171
5700	Superintendent, Tactical Electronic Warfare Division	Dr. J.A. Montgomery	767-6278
		MATERIALS SCIENCE AND COMPONENT TECHNOLOGY DIRECTORATE	
6000	Associate Director of Research	Dr. B.B. Rath	767-3566
6030	Head, Laboratory for Structure of Matter	Dr. J. Karle	767-2665
6100	Superintendent, Chemistry Division	Dr. J.S. Murday	767-3026
6300	Superintendent, Materials Science & Technology Division	Dr. D.U. Gubser	767-2926
6400	Director, Lab. for Computational Physics and Fluid Dynamics	Dr. J.P. Boris	767-3055
6600	Superintendent, Condensed Matter & Radiation Sciences Division	Dr. D.J. Nagel	767-2931
6700	Superintendent, Plasma Physics Division	Dr. S. Ossakow	767-2723
6800	Superintendent, Electronics Science & Technology Division	Dr. G.M. Borsuk	767-3525
6900	Center for Bio/Molecular Sciences and Engineering	Dr. J. Schnur	404-6000
		OCEAN AND ATMOSPHERIC SCIENCE AND TECHNOLOGY DIRECTORATE	
7000	Associate Director of Research	Dr. E.O. Hartwig	404-8690
7030	Head, Office of Research Support Services	Mr. G. Bower	601-688-4010
7100	Superintendent, Acoustics Division	Dr. E.R. Franchi	767-3482
7200	Superintendent, Remote Sensing Division	Dr. P. Schwartz (Acting)	767-3391
7300	Superintendent, Oceanography Division	Dr. W.B. Moseley	601-688-4670
7400	Superintendent, Marine Geosciences Division	Dr. H.C. Eppert, Jr.	601-688-4650
7500	Superintendent, Marine Meteorology Division	Dr. T.L. Tsui (Acting)	408-656-4721
7600	Superintendent, Space Science Division	Dr. H. Gursky	767-6343
		NAVAL CENTER FOR SPACE TECHNOLOGY	
8000	Director	Mr. P.G. Wilhelm	767-6547
8100	Superintendent, Space Systems Development Department	Mr. R.E. Eisenhauer	767-0410
8200	Superintendent, Spacecraft Engineering Department	Mr. H.E. Senasack, Jr. (Acting)	767-6411

*Additional Duty

Contributions by Divisions, Laboratories, and Departments

Employment Opportunities for
Entry-Level and Experienced Personnel

The *NRL Review* illustrates some of the exciting science and engineering carried out at the Naval Research Laboratory as well as the potential for new personnel.

NRL offers a wide variety of challenging positions that involve the full range of work from basic and applied research to equipment development. The nature of the research and development conducted at NRL requires professionals with experience. Typically there is a continuing need for electronics, mechanical, aerospace, ceramic, and materials engineers, metallurgists, computer scientists, and oceanographers with bachelor's and/or advanced degrees and physical and computer scientists with Ph.D. degrees. Opportunities exist in the areas described below:

Ceramic Engineers and Materials Scientists/Engineers. These employees are recruited to work on materials, microstructure characterization, electronic ceramics, solid-state physics, fiber optics, electro-optics, microelectronics, fracture mechanics, vacuum science, laser physics technology, and radio frequency/microwave/millimeter wave/infrared technology.

Electronics Engineers and Computer Scientists. These employees may work in the areas of communications systems, electromagnetic scattering, electronics instrumentation, electronic warfare systems, radio frequency/microwave/millimeter wave/infrared technology, radar systems, laser physics technology, radio-wave propagation, electron device technology, spacecraft design, artificial intelligence, information processing, signal processing, plasma physics, vacuum science, microelectronics, electro-optics, fiber optics, solid state, software engineering, computer design/architecture, ocean acoustics, stress analysis, and expert systems.

Mechanical Engineers. These employees may be assigned to spacecraft design, remote sensing, propulsion, experimental fluid mechanics, experimental structural mechanics, solid mechanics, elastic/plastic fracture mechanics, materials, finite-element methods, nondestructive evaluation, characterization of fracture resistance of structural alloys, combustion, and CAD/CAM.

Chemists. Chemists are recruited to work in the areas of combustion, polymer science, bioengineering and molecular engineering, surface science, materials, fiber optics, electro-optics, microelectronics, electron-device technology, and laser physics.

Physicists. Physics graduates may concentrate on such fields as materials, solid-state physics, fiber optics, electro-optics, microelectronics, vacuum science, plasma physics, fluid mechanics, signal processing, ocean acoustics, information processing, artificial intelligence, electron-device technology, radio-wave propagation, laser physics, ultraviolet/X-ray/gamma-ray technology, electronic warfare, electromagnetic interaction, communications systems, radio frequency/microwave/millimeter wave/infrared technology, and computational physics.

Oceanographers, Meteorologists, and Marine Geophysicists. These employees work in the areas of ocean dynamics, air-sea interaction, upper-ocean dynamics, oceanographic bio-optical modeling, oceanic and atmospheric numerical modeling and prediction, artificial intelligence applications for satellite analyses, benthic processes, aerogeophysics, marine sedimentary processes, and advanced mapping techniques. Oceanographers and marine geophysicists are located in Washington, D.C., and the Stennis Space Center, Bay St. Louis, Mississippi. Meteorologists are located in Washington, D.C., and Monterey, California.

254

APPLICATION AND INFORMATION

Interested applicants should submit an Application for Federal Employment (SF-171), an Optional Application for Federal Employment (OF-612), or a resume. The OF-612 and SF-171 can be obtained from local Office of Personnel Management and Human Resource Offices of federal agencies.

Direct inquiries to:

Naval Research Laboratory
Human Resources Office, Code 1813 RV 96
Washington, DC 20375-5324
(202) 767-3031

Location of NRL in the Capital Area

Subject Index

256

Fires, 183
Flight Support Detachment
  (NRL FSD), 26, 32
Focal Plane Evaluation Facility, 15
Free-electron maser, 110
Free-Surface Hydrodynamics
  Laboratory, 31
GAMBLE II, 19
Geolocation, 205
Global Imaging of the Ionosphere
  (GIMI), 24
Graphical Interface, 108
HERCULES, 205
High-Energy Pulsed Hydrogen
  Fluoride, Deuterium Fluoride
  Laser, 15
High-Power Microwave (HPM)
  Facility, 18
High-Resolution Atmospheric
  and Auroral Spectroscopy
  (HIRAAS), 24
High-temperature
  superconductivity, 195
Hispanic Employment Program
  (HEP), 238
Human-computer interaction, 181
Hydroxyl radical, 199
Hypervelocity Impact Facilities,
  18
Image intensifier, 205
Imaging radars, 171
Immunoassay, 97
Individuals with Disabilities
  Program (IWDP), 239
InfoNet, 25
Information Security Engineering
  Laboratory, 14
Information Technology, 14,
  32, 125
Ion Implantation Facility, 18
Information Technology and
  Communication, 129
Infrared, 159
Infrared detectors, 119
Infrared (IR) test chamber, 30
Instability, 117
Interfaces, 119
Intergovernmental Personnel
  Act Appointments, 242
Internal waves, 93
IR Missile-Seeker Evaluation
  Facility, 15
Joint multispectral program, 159
Karle, Dr. Isabella, iv

Kuroshio, 59
Laboratory for Advanced Material
  Synthesis (LAMS), 19
Laboratory for Computational
  Physics and Fluid Dynamics, 17
Land-based testing, 103
Large Optic, High-Precision
  Tracker, 15
Large-scale dynamics, 191
Laser explosion, 188
Laser facilities, 18
Laser sensing, 137
Lens antenna, 104
Littoral environment, 103
Localized, 117
Low cost, 104
Magnetic, 135
Map Data Formatting Facility,
  24, 28
Mask, 162
Materials Science and Technology,
  17, 32
Marine Corrosion Test Facility,
  27
Marine Geosciences, 23, 32, 33
Marine Meteorology Division
  Monterey, California
  (NRL-MRY), 24, 28
Mesoscale coastal nonhydrostatic,
  151
Meteorology, 151
Microcomputer Software Support
  Center, 240
Middle Atmosphere High
  Resolution Spectrograph
  Investigation (MAHRSI), 9
Midway Research Center (MRC),
  29
Millimeter wave source,
  110
Mississippi's Alliance for
  Minority Participation, 238
Multicast, 127
Multispectral, 159
Nanochannel glass, 162
Nanoelectronic Processing
  Facility (NPF), 19, 30
National Defense Science
  and Engineering Graduate
  Fellowship Program, 242
National Research Council
  (NRC)/NRL Cooperative
  Research Associate Program,
  241

Natural products, 49
Naval Center for Space
  Technology (NCST), 25
Naval Postgraduate School
  (NPS), 235
Navy Prototype Optical
  Interferometer (NPOI), 22
Navy Science Assistance
  Program (NSAP), 236
Near-field optical spectroscopy,
  140
Nearshore dynamics, 175
NICEnet, 14
Night vision, 205
Nike Krypton Fluoride Laser
  Facility, 10, 19
NRL Magnetic Observatory, 24
NRL Mentor Program, 237
NRL Review Awards, 230
NRL/United States Naval Academy
  (USNA) Cooperative Program
  for Scientific Interchange, 241
Numerical modeling, 149
Ocean Acoustics Research
  Laboratory, 31
Ocean currents, 173
Oceanography, 22
Ocean Science, 59
Office of Naval Research (ONR)
  Postdoctoral Fellowship
  Program, 241
Office of Research and
  Technology Applications
  Program (ORTA), 236
Optical measurements, 165
Optical probe shock, 188
Optical Sciences, 14, 30
Organic chemistry, 93
Oriented Scintillation
  Spectrometer (OSSE), 8, 24
Parallel High-Performance
  Computer/Graphics Facility, 17
Parallel processing, 185
Pattern Analysis Laboratory, 28
Patterning, 162
Penthouse Processing Facility
  (PPF), 19, 31
Pharos III Nd-laser facility,
  32
Phase change, 84
Phased arrays, 104
Photoelectron diffraction, 135
Plasma, 117
Plasma Physics, 18, 30, 32

258

Author Index